

**A mechanistic approach to understand the role of p90 ribosomal S6 kinases in
Prostate Cancer**

Ryan James Cronin

**A thesis submitted for the degree of
Doctor of Philosophy in Biochemistry**

School of Life Science

University of Essex

Date of submission December 2022

Abstract

The RSKs are known to be involved in many cancers, including Prostate Cancer (PCa), however the representation of the Ribosomal S6 Kinase (RSK) isoforms is skewed and there is little investigation into the RSK regulation of the Androgen Receptor (AR). Here we show in model African Green Monkey Kidney Fibroblast (COS-1 cells) that all RSKs regulate the AR transcriptional activity and interact with the AR in proximity. Analysis of PCa cell lines highlighted that all RSKs exhibited higher expression than the control but most significantly RSK2. We then transitioned to lymph node carcinoma of the prostate (LNCaP) cells as they are more biologically relevant, siRNA knockdown coupled with qPCR showed that key AR target genes was differentially regulated by the RSKs; RSK1 and RSK4 knockdown caused increased expression of NDRG1; RSK1 and RSK2 knockdown induced a decrease in TMPRSS2; RSK2 knockdown produced a significant decrease in PSA, respectively. To understand if these effects would translate to a cellular change we investigated proliferation, siRNA knockdown of RSK2 and RSK4 caused a significant decrease in LNCaP cells. Interestingly, investigation of RSK4 is also underrepresented in structural biology despite having a different mechanism from other isoforms. Here, we attempted to express, purify, and crystalize different domains of RSK4 to understand its mechanism of activation. Crystallization attempts were unsuccessful, potentially due proteolysis and chaperone contaminations. Kinetic assays showed that phospho-mimetic mutations were successful in creating a constitutively active mutant construct. Pull down assays experimentally showed that the AGC region of RSK4 is essential for the PDK1 independent activation. The multiple techniques used in this study strongly suggest that RSK are in fact involved in PCa signalling and warrant further investigation and highlight the nonredundant

functions of the RSK isoforms and a novel relationship between AR and RSK4.

Additionally, the pull-down assay highlighted that the AGC region of RSK facilitates interaction between the N- And C-terminal domains which has not been previously experimentally demonstrated thus supporting previous speculation around its activation mechanism.

Statement of Originality

I declare that the work within this document is of my own unless stated within the text.

Acknowledgements

I would like to thank Dr. Filippo Prischi and Dr. Greg Brooke for their continued support throughout my PhD it's been a long four years, but it is finally coming to an end. Both have not only supported me academically but emotionally by encouraging me to push through the hard times. We went through the global pandemic together and managed to publish a review. Both have not only helped me grow into a better scientist but a better person ready to go off on my own into a, hopefully, prosperous career. I would also acknowledge Kestutis Lapenas, my lab partner, for his support and the many laughs we shared. I would also like to thank my Fiancée, Georgie, for her continued love and support throughout our PhD journey together. Finally, I would like to acknowledge and express gratitude to Peter Nichols, who in his passing nobly created a PhD scholarship which I was fortunate enough to be awarded.

Abbreviations

α L – Inhibitory α -helix
Gamma-H2AX – Phospho-H2A histone family member X
AC – Affinity chromatography
ADT – Androgen deprivation therapy
AF – Activation function
AGC – PKA/PKG/PKC kinase
AIM – Autoinduction media
AKT – Protein kinase B
AMP-PNP – Adenylyl-imidodiphosphate
AP1 – Activator protein 1
AR – Androgen receptor
ARE – Androgen response element
ASK1 – Apoptosis signal-regulating Kinase 1
ATM – Ataxia telangiectasia mutated
ATP – Adenosine triphosphate
BAD - BCL-2 associated death protein
BAX – BCL-2 associated X protein
BCa – Breast Cancer
BCAR1 – Breast cancer anti-estrogen resistance protein 1
BCL-2 – B-Cell Lymphoma 2
BIC – Bicalutamide
CaCl₂ – Calcium chloride
CAMK – Calcium/Calmodulin- dependent protein kinase
cAMP – Cyclic adenosine monophosphate
CBP – CREB binding protein
Cdc - Cell division control
cDNA – complementary DNA
CDK – Cycling dependent kinase
Chk1/2 – Checkpoint kinase 1/2
CKAP2 – Cytoskeleton-associated Protein 2
CREB – cAMP responsive element binding protein
CRPC – Castrate resistant prostate cancer
C-spine – Catalytic spine
CTKD – C-terminal kinase domain
CTKDM – C-terminal kinase domain mutant
CTD – C-terminal domain
DBD – DNA binding domain
D-d – ERK D-domain
DHT – Dihydrotestosterone
DIAL – Dialysis buffer
DMEM - Dulbecco's modified eagle's medium
DNA – Deoxyribonucleotide acid
DSB – Double stranded break
dsDNA – double stranded DNA
E – Elution buffer

EDTA - Ethylenediaminetetraacetic acid
EGF – Epidermal growth factor
EGFR – Epidermal growth factor receptor
ERK – Extracellular signal-regulated kinase
EMT – Epithelial–mesenchymal transition
ER α – Estrogen receptor α
ETOH – Ethanol
FAK – Focal Adhesion Kinase
FBS – Foetal bovine serum
FRA1 – Fos related antigen 1
G-loop – Glycine -rich loop
Grb2 – Growth factor receptor bound protein 2
GDP – Guanosine diphosphate
GTP – Guanosine triphosphate
HCV – Hepatitis C virus
HE – Haemagglutinin-esterase
HM – Hydrophobic motif
HOXB13 – Homeobox B13
HPV 16 – Human papillomavims type 16
Hsp – Heat shock protein
IDH – Isocitrate dehydrogenase
IE – Ion exchange
IF – Interface
IGF – Insulin-like growth factor
ING3 – Inhibitor-of-growth protein 3
IPTG - isoproyl-b-D-thiogalactopyranoside
IRES – Internal ribosome entry site (IRES)
Itk – Interleukin-2 tyrosine kinase
JNK – c-Jun N-terminal kinase
LB – Luria broth
LBD – Ligand binding domain
LHRH – Luteinizing hormone-releasing hormone
LUC – Luciferase activity experiments
LY – LY294002
M2H – Mammalian-2-hybrid assay
MABC - Molecular apocrine breast cancer
MAPK – Mitogen activated protein kinase
MEK – Mitogen-activated protein kinase kinase
MIB – Mibolerone
MKK(n) – Mitogen-activated protein kinase kinase (n denotes a number)
Mre11 – Meiotic recombination 11
MRN – Mre11-Rad50-Nbs1
mRNA – messenger RNA
Nbs1 – Nijmegen breakage syndrome 1
NTD – N-terminal domain
p65 – Nuclear factor NF-kappa-B p65 subunit
p300 – E1A-associated protein

PBS – Phosphate buffered saline
PBST – Phosphate buffered saline – 0.1% tween
PCR – Polymerase chain reaction
PCa – Prostate cancer
PDK1 – Phosphoinositide-dependent kinase 1
PDVF – Polyvinylidene fluoride
PI3K – Phosphoinositide 3 Kinase
PIF – PDK1 interacting fragment
PKA – Protein kinase A
PKC – Protein kinase C
PSA – Prostate specific antigen
PTK6 – Protein tyrosine kinase 6
PTMs – Post-translational modifications
qPCR – Quantitative PCR
Rad50 – DNA repair protein RAD50
REs – Restriction enzymes
RNA – Ribonucleic acid
RPMI – Roswell park memorial institute
RPS6 – Ribosomal protein S6
R-spine – Regulatory spine
RSK – p90 ribosomal S6 kinase
RSK4 CTKD – RSK4 C-terminal kinase domain
RSK4 NTKD – RSK4 N-terminal kinase domain
RSK4 NL – RSK4 N-terminal kinase domain long
RSK4 NL3M – RSK4 N-terminal kinase domain long 3 mutations (S232E S389E S372E)
RT – Room temperature
RTK – Receptor tyrosine kinase
S6K – Ribosomal S6 kinase
SDS-PAGE – SDS polyacrylamide gel electrophoresis
SEC – Size exclusion chromatography
SFBS – double charcoal stripped FBS
SGK – Serum – and glucocorticoid-induced protein kinase
sHsps – Small heat shock proteins
siRNA – Short interfering RNA
SOS – sons of sevenless
SR – Steroid receptor
SRC – Steroid receptor co-activator
TGF- β – Transforming growth factor beta
TKL – Tyrosine kinase-like
TM – Turn motif
TMPRSS2 – Transmembrane protease serine 2
W1 – Wash buffer 1
W2 – Wash buffer 2
YB1 – Ybox binding protein 1

Contents

List of Tables	9
List of Figures	10
Chapter 1 – Literature review	12
1.1 – Prostate Cancer	13
1.1.1 – Development of Cancer	13
1.1.2 – Prostate Cancer	14
1.1.3 – Origin of Prostate Cancer	15
1.2 – The Androgen Receptor	18
1.2.1 – Androgen Receptor Expression and Function	18
1.2.2 – Androgen Receptor Structure	19
1.2.3 – Androgen Receptor Activation	22
1.2.4 – Androgen Receptor Post Translational Modifications	25
1.3 – The Ribosomal S6 Kinases	28
1.3.1 – Protein kinases	28
1.3.2 – RSK Structure	34
1.3.3 – RSK activation	37
1.4 – The role of the RSKs in Prostate Cancer signalling	41
1.4.1 – The role of RSKs in Prostate Cancer Proliferation	42
1.4.2 – The role of RSKs in cell cycle regulation	46
1.4.3 – The role of RSKs in cell motility	49
1.4.4 – The role of RSKs in therapy resistance	52
1.5 – Hypothesis and Objectives	57
Chapter 2 – Methods	58
2.1 – Antibiotic resistance and culture media preparation	58
2.2 – Molecular Biology	58
2.2.1 – Molecular Biology for Structural Studies	60
2.2.2 – Molecular Biology for Prostate Cancer signalling	60
2.2.3 – DNA plasmid amplification	60
2.2.4 – Plasmid mini/midi prep	61
2.2.5 – Gene amplification and site directed mutagenesis	63
2.2.6 – DNA fragment isolation	64
2.2.6.1 – Gene extraction / PCR cleanup	64
2.2.7 – DNA Double Digest	65
2.2.8 – Insert and Vector Ligation	66
2.2.9 – DNA verification	66
2.2.10 – Site directed Mutagenesis	67
2.3 – Recombinant Protein Expression	68
2.3.1 – Cell Harvesting	68
2.4 – Protein Purification	69
2.4.1 – Cell lysis	69
2.4.2 – Affinity Chromatography	70
2.4.3 – Ion Exchange Chromatography	70
2.4.4 – Size Exclusion Chromatography	71
2.4.5 – SDS-PAGE	71
2.5 – Crystallization	72
2.5.1 – Crystallization screening	72
2.5.2 – Crystallization optimization	74

2.6 – Protein Assays	76
2.6.1 – Kinase assay	76
2.6.2 – Pull down assay	77
2.6.3 – Western blotting	78
2.7 – Mammalian Cell Culture	80
2.7.1 – Passaging cells	82
2.7.2 – Cell counting and plating	82
2.7.3 – Calcium phosphate transfections	83
2.7.4 – Luciferase activity assay	84
2.7.5 – Mammalian-2-hybrid assay	86
2.7.6 – RSK siRNA knockdown	88
2.7.7 – RNA extraction	89
2.7.8 – Reverse Transcription	90
2.7.9 – qPCR	91
2.7.10 – WST-1 proliferation assay	93
Chapter 3 – Results – Characterization of RSK4 mechanism of activation	94
3.1 Introduction	94
3.2 – RSK4 N-Terminal Kinase Domain with AGC regulatory region S232E S389E S372E (RSK4 NL3M)	98
3.2.1 - Protein Purification and crystallization of RSK4 NL3M	98
3.3 – RSK4 C-Terminal Kinase Domain (RSK4 CTKD)	104
3.3.1 - Protein purification and crystallization of RSK4 CTKD	104
3.4 – RSK4 C-Terminal Kinase Domain T581E (RSK4 CTKDM)	116
3.4.1 - Protein purification and crystallization of RSK4 CTKDM	116
3.5 – RSK4 C-Terminal Kinase Domains role in activation	127
3.5.1 – RSK4 CTKDM is catalytically active	127
3.5.2 – Cross Talk between the RSK4 NTKD and the RSK4 CTKD	129
3.6 – Discussion	133
3.6.1 – Results Overview	133
3.6.2 – NL3M construct proteolysis	135
3.6.3 – C-terminal kinase domain does not crystallize	138
3.6.4 – RSK4 NTKD and CTKD interact via the AGC regulatory region	142
3.6.5 – Conclusion	143
Chapter 4 – Results – The role of RSKs in AR signalling and Prostate Cancer	145
4.1 – Introduction	145
4.2 – RSK-AR signalling pathway	147
4.2.1 – RSKs increase AR transcriptional activity	147
4.2.2 – RSKs interact with the AR in close proximity	150
4.2.3 – RSKs influence the AR transcriptional program	156
4.2.4 – The RSKs reduce proliferation in LNCaPs	163
4.3 – Discussion	166
4.3.1 – Results Overview	166
4.3.2 – RSK expression is elevated in Prostate Cancer	167
4.3.3 – RSKs regulate AR activity	169
4.3.4 – RSKs interact with the AR in proximity	173
4.3.5 – RSKs regulate LNCaP proliferation	175

4.3.6 – Conclusion	176
4.4 – Final Conclusion	178
Bibliography	179
Appendix	194

List of tables

Chapter 2	
Table 2.2.5.1 – Reaction mixture for PCR and Mutagenesis	63
Table 2.2.5.2 – Thermocycler program for PCR and Mutagenesis	63
Table 2.2.7.1 – Restriction enzyme double digest components, volumes, and concentrations	65
Table 2.2.8.1 – Ligation Reaction Mixture	66
Table 2.5.1.1 – Crystallization conditions used in screening	73
Table 2.5.2.1 – Traditional crystallization optimization of RSK4 CTKDM	75
Table 2.5.2.2 – Mixed matrix crystallization of RSK4 CTKDM	75
Table 2.5.2.3 – Seeding crystallization of RSK4 CTKDM	75
Table 2.6.1.1 – Kinase assay buffers	77
Table 2.6.2.1 – Pull down assay buffers	78
Table 2.7.1 – Cell lines models used	81
Table 2.7.3.1 – Calcium phosphate transfection components	83
Table 2.7.6.1 – QPCR siRNA transfection reaction mixtures	88
Table 2.7.6.2 – WST assay siRNA transfection reaction mixtures	88
Table 2.7.8.1 – Components of Reverse Transcription reaction	90
Table 2.7.9.1 – Reaction master mix for qPCR	92
Table 2.7.9.2 – qPCR cycling parameters	92
Chapter 3	
Table 3.6.2.1 – Components of Protease Inhibitor cocktail	136
Chapter 4	
Table 4.2.3.1 – Cell line, AR expression state and Ligand responsiveness	156

List of Figures

Chapter 1	
Figure 1.1.3.1 – Schematic representation of contributing mechanisms to prostate cancer progression	17
Figure 1.2.2.1 – Representations of Androgen Receptor Domains and Structure	21
Figure 1.2.3.1 – The Androgen Receptor Signalling Pathway	24
Figure 1.2.4.1 – Schematic representation of AR domain structure and phosphorylation sites	27
Figure 1.3.1.1 – Structure of common kinase catalytic core	29
Figure 1.3.1.2 – Hydrophobic spines define the internal architecture of RSK4	31
Figure 1.3.2.1 – Schematic representation of the RSKs domain structure	36
Figure 1.3.3.1 – Schematic representation of the RSK phosphorylation mechanism	40
Figure 1.4.1.1 – Summary of the role of the RSK family in Prostate Cancer proliferation	45
Figure 1.4.2.1 – Summary of the role of the RSK family in Prostate Cancer cell cycle regulation	48
Figure 1.4.3.1 – Summary of the role of the RSK family in Prostate Cancer cell motility	51
Figure 1.4.4.1 – Summary of the role of the RSK family in PCa progression and therapy resistance	56
Chapter 2	
Figure 2.2.1.1 – RSK domains cloned into plasmid vectors	59
Chapter 3	
Figure 3.1.1 – RSK4 NTKD has alternative binding to traditional AGC kinases	97
Figure 3.2.1.1 – SDS PAGE of Affinity chromatography of RSK4 NL3M	100
Figure 3.2.1.2 – SDS PAGE and chromatogram of Anion Exchange of RSK4 NL3M	101
Figure 3.2.1.3 – SDS PAGE and chromatogram of RSK4 NL3M SEC	102
Figure 3.2.1.4 – SDS PAGE of 10mg/ml RSK4 NL3M	103
Figure 3.3.1.1 – RSK alpha fold models	106
Figure 3.3.1.2 – SDS PAGE analysis of Affinity chromatography of RSK4 CTKD (AIM expression)	107
Figure 3.3.1.3 – SDS PAGE and chromatogram of RSK4 CTKD anion exchange (AIM expression)	108
Figure 3.3.1.4 – SDS PAGE and chromatogram of RSK4 CTKD Size exclusion (AIM expression) –	109
Figure 3.3.1.5 – SDS PAGE analysis of RSK4 CTKD at 10mg/ml (AIM expression)	110
Figure 3.3.1.6 – SDS PAGE analysis of Affinity chromatography of RSK4 CTKD (LB expression)	112
Figure 3.3.1.7 – SDS PAGE and chromatogram of RSK4 CTKD anion exchange (LB expression)	113
Figure 3.3.1.8 – SDS PAGE and chromatogram of RSK4 CTKD Size exclusion (LB expression)	114

Figure 3.3.1.9 – SDS PAGE analysis of RSK4 CTKD at 10mg/ml (LB expression)	115
Figure 3.4.1.1 – SDS-PAGE of RSK4 CTKDM affinity chromatography (AIM expression)	117
Figure 3.4.1.2 – SDS PAGE analysis and chromatogram of RSK4 CTKDM anion exchange (AIM expression)	118
Figure 3.4.1.3 – SDS PAGE analysis and chromatogram of RSK4 CTKDM Size exclusion (AIM expression)	119
Figure 3.4.1.4 – SDS PAGE analysis of RSK4 CTKDM at 10mg/ml (AIM expression)	120
Figure 3.4.1.5 – SDS PAGE analysis of RSK4 CTKDM affinity chromatography (LB expression)	121
Figure 3.4.1.6 – SDS PAGE analysis and chromatogram of RSK4 CTKDM anion exchange (LB expression)	122
Figure 3.4.1.7 – SDS PAGE analysis and chromatogram of RSK4 CTKDM Size exclusion (LB expression)	123
Figure 3.4.1.8 – SDS PAGE analysis of RSK4 CTKDM at 10mg/ml (LB expression)	124
Figure 3.4.1.9 – 100x magnification of RSK4 CTKDM crystal	125
Figure 3.5.1.1 – HTRF KinEASE assay of RSK4 CTKD and CTKDM	128
Figure 3.5.2.1 – RSK4 truncations used in western blotting	130
Figure 3.5.2.2 – Western blot of pull-down assay controls	132
Figure 3.5.2.3 – Western blot of pull-down assay binding elutions	132
Figure 3.6.1.1 – Model of RSK4 N-C terminal interaction	134
Chapter 4	
Figure 4.2.1.1 – RSK luciferase activity assay control	148
Figure 4.2.1.2 – AR luciferase activity assay	149
Figure 4.2.2.1 – Schematic representation of mammalian-2-hybrid mode of action	152
Figure 4.2.2.1 – Mammalian-2-hybrid assay of controls	154
Figure 4.2.2.2 – Mammalian-2-hybrid assay of AR-RSK	155
Figure 4.2.3.1– qPCR to monitor RSK expression in PCa cell lines	159
Figure 4.2.3.2– RSK expression is not altered by androgen stimulation	160
Figure 4.2.3.3 – siRNA knockdown of RSK coupled with qPCR of RSK1-4 expression in the presence of MIB	161
Figure 4.2.3.4 – siRNA knockdown of RSK coupled with qPCR to monitor expression of AR target genes	162
Figure 4.2.4.1 – WST hormone optimisation assay	164
Figure 4.2.4.2 – RSK siRNA knockdown WST assay	165

Chapter 1 – Literature Review

This chapter will outline the relevant literature available in the topic area to highlight the existing knowledge around the proteins of interest and how they are already known to influence cancer.

1.1 – Prostate Cancer

1.1.1 – Development of Cancer

Carcinogenesis processes are initiated by a plethora of different events, but all cancers have common features, first outlined by Hanahan and Weinberg 2000 (Hanahan & Weinberg 2000). The authors identified the hallmarks of cancer as: self-sufficiency in growth signals, insensitivity to anti-growth signals, acquisition of a blood supply, tissue invasion and metastasis, evasion of apoptosis and limitless cellular proliferation. These hallmarks were further expanded a decade later with the addition of two further hallmarks: reprogramming of energy metabolism and evading immune destruction (Hanahan & Weinberg 2011). Underlying these hallmarks and driving carcinogenesis is the accumulation of genetic and epigenetic changes which dysregulate cellular signalling. These mutations can be inherited or induced by environmental factors (Cuzick *et al.* 2014).

1.1.2 – Prostate Cancer

Prostate Cancer (PCa) is the leading cause of cancer related death in men in the UK. Each year, approximately 50,000 new cases of PCa are diagnosed and 12,000 patients will die from the disease (Cancer Research UK). Patients with non-aggressive localised PCa often undergo active surveillance or treatments such as surgery or brachytherapy (internal radiation) (Filson *et al.* 2015). The use of such techniques means that 87% of patients survive for five years or longer (Cancer Research UK). Patients with advanced disease are often faced with a malignant and more aggressive cancer. At this stage tumour growth is often dependent on the male sex hormone, androgen, therefore it is treated with antiandrogens, luteinizing hormone-releasing hormone (LHRH) agonists or a combination of both. Both of these treatments target androgen signalling but by different mechanisms: (i) antiandrogens elicit their effect by interacting with and inhibiting the Androgen Receptor (AR) at a protein level therefore preventing activation of the AR transcriptional program, whereas, (ii) LHRHs reduce the amount of circulating androgens within the body by pituitary downregulation therefore reducing activation of the AR (Pine *et al.* 2016). Despite the treatments extending the life expectancy of patients, there are associated side effects: sexual dysfunction, muscle atrophy, osteoporosis, hot flashes, fatigue, gynecomastia or anemia (Rhee *et al.* 2015). Additionally, there are more severe associated side effects such pneumonia, acute kidney injury, increased incidence of diabetes, and cardiovascular morbidity and mortality (Collier *et al.* 2012). Although initially successful for most patients these treatments invariably fail and disease progresses to Castration-Resistant Prostate Cancer (CRPC), which has limited treatment options hence identification of therapeutic molecules is needed.

1.1.3 – Origin of Prostate Cancer

The development of PCa is a sequential process induced by genetic and epigenetic alterations, however, the exact mechanism of initiation is still a matter of debate.

There are a number of inherited mutations which considerably increase the risk of developing PCa and can also determine PCa aggressiveness (Cuzick *et al.* 2014).

For example, whole exome sequencing identified that a single nucleotide polymorphism of the Homeobox B13 (HOXB13) gene increased the susceptibility of developing PCa (Brooke & Bevan 2009). Other factors such as age (Ferlay *et al.* 2010), ethnicity (Perez-Cornago *et al.* 2017) and lifestyle choices (Campi *et al.* 2019) have all been associated with increased PCa risk. Irrelevant of the origin of these genetic mutations, they cooperatively contribute to the development of prostatic intraepithelial neoplasia (PIN). The mutations associated with PIN are principally chromosomal deletions causing loss of function in tumour suppressor genes and thus increased cell proliferation (Gandhi *et al.* 2018). Further accumulation of mutations then drives disease progression and can cause PIN to develop into adenocarcinoma (Packer & Maitland 2016). Continued accumulation of genetic alterations such as gene duplications or gene fusions result in gain of function proteins and overactivation of proliferative pathways which drive disease progression (Gandhi *et al.* 2018). Analysis of patient samples show that multiple distinct mutations occur in advanced stage PCa but infrequently in the early stage disease (Brooke & Bevan 2009). Importantly many of these mutations have been shown to affect AR function (Pine *et al.* 2016). For example, dysregulation of the proliferative pathways mitogen activated protein kinase (MAPK) and phosphoinositide 3 kinase (PI3K) have been shown to activate the AR (Taylor *et al.* 2010). The final and most aggressive stage of PCa is CRPC. Paradoxically this transition occurs due to the

selective pressure caused from androgen deprivation therapy (ADT), cells with acquired pro-oncogenic alterations survive the therapy and proliferate. Many genetic mutations connected with CRPC are associated directly with the AR or with its regulatory signalling molecules (Matsumoto *et al.* 2013). AR ligand binding domain (LBD) mutations around the ligand binding pocket have been shown to reduce specificity of the AR for Dihydrotestosterone (DHT) and allow activation from other molecules such as glucocorticoids or even synthetic antagonists like hydroxyflutamide (Matsumoto *et al.* 2013) (Figure 1.1.3.1). AR gene amplifications which re-sensitize the cell to the low concentrations of circulating androgens during ADT have been identified in 30% of CRPC patients (Katzenwadel & Wolf 2015) (Figure 1.1.3.1). Most recently, AR splice variants have been identified. These variants do not possess a LBD resulting in constitutively active receptor and unregulated AR signalling (Wadosky & Koochekpour 2017) (Figure 1.1.3.1). Like the AR mutations, which allow for non-androgen ligands to activate the AR, dysregulation of co-regulators can also induce this ability. Both AR-associated protein 55 and β -catenin allow the AR to be activated by oestradiol. Dysregulated co-factors can also enable ligand-independent transcription (Figure 1.1.3.1). For example, c-Jun binds to the AR N-terminal domain (NTD) and facilitates post-translational modifications (PTMs), which cause the AR to become transcriptionally active. Similarly, phosphorylation of Steroid receptor co-activator (SRC-1) by MAPKs causes its recruitment to the AR which facilitates ligand-independent transcription (Edwards & Bartlett 2005) (Figure 1.1.3.1).

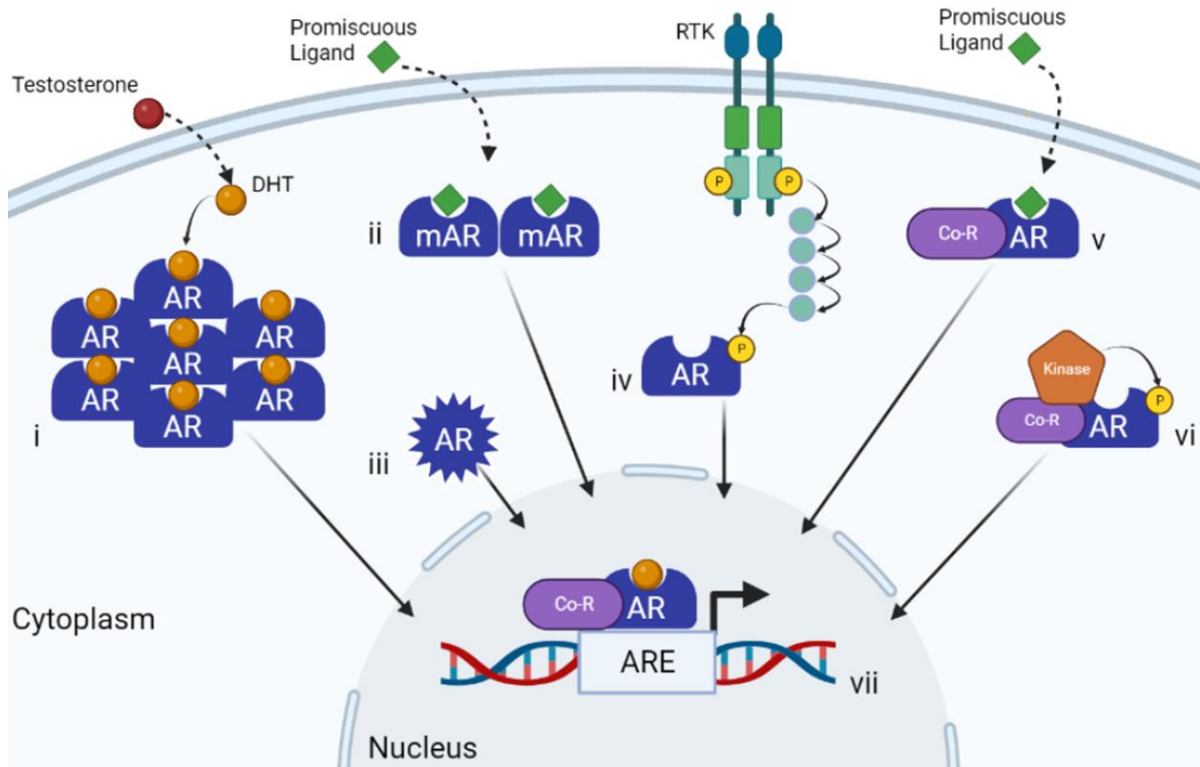


Figure 1.1.3.1 – Schematic representation of contributing mechanisms to prostate cancer progression – AR represents the androgen receptor, mAR represents mutant androgen receptor, RTK represents receptor tyrosine kinase, Co-R represents co-regulator. Dotted lines represent diffusion across the phospholipid bilayer, other lines represent interactions or translocation into the nucleus. i) AR amplification/overexpression sensitizes the cell to low levels of androgens circulating during ADT and ligand dependent transcription. ii) mutations in the AR allow promiscuous activation of the AR and ligand dependent transcription. iii) AR splice variants are constitutively active and for ligand-independent transcription. iv) overactive proliferative pathways can lead to post-translational modifications (PTMs) such as phosphorylations, activating the AR in a ligand independent manner. v) mutations in co-regulators can lead to promiscuous activation of the AR. vi) mutations in co-regulators can lead to altered recruitment of accessory proteins resulting in PTMs of the AR and ligand independent activation.

1.2 – The Androgen Receptor

1.2.1 – Androgen Receptor Expression and Function

The AR is a member of the Steroid Receptor (SR) family, the SRs are widely expressed throughout the body and regulate gene transcription to elicit many physiological functions. The AR functions as a transcription factor that regulates its cognate genes. However, different subsets of genes are transcribed dependent on tissue type and cellular conditions. The AR is primarily expressed in the male and female sexual organs (Dart *et al.* 2013). In males, the AR most significantly regulates the development and maintenance of the sexual reproductive organs, the testes and prostate (Shiraishi & Matsuyama 2017; Verze *et al.* 2016). In females the AR has been shown to contribute to the regulation of folliculogenesis, mammary gland development, and uterine morphology and development (Walters *et al.* 2009). Despite the association of the AR to sexual function (mostly due to being the cognate receptor to the male sex hormone testosterone), the AR is also expressed at secondary sites serving completely different functions. In male non-reproductive organs expressing AR the receptor is important in: bone density (Ting *et al.* 2002), sexual drive and aggression (Sato *et al.* 2004), development of the heart (Ikeda *et al.* 2005), metabolism homeostasis (Rana *et al.* 2011), muscle formation (MacLean *et al.* 2008) and regulation of the haemopoietic immune system (Lai *et al.* 2012).

1.2.2 – Androgen Receptor Structure

The AR has a modular domain structure consisting of the N-terminal domain (NTD), central DNA binding domain (DBD) and a C-terminal ligand binding domain (LBD) (Fig. 1.2.2.1.A). The DBD and LBD are connected by a linker region termed the hinge region. The DBD is composed of a conserved 66 amino acid central core followed immediately by a short unconserved extension into the hinge region. The conformation of the DBD forms two alpha helices and two zinc binding groups. One of the alpha helices is responsible for deoxynucleotide acid (DNA) recognition via the major groove, whilst the second is essential for hetero/homodimerisation (Rastinejad 2001). Additionally, the DBD is responsible for the selectivity of DNA response element binding. Properties like N-terminal flexibility, length of the hinge region and amino acid sequence determines SR positioning on DNA and in turn selectivity. Furthermore, the hinge region stabilises DNA binding by interacting with the minor groove of DNA (Helsen & Claessens 2014). The LBD is composed of a three layered alpha helical structure consisting of 12 α -helices (H1-H12), forming an 'alpha-helical sandwich' (Fig. 1.2.2.1.B). Ligand binding to the LBD causes a conformational change which creates a hydrophobic surface for coregulators to bind thus dictating which co-regulators will be recruited thus the transcriptional activity of the AR (Greschik *et al.* 2002). There are also additional regulatory regions within the AR, Activation Function 1 (AF1) and Activation Function 2 (AF2) (Fig. 1.2.2.1.A). AF1 is located in the flexible NTD meaning there are no crystal structures available for analysis into the structure-function relationship, however, the AF-1 is known to influence recruitment of co-regulators to the AR. AF2 is located in the LBD which has been structurally determined, analysis of the structure has revealed that there are key AF-2 helices in the domain, H1, H3, H5 and H12 (Figure 1.2.2.1.B) (Estébanez-

Perpiñá *et al.* 2007). AF-2 also determines AF1 activity by recruiting co-regulators which facilitate full transcriptional activity (Yu *et al.* 2020).

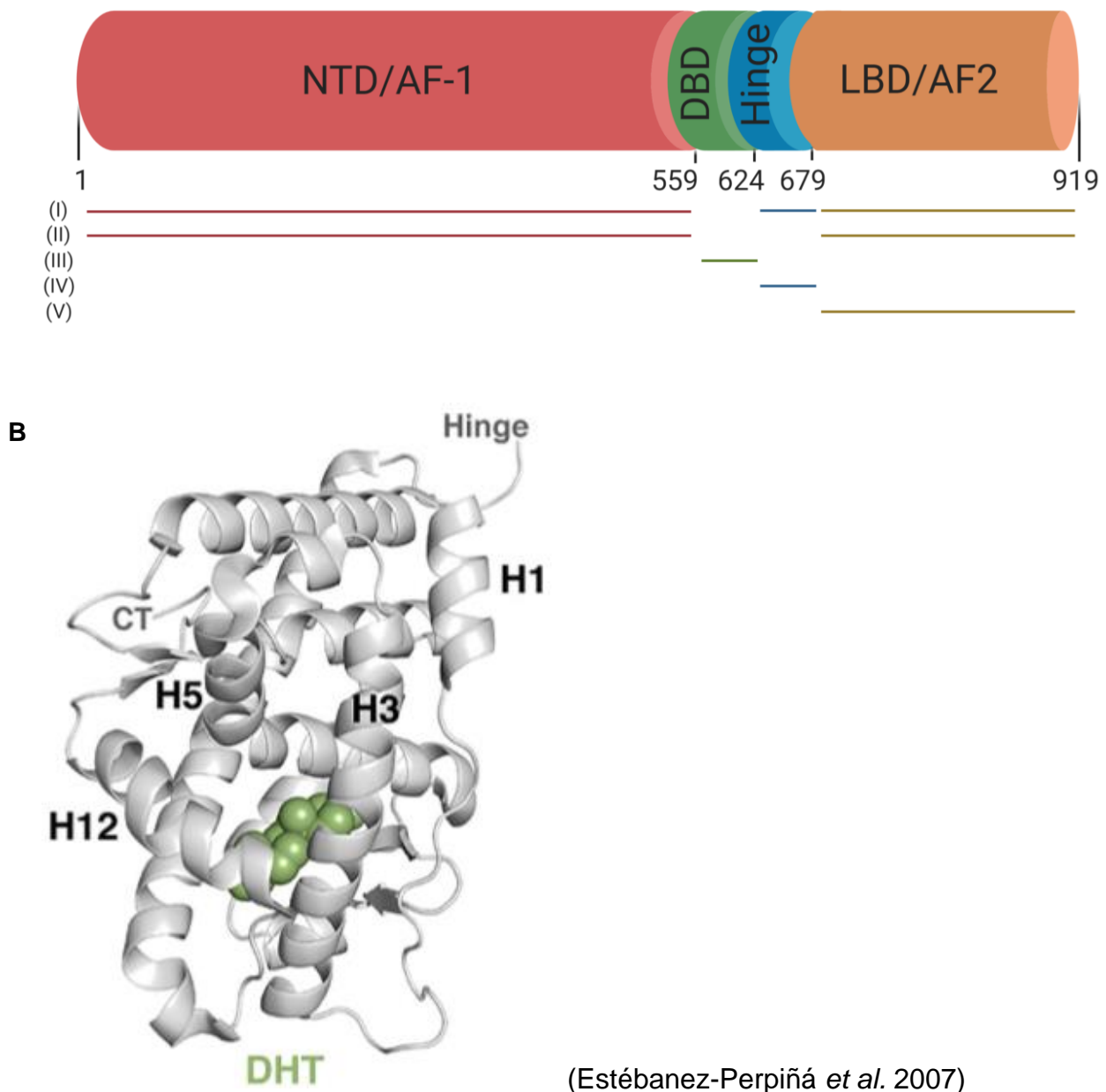


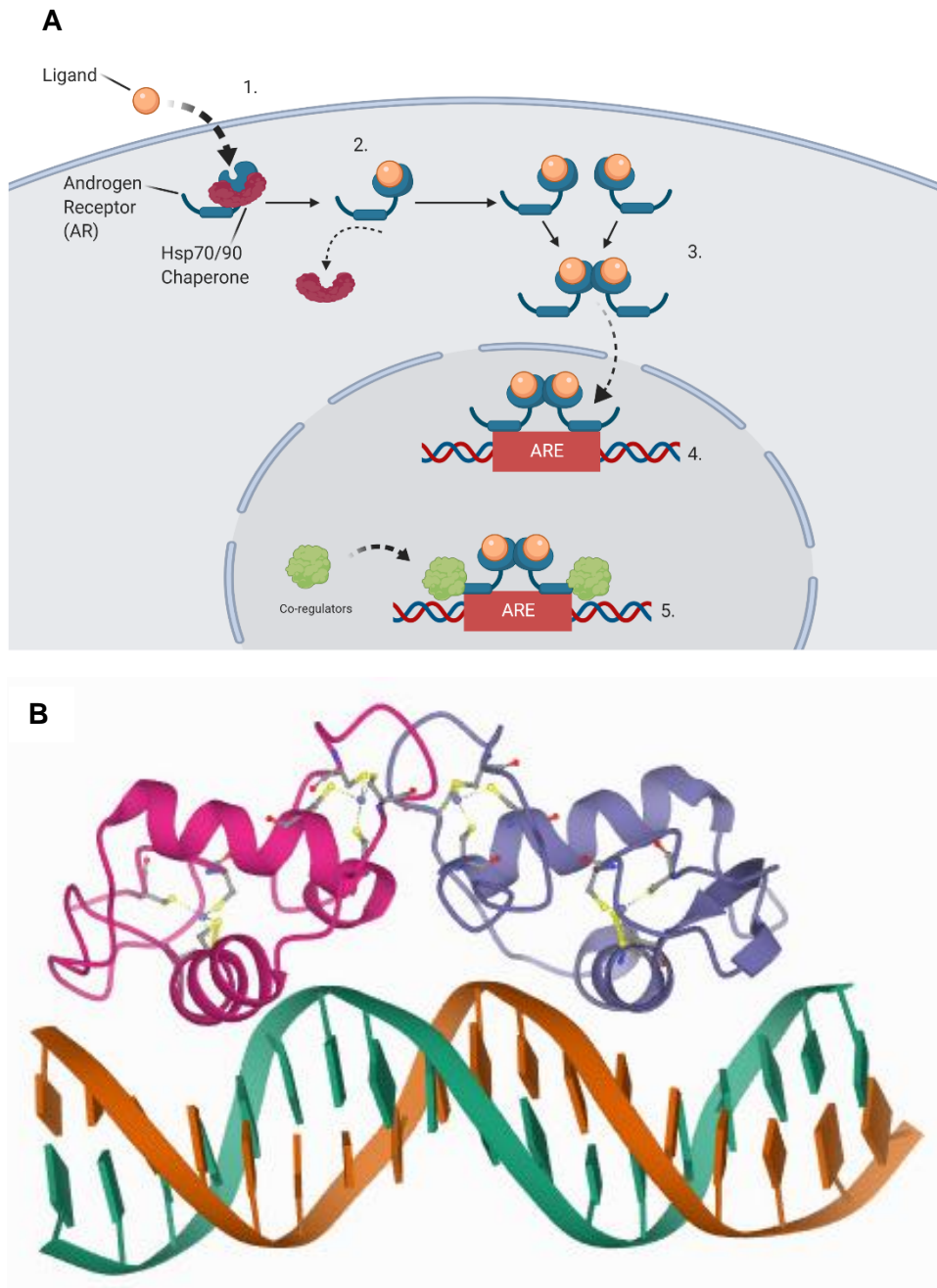
Figure 1.2.2.1 – Representations of Androgen Receptor Domains and Structure.

A) Schematic representation of the Androgen Receptor with its domains – The AR consists of an N-terminal Domain/Activation Function-1 (NTD/AF-1), DNA binding Domain (DBD), Hinge region and Ligand binding domain/Activation Function-2 (LBD/AF-2). Horizontal lines depict AR domains involved in (i) dimerization, (ii) transactivation and binding of coregulators, (iii) DNA binding, (iv) nuclear localization and (v) ligand binding. **B) Crystal Structure of the AR Ligand Binding Domain (2PIU)** – Ribbon representation of AR LBD highlighting the key helices of AF-2 when bound to small molecule DHT which is colored green, the hinge and C-terminal end of the protein (CT) are also labelled.

1.2.3 – Androgen Receptor Activation

In the absence of ligand, the AR is inactive and bound to chaperones (e.g. the heat shock proteins Hsp70 and Hsp90) in the cytoplasm which stabilize its structure and prevents its degradation (Fig. 1.2.3.1.A) (Dong *et al.* 2019). Testosterone passively diffuses through the phospholipid bilayer into the cytoplasm, upon where, 5- α -reductase converts it into DHT (van Royen *et al.* 2012). DHT then binds to the AR causing an allosteric change. The allosteric change occurs via the H12 α -helix, switching from a previous dynamic state to a fixed position closing the ligand binding pocket and further stabilizing the ligand (Nagy & Schwabe 2004). Furthermore, this stabilization of the AR causes the heat shock proteins to dissociate and promotes formation of homodimers (van Royen *et al.* 2012). It was shown by Yu *et al.* (2020) that surfaces of the LBD, DBD and NTD are involved in dimerization. The AR-Ligand complex translocates into the nucleus where it interacts with DNA androgen response elements (AREs). Once in proximity of DNA one of the zinc-finger like modules of the DBD interacts with the major groove of DNA. This is the recognition helix which interacts with AREs via specific DNA half sites (Schwabe *et al.* 1993). The half sites are found by utilising a series of hydrophilic residues which read the DNA sequence until recognition of the specific ARE (Fig.1.2.3.1.B) Homodimers increase selectivity of response elements due to varied orientation and space between half sites among the SRs (Roemer *et al.* 2006). Once bound to DNA the AR recruits co-regulators such as steroid receptor coactivator 1 (SRC-1) and basal transcriptional machinery, RNA polymerase II, to initiate gene expression (Tan *et al.* 2015). The positioning of H12 helix facilitates the AF-2 function and allows co-activators to interact with the newly formed coactivator interaction groove (Rastinejad *et al.* 2013). Co-regulators interact with this groove via LXXLL (L represents leucine

and X represents any amino acid) motifs. The LXXLL motifs interact with the AR via a hydrophobic cleft formed from H3, H4 and H12 helices. (Gronemeyer *et al.* 2004). Co-regulators often possess the ability to modify histones which in turn alter the local charge and cause changes in the structure of chromatin, for example, histone acetylases such as SRC-1 introduce acetyl modifications which relax the structure of chromatin and promote transcription whilst histone deacetylases act in the opposite fashion (Culig & Santer 2012). Beyond this AR activity can be modulated by PTMs such as phosphorylation or acetylation.



(Shaffer *et al.* 2004)

Figure 1.2.3.1 – The Androgen Receptor Signalling Pathway.

A) Schematic representation of Androgen Signalling – (1) Ligand diffuses across bilayer and binds to the AR. (2) Ligand binding causes a conformational change and dissociation of the Hsp complex. (3) Activated AR monomers homodimerize and translocate to the nucleus. (4) AR dimer binds to AREs located in the regulatory regions of target genes. (5) Co-regulators bind to receptor and promote target gene transcription. **B) – Crystal structure of AR bound to Androgen Response Element (1R4I)** – DNA can be visualised with green and orange whilst the AR monomers of the AR homodimer can be seen via pink and purple.

1.2.4 – Androgen Receptor Post Translational Modifications

AR activity can be modulated by several different PTMs, i.e. acetylation, SUMOylation, methylation, ubiquitination, phosphorylation. (i) Acetylation of the AR occurs within the hinge region. Addition of an acetyl group results an increase in transcriptional activity and cell growth (Anbalagan *et al.* 2012). It has been shown in response to the Androgen, DHT, acetylation increases AR transcriptional activity by enhancing binding with its co-regulator histone acetyltransferase p300 (p300)/ cAMP response element-binding protein (CREB) binding protein (CBP) (Fu *et al.* 2003). Interestingly, p300/CBP and other well established AR co-regulators have been shown to directly acetylate the AR (Anbalagan *et al.* 2012). (ii) SUMOylation is the covalent attachment of a small amino acid chain. The AR can be sumoylated on two sites Lys 386 and Lys 520 in response to androgen treatment. Interestingly, these sumoylation sites were shown to have opposing regulative control of AR activity. Sumoylation of K386 reduces AR transcriptional activity whereas sumoylation of K520 on its own or in conjunction with K386 enhances transcriptional activity (Kaikkonen *et al.* 2009). (iii) There is one methylation site on the AR, but the exact position of this PTM is debated across literature. Gaughan *et al.* (2011) state that the methylation is on Lys 632 whereas Ko *et al.* (2011) state that it occurs on Lys 630. Despite this contrast, both data agree that the AR was methylated by the methyltransferase SET9 and this enhances AR transcriptional activity by facilitating N-C terminal interactions. This methylation induced conformational change promotes association to androgen target genes and enhanced target gene expression (Gaughan *et al.* 2011; Ko *et al.* 2011). (iv) Ubiquitination of the AR lead to degradation via the proteasome pathway. A constant cycle of protein synthesis and degradation exists to tightly regulate the AR transcriptional program (Faus &

Haendler 2006). (v) The most significant PTM of the AR is phosphorylation. The AR has several phosphorylation sites within the protein which spans all domains of the protein, most of which have been experimentally validated to alter AR transcriptional activity by facilitating interactions with co-regulators and other molecules. The NTD can be highly phosphorylated with the majority being inside AF1; S16, S81, S94, S213, Y223, S256, Y267, T282, S293, S308, Y363, S424, S515 and Y534. There are also additional phosphorylations within the DBD at S578, the hinge region at S650 and the LBD at S791, Y850 (Koryakina *et al.* 2014) (Figure 1.2.4.1). The most frequent phosphorylation of the AR is on S81. This phosphorylation is amplified in response to androgenic stimulation of the AR and is primarily phosphorylated by cyclin dependent kinase (CDK) 1/5/9, which stabilises the AR causing protein levels to rise and increases its transcriptional activity (Gordon *et al.* 2010). More kinases have been identified to phosphorylate the AR and influence its transcriptional program (Wen *et al.* 2020). Among these kinases the p90 Ribosomal S6 Kinase (RSK) family is of particular interest as they have been shown to influence a range of essential cellular processes in healthy and cancerous cells. Despite initial studies by Clark *et al.* 2005 linking RSK1 to AR activation and disease progression (Clark *et al.* 2005), limited data are currently available for the role the whole RSK family has in PCa.

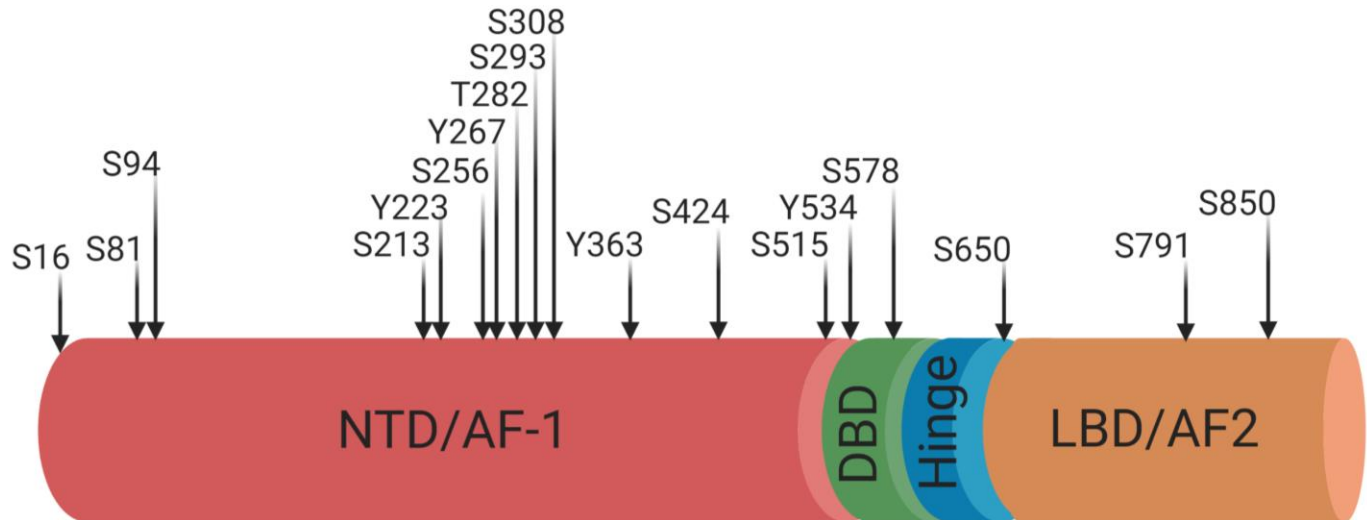


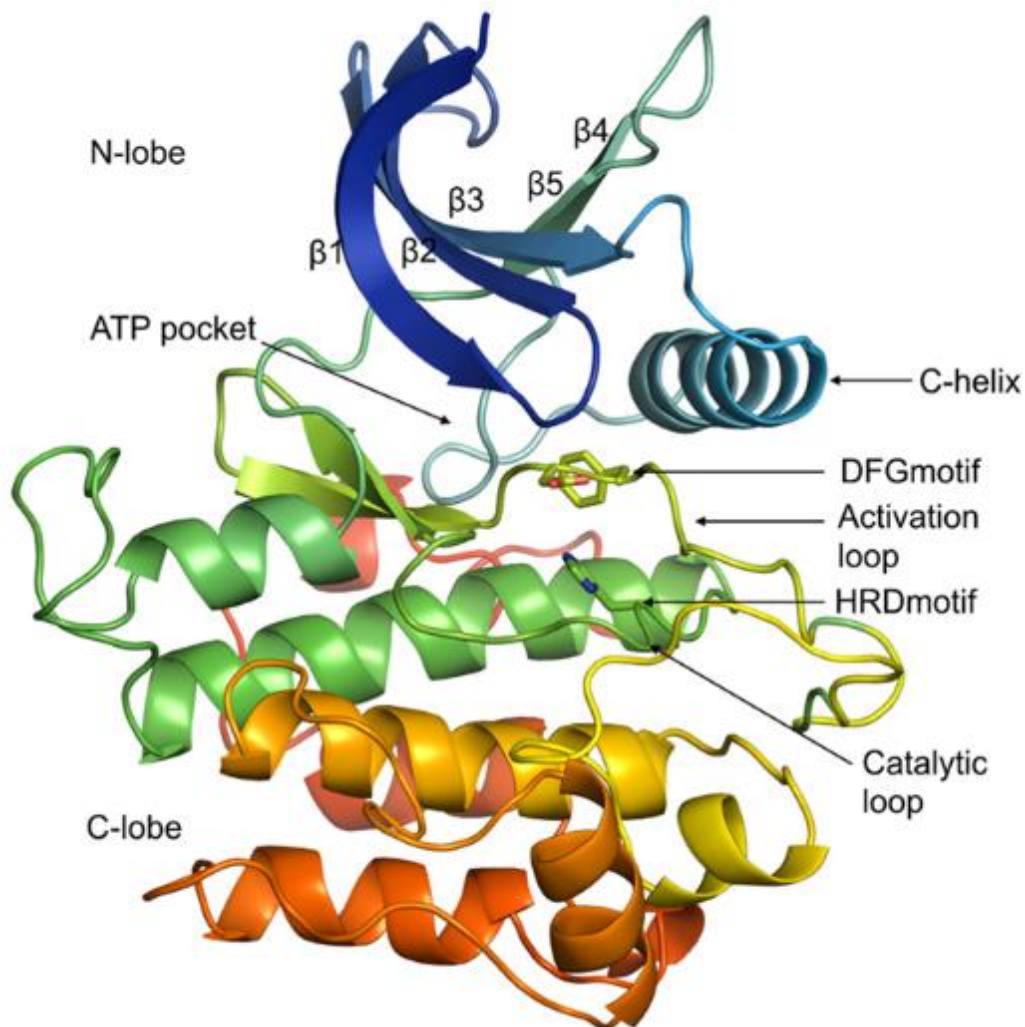
Figure 1.2.4.1 – Schematic representation of AR domain structure and phosphorylation sites - The AR consists of an N-terminal Domain/Activation Function-1 (NTD/AF-1), DNA binding Domain (DBD), Hinge region and Ligand binding domain/Activation Function-2 (LBD/AF-2). Phosphorylation sites are highlighted with black arrows with corresponding residue numbers.

1.3 – The Ribosomal S6 Kinases

1.3.1 – Protein Kinases

Kinases are responsible for transmitting cellular signals which result in a molecular effect. These proteins are essential in many processes, 538 human kinases have been identified which constitutes about 1.7% of all human genes, interestingly this remains a similar proportion across most eukaryotes independent of genome size (Fabbro *et al.* 2015; Manning *et al.* 2002). Kinases can then be split into two main categories serine/threonine kinases or tyrosine kinases, with regards to which amino acid they phosphorylate (Endicott *et al.* 2012). All kinases share a common catalytic domain comprised of two lobes. The N-terminal lobe is composed of five β -sheets and a single α -helix (C-helix). The N-lobe contains the conserved Gly-rich loop (G-loop) which is present between β 1 and β 2 strands, this motif is important in coordinating adenosine triphosphate (ATP) (Kornev *et al.* 2006). The C-terminus of the C-helix extends into the hinge region and is anchored by the C-lobe whereas the N-terminus of the C-helix interacts with the activation loop. Correct positioning of the N-terminus of C-helix is essential for catalysis to allow interaction between the active Lys of the AXK-motif in β 3 and the Glu of the C-helix to form a critical salt bridge which in turn allows the Glu to interact with ATP (Fabbro *et al.* 2015). The C-lobe is the larger of the two catalytic core domains and is comprised of mostly α -helices and four β -sheets. β 6 and β 7 contain the very important catalytic loop which contains the Y/HRD motif; the Asp of this motif is responsible for orientating the hydroxyl acceptor of the substrate peptide; the Tyr/His of this motif forms hydrophobic contacts with the Phe of the DFG-motif. The activation loop is present in β 9 and extends from the DFG motif. The DFG motif is responsible for positioning the Asp of the Y/HRD motif in the

catalytic loop. Additionally the Asp of this motif binds Mg^{2+} which is essential for coordinating the β and γ phosphates of ATP (Goldsmith *et al.* 2007).



(Modi & Dunbrack 2019)

Figure 1.3.1.1 – Structure of common kinase catalytic core – Crystal structure of ISNR kinase, PDB 1GAG. The N-lobe is comprised of mostly β -sheets and extends into the C-helix. The C-lobe is comprised of mostly α -helices. The C-helix stabilizes the activation loop orientation, in turn allowing the DFG motif of the activation loop and the HRD motif of the catalytic loop to interact creating a favourable orientation for catalysis. The change in colours represent transition into a new distinct region of secondary structure.

The motifs of each lobe possess specific essential functions for kinase catalysis however the kinase conformational changes can also be categorized into spines during transition from active to inactive state. There are two spines which span both lobes of the core; the catalytic spine (C-spine) and the regulatory spine (R-spine). The R-spine contains two residues from the C-lobe and two residues from the N-lobe. The residues from the C-lobe are: (i) from the Y/HRD motif in the catalytic loop (RS1) and (ii) from the DFG motif in the activation loop (RS2). The residues from the N-lobe are: (i) from the C-helix (RS3) and (ii) from the β 4 strand. The R-spine is anchored to the α F-helix through a conserved aspartate. A 'shell' of hydrophobic residues (two from the C-helix- β 4 loop and one from β 5) support the spine (Meharena *et al.* 2013). When the R-spine is formed the state of the kinase changes from open to intermediate, this normally occurs via phosphorylation of the activation loop. Binding of ATP promotes the transition of the kinase from intermediate to closed (inactive to active) and the formation of the C-spine. Finally the binding of substrate allows final transition from intermediate to closed conformation (Meharena *et al.* 2016).

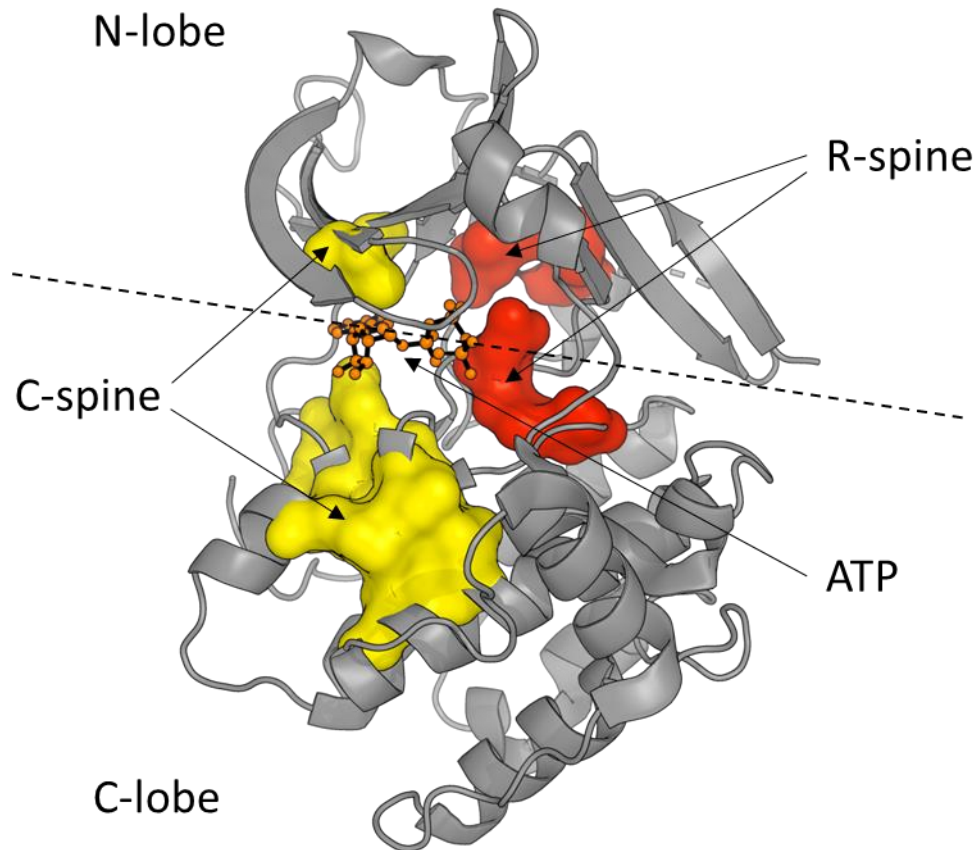


Figure 1.3.1.2 - Hydrophobic spines define the internal architecture of RSK4 - Two hydrophobic spines, the regulatory-spine (R-spine) and the catalytic-spine (C-spine), span across both lobes of the kinase core and provide a firm but flexible connection between the two lobes. The regulatory spine (red filled globular space) moves the kinase into an intermediate but inactive state most often due to a phosphorylation event. The catalytic spine (yellow filled globular space) is completely formed after the binding of ATP and promotes formation of an active state which occurs when interaction with substrate occurs. The dashed line across the picture depicts the two different lobes of the kinase core.

The overall purpose of these conserved motifs and spines is to position both the kinase and its substrate in the correct orientation for γ -phosphate transfer from ATP to the hydroxyl acceptor of a serine/threonine or tyrosine (Figure 1.3.1.1). The transfer occurs when the nucleophilic attacking group (OH) comes into proximity with the leaving group (phosphate ester oxygen). Here the Mg^{2+} positive charge stabilizes the significant amount of negative charge which develops from the bridging oxygen (Endicott *et al.* 2012). The chemical intermediate of this reaction could occur in two ways, however, there is data to support a dissociative mechanism by where the bond to the leaving group breaks before the bond by the attacking group is made. The reaction is catalysed by aspartate through base catalysis and the transfer of proton occurs by acid catalysis. The rate limiting step of this reaction is the release of products (adenosine diphosphate and phosphorylated protein) (Endicott *et al.* 2012).

Although all kinases share the same catalytic core and mechanism the regions outside of this vary considerably leading to the formation of kinase super families based on primary sequence identity: RTK (Receptor tyrosine kinase), TKL (Tyrosine kinase-like), STE (yeast sterile kinase homologs), CK1 (Casein Kinase 1 kinase), CMGC (CDK, MAPK, GSK, CLK kinases), CAMK (Calcium/Calmodulin-dependent kinases) and AGC (PKA/PKG/PKC kinases). However, not all kinases fit into these classifications and a small proportion of kinases are classified as 'Other' (Manning *et al.* 2002). Of particular interest are the AGC and the CAMK families as uniquely the RSKs possess two distinct kinase domains. Both the AGC kinases and CAMKs follow the generic catalytic core structure but have some definitive features associated with each family. The key AGC kinase features are the Hydrophobic Motif (HM) and the Turn Motif (TM). The HM is located on the C-terminal tail which

extends from the C-lobe and wraps around the N-lobe to interact with the hydrophobic pocket, this in turn stabilises the active conformation of the C-helix. The TM is also located on the C-terminal tail but precedes the HM. The TM assists the C-helix in wrapping around the N-lobe and in turn promotes correct positioning of the HM at the HM pocket (Pearce *et al.* 2010). Key features of the CAMKs are the autoinhibitory helix which is present in the N-lobe, a Ca^{2+} /calmodulin binding site and a C-terminal oligomerisation domain. The autoinhibitory domain regulates the activity of the kinase by stabilising the inactive conformation of the protein and preventing substrate from binding in the substrate binding pocket thus preventing its kinase activity. When Ca^{2+} /Calmodulin binds to the protein it displaces the autoinhibitory domain and opens the catalytic site and allows for subsequent phosphorylation of substrate (Sakkiah *et al.* 2017). The C-terminal oligomerisation domain is responsible for organising large oligomers which are paramount in signal transduction and regulation of protein activity (Rellos *et al.* 2010).

1.3.2 – RSK Structure

The ribosomal S6 kinase (RSK) family is composed of four isoforms, RSK1/2/3/4. The RSKs are a unique family of kinase containing two distinct kinase domains in the same polypeptide chain. This originated from an ancestral gene fusion event and not a gene duplication event since the N-Terminal Kinase Domain (NTKD) belongs to the AGC kinase family whereas the C-Terminal Kinase Domain (CTKD) belongs to the CAMK family (Jones *et al.* 1988). The isoforms share a high level of sequence similarity in their two catalytic domains, while there is reduced conservation in the N- and C-termini. The NTKD and CTKD are connected by a linker region which contains the TM and HM which are essential for AGC regulation (Yang *et al.* 2002b). The C-terminus contains two further regulatory regions the ERK D-domain (D-d) which is the docking site for ERK and the autoinhibitory domain which regulates the CAMK domain by interacting with the D-d to reduce affinity for ERK (Lara *et al.* 2013) (Figure 1.3.2.1). Interestingly the RSKs have been shown to have an abnormal NTKD than that of other kinases explained in chapter 1.3.1. The NTKD of RSK2 was shown to have a displaced C-helix and subsequently, the well-established salt bridge between the β 3 strand and the C-helix does not occur. This occurs due an extra β -sheet in the N-lobe, the β B-sheet. This β B-sheet replaces the C-helix's function of stabilising the N-lobe in active conformation (Malakhova *et al.* 2009). The C-terminus follows the general bilobed kinase fold however due to its CAMK nature it exhibits an autoinhibitory function. This arises from the positioning of an inhibitory α -helix (α L). α L causes a change in the orientation of the Glu from the C-helix which in turn causes the formation of an ionic pair with a Lys and prevents Glu from binding ATP in RSK2. Interestingly despite high sequence identity this does not occur in RSK1 (Li *et al.* 2012). The α L in RSK1 is fixed by ionic interaction and hydrogen bonding in the

substrate binding groove acting a pseudo-substrate subsequently preventing substrate binding. Furthermore, the inhibition of substrate binding caused a reduced binding affinity to ATP thus favouring the inactive state (Li *et al.* 2012). This autoinhibitory function is directly linked to the binding of ERK to RSK. RSK and ERK form a complex preceding phosphorylation when both proteins are in the inactive state. Through the use of kinetic studies it was shown that the linear motif of RSK causes a transition from disordered to ordered structure when ERK binds. Crystal structure analysis showed that the activation loop of the RSK CTKD was positioned in the catalytic site of ERK awaiting phosphorylation (Alexa *et al.* 2015). The proteins associate through two interfaces, interface 1 (IF1) utilises a series of hydrogen bonds, salt bridges and Van de Waal interactions whereas interface 2 (IF2) follows the generic kinase features mentioned in chapter 1.3.1 for example the essential Glu of the C-helix positioned to interact with ATP. Molecular dynamic simulations suggested that the IF1 contacts are had limited molecular movement thus it was suggested that this interface acts as the docking groove whereas IF2 was dynamic which allows for readjustments for optimal surface interactions. The major contact between the two proteins of the IF2 was between the APE motif of RSK and the P loop of ERK, which creates a pivoting point to allow IF2 adjustments. Following phosphorylation of ERK complete alignment occur allowing activation of RSK (Alexa *et al.* 2015).

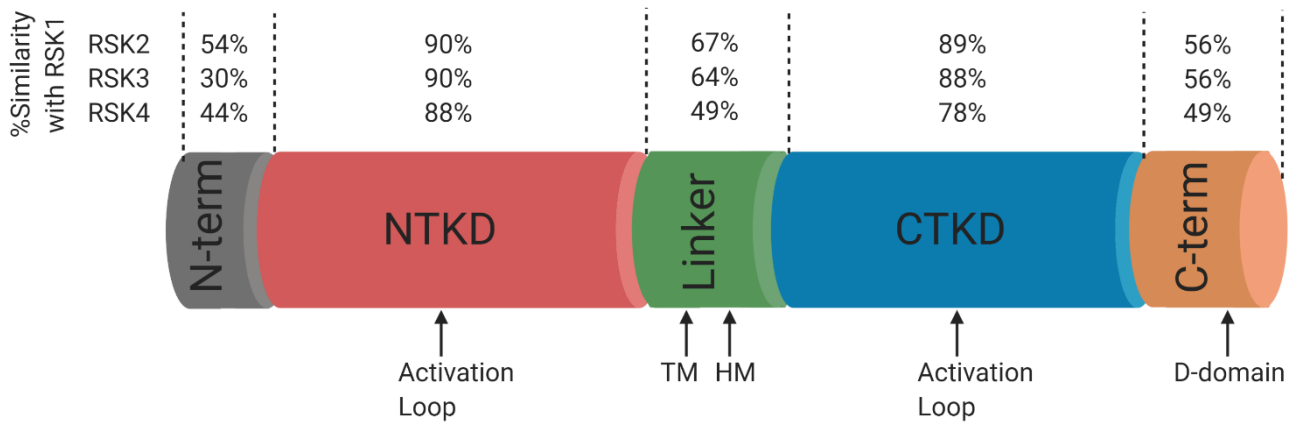


Figure 1.3.2.1 – Schematic representation of the RSKs domain structure –

Percentage sequence similarity of the RSK1 and RSK2/3/4 domains: N-terminal region (N-term), N-terminal kinase domain (NTKD); linker region (Linker); C-terminal kinase domain (CTKD) and the Cterminus (C-term). Motifs are highlighted in the structure with black arrows: Activation loop(s); Hydrophobic Motif (HM); Turn Motif (TM); ERK Docking Domain (D-domain).

1.3.3 – RSK activation

The RSKs are the downstream effectors of the MAPK pathway therefore in healthy cells the RSKs are activated in response to a tightly regulated stimulus. Extracellular RTK stimulation by growth factors or hormones leads to the dimerization of their cytoplasmic domains and autophosphorylation occurs (Hilger *et al.* 2002). The phosphorylated tyrosines present on the RTK are recognised by Growth-factor-receptor-bound-protein 2 (Grb2) which in turn recruits Sons Of Sevenless (SOS). SOS is a guanine exchange factor which causes the Guanosine diphosphate/Guanosine triphosphate (GDP/GTP) exchange in membrane bound Ras which causes a conformation change into its active conformation (Hilger *et al.* 2002). Active Ras then recruits the MAPK Raf to the cell membrane and activates the protein. Raf then phosphorylates two serine residues on the kinase mitogen-activated protein kinase kinase 1/2 (MEK1/2) which in turn phosphorylates ERK1/2 (Kolch 2000). Phosphorylated ERK1/2 binding to the RSKs then initiates the sequential phosphorylation mechanism of the RSKs. ERK1/2 dock onto the D-d and phosphorylate the CTKD on the activation loop (Dümmeler *et al.* 2005). This enables the catalytic activity of the CTKD which in turn phosphorylates the HM. This creates the Phosphoinositide-dependent kinase-1 (PDK1) docking site within the PDK1 Interacting Fragment (PIF), which is most likely caused by conformational changes as a result of the phosphorylations (Frödin *et al.* 2000). ERK then phosphorylates two further residues in the TM which stabilises HM interactions and facilitates further C-terminal conformational changes. The binding of PDK1 to RSKs' PIF induces PDK1 catalytic activity, which results in the phosphorylation of the NTKD activation loop (Pearce *et al.* 2010). PDK1 then dissociates leaving the RSK fully catalytically active. Interestingly, data has shown that RSK4 is activated independently of PDK1

since inhibition of PDK1 did not halt RSK4 activity (Dümmmler *et al.* 2005). Recently it has been suggested through the use of crystal structures and docking simulations that in the absence of PDK1 the HM of RSK4 invoking autophosphorylation of the NTKD activation loop (Chrysostomou *et al.* 2021). The NTKD auto-phosphorylates the autoinhibitory domain reducing the affinity to ERK1/2 and producing a negative feedback loop for RSK activation (Figure 1.3.3.1). This is not present in RSK3 which could be linked to its longer ERK1/2 binding. The RSKs are inactivated by removal of these phosphorylations by phosphatases (Romeo *et al.* 2012; Roux *et al.* 2003) (Figure 1.3.3.1). Active RSKs can then phosphorylate a wide range of substrates (Anjum & Blenis 2008; Romeo *et al.* 2013). In an early attempt to identify substrate specificity, Philip Cohen's group, using a library of peptides related to the N-terminus of glycogen synthase, showed that RSKs preferentially phosphorylate S residues over T and target substrates containing a consensus motif RXRXXpS or RRXpS (Leighton *et al.* 1995; Stokoe *et al.* 1993). More recently, Roux and coworkers suggested that RSKs preferentially phosphorylate substrates containing the RXRXXpS sequence, highlighting the requirement for R residues at position -5 and -3 (Cargnello & Roux 2011). Analysis of consensus sequences recognized by individual protein kinases reveals high level of similarities among basophilic kinases, which includes the majority of known Ser/Thr protein kinases (Pinna & Ruzzene 1996). This is in line with earlier evidence showing that some AGC kinases can redundantly phosphorylate overlapping sites on substrates, further complicating the assignment of a specific substrate to a kinase within a signalling pathway (Manning & Cantley 2007; Mendoza *et al.* 2011). Indeed, several RSKs substrates can also be targeted by p70 ribosomal S6 kinase (S6K), Protein Kinase B (Akt), Protein Kinase A (PKA) and serum- and glucocorticoid-induced protein kinase (SGK) (Manning &

Cantley 2007; Mendoza *et al.* 2011). While RSKs, and kinases in general, preferentially phosphorylate residues within the consensus motif, recent structural and biochemical studies have shown that substrate recognition can be driven by docking interactions with regions distant from the phosphorylation and the kinase catalytic sites. It has also been shown that temporally and spatially regulated complex interactions are required for substrate phosphorylation *in vivo* (Miller & Turk 2018). This is in line with evidence suggesting that RSK-isoform specific features (Romeo *et al.* 2012; Sulzmaier & Ramos 2013) and substrate recognition (Gógl *et al.* 2018) may be driven by the non-conserved N- and/or C-terminus, which are far from the kinase catalytic pocket.

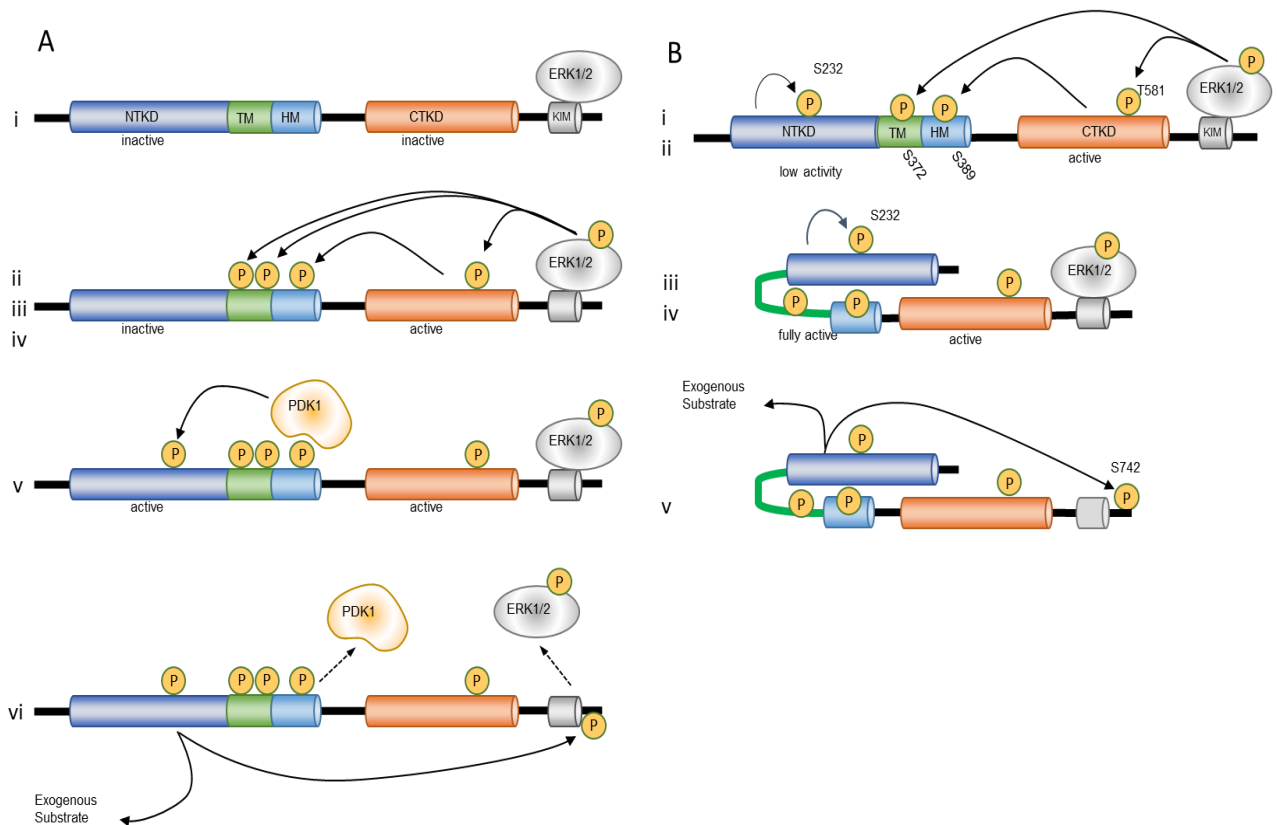


Figure 1.3.3.1 – Schematic representation of the RSK phosphorylation mechanism - **A) RSK1-3 activation mechanism:** (i) ERK is bound to the conserved D-d region at the C-terminus of RSK; (ii) active ERK phosphorylates the activation loop of the RSK-CTKD; (iii) active RSK-CTKD phosphorylates the HM; (iv) ERK or RSK-CTKD (still unclear) phosphorylates TM; (v) PDK1 binds on the phosphorylated HM and phosphorylates the activation loop; (vi) PDK1 dissociates and active RSK-NTKD phosphorylates substrates and itself near the D-d causing ERK dissociation. **B) RSK4 activation mechanism:** - (i) ERK is bound to the conserved D-d region at the C-terminus of RSK4; (ii) active ERK phosphorylates T581 on the activation loop of the RSK-CTKD (that activates RSK4-CTKD) and S372; (ii) RSK4-CTKD phosphorylates in turn S389; (iii) binding of the phosphorylated HM on the phosphate-binding pocket increase NTKD auto-phosphorylation activity; (iv) NTKD gets phosphorylated on S232 and is then able to phosphorylate substrates. (v) NTKD phosphorylates the D-d causing ERK dissociation.

1.4 – The role of the RSKs in Prostate Cancer signalling

The RSKs are the most downstream effectors of the MAPK pathway. The activation of these proteins allows phosphorylation of a range of substrates, for example glycogen synthase kinase 3, which leads to changes in several cellular processes. RSKs were initially discovered for their ability to phosphorylate the Ribosomal Protein S6 (RPS6), a component of the ribosomal 40S subunit (Erikson & Maller 1986). The discovery of the S6K1/2 two years later raised questions to which kinases primarily phosphorylate RPS6 kinase. Interestingly, in human the S6Ks phosphorylate RPS6 on four clustered Ser residues at the C-terminus of the protein (Ser235, Ser236, Ser240 and Ser244), while the RSKs phosphorylate only two (Ser235 and Ser236) (Roux *et al.* 2007). The difference between these two sets of phosphorylations remains elusive, but it has been speculated to have a role in fine-tuning cellular response to different growth signals (Roux *et al.* 2007). In addition to this the RSKs have been shown to have roles in cell proliferation, cell cycle regulation, cell motility and therapy resistance which was comprehensively reviewed by Cronin *et al.* 2021. In particular the RSKs regulate gene expression through either a direct or indirect manner, for example, RSK has been shown to regulate 228 genes in kidney epithelial cells (Doehn *et al.* 2009). RSK1/2 have been considered the prototypical RSKs and RSK3/4 have been largely neglected. This is particularly relevant in PCa, where, despite initial evidence linking RSKs to disease progression, there are no studies investigating RSK3/4 roles in PCa.

1.4.1 – The role of RSKs in Prostate Cancer Proliferation

Clark *et al.* (2005) described one of the first studies to show RSK regulation of PCa. They highlighted that RSK2 regulates proliferation in the PCa cell lines LNCaP and PC3. Analysis of PCa patient biopsies showed elevated protein levels of RSK1/2 by 2.5-3.5 fold than that of normal prostate tissue (Clark *et al.* 2005). Furthermore, overexpression and hyperactivation of RSK2 caused an increase in Prostate Specific Antigen (PSA) in LNCaP. Elevated levels of PSA have a strong correlation with PCa progression and measuring the concentration of PSA in the blood has been used in diagnosis and treatment decision making for many years (Jakobsen *et al.* 2016). RSK2 was shown to indirectly increase the expression of PSA via regulation of the AR transcriptional program via regulation of the AR co-regulator p300/CBP (Clark *et al.* 2005). Interestingly, the RSKs have been shown to bind to the CH3 domain of p300 and antagonistically regulate transcription of CREB (Chan & La Thangue 2001). In a similar mechanism but converse manner RSK2 binding to p300 was shown to agonistically regulate the AR transcriptional program, increasing PSA expression 5-fold. This was further validated by using a known p300 binding partner, E1A a viral oncoprotein, which competes for association with p300/CBP against RSK2. Co-transfection of LNCaP cells with E1A, RSK2 and p300 reduced PSA expression 2- to 3-fold than when the cells were transfected with only RSK2 and p300 (Clark *et al.* 2005). Debate as to whether the RSKs directly co-regulate or phosphorylate the AR. (Figure 1.4.2.1).

RSK1 was also shown to regulate cell proliferation in PCa by promoting cell survival and inhibiting apoptosis. Initial analysis of PCa patient samples showed that RSKs

were highly phosphorylated and localized to the nucleus of bone metastases which is not present in other stages of PCa progression. Overexpression of constitutively activated RSK1 in PCa cell line C4-2B, injected into femurs of mice models, enhanced tumour growth and increased cell survival (Yu *et al.* 2015). Concurrently, knockdown of RSK1, and to a lesser extent RSK2, caused a reduction in osteolytic lesions in PC3 cells injected into mouse femurs. Interestingly this challenges the research from Clark *et al.* (2005) which showed inhibition of RSKs using SL0101 significantly reduced proliferation in LNCaP and PC3 cells, whereas Yu *et al.* (2015) showed overexpression of RSK1 in C4-2B and knockdown of RSK1 in PC3 cells increased and decreased anchorage-independent growth respectively. Yu *et al.* (2015) highlighted that RSK1 elicited these effects by causing a reduction of p38 MAPK and c-Jun N-terminal Kinase (JNK) phosphorylation, reducing the expression of both Inhibitor-of-Growth protein 3 (ING3) and Cytoskeleton-Associated Protein 2 (CKAP2) and increasing the expression of protein tyrosine kinase 6 (PTK6) (Jin *et al.* 2013). Previous studies have presented similar outcomes, RSK2 inactivates Apoptosis Signal-regulating Kinase 1 (ASK1) by phosphorylating it on T1109 and T1326. This inhibits ASK1 phosphorylation of Mitogen-Activated Protein Kinase Kinase 4/7 (MKK4/MKK7) and MKK3/MKK6 and in turn inhibits the activation of JNK and p38 MAPK resulting in inhibition of apoptosis (Jin *et al.* 2013). JNK and p38 activate apoptosis by promoting increased expression of the proapoptotic protein BAX, Cytochrome C, increased activity of caspase 3 and reduced expression of anti-apoptotic protein B-Cell Lymphoma 2 (BCL-2) (Joo & Yoo 2009). The pro-metastatic function of RSK1 in PCa was also linked to the activation of an RSK-dependent transcriptional programme. Overexpression of RSK1 in C4-2B4 caused a moderate reduction of ING3 and CKAP2 mRNA levels (65% and 80% respectively), and a

significant (~40 fold) increase in PTK6 mRNA levels (Yu *et al.* 2015). This is linked to the ability of RSK1/2 to directly phosphoregulate CREB, causing changes in expression of its transcriptional targets in metastatic Cancers (Jin *et al.* 2013; Yu *et al.* 2015). PTK6 is a kinase that is expressed in various epithelia and is commonly found overexpressed in PCa (Zheng *et al.* 2012). While PTK6 is localized in the nucleus of healthy cells, it accumulates in the cytoplasm and cell membrane in PCa, where it positively contributes to Epithelial–mesenchymal transition (EMT) by activating Akt, Focal Adhesion Kinase (FAK) and breast cancer anti-estrogen resistance protein 1 (BCAR1), which is coupled with increased cell survival and drug resistance (Zheng *et al.* 2013). ING3 is a tumour suppressor expressed in various species and cancer types. Recent data suggests that an increased level of ING3 in PCa promotes cell proliferation and migration (Almami *et al.* 2016; Nabbi *et al.* 2017). Nabbi *et al.* 2017 showed that ING3 potentiates activation of the AR and increases expression of targeted genes. However, Nabbi *et al.* 2017 also hypothesized that ING3 may not be required for AR, but may be involved in inhibition of apoptosis in an RSK-dependent manner (Nabbi *et al.* 2017) (Figure 1.4.2.1).

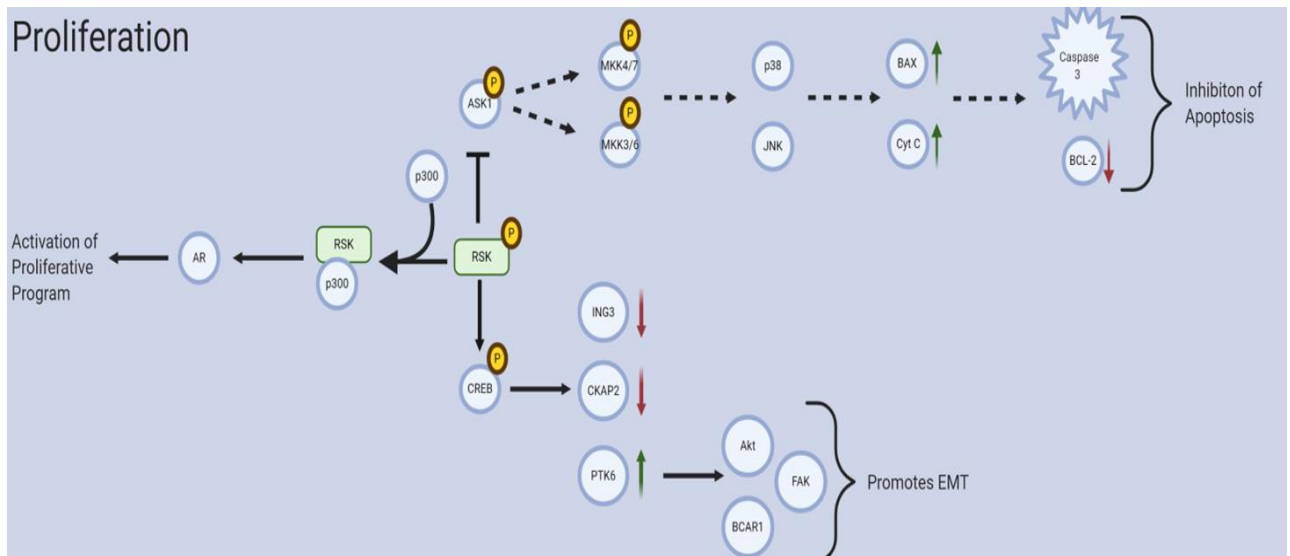


Figure 1.4.1.1 – Summary of the role of the RSK family in Prostate Cancer proliferation – Schematic representation of how RSK signalling regulates PCa proliferation. Solid arrows depict signalling events while dashed arrows depict signalling events inhibited by RSKs. Red arrows depict a decrease in expression while green arrows depict an increase in expression. Brackets are used to summarize the overall cellular outcome.

1.4.2 – The role of RSKs in cell cycle regulation

RSK1/2 were shown to inhibit Double Stranded Break (DSB) regulation resulting in G2/M checkpoint progression, in PC3 cells (Chen *et al.* 2013). In healthy cells, DSBs in DNA are recognized by the meiotic recombination 11(Mre11)-DNA repair protein RAD50(Rad50)-Nijmegen breakage syndrome 1(Nbs1) ((Mre11-Rad50-Nbs1) (MRN)) complex which then recruits the kinase ataxia telangiectasia mutated (ATM) which in turn phosphorylates several targets such as p53, Checkpoint kinase 1/2 (Chk1/2), BRACA1, Nbs1, H2A histone family member X (γ -H2AX) (Kastan & Lim 2000; Kim *et al.* 1999) resulting in cell cycle arrest and DNA repair or apoptosis (Jackson 2001). When this pathway becomes dysregulated it leads to the accumulation of DNA damage, mutations or loss of segments of chromosomal DNA which results in diseases including Cancer (Chen *et al.* 2013; Lavin 2007). Chen *et al.* (2013) used a combination of RSK activation with PMA and RSK inhibition with SL0101 to infer that RSK1/2 was causing a decrease in ATM phosphorylation. Further experimentation revealed that RSK1/2 phosphorylate the Mre11 component of the MRN complex, inhibiting its ability to bind to double stranded DNA (dsDNA). This prevents the recruitment of ATM to DSBs and in turn its activation (Chen *et al.* 2013). The RSK-dependent inactivation of ATM resulted in decreased phosphorylation of its substrates Nbs1 and γ -H2AX and G2/M progression and proliferation despite the presence of DSBs (Chen *et al.* 2013). Progression through the G2/M checkpoint with the accumulation of DSBs has the potential to cause disease and accelerate disease progression by allowing the replication of damaged DNA, this is likely to cause further mutations in recurring manner (Löbrich & Jeggo 2007). (Figure 1.4.2.2).

RSK1/2 have also been shown to regulate G2/M progression in PC3 cells by a different set of proteins, cell division control (Cdc) 25A and B. Cdc25 isoforms control the G2/M checkpoint via formation of Cyclin Dependent Kinase (CDK) complexes. There are several kinases which phosphorylate the Cdc25 isoforms (Wu *et al.* 2014). Interestingly, to further confine the regulation of the G2/M checkpoint many of the kinases responsible for phosphorylating the proteins are also downstream substrates of the Cdc25 isoforms creating a feed forward mechanism (Boutros *et al.* 2013). The RSKs were shown to phosphorylate Cdc25 A and B on residues S293/295 and S353/T355 respectively which causes an increase in M-phase inducing activities of PC3 cells (Wu *et al.* 2014). Furthermore, due to the RSKs not being a Cdc25 isoform substrate Wu *et al.* (2014) hypothesized that RSKs could be responsible for initiating the G2/M feed forward mechanism by phosphorylating Cdc25 A and B. Additionally, the RSK regulation of Cdc25 could be further intertwined with PCa signalling due to the Mre11 phosphorylation. As previously mentioned phosphorylation of Mre11 inhibits the activation of ATM (Chen *et al.* 2013). This inhibition could prevent ATM activation of its downstream kinases Chk1 and Chk2, this could also stop Chk1 from phosphorylating Cdc25A thus inhibiting its degradation. The accumulation of Cdc25A which dephosphorylates inhibitory phosphorylations on CDK (e.g. CDK1 Y14 and Y15) complexes could in turn prevent cell cycle arrest (Boutros *et al.* 2007). (Figure 1.4.2.2).

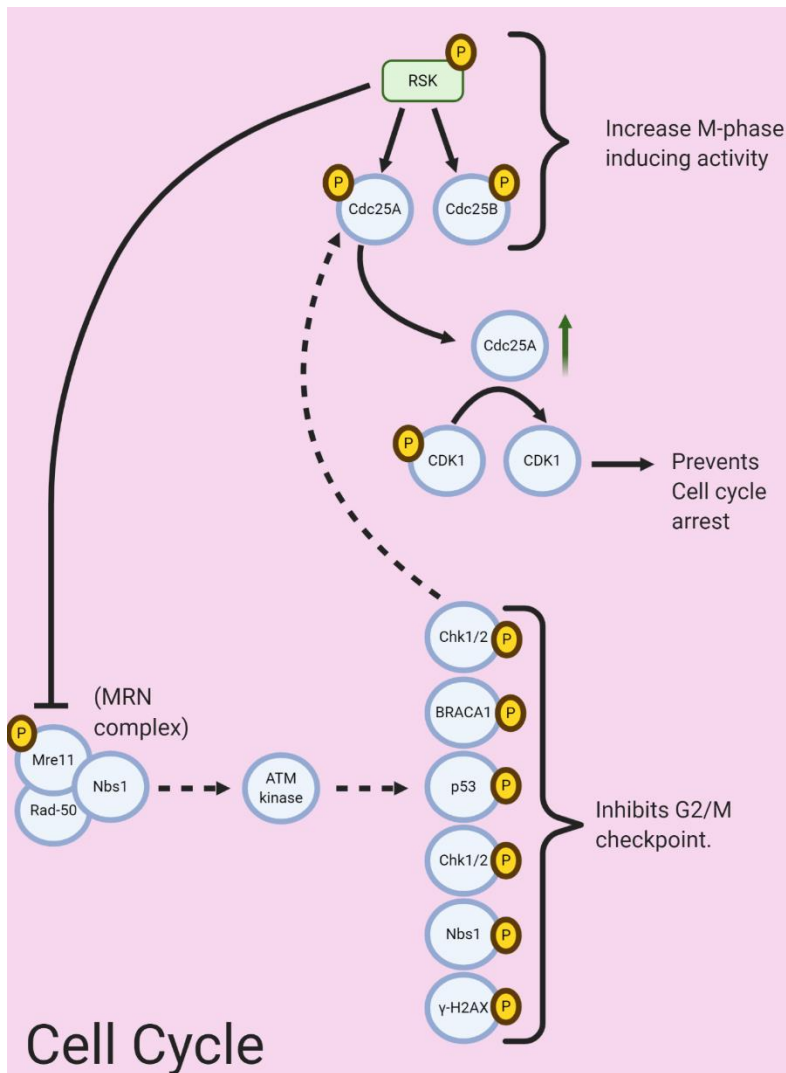


Figure 1.4.2.1 – Summary of the role of the RSK family in Prostate Cancer cell cycle regulation – Schematic representation of how RSK signalling regulates PCa cell cycle regulation. Solid arrows depict signalling events while dashed arrows depict signalling events inhibited by RSKs. Red arrows depict a decrease in expression while green arrows depict an increase in expression. Brackets are used to summarize the overall cellular outcome.

1.4.3 – The role of RSKs in cell motility

The RSKs have been shown to regulate cell motility across a range of cancers (Sulzmaier & Ramos 2013). More specifically, in PCa RSK1/2 have been shown to regulate a conserved pro-motility program in both healthy and tumorigenic prostate cells (Doehn *et al.* 2009). Through the use of a series of selective inhibition experiments Doehn *et al.* (2009) showed that the RSKs regulate multilayering, wound healing, chemotaxis and cell invasiveness via the Fos-related Antigen 1 (FRA1) transcriptional program across multiple cell types including PCa cell lines. However, the method in which the RSKs induce these changes varies between cell types, for example in MCF10A Breast Cancer (BCa) cells RSK caused an increase in FRA1 expression, while in MDCK cells RSK induced an increase in FRA1 phosphorylation/activation. Although Doehn *et al.* (2009) showed evidence of RSK phosphorylation of FRA1, the location of this residue was not experimentally validated but instead they assumed that RSK would phosphorylate FRA1 at S252 based on RSK phosphorylation of FRA1 homologue c-Fos (Doehn *et al.* 2009). Doehn *et al.* (2009) also highlighted that this could contribute to cell motility autocrine loop which has also been shown to exist in squamous cell carcinomas (Marinkovich 2007). FRA1 has been shown to regulate approximately 23% of the genes which highlights a large potential for therapeutic treatment. FRA1 has also been linked to the transition from androgen responsive PCa to CRPC. Kavya *et al.* (2017) used LNCaP and PC3 cells to mimic early and late stages of disease. Experiments highlighted that FRA-1 expression was upregulated in PC3 cells in response to DHT but remained unaffected when treated with Bicalutamide (BIC) which was not exhibited for most other activator protein 1 (AP1) components in LNCaPs. Additionally, Kavya *et al.* (2017) hypothesized that these cellular signalling

events may be a result of non-genomic cascades such as the Ras/Raf/MAPK or PI3K pathways which highlights another potential signalling node where the RSKs could contribute to PCa (Figure 1.4.2.3).

RSK2 has also been shown to regulate a conserved pro-motility program through the inactivation of integrin β (Gawecka *et al.* 2012). The conserved pro-motility program was demonstrated across multiple cell lines including PCa cell line DU145. RSK2 phosphorylates filamin A at S2152 which promotes its association to integrin β tails, forming a RSK2/filamin A/ integrin β complex. This complex formation disrupts association of integrin with the actin cytoskeleton thus prevents the formation of actin stress fibers, therefore promoting cell motility (Gawecka *et al.* 2012). Additionally, a similar pro-motility program has been reported in squamous carcinoma and colon cancer cells. Epidermal growth factor (EGF) stimulation of cells was shown to cause a reduction in cell adhesions by the same model demonstrated by Gawecka *et al.* (2012). EGF stimulation also activated the Rho/Rho kinase pathway which contributes to the phosphorylation of Filamin A, although, it was deduced that RSKs are the predominant kinase responsible (Vial & McKeown-Longo 2012). Filamin A was further associated with PCa by Sun *et al.* (2014) whose analysis of a group of patient samples showed reduced expression of filamin A which was also significantly correlated to lymph node metastasis. Experiments on PC3 cells showed transfection of filamin A caused a reduction in the survival fraction and a significant reduction in migration and invasion (Sun *et al.* 2014), in line with previous data from Gawecka *et al.* (2012). (Figure 1.4.2.3).

1.4.4 – The role of RSKs in therapy resistance

As previously mentioned, the common treatment for PCa is ADT, which aims to reduce activation of the AR and its transcriptional program which is the accepted driver of PCa. ADT elicits this by reducing the amount of circulating androgens and by using competitive inhibitors (Katzenwadel & Wolf 2015). Despite this, most patients will transition to CRPC, a therapy resistant form of PCa. The RSKs have been shown to regulate some of the current proposed mechanisms for the transition to CRPC (Zarif & Miranti 2016). One of these proposed events is that increased AR expression re-sensitizes the cell to the low concentrations of androgens present during ADT. RSK1 was shown to regulate the AR transcriptional program via YB1 in LNCaPs in response to androgen depletion (Shiota *et al.* 2014). Androgen depletion caused an increase in AR expression and increased phosphorylation of RSK1 and YB1. Treatment with anti-androgen Enzalutamide also exhibited the same outcomes. These events were further validated with the use of RSK inhibitor SL0101 and siRNA knockdowns (Shiota *et al.* 2014). Interestingly combinational use of SL0101 and enzalutamide showed synergistic tumour suppressor capabilities in both LNCaPs cells and the castration resistant cell line C4-2 (Shiota *et al.* 2014). Earlier work from the same group (Shiota *et al.* 2011) highlighted the ability of YB1 to regulate AR transcription in PCa cells. RSK1 phosphorylation of YB1 at S102 causes YB1 nuclear translocation and binding to its cognate Y-box and in turn regulate the AR transcriptional program (Shiota *et al.* 2011, 2014). This was shown to promote cell survival and invoke therapy resistance by enhancing the expression of cyclin D1, E2F-1 and phosphorylation of Retinoblastoma protein (Rb) (Shiota *et al.* 2014). Interestingly, Law *et al.* (2010), managed to overcome RSK/YB1 induced therapy resistance by using a cell permeable peptide which competes with YB1 for RSK2.

This caused a reduction of YB1 S102 phosphorylation and in turn reduced YB1 translocation to the nucleus which inhibited the growth of PCa and BCa cell lines (Law *et al.* 2010). (Figure 1.4.2.4).

In a similar manner treatment of PCa cell line PC3, DU145, LNCaP and 22Rv1 cells with RSK inhibitor PMD-026 exhibited an anti-cancer effect, most significantly with 22Rv1 cells. This was shown to be exhibited through RSK/YB1 signalling as phosphorylation of both RSK and YB1 were reduced when cells were treated with PMD-026 inhibitor (Ushijima *et al.* 2022). A reduction in AR splice variant, AR V7, at both the mRNA and protein level was also confirmed by qualitative PCR (qPCR) and western blotting. Co-treatment of PMD-026 with enzalutamide or darolutamide enhanced the reduction in RSK and YB1 phosphorylation and increased the amount of cleaved poly-ADP ribose polymerase (an indicator of apoptosis) and the amount of cell, accumulating in G2/M.

RSK1 was also shown to promote resistance to LY294002 (LY), a PI3K inhibitor (Chao & Clément 2006). LY treatment of LNCaPs causes apoptosis however when co-treated with EGF the LY induced cell death was inhibited. Using western blotting it was shown that BAD, ERK1/2 and RSK1/2 were phosphorylated in response to EGF. Further siRNA knockdown experiments were used to illustrate that RSK1 phosphorylation of BAD at S75 caused its inactivation and prevented BAD/BAX mediated LY induced apoptosis (Chao & Clément 2006).

In a comparable manner, Insulin-like Growth Factor (IGF) signalling activated both the MAPK and PI3K/Akt pathways promoting resistance to cycloheximide through Hsp27 regulation (Zoubeidi *et al.* 2010). Using both human PCa tissues and PCa cell lines it was shown that Hsp27 expression correlates with PCa progression.

Furthermore, Hsp27 protein levels and phosphorylation state were elevated in response to androgen ablation. Using both *in vitro* and *in vivo* methods it was demonstrated that RSK directly interacts with and phosphorylates Hsp27 (Zoubeidi *et al.* 2010). Hsp27 plays a role in the regulation of AR activity via facilitating the movement of the AR into the nucleus thus if RSK can phosphorylate Hsp27 then it may influence the movement of the AR into the nucleus and in turn its transcriptional activity (Zoubeidi *et al.* 2007). This was further validated through the use of RSK inhibition with siRNA knockdowns and employing the use of overexpressing inactive RSK which reversed the IGF induced Hsp27 phosphorylation (Zoubeidi *et al.* 2010). By an unknown mechanism, Hsp27 phosphorylation potentiates the IGF-I induced activation of Akt, ERK and RSK, which was validated through Hsp27 knockdown. Furthermore, the potentiation of the IGF-I signal increased phosphorylation of BAD on S75 and S99 causing the formation of BAD - 14-3-3 complexes via Akt, ERK and RSK. This causes sequestering of BAD to the cytoplasm and prevents the apoptotic program (Zoubeidi *et al.* 2010). Interestingly, the work of Chao & Clément (2006) identified an additional phosphorylation site of BAD at S99. This could possibly be due to the convergence of the PI3K and MAPK pathways, previously characterized in BCa, which could also exist in PCa. These studies revealed that IGF-I can stimulate transactivation of the EGF-receptor (EGFR) in the absence of EGF which results in MAPK pathway activation and phosphorylation of BAD (Gilmore *et al.* 2002). ZD1839, an EGFR inhibitor, was shown to induce apoptosis by inhibiting

MAPK activation and BAD dephosphorylation on S75. However, phosphorylation of BAD on S99 was not altered by ZD1839, confirming that this phosphorylation was independent of the EGFR-MAPK pathway and was indirectly targeted by PI3K. However, S99 was not sufficient to maintain survival when cells were treated with ZD1839 (Gilmore *et al.* 2002). Similar survival mechanisms were also identified in melanoma cells which develop chemoresistance via RSK inactivation of BAD (Eisenmann *et al.* 2003).

Interestingly, earlier work by Zoubeidi *et al.* (2010) in LNCaPs highlighted ligand-dependent activation of the AR through Hsp27 phosphorylation of S78 and S82 via p38 MAPK phosphorylation. This phosphorylation caused Hsp27 to displace Hsp90 from the AR and facilitate translocation to the nucleus. Hsp27 then promoted AR interaction with its cognate AREs and enhancing AR transcriptional activity (Zoubeidi *et al.* 2007). Furthermore, this mechanism has been established in the AR dependent molecular apocrine breast cancer (MABC) leading to DHT dependent proliferation thus promoting tumorigenic and metastatic capabilities. Specifically this was attributed to Hsp27 phosphorylation on S82 (Liu *et al.* 2018). Considering these data (Liu *et al.* 2018; Zoubeidi *et al.* 2007, 2010) it seems plausible that the RSKs could be further regulate PCa beyond the current research and presents an unexplored area for further investigation. (Figure 1.4.2.4).

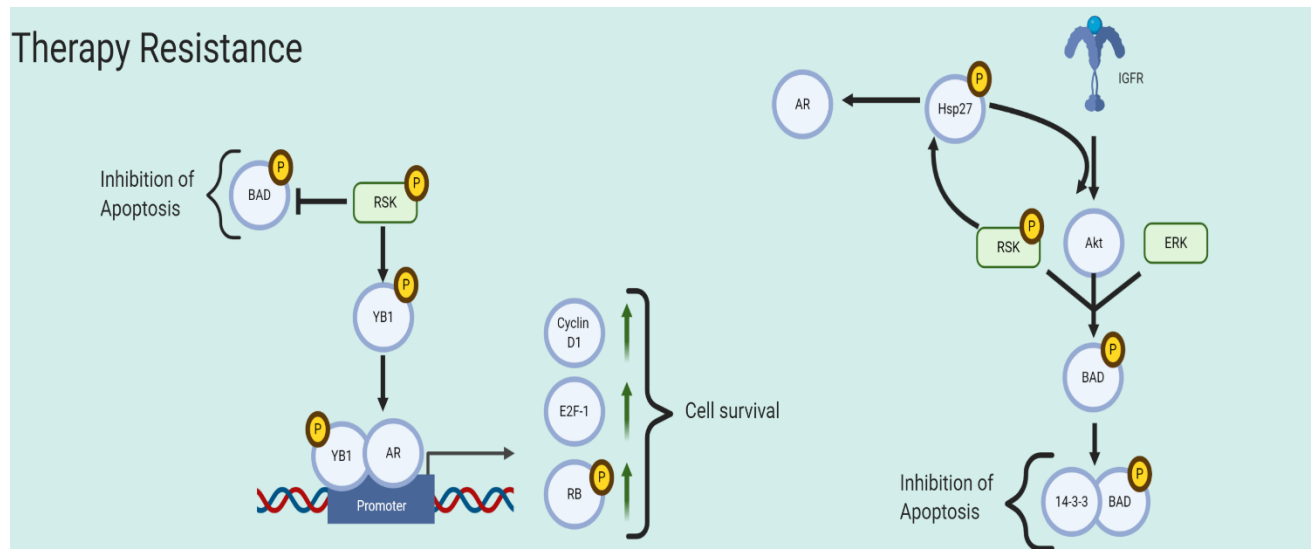


Figure 1.4.4.1 – Summary of the role of the RSK family in PCa progression and therapy resistance – Schematic representation of how RSK signalling regulates PCa therapy resistance. Solid arrows depict signalling events while dashed arrows depict signalling events inhibited by RSKs. Red arrows depict a decrease in expression while green arrows depict an increase in expression. Brackets are used to summarize the overall cellular outcome.

1.5 – Hypothesis and Objectives

Structural Hypothesis: RSK4 activation mechanism varies from RSK1-3 by NTKD-CTKD interactions in an inactive state

Structural Objectives:

1. Solve crystal structure of RSK4 CTKD
2. Solve crystal structure of RSK4 NL3M
3. Solve Co-crystal structure of RSK4 CTKD/NL3M
4. Carry out binding studies between RSK4 CTKD/NTKD

Prostate Cancer Signalling Hypothesis: RSKs influence the AR transcriptional program via direct/indirect mechanism.

Prostate Cancer Signalling Objectives:

1. Determine if RSKs interacts with the AR
2. Determine if the RSKs are downregulated/upregulated in PCa cell lines
3. Determine if the RSKs regulate the AR transcriptional program
4. Determine if the RSKs regulate proliferation in PCa cell lines

Chapter 2 – Methods

This chapter outlines the materials and methods used for the experiments outlined in this thesis.

2.1 – Antibiotic resistance and culture media preparation

All forms of bacterial growth media were prepared with ultra-pure water, sterilized by autoclaving and supplemented with antibiotics prior to inoculation. Cultures were then inoculated with cells that were transformed with varied vector depending on the experiment. *E.coli* cells carrying pETM-14 vectors inoculations were supplemented with 50 µg/ml Kanamycin (Thermo Fisher Scientific) whilst pGEX-6p-1, pcDNA 3.1 (+) and pM vector inoculations were supplemented with 100 µg/ml of Ampicillin (Thermo Fisher Scientific).

2.2 – Molecular Biology

2.2.1 – Molecular Biology for Structural Studies

PCR was used to amplify specific domains and regions of RSK4 DNA, exon sequences from existing sequence verified RSK-pGEX-6p-1 was used. The domains were then subcloned into vectors and phospho-mimetic site-specific mutations were created using existing template. DNA encoding RSK4 CTKD (spanning residues 420-686) was subcloned into the pETM-14 vector using NcoI and XhoI restriction enzymes (REs) for expression with a PreScission Protease-cleavable N-terminal Hexa-histidine tag (N-His) (Appendix Table 1), following this site directed mutagenesis was used to create a phospho-mimetic mutation at T581E creating the construct RSK4 CTKD Mutant (CTKDM) using mutagenesis primers (Appendix table

1) (Figure 2.2.1). DNA encoding RSK4 NTKD and AGC regulatory region (RSK4 NL) (spanning residues 48-401) and NTKD and AGC regulatory region with three mutations (RSK4 NL3M) were subcloned into the pETM-14 vector using *Nco*I and *Xho*I restriction sites for expression with PreScission Protease-cleaveable N-His (Appendix table 1) (Figure 2.2.1). The constructs already mentioned were created for the purpose of protein expression in *E.coli* cells.

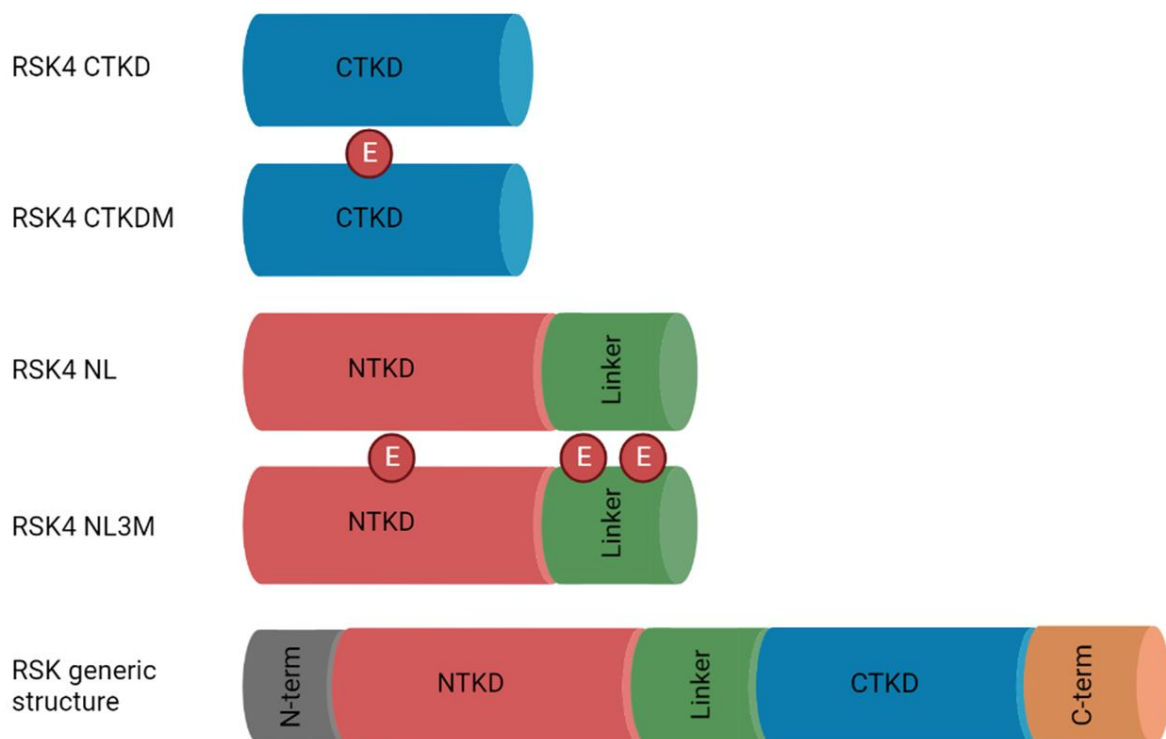


Figure 2.2.1.1 – RSK domains cloned into plasmid vectors – schematic representation of the RSK domains cloned into varied vectors for further experiments. Grey represents the flexible N-terminal region, NTKD represented in red, Linker region represented in green, CTKD represented in blue and flexible C-terminal region in orange. Red E represents phosphomimetic mutations to glutamic acid.

2.2.2 – Molecular Biology for Prostate Cancer Signalling

PCR was used to amplify RSK1-4 DNA exon sequences (Chapter 2.2.5). The full length genes were sub-cloned into the pM plasmid for mammalian-2-hybrid experiments (M2H) using varied combinations of restriction sites; EcoRI and Sall for RSK1/3, BamHI and HindIII for RSK2 and BamHI and EcoRI for RSK4 (Appendix Table 2) all enzymes were purchased from Thermo Fisher Scientific. Full length genes were cloned into pCDNA 3.1 (+) for Luciferase activity experiments (LUC) using restriction sites KpnI and NotI for RSK1-4 (Appendix table 2) (Figure 2.2.1.1). All restriction enzymes used were from thermo scientific.

2.2.3 – DNA plasmid amplification

1 µl of DNA or 5 µl of ligation mixture was added to chemically competent DH5α *E. coli* cells (Thermo scientific) and incubated on ice for 30 minutes. The cells were then heat shocked in 42 °C water for 45 seconds. Cells were then rested on ice for 2 minutes. 500 µl of Luria Broth (LB) (Merck), or 200 µL in the case of agar plating, was added to the cells prior to a one hour incubation at 37 °C with agitation. The cells were then inoculated into culture media containing 100 µg/ml of ampicillin for pGEX-6p-1 vectors or 50 µg/ml of kanamycin for pETM-14 vectors and incubated at 37 °C overnight. In the case of a midi prep, the 10 ml overnight culture was inoculated into 200 ml of media containing relevant antibiotics and incubated until the OD₆₀₀ reached between 2-4. A class II microbiological safety cabinet was used when necessary to reduce the chance of contamination.

2.2.4 – Plasmid mini/midi prep

Amplified DNA was extracted from cells using the GeneJet Plasmid miniprep kit (Thermo Fisher Scientific). Cell cultures were centrifuged for 12 minutes at 4000G. Supernatant was discarded and cell pellet was re-suspended in 250 μ l of resuspension buffer, lysed with 250 μ l of lysis buffer and 350 μ l of neutralization buffer added, at each stage mixing was undertaken. The solution was centrifuged at 11,400G for 12 minutes. 800 μ l maximum of supernatant was transferred to a miniprep column and centrifuged for one minute at 11,400G. 500 μ l of wash buffer was added to the column, incubated at RT for three minutes then centrifuged for one minute at 11,400G. This was repeated once more. The column was then centrifuged for two minutes at 11,400G to remove the residual wash buffer and transferred to an Eppendorf microcentrifuge tube. 30 μ l of type I water was added and the column left to stand at RT for 3 minutes before centrifugation at 11,400G for one minute to elute the DNA.

RBC bioscience fast ion plasmid midi advance kit was used to generate high-purity plasmids for mammalian cell transfection. 200 ml of cells were centrifuged at 6000G for 15 minutes at 4 °C. The supernatant was discarded, and the cells were resuspended in 10 ml of PM1 buffer. The cells were then transferred to a 30 ml centrifuge tube and 10 ml of PM2 buffer was added. The solution was mixed by inverting 10-15 times and incubated at RT for five minutes. A PMI column was equilibrated with 10 ml of PEQ buffer during this incubation time. 10 ml of PM3 buffer was added to the solution and mixed by inverting and incubated at RT for 5 minutes. The solution was then centrifuged 15000G for 15 minutes at 4 °C. The supernatant

was transferred to the equilibrated column and allowed load under gravity. The column was then washed with 15 ml of PWA buffer by gravity flow. 10 ml of PEL buffer was added to the column and the eluted DNA was collected in a sterile 30 ml centrifuge tube. 7.5 ml of isopropanol was added, mixed by inverting and then incubated at RT for 5 minutes. The mixture was centrifuged at 20,000G for 30 minutes at 4 °C. The supernatant was discarded and 5 ml of 70% ethanol was added and the sample was centrifuged at 20,000G for 10 minutes at 4 °C. The supernatant was discarded, and the DNA pellet was allowed to dry at RT. Once dried the pellet was resuspended with 100-250 µl, dependent on size, of sterile ultrapure water and transferred to a sterile 1.5 ml Eppendorf tube.

2.2.5 – Gene amplification and site directed mutagenesis

Reaction mixtures for Polymerase chain reaction (PCR) and mutagenesis were prepared (Table 2.2.5.1) and PCR was performed using a thermocycler (Techne, TC-412) following set parameters (Table 2.2.5.2).

Table 2.2.5.1 – Reaction mixture for PCR and Mutagenesis – PCR reagents with a (*) were obtained from thermos fisher scientific.

Component	Amount
*Phusion DNA Polymerase GC buffer (5X)	6 μ l
Template DNA	20-50 ng
Primer 1 (125 ng)	1 μ l
Primer 2 (125 ng)	1 μ l
*ddNTPs (10 mM)	1 μ l
*Phusion DNA Polymerase (2 U/ μ l)	1 μ l
H ₂ O	To a final volume of 30 μ l

Table 2.2.5.2 – Thermocycler program for PCR and Mutagenesis

Process	Temperature	Time	Cycles
Initial Denaturation	98	5min	1
Denaturation	98	1min	30 ^P / 18 ^M
Annealing	X ^P / 55 ^M	1min	
Extension	72 ^P / 68 ^M	2min ^P / 12min ^M	
Final Extension	72 ^P / 68 ^M	10min	1

^P = PCR reaction, ^M = Mutagenesis reaction

X = varied annealing temperature dependent on the template; RSK4 NL/NL3M 55°C, RSK4 CTKD(M) 59°C, RSK1-3 M2H 60°C, RSK4 M2H 57°C, RSK1-4 LUC 60°C.

2.2.6 – DNA fragment isolation

Following DNA amplification, DNA was prepared by adding 5µl of 1:1000 dilution of gel red (Sigma-Aldrich) and 1X of Agarose gel loading dye (6X) (Alfa Aesar). The samples were analyzed for successful amplification of a correctly sized gene via comparison to a 1kb Gene Ruler (Thermo Fisher Scientific) via gel electrophoresis (100V, 50min) using a 1% (w/v) agarose gel. The DNA was excised from the gel and isolated using the Nucleospin Gel and PCR Clean-up Kit (Machery-Nagel) (Chapter 2.2.6.1).

Following site directed mutagenesis samples were cleaned using the PCR cleanup protocol of the Nucleospin Gel and PCR Clean-up Kit (Machery-Nagel) (Chapter 2.2.6.1).

2.2.6.1 – Gene extraction / PCR cleanup

All centrifugations were carried out at 11,400G. For DNA extraction the agarose gel was solubilized with Solubilization buffer 100 µl to 100 mg of gel, heated at 55 °C for 10 minutes whilst vortexing regularly. The solution was added to the centrifuge column and centrifuged for one minute and flow through discarded. For PCR cleanup the total volume of sample was brought to 50 µl with the water and then 100 µl of solubilization buffer was added. The solution was then added to the centrifuge column, centrifuged for 1 minute and flow through discarded. From this point both methods converge. 500 µl of wash buffer was added, incubated for 3 minutes then centrifuged for 1 minute and flow through discarded. This was repeated once. The column was then centrifuged for 2 minutes and then transferred to an Eppendorf

microcentrifuge tube. 30 μ l of water was incubated for 3 minutes prior to a 1 minute centrifugation to elute the DNA.

2.2.7 – DNA Double Digest

1-2 μ g of Insert and vector DNA were double digested for three hours at 37 °C using the corresponding restriction enzymes (Chapter 2.2.1/2.2.2). DNA reaction mixture (Table 2.2.7.1) was prepared with 5 μ l of 1:1000 dilution of gel red (Sigma-Aldrich) and 1X of Agarose gel loading dye (6X) (Alfa Aesar), electrophoresis was used to ensure linearization by comparison to 1 kb DNA ladder (Thermo Fisher Scientific), digested and undigested vector controls. This was carried out on a 1% (w/v) agarose gel at 100 V for 50 minutes. The linearized vector DNA was then extracted (chapter 2.2.6.1). Insert DNA was isolated using a PCR cleanup (Chapter 2.2.6.1).

Table 2.2.7.1 – Restriction enzyme double digest components, volumes, and concentrations

Volume	Component
5 μ l	10X FD buffer
1 μ l	1 st RE (Thermo Scientific, 10U/ μ l)
1 μ l	2 nd RE (Thermo Scientific, 10U/ μ l)
X μ l = 1-2 μ g	Insert/Vector DNA
Make up to 50 μ l	H ₂ O

X= varied volume dependent on DNA concentration

2.2.8 – Insert and Vector Ligation

Ligation reaction mixtures were made containing 100 ng of digested vector DNA and 100-300 ng of insert DNA in the ratios 1:1, 1:2, and 1:3 (Vector: Insert) and incubated with T4 DNA ligase (5U / μ l) (Thermo Fisher Scientific) at Room Temperature (RT) overnight (Table 2.2.8.1)

Table 2.2.8.1 – Ligation Reaction Mixture

Amount	Component
1X	10X T4 DNA ligase buffer
100ng	Digester vector DNA
100-300ng	Digested insert DNA
1 μ l	T4 DNA ligase (5U/ μ l)
Make up to final volume of 20-30 μ l	H ₂ O

2.2.9 – DNA verification

Overnight ligation reactions were used for transformation of *E.coli* (Chapter 2.2.5) on LB agar plates. LB cultures were inoculated with single colonies and grown overnight at 37°C. DNA was then isolated (Chapter 2.2.4). A sample of the isolated DNA was subject to a double digest check. The same corresponding REs were used as prior to ligation and incubated for 3 hours at 37 °C. The sample was then analyzed via gel electrophoresis using 1% (w/v) agarose gel for 50 minutes at 100 V and visualized on a UV light. Control samples of undigested (300ng) and digested vector (300ng), 1 kb GeneRuler DNA ladder (Thermo Fisher Scientific) were also ran alongside for comparison. Following this a DNA sample was sent for external sanger sequencing (Eurofins) for complete gene sequencing.

2.2.10 – Site directed mutagenesis

Mutations were created by PCR using the QuickChange II XL site directed mutagenesis protocol. Plasmid-insert DNA was prepared and amplified (chapter 2.2.5) using the primer pairs to bring about the desired mutation (Table 2.2.1.1). Following this the parental DNA was digested by overnight incubation with 1 μ l of DPNI (10U/ μ l) (Thermo Fisher Scientific) which preferentially digests methylated DNA. The DPNI digested DNA was amplified (chapter 2.2.3) and isolated (chapter 2.2.4) followed by external sanger sequencing to verify if the mutagenesis was successful.

2.3 – Recombinant Protein Expression

Media for precultures and protein expression was sterilized by autoclaving and supplemented with the appropriate antibiotics before being inoculated with transformed BL21-DE3 cells. Expression cultures were 1 L of media inside a 2.5 L Erlenmeyer flask, precultures were 10 ml LB culture in universal containers. BL21-DE3 cells were transformed with expression vector DNA following the same protocol as Chapter 2.2.2. Following overnight incubation, auto-induction media (AIM) (Foremedium) or LB-broth media all 10 ml of the preculture was added to the expression culture. AIM cultures were incubated for 1 hour at 37 °C and then overnight at 20 °C. LB cultures were incubated until Optical Density at 600nm of 0.5-0.6 was reached then 250 µM (final concentration) of isopropyl-b-D-thiogalactopyranoside (IPTG) was added to induce protein expression. Cells were then incubated at 20°C for 20 hours before being harvested by centrifugation.

2.3.1 – Cell Harvesting

Following protein expression cells were harvested by centrifugation at 4,000G for 15 minutes at 4 °C. Pelleted media was discarded, and the pellet was transferred to a falcon tube for storage. Residual cell pellet was recovered by washing containers with PBS and spinning cells for a further 15 minutes at 4000G. The falcon tube was then labeled and stored in a -80 °C freezer to aid with lysis.

2.4 – Protein Purification

Three purification techniques were used to obtain suitable purity for later crystallography techniques: Affinity Chromatography (AC), Ion Exchange Chromatography (IE) and Size Exclusion Chromatography (SEC). Purification steps were carried out on ice when suitable. Buffers were made immediately prior to purification. When % buffer B is referred to, the remaining % of the buffer is made of buffer A (Appendix table 3).

2.4.1 – Cell lysis

Frozen cell pellets were re-resuspended with 4X volume of wash buffer 1 (W1) (Appendix Table 3) to volume of pellet (ml). 0.1 µg/ml DNase (Thermo Fisher Scientific) and one protease cocktail inhibitor tablet (Thermo Fisher Scientific) were added directly to the resuspended cells. This was then agitated on ice for 1 hour. The cells were then lysed mechanically through an emulsiflex between 12,000-15,000 PSI. This was repeated 2-3 times dependent on the viscosity of the cell lysate. The soluble and insoluble fractions of the cell lysate were then separated by centrifugation at 18,000G for 50 minutes at 4 °C. Samples were taken from both cell lysate and the soluble fraction and mixed with 2X lameli loading dye to be analyzed via sodium dodecyl-sulfate polyacrylamide gel electrophoresis (SDS-PAGE) (Chapter 2.4.5).

2.4.2 – Affinity Chromatography

A 5 ml HisTrap FF crude Ni-NTA column (Cytiva) or a 5ml GSTrap (Cytiva) was connected to a peristaltic pump. All steps were carried out using a flow rate of 2 ml/min. The columns used were pre-equilibrated with 25 ml of water followed by 25ml of wash buffer 1 (W1) (Appendix Table 3). All samples flow throughs were collected. The soluble fraction from Chapter 2.4.1 was applied to the column. The column was then washed with 50 ml of W1. The column was then washed a second time with 50 ml of wash 2 buffer (W2) (Appendix Table 3). The protein was then eluted with elution buffer (E) (Appendix Table 3). Samples of all the flow throughs were taken and mixed and analyzed via SDS-PAGE (Appendix Table 3). The elution sample was dialyzed overnight in dialysis buffer (DIAL) (Appendix Table 3) at 4 °C. Addition of Human Rhinovirus 3C protease (PreScission protease) at 4 units/mL was necessary if removal of protein tag was desired.

2.4.3 – Ion Exchange Chromatography

Ion exchange was performed on an AKTA pure with a 5 mL High Performance Sulphopropyl (HP SP) column (Cytiva) or High Performance Quaternary Ammonium (HP Q) columns (Cytiva). All steps were carried out at 2 ml/min. Columns were pre-equilibrated with 25 ml of a 5% buffer B (Appendix Table 3). Sample was loaded onto the column via peristaltic pump. Columns were washed with 25 ml of 5% buffer B and eluted using a linear gradient of 5-40% buffer over 80 ml (Appendix Table 3). Based on the chromatogram samples were taken for SDS-PAGE analysis (Chapter 2.4.5) and the relevant fractions were incubated overnight.

2.4.4 – Size Exclusion Chromatography (SEC)

A HiLoad 16/60 superdex 200 or 75 column (16 x 600mm) with column volume 120 ml was used for Size Exclusion Chromatography (Cytiva). SEC was performed on the AKTA pure. The column was equilibrated with 120 ml of SEC buffer (Appendix Table 3). Protein samples were pooled concentrated to 5 ml, then loaded via the injection loop. The flow rate was 0.75 ml/min throughout using SEC buffer. Again based on the chromatogram, samples were taken for SDS-PAGE analysis (Chapter 2.4.5) and the relevant fractions were pooled together, concentrated, aliquoted into 250µl samples, frozen in liquid nitrogen and stored in a -80 °C freezer.

2.4.5 – SDS-PAGE

Protein samples were prepared with 2X laemmli loading dye (Appendix Table 6) and heated to 90°C for 10 minutes followed by loading the samples into the wells of the 12% SDS gel. Samples were separated via electrophoresis at 200 V for 50 minutes. Proteins were stained with Coomassie stain (Thermo Fisher scientific). Cell lysate, soluble fraction and flow through were prepared at a higher dilution than other samples (1:3) and 3 µl were loaded. All other samples were diluted 1:1 and 10 µl were loaded. 5µl of Protein ladder (Thermo Fisher Scientific) was run in all SDS-PAGE gels for verification of size.

2.5 – Crystallization

Following obtaining protein at a high purity crystallography was pursued. Crystal screening is the initial step which has a broad systematic approach to find conditions which are favorable for crystal growth. This is then proceeded by large volume crystal condition optimization to increase the quality of the protein crystal and produce crystals in a more reproducible way.

2.5.1 – Crystallization screening

Following purification crystallization trials were undertaken. Protein samples were supplemented with 500 μ M Adenylyl-imidodiphosphate (AMP-PNP) and 1 mM $MgCl_2$ prior to being screened. Varied concentrations of protein were used across a series of purchased crystallography screens at either 1:1 or 1:2 volume ratios of protein to reservoir buffer were used, where 1=100nl. The protein sample was loaded onto the gryphon robot and a program was executed creating 96 conditions per ratio, if desired, both ratios could be applied to the same plate/screen. The plates were then sealed and stored at 16 °C. These conditions can be shown by (Table 2.5.1.1). 70 μ l reservoirs were used throughout the screens.

Table 2.5.1.1 – Crystallization conditions used in screening – numbers dictate what concentration of each protein was used for each condition.

Crystallisation screen	Protein constructs				
	RSK4 NL3M Untagged (mg/ml)	RSK4 CTKD tagged (mg/ml)	RSK4 CTKD untagged (mg/ml)	RSK4 CTKDM tagged (mg/ml)	RSK4 CTKDM Untagged (mg/ml)
Proplex	5, 7.5, 10	5, 7.5, 10	5, 7.5, 10	5,6,6.5,7,7.5, 8,9,10	5,6,6.5,7,7.5, 8,9,10
PACT	5, 7.5, 10	5, 7.5, 10	5, 7.5, 10	5,6,6.5,7,7.5, 8,9,10	5,6,6.5,7,7.5, 8,9,10
Peg/lon	5, 7.5, 10	5, 7.5, 10	5, 7.5, 10	5,6,6.5,7,7.5, 8,9,10	5,6,6.5,7,7.5, 8,9,10
JCSG	5, 7.5, 10	5, 7.5, 10	5, 7.5, 10	5,6,6.5,7,7.5, 8,9,10	5,6,6.5,7,7.5, 8,9,10
Structure	5, 7.5, 10	5, 7.5, 10	5, 7.5, 10	5,6,6.5,7,7.5, 8,9,10	5,6,6.5,7,7.5, 8,9,10
PGA	5, 7.5, 10	5, 7.5, 10	5, 7.5, 10	5,6,6.5,7,7.5, 8,9,10	5,6,6.5,7,7.5, 8,9,10

2.5.2 – Crystallization optimization

Following successful identification of crystal conditions for RSK4 CTKDM hanging droplet plates were created. Either 1 μ l or 2 μ l of RSK4 CTKDM was mixed with equal volume of 0.1M HEPES (Sigma Aldrich) of varied concentrations (Table 2.5.2.1) (1:1 ratio protein:buffer) overhanging 1 ml reservoirs. The pH of 0.1 M HEPES buffer and the amount of PEG4000 (Sigma Aldrich) was changed to create a range of conditions (Table 2.5.2.1). Additionally, mixed matrix crystallization was undertaken. 2 μ l of varied concentrations of RSK4 CTKDM was added to 4 μ l of 0.1M HEPES buffer. pH and PEG concentrations were also varied (Table 2.5.2.2). Finally seeding crystallization trials were undertaken. In all steps throughout this process the exact buffer in the kit was used. A seed stock was prepared by taking the crystal and adding it to 50 μ l of buffer in an Eppendorf. This was then vortexed. The seed stock was diluted in series by removing 5 μ l of the previous solution and mixing with 45 μ l of buffer. This created a range of seed dilutions (Table 2.5.2.3). Following this 1 μ l of seed stock was mixed with 1 purified protein over a hanging drop reservoir of 1 ml. This was done for each seed dilution and at varied concentrations of RSK4 CTKDM (Table 2.5.2.3).

Table 2.5.2.1 – Traditional crystallization optimization of RSK4 CTKDM – 1 μ l or 2 μ l of varied concentrations of RSK4 CTKDM were mixed with equal volumes of HEPES buffer at varied pH and varied PEG concentrations. Numbers in cells correspond to the concentration (mg/ml) of RSK4 CTKDM used.

	% PEG 4000					
0.1 M HEPES pH	9	11	13	15	17	19
6.8	6.9,7,7.1	6.9,7,7.1	6.9,7,7.1	6.9,7,7.1	6.9,7,7.1	6.9,7,7.1
7	6.9,7,7.1	6.9,7,7.1	6.9,7,7.1	6.9,7,7.1	6.9,7,7.1	6.9,7,7.1
7.2	6.9,7,7.1	6.9,7,7.1	6.9,7,7.1	6.9,7,7.1	6.9,7,7.1	6.9,7,7.1

Table 2.5.2.2 – Mixed matrix crystallization of RSK4 CTKDM – 2 μ l of varied concentrations of RSK4 CTKDM were mixed with 4 μ l of HEPES buffer at varied Ph and varied PEG concentrations. Numbers in cells correspond to the concentration (mg/ml) of RSK4 CTKDM used.

	% PEG 4000					
0.1 M HEPES Ph	9	11	13	15	17	19
6.8	6.9,7,7.1	6.9,7,7.1	6.9,7,7.1	6.9,7,7.1	6.9,7,7.1	6.9,7,7.1
7	6.9,7,7.1	6.9,7,7.1	6.9,7,7.1	6.9,7,7.1	6.9,7,7.1	6.9,7,7.1
7.2	6.9,7,7.1	6.9,7,7.1	6.9,7,7.1	6.9,7,7.1	6.9,7,7.1	6.9,7,7.1

Table 2.5.2.3 – Seeding crystallization of RSK4 CTKDM – 1 μ l of seed stock dilution at varied seed stock dilutions was mixed with 1 μ l of RSK4 CTKDM at varied concentrations. Numbers in the wells represent the concentration (mg/ml) of RSK4 CTKDM used.

	Seed Stock dilution					
	1×10^0	1×10^{-1}	1×10^{-2}	1×10^{-3}	1×10^{-4}	1×10^{-5}
Concentrations of RSK4 CTKDM used	6.9	6.9	6.9	6.9	6.9	6.9
	7	7	7	7	7	7
	7.1	7.1	7.1	7.1	7.1	7.1

2.6 – Protein Assays

To evaluate the activity of the RSK4 CTKDM construct, kinase assays were used to compare activity to RSK4 CTKD (Chapter 2.6.1). Pull down assays were also conducted to investigate the binding interactions between the N-terminal region and C-terminal region of RSK4 (Chapter 2.6.2).

2.6.1 – Kinase assay

The HTRF KinEASE kit (cisbio) was used to undertake the kinase assays. These assays were carried out on 384 well plate. Protein samples used were very concentrated so were series diluted with kinase buffer (Table 2.6.1.1). 5 μ M of kinase was added to the wells, not exceeding 6 μ l volume, if the protein volume was below 6 μ l the rest of this volume was made up with the kinase buffer (Table 2.6.1.1). 2 μ l of 1.25 μ M substrate 1 (S1) was added to the wells (final concentration 0.25 μ M). 2 μ l of ATP buffer (Table 2.6.1.1) was added to the wells, this was always added last as this initiates the reaction (final ATP concentration 1 mM). Over a series of pre-selected time points the reactions were stopped by the addition of 1 μ l of 20 mM ethylenediaminetetraacetic acid (EDTA) (Sigma Aldrich) to a Final concentration of 2 mM . Once all time points were stopped 5 μ l of 0.125 μ M Streptavidin-XL665 was added to all wells (final concentration 15.61 nM). 5 μ l of the STK antibody-cryptate was then added to all wells. The reaction was then covered with tin foil to prevent light degradation and incubated at room temperature for 1 hour before being quantified on the clariostar plate reader. Following this, the data was analyzed.

Table 2.6.1.1 – Kinase assay buffers

Buffer	Buffer Composition
Kinase buffer	25 mM Tris-HCl pH 8, 150 mM NaCl, 5 % (v/v) glycerol), 2 mM MgCl ₂
ATP buffer	25 mM Tris-HCl pH 8, 150 mM NaCl, 5 % (v/v) glycerol), 2 mM MgCl ₂ , 5 mM ATP

2.6.2 – Pull down assay

RSK4 CTKD, CTKDM and NL3M were already available from previous purifications. However, RSK4 NTKD and NL needed to be purified prior to the pull down assay. Both proteins were subjected to Affinity Chromatography (Chapter 2.4.2) followed by Size Exclusion (Chapter 2.4.4). For the pull-down assay agarose resin with covalently attached glutathione was used to bind GST tagged proteins. The assay was carried out in 1 ml gravity flow columns (Bio Rad). 150 µl of resin (Merck) was used for all samples. Resin was pre-equilibrated with wash buffer (Table 2.6.2.1). 300 µl of 50 µM RSK4 NTKD, NL and NL3M were incubated with resin for 1 hour at RT. For the control experiments 500 µl of 200 µM RSK4 CTKD and CTKDM were also incubated with resin for 1 hour at RT. The resin was then washed with 5 ml of wash buffer in 500 µl volumes. Each flow through was collected for analysis. For binding experiments, 500 µl of 200 µM RSK4 CTKD and CTKDM was incubated with 300 µl of 50 µM RSK4 NTKD, NL and NL3M, for 1 hour at RT and then washed as previously described. Both samples and controls were then eluted with elution buffer (Table 2.6.2.1). Samples were then analysed by SDS-PAGE (Chapter 2.4.5) with the omission of pre-stained Protein ladder, instead a non-stained ladder was used. The SDS gel was then analysed by western blotting (Chapter 2.6.3).

Table 2.6.2.1 – Pull down assay buffers

Buffer	Composition
Wash buffer	25 mM Tris-HCl pH 8, 50 mM NaCl, β -mercaptoethanol, 5 % glycerol, 1 mM MgCl ₂ , 500 μ M ATP.
Elution buffer	25 mM Tris-HCl pH 8, 50 mM NaCl, β -mercaptoethanol, 5 % glycerol, 1 mM MgCl ₂ , 500 μ M ATP, 10 mM reduced glutathione.

2.6.3 – Western blotting

Once SDS-PAGE was complete the proteins in the gel were transferred onto a Polyvinylidene fluoride (PDVF) membrane (Bio Rad). Five pieces of electrode paper were soaked in transfer buffer (Appendix Table 9) and placed on the BIO-RAD trans-blot semi-dry transfer cell. A piece of PDVF membrane was soaked in methanol, then soaked in transfer buffer and placed on top of the electrode paper. A small amount of transfer buffer was poured on top to retain moisture. Five additional pieces of soaked electrode paper were placed on top of the PDVF membrane and rolled to remove air bubbles. Electrode plates were then dampened with transfer buffer to ensure complete current flow. The proteins were then transferred onto the membrane for two hours at 15 V and 100 mA.

Following protein transfer, 1 g of powdered milk (Tesco) was dissolved in 20 ml of Phosphate buffered saline-0.1% tween (PBST) (Thermo Fisher Scientific) creating a 5% PBST-milk solution. The PBST-milk was incubated with PVDF membrane and incubated for 30 minutes to block pores on the membrane. The block was removed, and primary antibodies (also made in PBST-milk) were incubated overnight at 4 °C with slow rotation (Appendix Table 4). The next day primary antibody was removed,

and the membrane was washed with 5 ml of PBST for 5 minutes whilst rotating at RT. This was repeated two more times. The membrane was blocked with PBST for 15 minutes at RT with rotation. Secondary antibodies (Appendix table 4) were then incubated with the membrane for one hour at RT whilst rotating. The wash steps were repeated, but an additional PBS wash for 5 minutes was added. 350 μ l of Luminata Forte Western Horseradish peroxidase substrate (Merck) was continuously pipetted over the membrane for 3 minutes. The membrane was then placed in a plastic film and bands visualized using a Fusion FX Viber Lourmat.

2.7 – Mammalian Cell Culture

All cell lines (Table 2.7.1) were supplied by Dr. Greg N Brooke, University of Essex. Different cell lines were maintained in either Dulbecco's Modified Eagle Medium (DMEM) (Gibco) or Roswell Park Memorial Institute 1640 (RPMI) (Gibco), additionally, double charcoal stripped versions of both medias were also used (Gibco) which have been further processed to remove additional components from the media which could interfere with experimental design. The double charcoal stripped versions of each media will be referred to as 'stripped media' whilst the standard nomenclature will be used for the 'unstripped' media. Both DMEM and RPMI were supplemented with 10% foetal bovine serum (FBS) (Gibco) whereas both the stripped DMEM and RPMI were supplemented with 5% double charcoal stripped FBS (SFBS) (Gibco). All media were also supplemented with an antibiotic cocktail, PSG; Penicillin (100U), Streptomycin (0.1mg/ml) and L-Glutamine (2mM) (Gibco). All cell culture work was performed under sterile conditions inside a Class II flow cabinet. Cells were incubated in humidified air 5% CO₂ at 37 °C. A variety of cells were used throughout these experiments and different media used to grow them (Table 2.7.1).

Table 2.7.1 – Cell lines models used – Cell name stated in right column, a description of each cell line and their origin in middle column and the media used to maintain these cell lines in the right column.

Cell Line	Description	Media
COS-1	A fibroblast-like cell that was isolated from the kidney of an African green monkey.	DMEM
PNT1A	Normal prostatic epithelial cells that have been immortalized by SV40.	RPMI-1640
LNCaP	Epithelial-like morphology. Derived from metastatic lymph node lesion.	RPMI-1640
C42	Epithelial-like morphology. Derived from xenograft tumor of castrated mouse which was originally propagated from LNCaP.	RPMI-1640
C42B	Epithelial-like morphology. Derived from xenograft of bone metastasis which was originally propagated from C42.	RPMI-1640
22RV1	Epithelial-like morphology. Derived from xenograft of castration-induced regression which was originally propagated from CWR22.	RPMI-1640
DU145	Epithelial-like morphology. Derived central nervous system metastasis of human patient.	RPMI-1640

2.7.1 – Passaging cells

Cells were passaged every time they reached 70-80% confluency. Old media was removed and cells were washed with PBS. Dependent on the flask size, 0.25-0.75 ml of trypsin/EDTA (Gibco) was added directly to the cells. The cells were incubated with the trypsin for a few minutes at room temperature to detach the cells from the flask surface. The trypsinised cells were resuspended in 10 ml of relevant media (Table 2.7.1) and based on confluency the desired volume of cells was added to a new flask containing the relevant fresh media and returned to the incubator.

2.7.2 – Cell counting and plating

If cells were needed for an experiment they were passaged as described in Chapter 2.7.1 but dependent on the experiment type and the cell line used then the choice of media to resuspended the cells would differ (stated in relevant chapter). Once the cells were resuspended in the desired media, they were counted to ensure consistent numbers of cells per well of a plate. 0.5 ml of cells were diluted into 4.5 ml of media dilution. The cells were then mixed and two 10 μ l samples were taken and applied to a hemocytometer. The cells were then counted across 10 grids present on the hemocytometer and based on this number the cell density was calculated. This would then determine the volume of media to dilute the cells with, whilst also considering the total volume of cells needed for the experiment. The cells were then mixed and plated which again varied dependent on experiment (stated in relevant chapter). The plates were then incubated at 37 °C overnight.

2.7.3 – Calcium phosphate transfections

COS-1 cells were transfected with DNA for mammalian-2-hybrid (M2H) assays or luciferase activity assays. Transfection master mix (Table 2.7.3.1) were prepared to reduce variability between samples. Master mixes were prepared and then split between conditions, DNA for the relevant conditions were then added. Each DNA mixture was supplemented with sterile filtered CaCl₂ (Sigma Aldrich) and Borine buffered saline (BBS) (Sigma Aldrich) utilizing the swirling and bubbling method to mix the reagents (Table 2.7.3.1). Mixtures were left to incubate at RT for 15 minutes prior to transfection. 100 µl of transfection mixture was pipetted dropwise into each well of a 24 well plate and incubated for 20-24 hours.

Table 2.7.3.1 – Calcium phosphate master mix – Vector 1 and Vector 2 correspond to varied combinations of vectors co-transfected into COS-1 cells. * the luciferase reporter plasmids were 5GAL-LUC for M2H and TAT-GRE-E1B-LUC for luciferase assays.

Component	Volume Per well (µl)
Luciferase reporter plasmid (500 ng/ul)*	2
Bos-β-galactosidase (10 ng/ul)	1
Vector 1 (100 ng/ul)	1
Vector 2 (100 ng/ul)	1
2 M CaCl ₂	5
BBS	50
H ₂ O	40

2.7.4 – Luciferase activity assay

The Luciferase assay is a reporter assay, it operates via the transcription of the luciferase gene *in vitro*. When the cells are lysed the luciferase enzyme is released and interacts with other reagents to produce light, this can be quantified as an indirect measure of gene expression of the reporter system and thus activity of the transcriptional activity. COS-1 cells were counted and plated into 24 well plates (Chapter 2.7.2) using stripped DMEM media at a cell density of 1×10^5 . COS-1 cells were then transfected (Chapter 2.7.3) with varying combinations of vectors to investigate possible interactions between the RSKs and AR. COS-1 cells were co-transfected with; pVP16-AR and pM-LXXLL or pVP16-AR and pcDNA3.1-RSK1-4 (Table 2.7.3.1). Following transfection, cells were incubated for 20-24 hours. The media was removed, cells washed with 1 ml of PBS twice and stripped DMEM media supplemented with 1 nM synthetic Mibolerone (MIB) was added or 1 μ l of Ethanol (ETOH) was added to maintain a consistent volume for the control. Cells were incubated for 20-24 hours. Following this media was removed, cells were washed twice with 1 ml of PBS and then lysed using 60 μ l of 1X Cell Culture Lysis Reagent (Promega) diluted from the 4X concentrated stock. The plate was frozen for 15 minutes at -80 °C. 20 μ l of cell lysate was taken from each well and added to a 96 well plate. 20 μ l of Luciferase Substrate (Promega) was added to each well, the plate was covered with foil, rotationally mixed for 15 minutes at RT and luminescence quantified on a FLUOstar Omega plate reader. For β -galactosidase, 5 μ l of cell lysate was taken from each well and added to a 96 well plate. 50 μ l of Tropix Galacton-Plus (Thermo Fisher Scientific) was added per well, the plate was covered, mixed rotationally for one hour at RT and luminescence quantified on a FLUOstar Omega plate reader.

All experiments were completed in triplicate and averaged (with anomalies removed). The luciferase data was normalized by dividing it by the β -galactosidase data. These values were then made relative to the AR in the presence of MIB. This process was repeated for every experimental repeat. The mean from each experimental repeat was then averaged to give the final relative activity value and the same data was also used to determine the standard error. This data was also used for statistical analysis on graph pad prism. A One-way ANNOVA was performed with Sidak's post hoc to determine statistical significance in relation to AR in the presence of MIB.

2.7.5 – Mammalian-2-hybrid assay

COS-1 cells were counted and plated into 24 well plates (Chapter 2.7.2) using stripped DMEM media at a cell density of 1×10^5 . COS-1 cells were transfected (Chapter 2.7.3) with varying combinations of vectors to investigate possible interactions between the RSKs and AR. COS-1 cells were co-transfected with; pVP16-AR and Empty pM; Empty pVP16 and pM-LXXLL; pVP16-AR and pM-LXXLL; pVP16-AR and pcDNA3.1-RSK1-4 (Table 2.7.3.1). Following transfection, cells were incubated for 20-24 hours. The media was removed, cells washed with 1 ml of PBS twice and stripped DMEM media supplemented with 1 nM MIB or 1 μ l of ETOH was added. Cells were incubated for 20-24 hours. Following this media was removed, cells were washed twice with 1 ml of PBS and then lysed using 60 μ l of 1X Cell Culture Lysis Reagent (Promega). The plate was frozen for 15 minutes at -80°C . 20 μ l of cell lysate was taken from each well and added to a 96 well plate. 20 μ l of Promega Luciferase Substrate was added to each well, the plate was covered with foil, rotationally mixed for 15 minutes at RT and luminescence quantified on a FLUOstar Omega plate reader. For β -galactosidase, 5 μ l of cell lysate was taken from each well and added to a 96 well plate. 50 μ l of Tropix Galacton-Plus was added per well, the plate was covered, mixed rotationally for one hour at RT and luminescence quantified on a FLUOstar Omega plate reader.

All experiments were performed in triplicate and averaged (with anomalies removed). The luciferase data was normalized by dividing it by the β -galactosidase data (Luciferase/ β -gal). These values were then made relative to the AR + LXXLL in the presence of MIB. This process was repeated for every experimental repeat. The data

from all experimental repeats was then averaged to give a final value, the same data was also used to determine the standard error. The same data was also used for statistical analysis on graph pad prism. A One-way ANNOVA was performed with Sidak's post hoc to determine statistical significance.

2.7.6 – RSK siRNA knockdown

siRNAs interfere with the translation of proteins, by transfecting cells with siRNA the levels of the targeted protein are reduced and in turn the effects they have on cellular function are also reduced and lead to inferring protein function. LNCaP cells were counted and plated (Chapter 2.7.2) into 6-well plates using RPMI media at a cell density of 4×10^5 . The old RPMI media was removed from the LNCaP cells and then washed with 1 ml of PBS twice and then 1 ml of stripped RPMI media was added to the wells. siRNA duplexes were mixed with Optimem media by vortexing and pulse spinning in a benchtop centrifuge (Table 2.7.6.1/2). In a separate tube, Optimem (Gibco) and transfection reagent, RNAiMAX (Invitrogen), were mixed by flicking (Table 2.7.6.1/2). The RNAiMAX solution and siRNA solution were mixed by flicking. The final solution was then incubated at RT for 10 minutes prior to being transfected into the LNCaP cells in a drop wise manner (Table 2.7.6.1/2). The cells were then incubated with siRNA for 72 hours. Varied volumes of the reagents were used dependent on experiment type (Table 2.7.6.1/2). Cells were then supplemented with either 1 nM MIB or 1 μ l of ETOH. Cells were then incubated for 24 hours for qPCR experiments or five days for WST assay experiments.

Table 2.7.6.1 – QPCR siRNA transfection reaction mixtures

Mixture	Components per well
siRNA solution	5 μ l of 10 μ M siRNA, 45 μ l Optimem
RNAiMAX solution	1.13 μ l RNAiMAX, 48.87 μ l Optimem
Total Volume 100 μl	

Table 2.7.6.2 – WST assay siRNA transfection reaction mixtures

Mixture	Components per well
siRNA solution	0.2 μ l of 10 μ M siRNA, 9.8 μ l Optimem
RNAiMAX solution	0.075 μ l RNAiMAX, 9.925 μ l Optimem
Total Volume 20 μl	

2.7.7 – RNA extraction

The RNAeasy kit (Qiagen) was used for RNA extraction. Media was removed from the plate and 350µl of RTL buffer was added to the cells. To aid lysis and removal of the cells from the surface of the well a pipette tip was used to scrape the well and the lysate was transferred to an Eppendorf. 350 µl of 70% ETOH was added to the samples and mixed by pipetting. The sample was then transferred to a RNAeasy spin column and centrifuged for 15 seconds at 8000G. 700 µl of RW1 buffer was added to the column and centrifuged for 15 seconds at 8000G; the flow through was discarded. 500 µl of RPE buffer was then added and centrifuged for 15 seconds at 8000G. 500 µl of RPE buffer was then added and centrifuged for 2 minutes at 8000G. The column was then centrifuged at 8000G for 1 minute to removal residual buffer. At each step, the flow through was discarded. The column was then transferred to a clean Eppendorf and eluted with 30 µl of Ultra pure water via 1 minute centrifugation at 8000G. RNA was quantified using a nanodrop and stored at -80 °C.

2.7.8 – Reverse Transcription

RNA was reverse transcribed into complementary DNA (cDNA) using a reverse transcription kit (Lunascript). RNA and reagents were thawed on ice. Samples were mixed by flicking and pulse spinning prior to preparation of the reaction mixtures. Reaction mixtures were prepared (Table 2.7.8.1) The samples were then incubated for 2 minutes at 25 °C, 10 minutes at 55 °C and 5 minutes at 95 °C in a thermocycler. The samples were then further diluted (1:8) with 140 µl of nuclease free water (Thermo Fisher Scientific) and stored for qPCR.

Table 2.7.8.1 – Components of Reverse Transcription reaction

Component	Volume added
LunaScript RT supermix (5X)	4 µl
RNA sample	Variable (up to 1 µg)
RNA/Nuclease free water	Remainder up to 20 µl

2.7.9 – qPCR

To undertake qPCR experiment a series of techniques were used. LNCaP cells were passaged (Chapter 2.7.1). Cells were then counted and plated into 6 well plates (Chapter 2.7.2) using RPMI media at a cell density of 4×10^5 . The cells were then transfected and treated (Chapter 2.7.6). The RNA was then extracted (Chapter 2.7.7) and then reverse transcribed into cDNA (Chapter 2.7.8) which could then be used in the qPCR experiment. cDNA used for PCa cell line qPCR experiments were provided by A.Ekperouh. qPCR reactions were carried out in a 96 well plate and amplification was quantified using a BIO RAD CFX connect Real Time System. The qPCR reactions were completed using the Quantitect SYBR Green PCR Kit (Qiagen). All reaction mixtures were prepared on ice. Reaction master mixtures were made with qPCR primers (Appendix Table 5) and SYBR green (Thermo Fisher Scientific) (Table 2.7.9.1). 6 μ l of the master mixes were aliquoted into the wells followed by 4 μ l of cDNA. The plate was sealed and spun. The qPCR protocol was then ran (Table 2.7.9.2). The data was then analyzed.

All experiments were performed in triplicate and averaged (with anomalies removed). To calculate the change in expression an internal control, the house keeping gene L19, was used. The expression of this gene should not alter during experiments thus accounts for fluctuations of cell number. The L19 Cycle Threshold (CT) averages were then subtracted from the RSK CT averages (for RSK expression) or the AR target gene CT averages (for target gene expression in the presence of RSK siRNA) (delta CT). The data was then normalized to the external control to allow for comparison. In the case of siRNA knockdowns, the control was to the non-targeting siRNA as this should not have caused any change to the cells whereas for the PCa cell lines PNT1A was used as it is the 'healthy state' of prostate epithelial cells thus

allows comparison of changes in RSK expression in relation to PCa disease state. The normalization was achieved by using the delta CT value of the external control (non-targeting siRNA in the presence of ETOH or PNT1A) and subtracting this value from the other conditions (delta CT/delta CT). The delta CT/delta CT value was then used as the indices of 2, $2^{(\text{deltaCT}/\text{deltaCT})}$ to give the relative change in expression. This was then used as the final value for one experimental repeat. This was then repeated for additional experimental repeats and averaged. The data of all repeats was then subjected to statistical testing in graph prism pad. One-way ANNOVA was selected and followed by Sidaks post-hoc test to give levels of significance.

Table 2.7.9.1 – Reaction master mix for qPCR

Component	Volume added (per well)
Forward qPCR primer	0.5 µl of 10µM
Reverse qPCR primer	0.5 µl of 10µM
2X SYBR PCR master mix	5 µl

Table 2.7.9.2 – qPCR cycling parameters

Step and Temperature	Time	Number of Cycles
Initial denaturation (95 °C)	2 minutes	1
Denaturation (95 °C)	5 seconds	40
Annealing/Extension/Data collection (60 °C)	10 seconds	
Melt Curve (65-89.6 °C)	+0.3 °C every 5 seconds	1

2.7.10 – WST-1 proliferation assay

LNCaP cells were passaged (Chapter 2.7.1). Cells were then counted and plated into 96 well plates (Chapter 2.7.2) using stripped RPMI media at a cell density of 4×10^3 . The cells were then transfected and treated (Chapter 2.7.5) prior to the WST assay. 10 μ l of WST-1 reagent (Roche) was then added to all wells and absorbance at 450 nm wavelength was recorded using a FLUOstar Omega plate reader every five minutes for 20 minutes. The data was then analysed.

The hormone optimization experiments were completed in triplicate and average. This was repeated for each experimental repeat. The mean from each experimental repeat was then averaged to give a final absorbance value. These values were also used to generate standard error bars.

The WST siRNA knockdown experiments were completed in triplicate and then averaged (anomalies removed). The average of each condition, for example RSK1 KD treated with MIB, were then normalized to the external control (non-targeting siRNA treated with ETOH) by dividing it by the average of the non-targeting control giving relative proliferation. This was repeated for each experimental repeat. The mean of each experimental repeat was then averaged to give the final value for each condition. The same data was used to determine standard error bars and statistical significance in graph pad prism. A one-way ANNOVA was performed with Sidaks post hoc test.

Chapter 3 – Results – Characterisation of RSK4 mechanism of activation

3.1 – Introduction

Kinases share a common structure composed of two lobes, the N-lobe and the C-lobe. Both lobes possess key regions which are necessary for the catalytic activity of a kinase. Most significantly two regions from each lobe; the C-helix and β 4 strand (N-lobe); the Y/HRD motif and DFG motif (C-lobe) (Meharena *et al.* 2013). These regulatory regions orientate both the kinase and substrate in optimal positions for the transfer of γ -phosphate transfer from ATP to hydroxyl acceptor on the substrate. The RSKs uniquely possess two distinct kinase domains the NTKD (AGC) and the CTKD (CAMK) which is connected by a linker region (Endicott *et al.* 2012). Most AGC kinases possess a conserved hydrophobic motif (HM: F-X-X-F-S/T-F/Y) on their C-terminal region (linker region in RSKs), which is phosphorylated to achieve maximal activity (Pearce *et al.* 2010). RSKs activation requires an extensive level of interaction among the NTKD, the CTKD and the linker region, and the exact relationship among these 3 functional regions of the RSKs are still unclear. Indeed, classically, a heterokinase phosphorylates the HM (pHM) which wraps around the N-lobe where a phosphate-binding pocket is localized, and stabilizes the active conformation of the C-helix (Frödin *et al.* 2002; Hindie *et al.* 2009; Yang *et al.* 2002b, 2002a). For RSKs, the CTKD phosphorylates the HM, which in RSK1-3, but not RSK4, acts to recruit PDK1. PDK1 then phosphorylates the NTKD activation loop, resulting in RSKs activation and substrate phosphorylation.

However, RSK4 activation is PDK1 independent (Dümmeler *et al.* 2005), and it has been suggested that the binding of the pHM to the RSK4 NTKD increases its autophosphorylation rate (Chrysostomou *et al.* 2021). Structural superimposition between RSK4 NTKD and PDK1, protein kinase C β 2 (PKC β 2), AKT1, AKT2 that were crystallised in presence of their phosphorylated (or phospho-mimic mutant) C-term, revealed that the phosphate-binding pocket of the RSK4 NTKD is different from that of the classical AGC kinases (Figure 3.1.1). This difference is a result of the β B-sheet that alters the binding surface. Recently, Chrysostomou *et al.* (2021) used a docking model for the NTKD bound to the pHM coupled with Markov transient analysis to show how the binding of the pHM to a non-conventional phosphate binding pocket caused protein activation via the DFG motif. This non-conventional model of activation and, more generally, the global RSK allosteric regulation mechanism differs substantially from that of other kinases.

Attempts to crystallise the RSK4 full length and gain a better understanding of the relative orientation of the NTKD and CTKD in the inactive and active states have failed. The AlphaFold model for RSK4 is substantially different from the crystal structure of the NTKD, as it presents a classic kinase fold like that of other AGC kinases. Furthermore, the NTKD and CTKD of RSK4 interact using an extended surface and are placed in a face-to-back orientation, with the HM wrapped around the N-lobe of the NTKD, far from the active site of the CTKD (Figure 3.3.1.1.A). Additionally, previous studies have suggested that the ERK1/2 is always bound to the CTKD in a resting state and dissociates only upon RSK autophosphorylation on the C-term (Gao *et al.* 2012). Considering the deviance from classical NTKD

interactions and the CTKD crystal structure opposing alpha fold predictions, RSK4 mechanism of activation warrants further investigation.

To elucidate the relationship between the RSK4 NTKD and CTKD a series of experiments were conducted; (i) RSK4 NL3M purification and crystallization to determine the structure of RSK4 NTKD in an active intermediate state; (ii) RSK4 CTKDM purification and crystallization to determine the difference in structure of active and inactive state of RSK4 CTKD; (iii) Kinase assay to determine the activity of the RSK4 CTKD constructs; (iv) Pull-down assay to determine binding between RSK4 CTKD and NTKD (Figure 2.2.1.1).

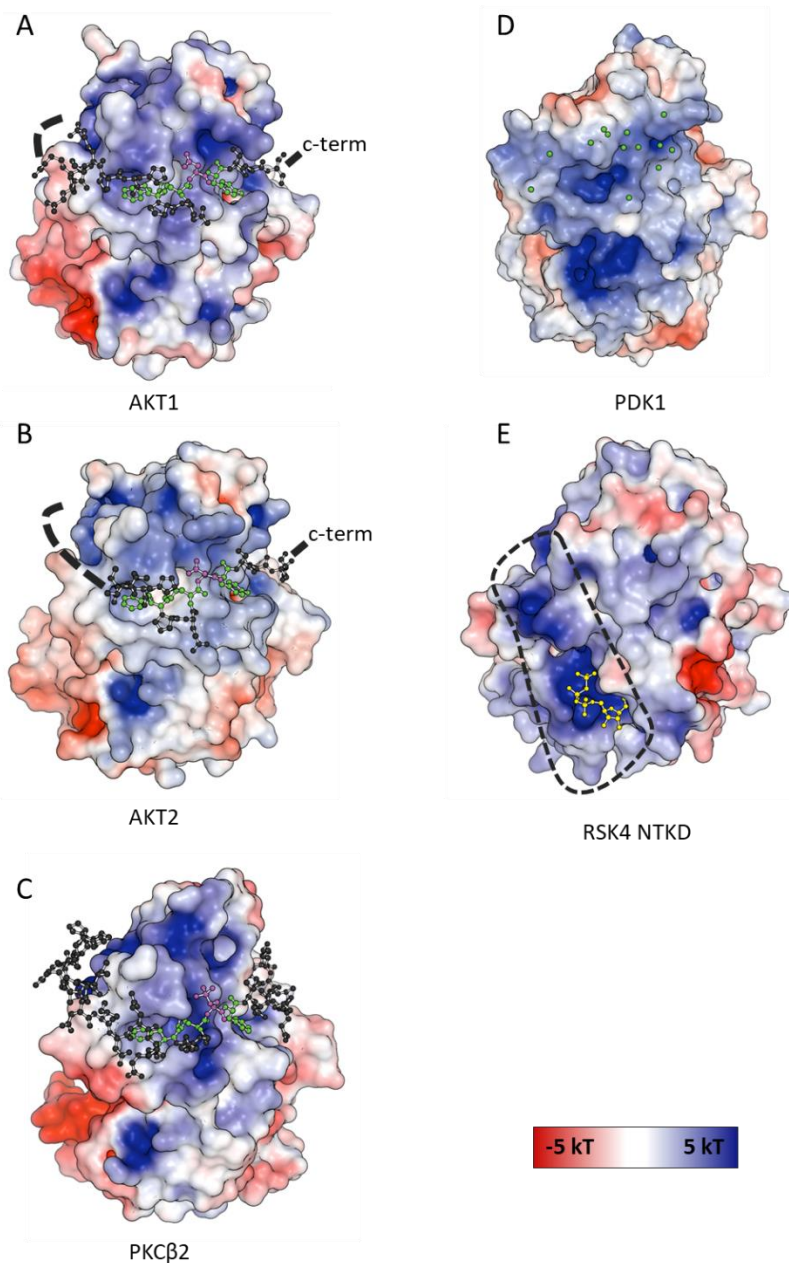


Figure 3.1.1 – RSK4 NTKD has alternative binding to traditional AGC kinases – (A) AKT1, (B) AKT2, (C) PKCβ2 with positive potential in blue and negative potential in red, respectively, from 5 to -5 kT. The phosphorylated C-term is shown as grey ball-and-stick representation, with the hydrophobic residues of the HM in green and in magenta D473, D474 (phospho-mimetic mutant) and pS660 respectively for AKT1, AKT2 and PKCβ2. (D) Electrostatic surface potential representation of PDK1. Green spheres represent the position of residues known to be involved in the binding of the phosphorylated HM of target kinases (K76, K115, I119, R131, L145, F147, T148, Q150, L155, Y156 and F157). (E) Electrostatic surface potential representation of RSK4 NTKD. The second molecule of AMP-PNP is represented in yellow as ball-and-stick.

3.2 – RSK4 N-Terminal Kinase Domain with AGC regulatory region S232E

S389E S372E (RSK4 NL3M)

3.2.1 - Protein Purification and crystallization of RSK4 NL3M

Increasing evidences show that RSK4 is activated in a PDK1 independent manner (Chrysostomou *et al.* 2021). It is hypothesized that the NTKD of RSK4 reaches maximal activity upon binding of the phosphorylated HM to the NTKD. To understand the role of RSK4 regulatory regions in the activation mechanism, the RSK4 NL3M construct was used with the aim to purify and crystalize the protein. This construct spans residues 48-401 which includes the HM region and contains 3 phospho-mimetic mutations S232E, S389E and S372E. The phospho-mimetic mutations replace serine with glutamic acid, which mimics the fully phosphorylated state of serine containing a 2- charge as is the charge of glutamic acid. Furthermore, this replacement of amino acid dictates the 2- charged state cannot be removed by endogenous phosphatases thus keeping the domain in a constitutively active state. The RSK4 NL3M construct was produced with an N-terminal GST fusion tag. The recombinant protein was expressed in *E. coli* using AIM (Chapter 2.3) and purified via affinity chromatography using a GSTrap (Chapter 2.4.2). From SDS analysis it was clear that the first stage of the purification recovered a high quantity of protein (Figure 3.2.1.1), evident by the single band at approximately 67kDa. Following tag cleavage with PreScission protease, 3 major bands were visible on the SDS-PAGE gel: 42kDa, 40kDa and 27kDa, which correspond, respectively, to the PreScission protease, RSK4 NL3M and GST (Figure 3.2.1.1). Anion exchange was used with the aim to remove the remaining contaminants (Chapter 2.4.3). This second purification step was successful in removing the precision protease and most GST contaminants (Figure 3.2.1.2.A). However, based on the SDS analysis, due to the presence of

several closely sized bands under the most abundant band it would suggest that proteolytic cleavage is occurring in the sample, lanes 3-6 of Figure 3.2.2.A. The samples eluted between 170-210 mM NaCl (Figure 3.2.1.2.B) were collected and purified further using size exclusion chromatography (SEC). This was largely unsuccessful as the contaminants present in the load of SEC (Figure 3.2.1.3.A) remained in the final concentrated sample (Figure 3.2.1.4). Nevertheless, samples were collected and concentrated to approximately 4 mg/ml. Prior to crystal trials the sample was concentrated to 10mg/ml in presence of 500 μ M AMP-PNP and 1 mM $MgCl_2$ (Figure 3.2.1.4) with an overall final estimated ~90% purity (not considering the possible RSK4 NL3M degradation). This purified sample was used for crystallography screening (Table 2.5.1.1). Crystallisation trials were set up using commercially available sparse-matrix screens: PEG/Ion (Hampton Research), JCSG+ (Molecular Dimensions), ProPlex (Molecular Dimensions), Structure Screens (Molecular Dimensions), PACT Premier (Molecular Dimensions) and PGA (Molecular Dimensions) (Appendix table 6). The Gryphon liquid handling robot was used to set up crystallisation drops with either 1:1 or 1:2 volume ratios of protein to reservoir using 5, 7.5 and 10 mg/ml of protein. The plates were then incubated at 16°C. However, no crystals were obtained.

The result of these purifications and attempted crystallization trials suggest that the sample is heterogeneous, which in turn hindered the crystallization process. This likely occurred due to accessibility of the N-term region to endogenous proteases. To prevent this, the expression plasmid was changed (pETM-14) producing a new His tag RSK4 NL3M construct which could help restrict access from proteases

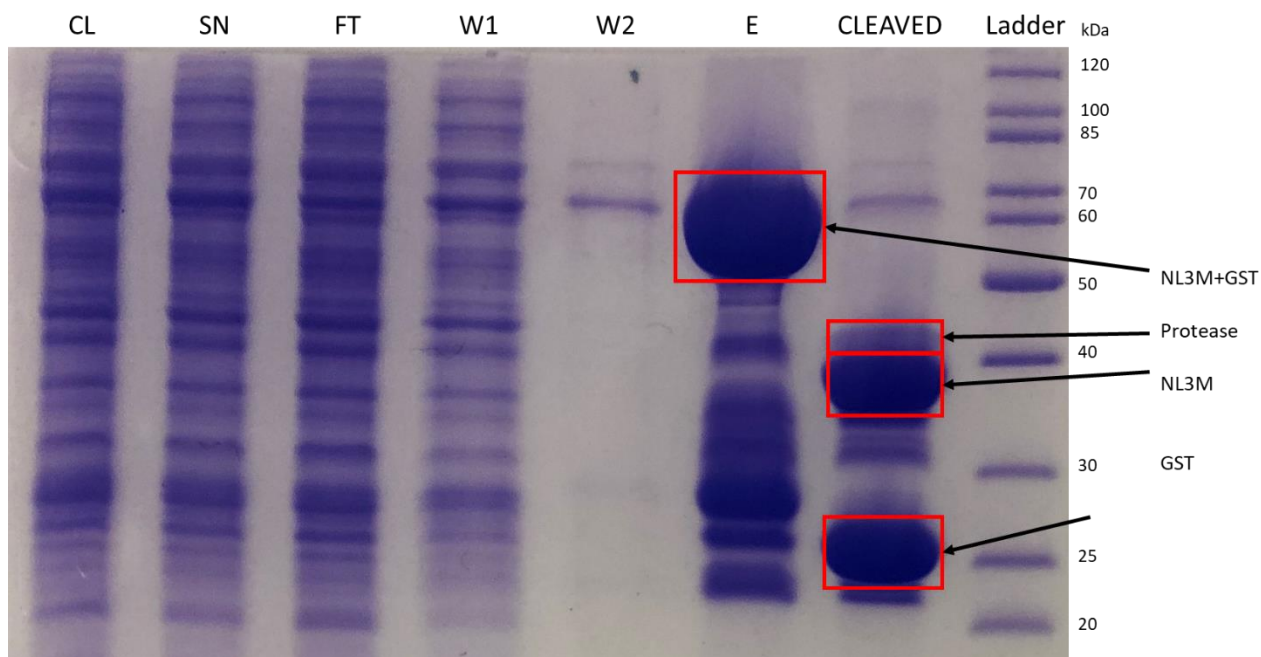


Figure 3.2.1.1 – SDS PAGE of Affinity chromatography of RSK4 NL3M - The GST-tag based purification was carried out on a GStrap HP 5ml column at a constant flow rate of 2ml/min was used. 5 μ l of protein ladder mixed with loading dye was used (Ladder). 10 μ l of samples mixed with 2X lamelli loading dye were loaded onto an SDS-PAGE gel for 45 minutes at 200V. The gel was then stained with Coomassie blue stain for 1 hour and then destained overnight. Red boxes were used to highlight which bands correspond to which protein. CL=Cell Lysate, SN=Supernatant, FT=Flow Through, W1=Wash 1, W2=Wash 2, E= Elution, CLEAVED=after precision protease digestion.

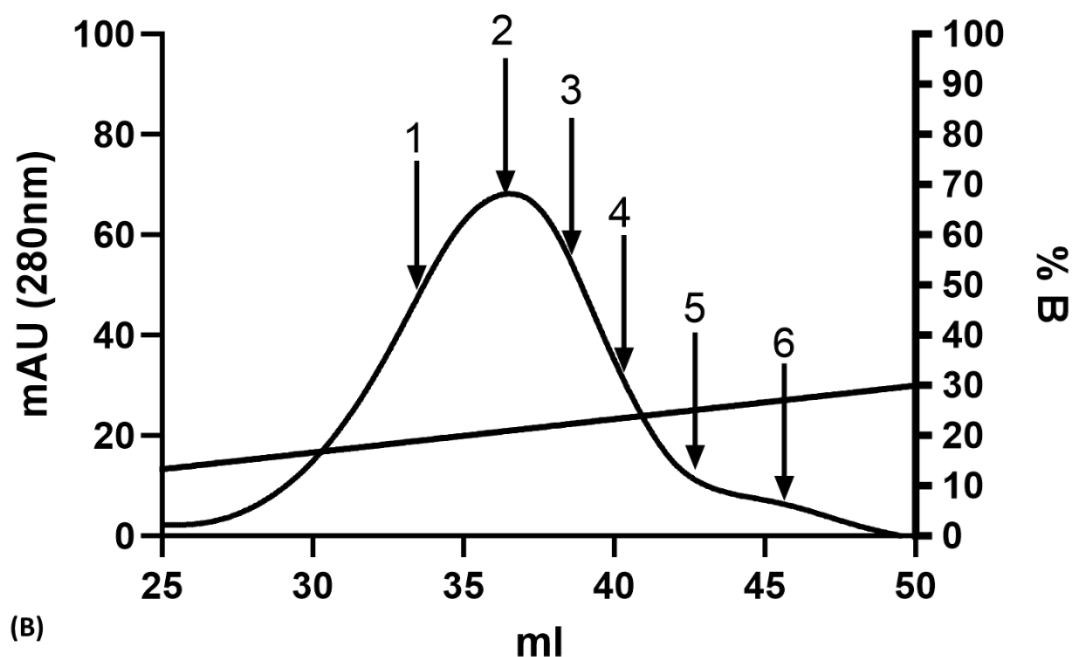
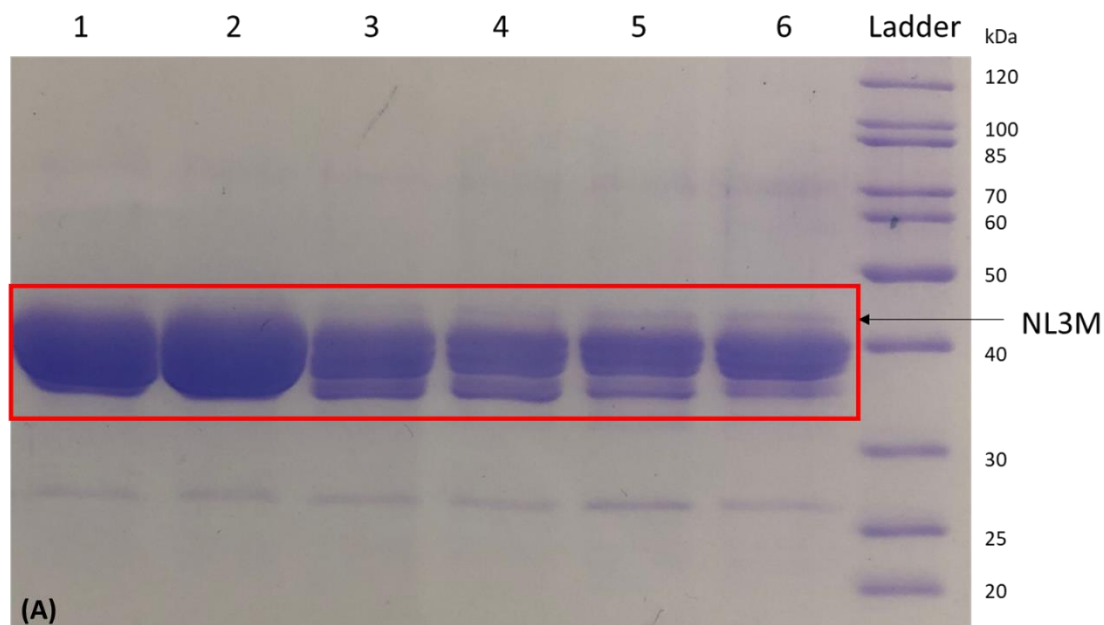


Figure 3.2.1.2 – SDS PAGE and chromatogram of Anion Exchange of RSK4

NL3M - A) The purification was completed on a 5ml HiTrap Q HP where 1ml/min flow rate was used. 5 μ l of ladder and 10 μ l of samples mixed with 2X lamelli loading dye were loaded onto an SDS-PAGE gel for 45 minutes at 200V. The gel was then stained with Coomassie blue stain for 1 hour and then destained overnight. Numbers above SDS correspond to the points on B in which samples were taken. B) Chromatogram data for corresponding experiment. The x-axis represents volume of buffer (ml) which had been applied to the column, the left Y-axis shows the absorbance (mAU) at 280nm and the right Y-axis depicts the % of buffer B.

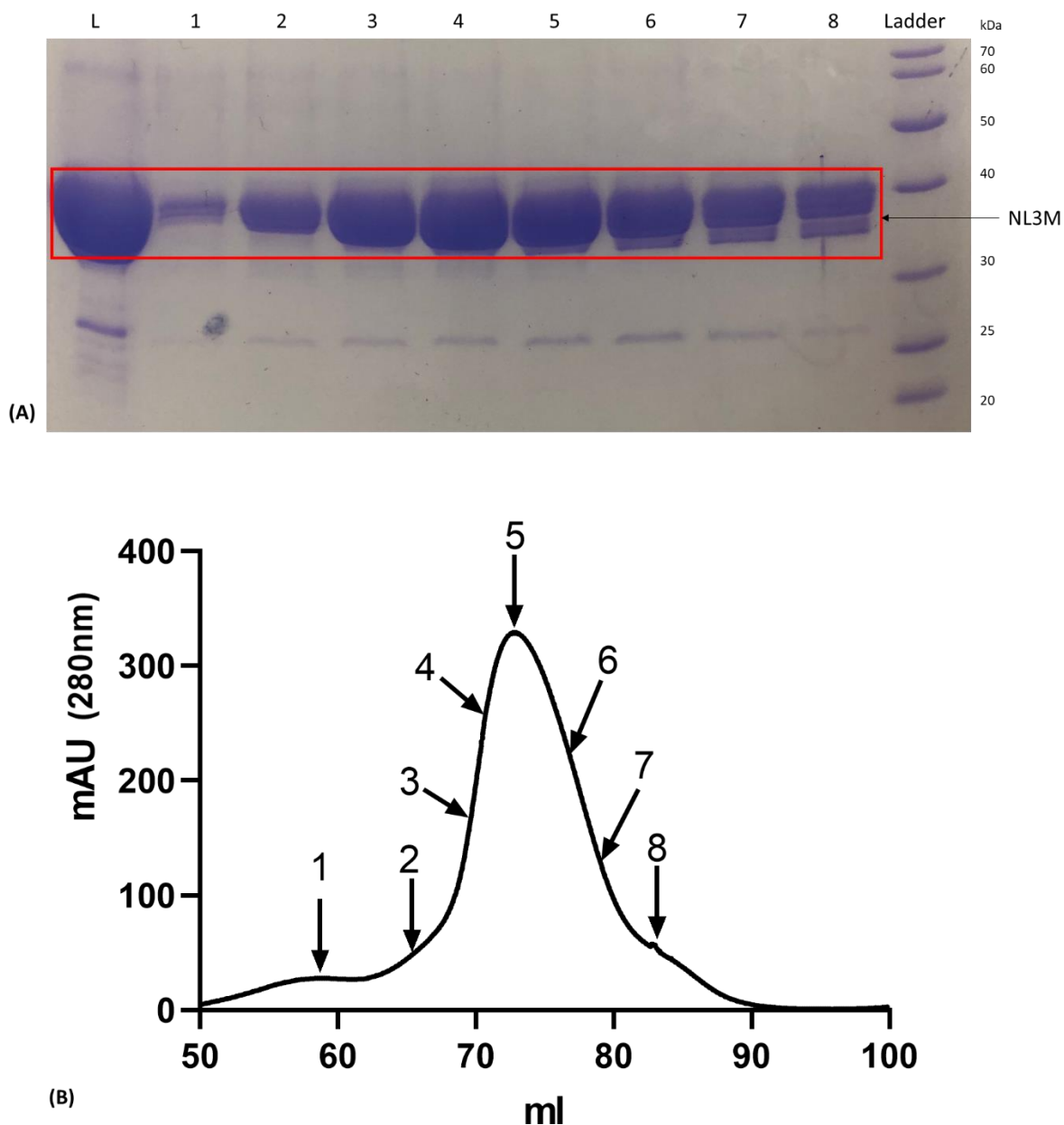


Figure 3.2.1.3 – SDS PAGE and chromatogram of RSK4 NL3M SEC - A) A Superdex 75 G 16/60 was used for the gel filtration purification, flow rate of 1 ml/min was used. 5 μ l of ladder and 10 μ l of samples mixed with 2X lamelli loading dye were loaded onto an SDS-PAGE gel for 45 minutes at 200V. The gel was then stained with Coomassie blue stain for 1 hour and then destained with destain buffer overnight. Numbers above SDS correspond to the points on B in which samples were taken. B) Chromatogram data for corresponding experiment. The x-axis represents volume of buffer (ml) which had been applied to the column, the Y-axis shows the absorbance (mAU) at 280nm

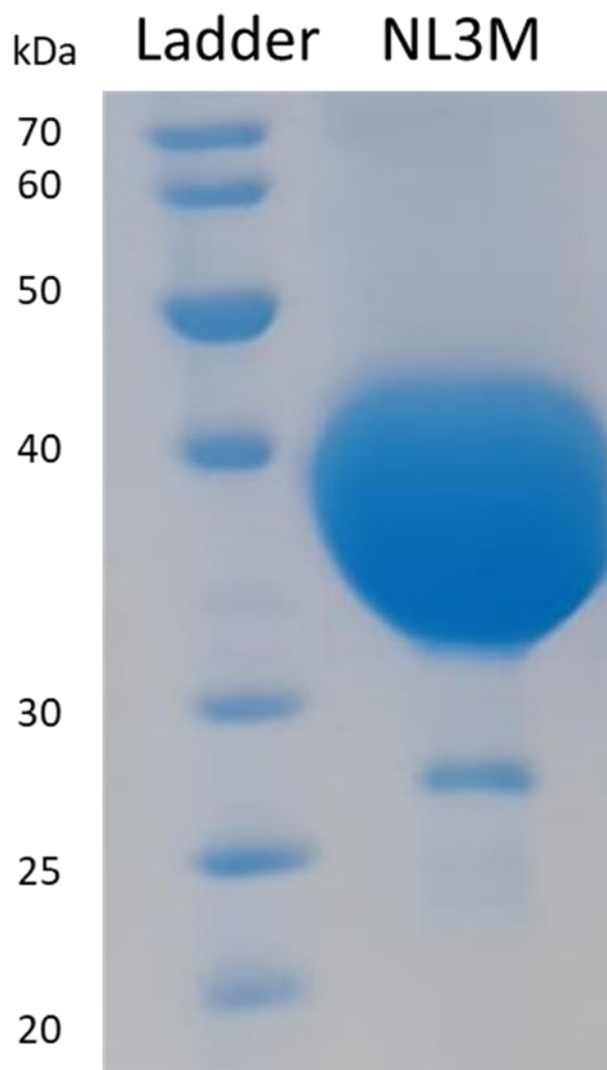


Figure 3.2.1.4 – SDS PAGE of 10mg/ml RSK4 NL3M - 5 μ l of ladder and 10 μ l of sample was mixed with 2X lamelli loading dye were loaded onto an SDS-PAGE gel for 45 minutes at 200V. The gel was then stained with Simply blue stain for 1 hour and then destained overnight.

3.3 – RSK4 C-Terminal Kinase Domain (RSK4 CTKD)

3.3.1 - Protein purification and crystallization of RSK4 CTKD

Superposition of the structures of RSK1 CTKD in complex with ERK2 (Alexa *et al.* 2015) and RSK1 AlphaFold model show that the model is not in agreement with the experimental structures, as according to the model, ERK2 would clash with the NTKD (Figure 3.3.1.1). This suggests that the AlphaFold model is not representative of a resting or early stage of the kinase activation. Lack of structural data on RSK intermediate stages of activation prevent us from assessing if, the AlphaFold model is representative of late stage RSK activation. Thus, more structural studies on the RSK4 CTKD alone and in complex with the RSK4 NL3M are needed to clarify the roles different domains play in protein regulation. The RSK4 CTKD was cloned into a pETM14 plasmid, which produced a N-terminal His-tag fused protein (Chapter 2.2.1). The recombinant protein was expressed in *E. coli* using AIM (Chapter 2.3). RSK4 CTKD, similarly to RSK4 NL3M, was initially purified using affinity chromatography using a HisTrap Crude FF (Chapter 2.4.2). SDS analysis of the purification showed a single band at 27kDa, this doesn't coincide directly with the molecular weight of the RSK4-CTKD sequence of 31.3 kDa. However, analysis across all samples shows substantial overexpression of a protein with an apparent molecular mass of 27 kDa (Figure 3.3.1.2). Protein sample was further purified via anion exchange chromatography (Chapter 2.4.3). RSK4-CTKD showed low solubility in low salt buffers and precipitated during the initial steps of sample dilution and injection in the ion exchange column. This was overcome with two optimizations: i) instead of concentrating the protein and then diluting it with CTKD Buffer A (Appendix Table 3) to promote binding with the column resin, a more "gentle" overnight dialysis in low salt buffer was carried out; ii) the salt concentration for the ion exchange equilibration

buffer was increased from 0 Mm to 50 Mm NaCl. These were successful in preventing protein precipitation. However, this second step of purification failed to remove high molecular mass contaminants via ion exchange chromatography (Figure 3.3.1.3.A/B). The protein samples collected eluted over the range of 200-300 Mm NaCl which correspond to lanes 3-7 (Figure 3.3.1.3.A/B). Size exclusion chromatography was then used to further purify RSK4 CTKD. The first half of the peak contained more contaminants thus fractions corresponding to the second half of the elution peak were pooled together and concentrated to approximately 4 mg/ml and stored (Figure 3.3.1.4.A/B). In a similar manner to RSK4 NL3M, concentrated protein (5, 7.5 and 10 mg/ml) was supplemented with 500 Mm AMP-PNP and 1 Mm MgCl₂ (Figure 3.3.1.5). Crystallisation trials were set up using commercially available sparse-matrix screens (Table 2.5.1.1) using the Gryphon liquid handling robot at 1:1 or 1:2 volume ratios of protein to reservoir and incubated at 16 °C.

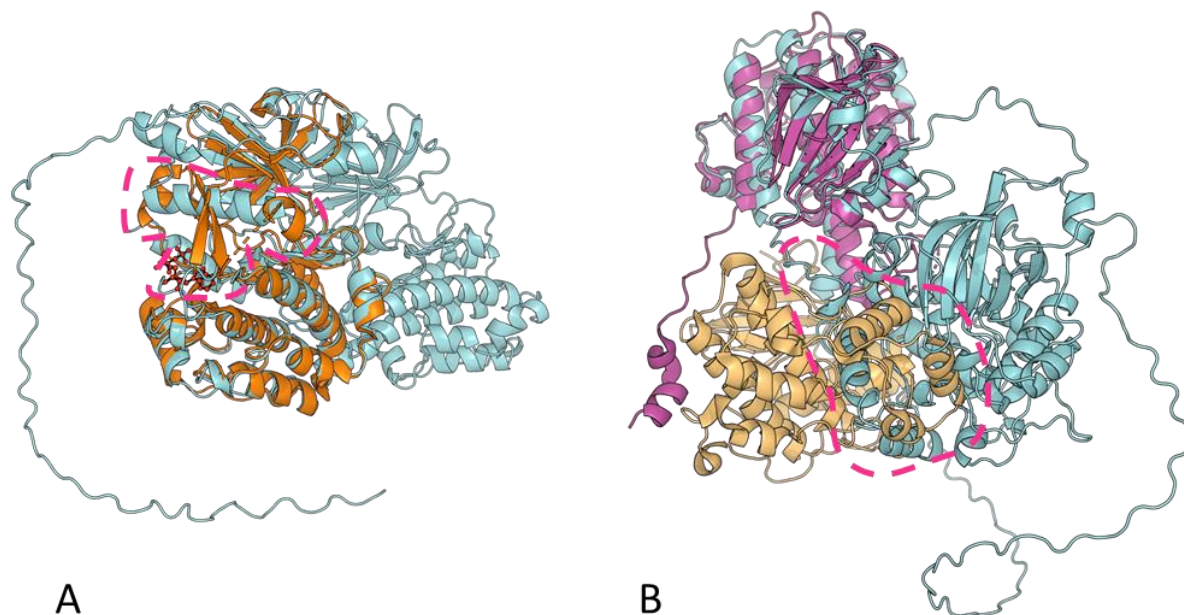


Figure 3.3.1.1 – RSK alpha fold models - A) Cartoon representation of RSK4 AlphaFold model (in cyan) superimposed to RSK4 NTKD structure (in orange). The model shows a classic kinase fold, which differs from the experimental structure (highlighted in pink dotted line). **B) Cartoon representation of RSK1 AlphaFold model (in cyan) superimposed to RSK1 CTKD (in purple) in complex with ERK2 (in light orange).** The resting state position of ERK2 is not compatible with the model, as this would result in a clash between ERK2 and the NTKD (highlighted in pink dotted line).

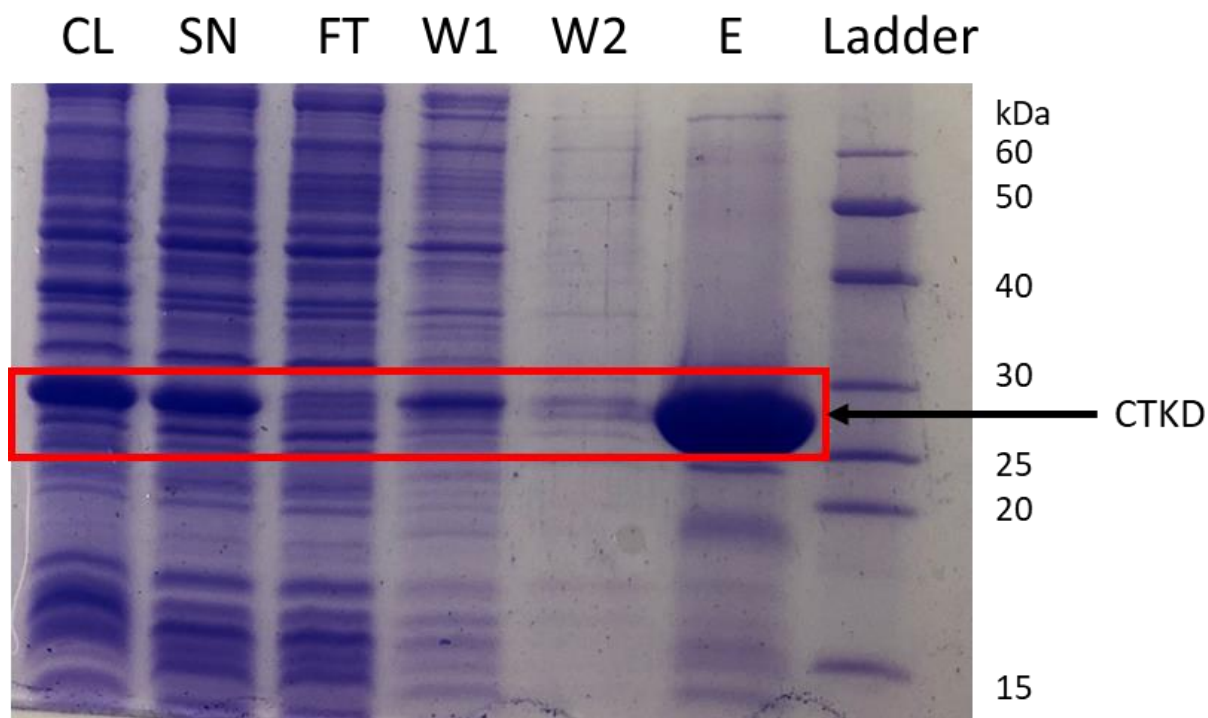
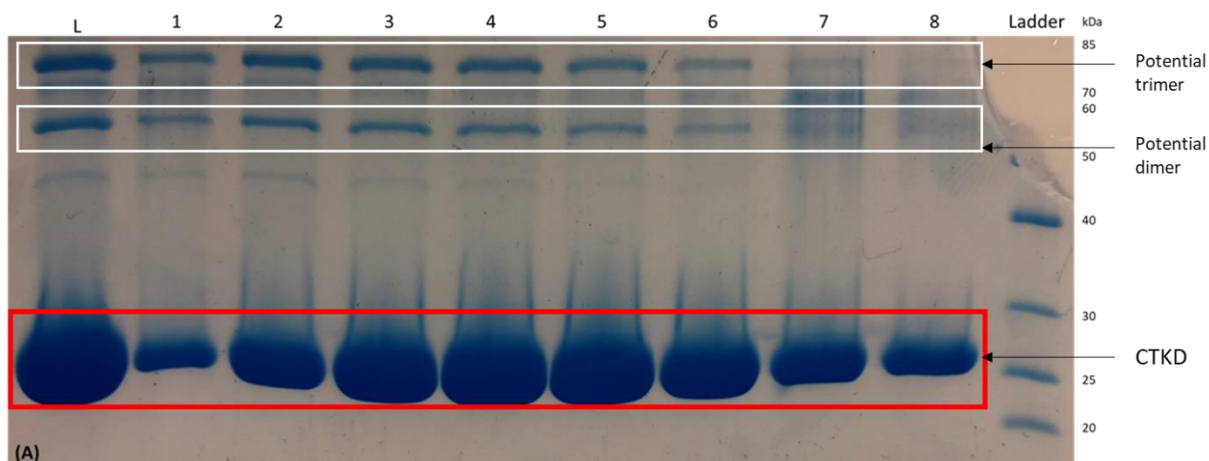
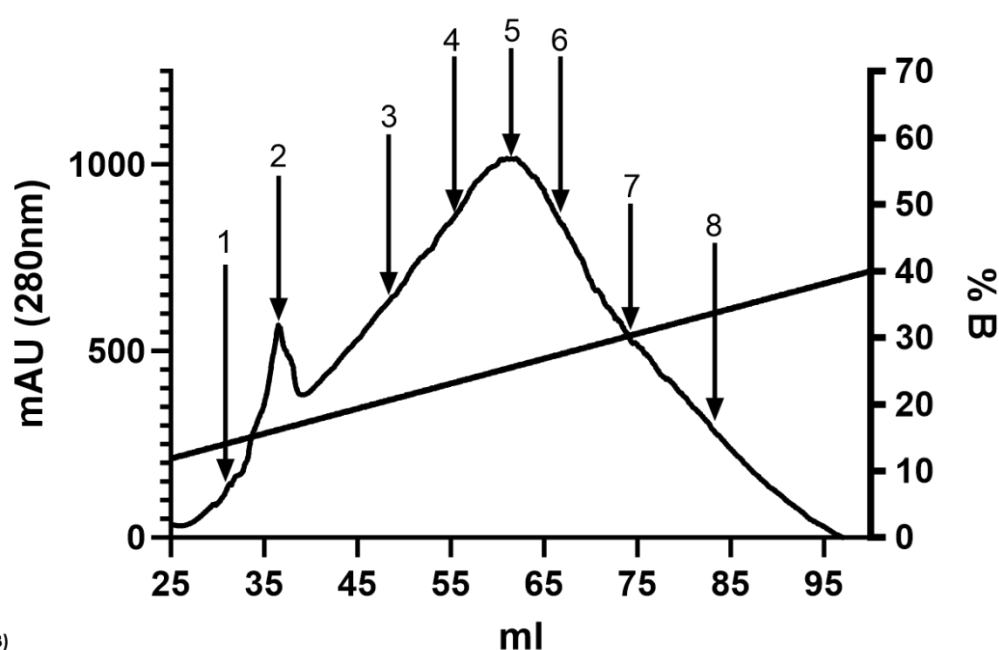


Figure 3.3.1.2 – SDS PAGE analysis of Affinity chromatography of RSK4 CTKD (AIM expression) - The Hexa-histidine tag based purification was carried out on a His trap crude FF 5ml column at a constant flow rate of 2ml/min was used. 5 μ l of ladder mixed with loading dye was used. 10 μ l of samples mixed with 2X lamelli loading dye were loaded onto an SDS-PAGE gel for 45 minutes at 200V. The gel was then stained with Coomassie blue stain for 1 hour and then destained overnight. Red boxes were used to highlight which bands correspond to the CTKD. CL=Cell Lysate, SN=Supernatant, FT=Flow Through, W1=Wash 1, W2=Wash 2, and E= Elution.



(A)



(B)

Figure 3.3.1.3 – SDS PAGE and chromatogram of RSK4 CTKD anion exchange (AIM expression) – A) The purification was completed on a 5ml HiTrap Q HP where 1ml/min flow rate was used. 5 μ l of ladder and 10 μ l of samples mixed with 2X lamelli loading dye were loaded onto an SDS-PAGE gel for 45 minutes at 200V. The gel was then stained with Coomassie blue stain for 1 hour and then destained overnight. Numbers above SDS correspond to the points on B in which samples were taken. B) Chromatogram data for corresponding experiment. The x-axis represents volume of buffer (ml) which had been applied to the column, the left Y-axis shows the absorbance (mAU) at 280nm and the right Y-axis depicts the % of buffer B.

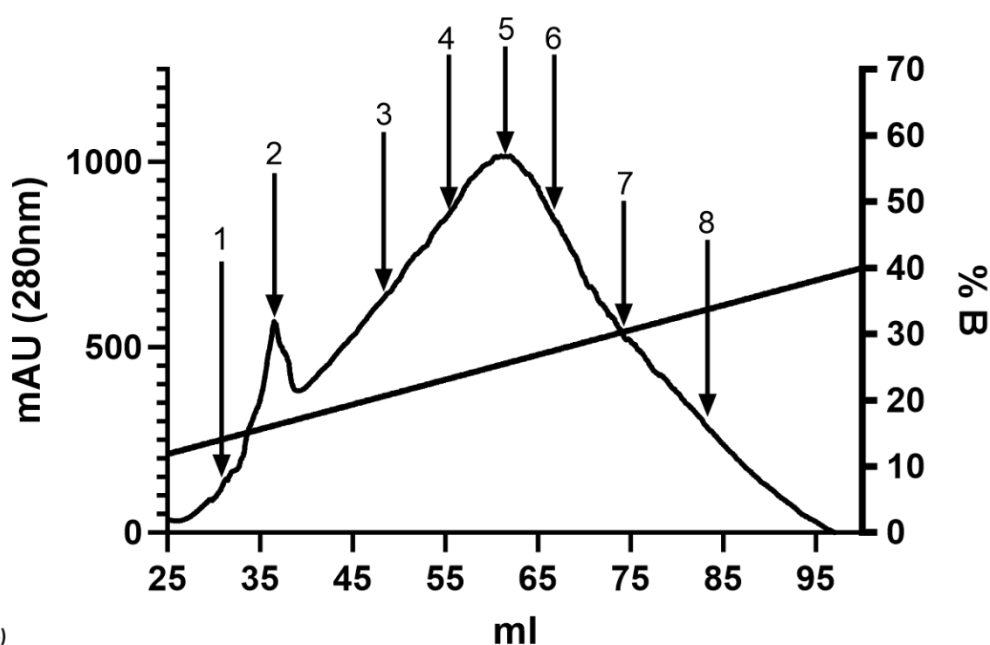
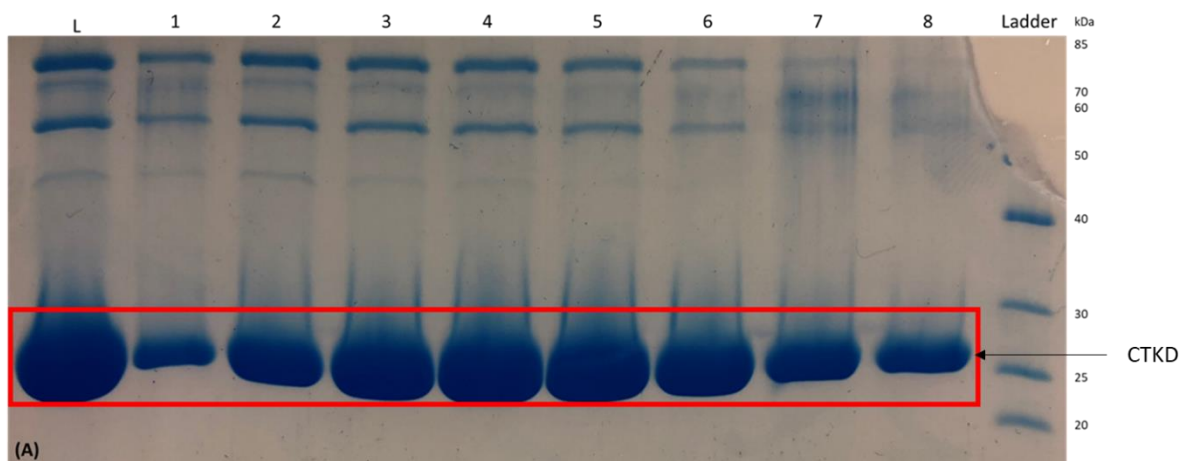


Figure 3.3.1.4 – SDS PAGE and chromatogram of RSK4 CTKD Size exclusion (AIM expression) – A) A Superdex 75 G 16/60 was used for the size exclusion purification, flow rate of 1ml/min was used. 5 μ l of ladder and 10 μ l of samples mixed with 2X lamelli loading dye were loaded onto an SDS-PAGE gel for 45 minutes at 200V. The gel was then stained with Coomassie blue stain for 1 hour and then destained with destain buffer overnight. Numbers above SDS correspond to the points on B in which samples were taken. B) Chromatogram data for corresponding experiment. The x-axis represents volume of buffer (ml) which had been applied to the column, the Y-axis shows the absorbance (mAU) at 280nm

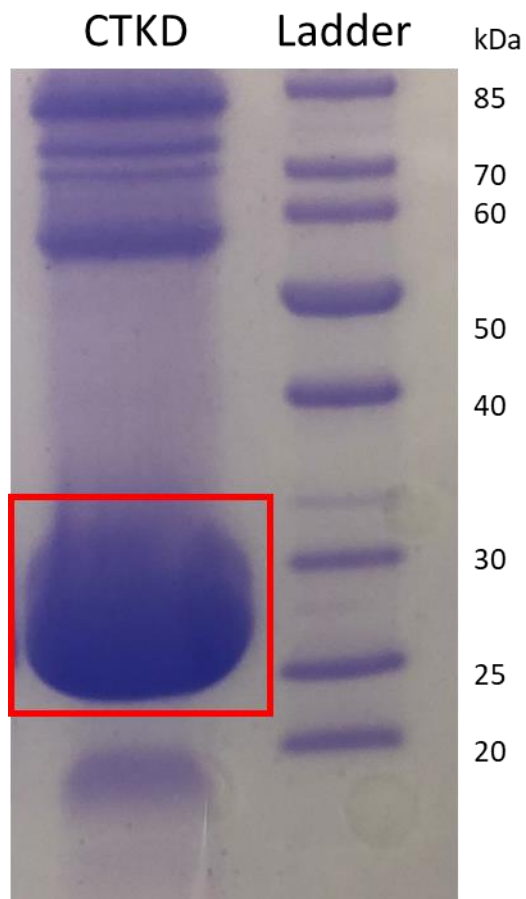


Figure 3.3.1.5 – SDS PAGE analysis of RSK4 CTKD at 10mg/ml (AIM expression) - 5 μ l of ladder and 10 μ l of sample was mixed with 2X lamelli loading dye were loaded onto an SDS-PAGE gel for 45 minutes at 200V. The gel was then stained with Coomassie blue stain for 1 hour and then destained overnight. Red box depicts which band is the protein of interest RSK4 CTKD.

To evaluate if the failed crystallisation trials were due to excessive level of contaminations (Figure 3.3.1.5) (Kim *et al.* 2008), the expression media was changed to LB. In fact, while AIM media has been shown to improve protein production in bacterial system (Studier 2005), it is a complex media which favors cell growth, resulting in a lower recombinant protein:bacterial proteins ratio. Following the same purification protocol as optimized for the RSK4 CTKD produced in AIM media, it was possible to see a reduction in contaminants during affinity chromatography (Figure 3.3.1.6). However, upon sample concentration, clear high molecular weight contaminants were visible in both the ion exchange (Figure 3.3.1.7) and size exclusion (Figure 3.3.1.8) elution samples. Crystal trials were then conducted for the new RSK4 CTKD sample but again yielded no crystals (Table 2.5.1.1). Overall, the final RSK4 CTKD sample had a reduced level of contaminants when expressed in LB (Figure 3.3.1.9), but it is still not possible to rule out that the presence of high molecular weight proteins prevented protein crystallization.



Figure 3.3.1.6 – SDS PAGE analysis of Affinity chromatography of RSK4 CTKD (LB expression) - The Hexa-histidine tag based purification was carried out on a His trap crude FF 5ml column at a constant flow rate of 2ml/min was used. 5 μ l of ladder mixed with loading dye was used. 10 μ l of samples mixed with 2X lamelli loading dye were loaded onto an SDS-PAGE gel for 45 minutes at 200V. The gel was then stained with Simply blue stain for 1 hour and then destained overnight. Red boxes were used to highlight which bands correspond to RSK4 CTKD. CL=Cell Lysate, SN=Supernatant, FT=Flow Through, W1=Wash 1, W2=Wash 2, and E= Elution.

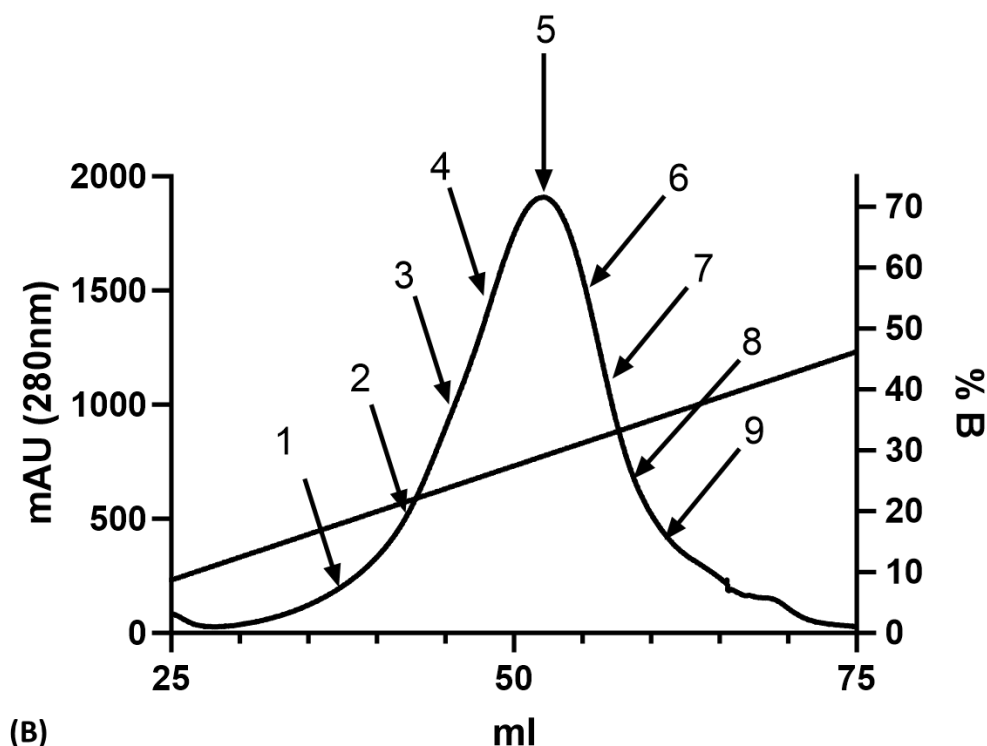
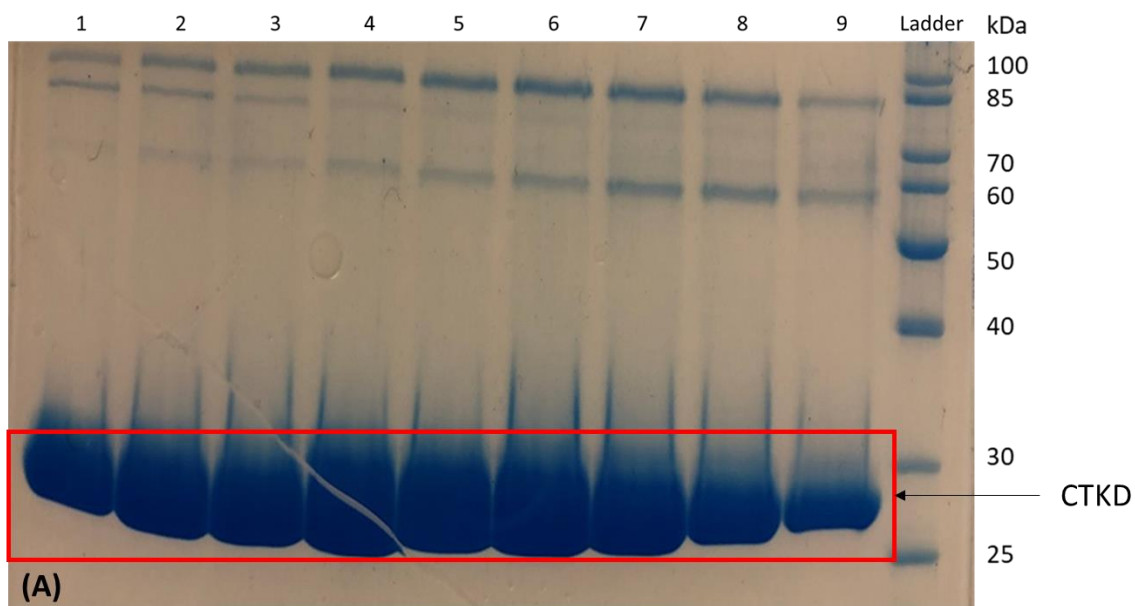


Figure 3.3.1.7 – SDS PAGE and chromatogram of RSK4 CTKD anion exchange (LB expression) – A) The purification was completed on a 5ml HiTrap Q HP where 1ml/min flow rate was used. 5 μ l of ladder and 10 μ l of samples mixed with 2X lamelli loading dye were loaded onto an SDS-PAGE gel for 45 minutes at 200V. The gel was then stained with Simply blue stain for 1 hour and then destained overnight. Numbers above SDS correspond to the points on B in which samples were taken. B) Chromatogram data for corresponding experiment. The x-axis represents volume of buffer (ml) which had been applied to the column, the left Y-axis shows the absorbance (mAU) at 280nm and the right Y-axis depicts the % of buffer B.

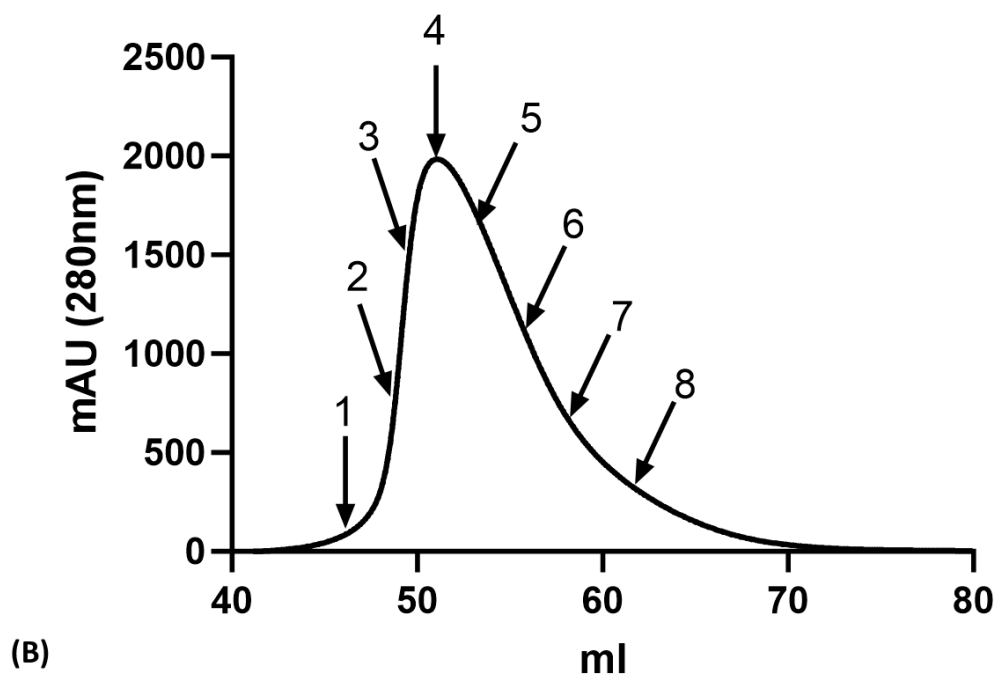
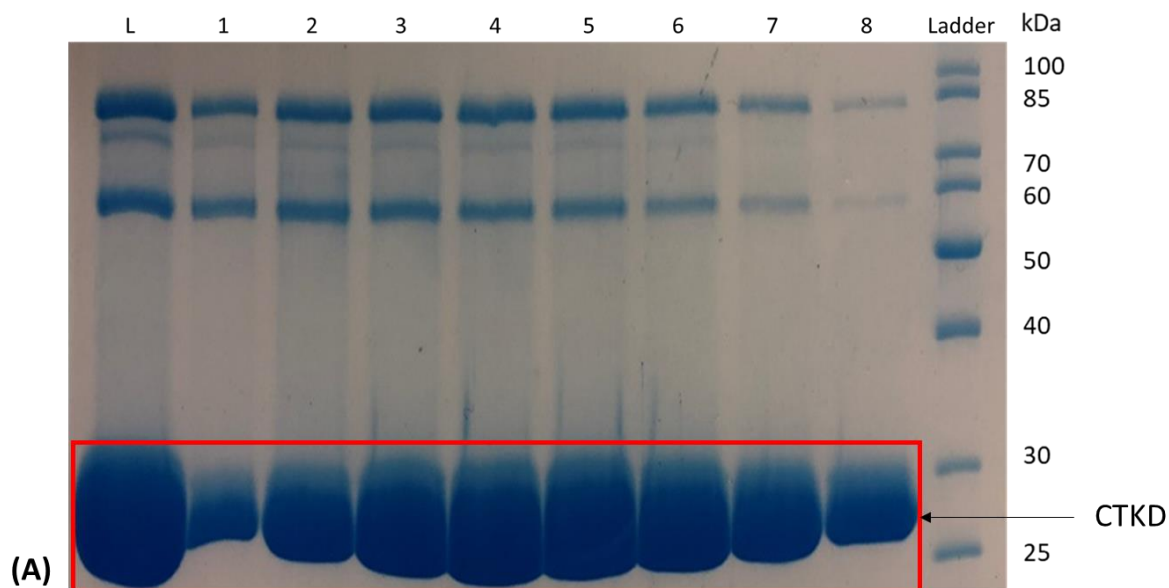


Figure 3.3.1.8 – SDS PAGE and chromatogram of RSK4 CTKD Size exclusion (LB expression) – A) A Superdex 75 G 16/60 was used for the size exclusion purification, flow rate of 1ml/min was used. 5 μ l of ladder and 10 μ l of samples mixed with 2X lamelli loading dye were loaded onto an SDS-PAGE gel for 45 minutes at 200V. The gel was then stained with Simply blue stain for 1 hour and then destained with destain buffer overnight. Numbers above SDS correspond to the points on B in which samples were taken. B) Chromatogram data for corresponding experiment. The x-axis represents volume of buffer (ml) which had been applied to the column, the Y-axis shows the absorbance (mAU) at 280nm.

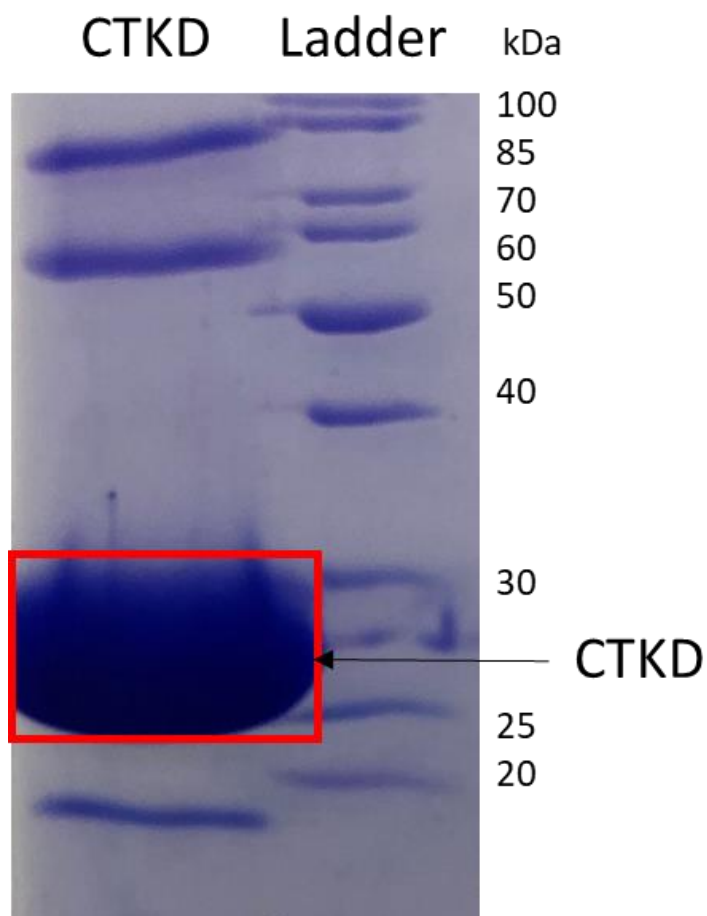


Figure 3.3.1.9 – SDS PAGE analysis of RSK4 CTKD at 10mg/ml (LB expression)

- 5 μ l of ladder and 10 μ l of sample was mixed with 2X lamelli loading dye were loaded onto an SDS-PAGE gel for 45 minutes at 200V. The gel was then stained with Coomassie blue stain for 1 hour and then destained overnight. Red box depicts which band is the protein of interest RSK4 CTKD.

3.4 – RSK4 C-Terminal Kinase Domain T581E (RSK4 CTKDM)

3.4.1 - Protein purification and crystallization of RSK4 CTKDM

In an attempt to produce a more stable RSK4 CTKD and achieve higher final sample purity, a new RSK4 CTKD construct was cloned. Previous studies on the NTKD (Chrysostomou *et al.* 2021) have shown that inserting a phospho-mimetic mutation on the kinase activation loop causes protein activation and increased protein stability. As such, a phospho-mimetic mutation on the CTKD activation loop, T581E, was incorporated into the kinase activation loop creating RSK4 CTKDM. The recombinant protein was expressed in *E.coli* using AIM and purified using the same protocol optimized for RSK4 CTKD. SDS analysis revealed a single band at 27kDa which coincides with RSK4 CTKD (Figure 3.4.1.1). Despite the presence of high molecular weight contaminants, the ratio of RSK4 CTKDM:bacterial proteins is higher than in the RSK4 CTKD sample. Further analysis of SDS-PAGE from anion exchange (Figure 3.4.1.2) and size exclusion (Figure 3.4.1.3) Chromatographies continued to show a higher level of purity of the RSK4 CTKDM samples when compared to the RSK4 CTKD. Once concentrated to 10 mg/ml it was clear that the phospho-mimetic mutation of RSK4 CTKDM had allowed to reach a higher level of sample purity, suitable for crystallization trials (Figure 3.4.1.4). Similarly, to RSK4 CTKD, varied concentrations of RSK4 CTKDM (Table 2.5.1.1) were supplemented with 500 μ M AMP-PNP and 1 mM MgCl₂. Crystallisation trials were set up using commercially available sparse-matrix screens (Table 2.5.1.1). The Gryphon liquid handling robot was used to set up crystallisation drops with either 1:1 or 1:2 volume ratios of protein to reservoir. The plates were then incubated at 16°C. Similarly, to RSK4 CTKD no crystals were obtained.

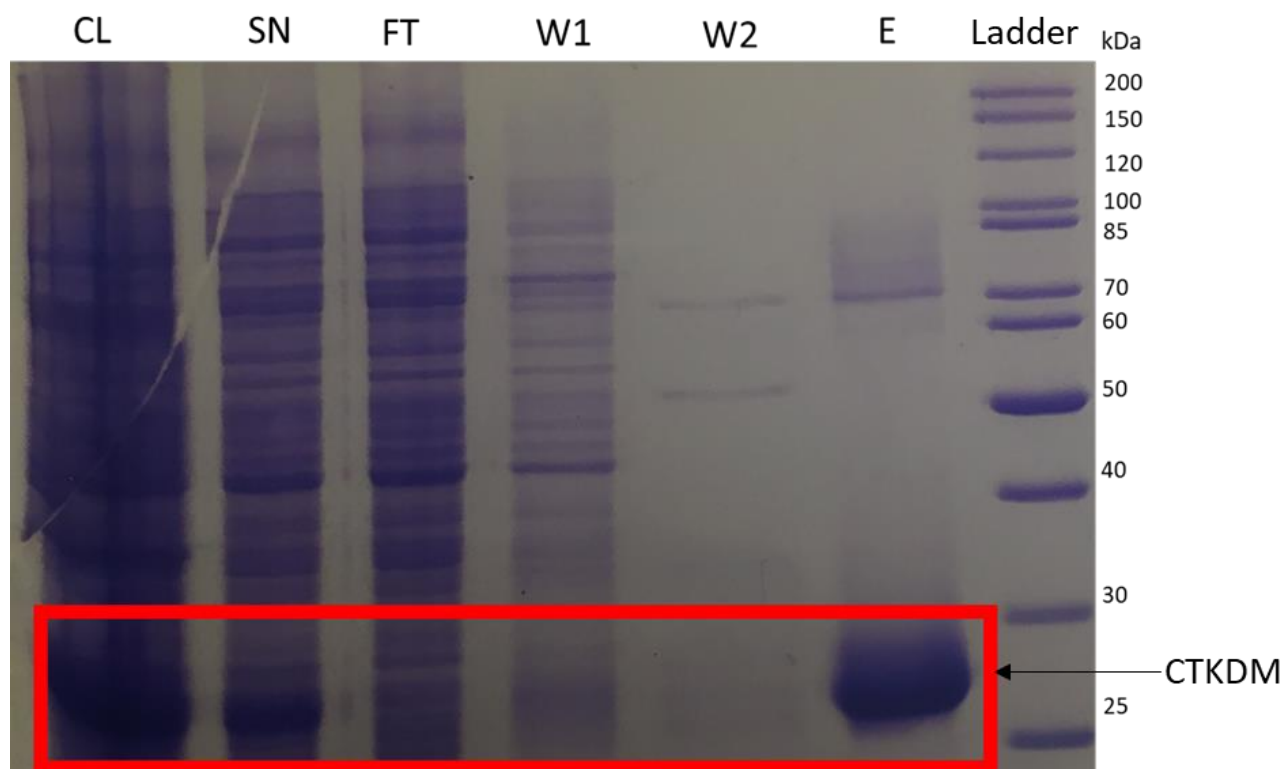


Figure 3.4.1.1 – SDS PAGE analysis of RSK4 CTKDM affinity chromatography (AIM expression) – The Hexa-histidine tag based purification was carried out on a His trap crude FF 5ml column at a constant flow rate of 2ml/min was used. 5 μ l of ladder mixed with loading dye was used. 10 μ l of samples mixed with 2X lamelli loading dye were loaded onto an SDS-PAGE gel for 45 minutes at 200V. The gel was then stained with Coomassie blue stain for 1 hour and then destained overnight. CL=Cell Lysate, SN=Supernatant, FT=Flow Through, W1=Wash 1, W2=Wash 2, and E= Elution.

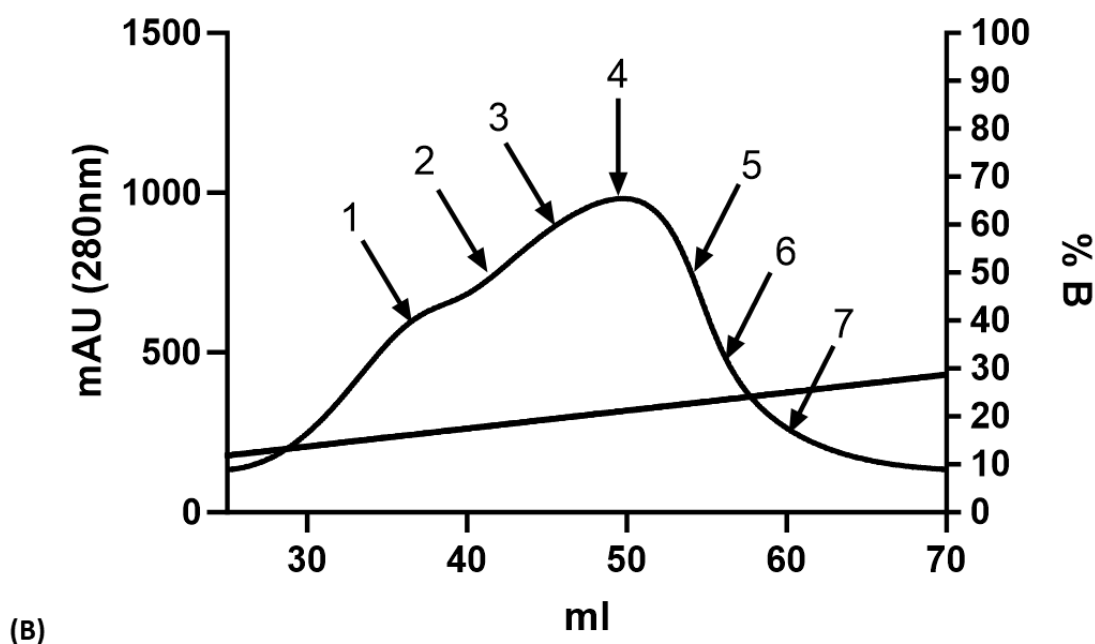
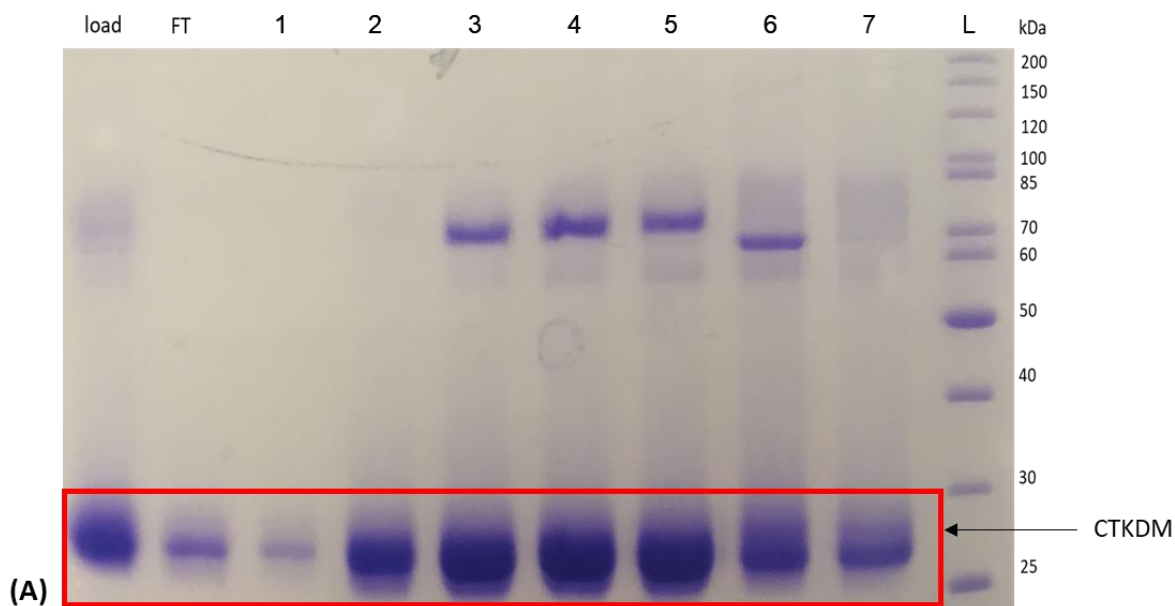


Figure 3.4.1.2 – SDS PAGE analysis and chromatogram of RSK4 CTKDM anion exchange (AIM expression) – A) The purification was completed on a 5ml HiTrap Q HP where 1ml/min flow rate was used. 5 μ l of ladder and 10 μ l of samples mixed with 2X lamelli loading dye were loaded onto an SDS-PAGE gel for 45 minutes at 200V. The gel was then stained with Coomassie blue stain for 1 hour and then destained overnight. Numbers above SDS-PAGE correspond to the points on B in which samples were taken. B) Chromatogram data for corresponding experiment. The x-axis represents volume of buffer (ml) which had been applied to the column, the left Y-axis shows the absorbance (mAU) at 280nm and the right Y-axis depicts the % of buffer B.

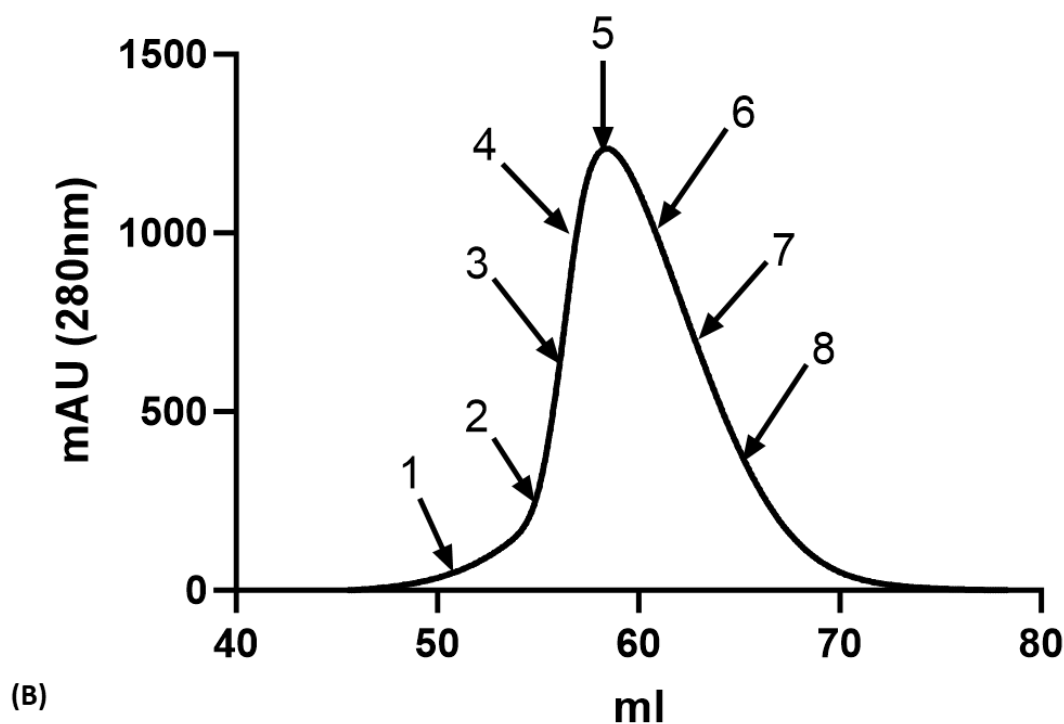
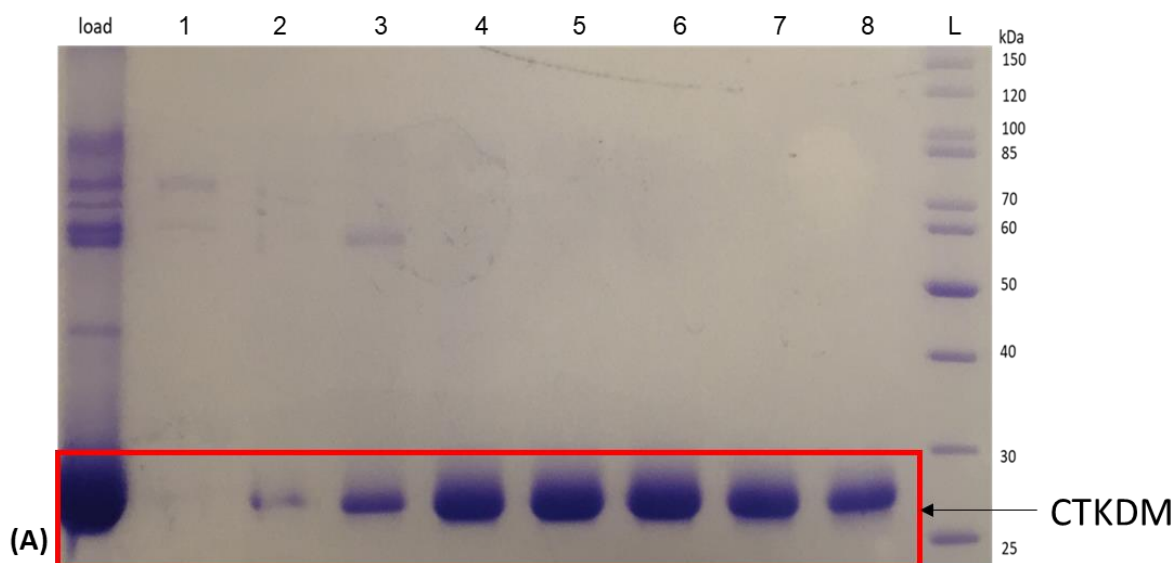


Figure 3.4.1.3 – SDS PAGE analysis and chromatogram of RSK4 CTKDM Size exclusion (AIM expression) – A) A Superdex 75 G 16/60 was used for the size exclusion purification, flow rate of 1ml/min was used. 5 μ l of ladder and 10 μ l of samples mixed with 2X lamelli loading dye were loaded onto an SDS-PAGE gel for 45 minutes at 200V. The gel was then stained with Coomassie blue stain for 1 hour and then destained with destain buffer overnight. Numbers above SDS correspond to the points on B in which samples were taken. B) Chromatogram data for corresponding experiment. The x-axis represents volume of buffer (ml) which had been applied to the column, the Y-axis shows the absorbance (mAU) at 280nm.

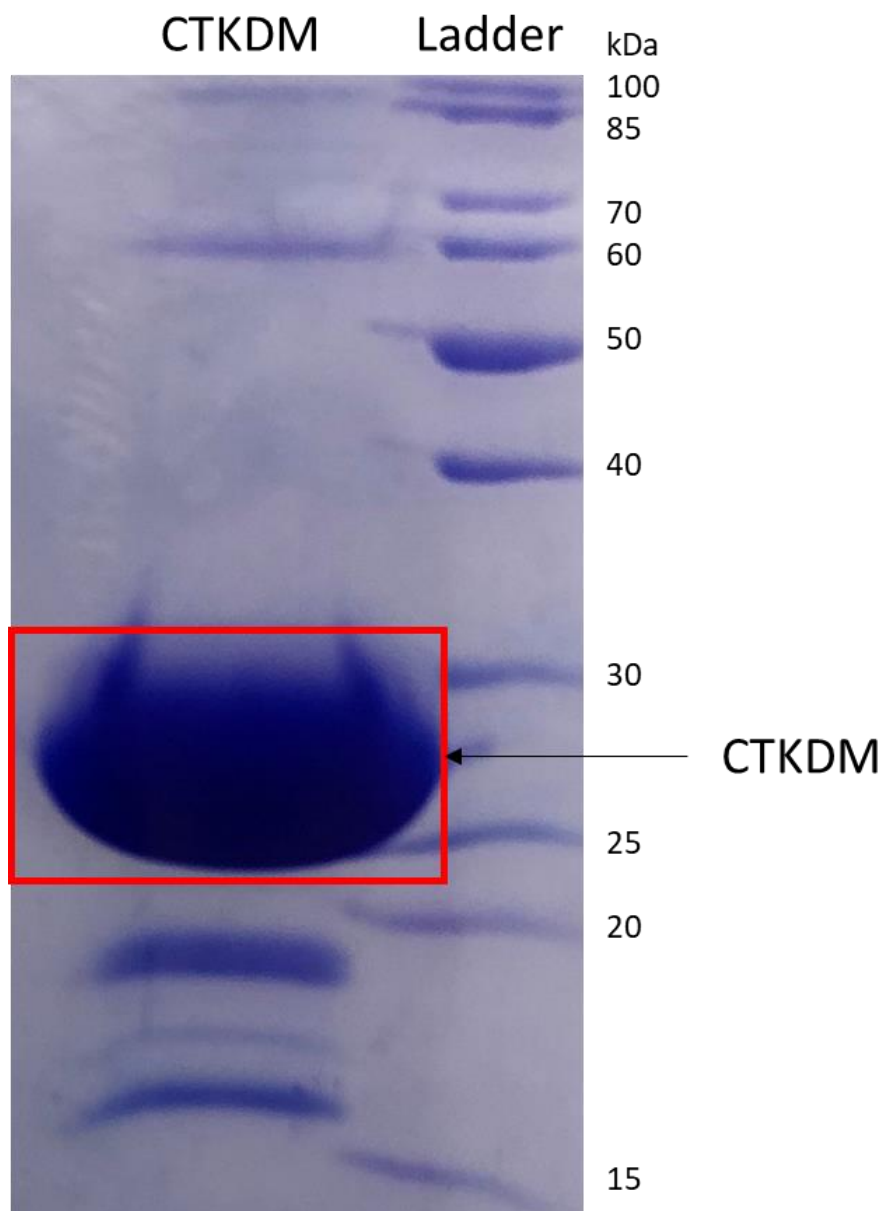


Figure 3.4.1.4 – SDS PAGE analysis of RSK4 CTKDM at 10mg/ml (AIM expression) – 5 μ l of ladder and 10 μ l of sample was mixed with 2X lamelli loading dye were loaded onto an SDS-PAGE gel for 45 minutes at 200V. The gel was then stained with Coomassie blue stain for 1 hour and then destained overnight. Red box depicts which band is the protein of interest RSK4 CTKDM.

For RSK4 CTKD, an improvement in purity was observed by changing the expression media from AIM (Figure 3.3.1.4) to LB (Figure 3.3.1.8). The same approach was applied to RSK4 CTKDM. Using the same optimized purification protocol, no improvement in purity was observed (figure 3.4.1.5-7). However, this is most likely due to varied concentrations of samples across experiments, as when the final RSK4 CTKDM AIM (Figure 3.4.1.4) and LB (Figure 3.4.1.8) samples were compared a reduction in contaminants is clear. Crystal trials were then conducted with RSK4 CTKDM LB samples in the same manner as previously mentioned (Table 2.5.1.1). This process yielded one potential crystal (Figure 3.4.1.9). Following this the condition optimization was attempted using traditional hanging droplet plates keeping a ratio of 1:1 protein:reservoir, while pH of buffer and the amount of PEG4000 were changed (Table 2.5.2.1). Additionally, a mixed matrix approach was attempted: 2 μ l of varied concentrations of RSK4 CTKDM were added to 4 μ l of buffer, while also screening for optimal pH and PEG concentrations (Table 2.5.2.2). However, it was not possible to reproduce RSK4 CTKDM crystallization. Attempts to reproduce crystallisation using original solutions and gryphon robot produced no crystals. Seeding plates were also set up in the traditional manner yet still yielded no additional crystals suggesting the identified crystal was most likely a salt crystal (Table 2.5.2.3).

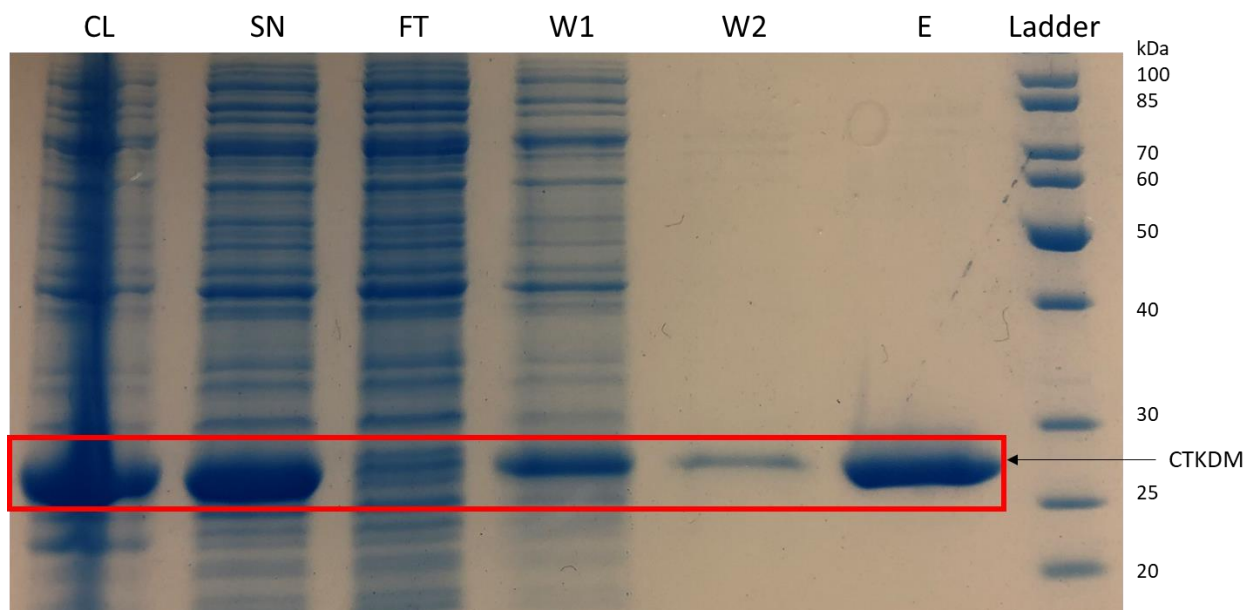


Figure 3.4.1.5 – SDS PAGE analysis of RSK4 CTKDM affinity chromatography (LB expression) – The Hexa-histidine tag based purification was carried out on a His trap crude FF 5ml column at a constant flow rate of 2ml/min was used. 5 μ l of ladder mixed with loading dye was used. 10 μ l of samples mixed with 2X lamelli loading dye were loaded onto an SDS-PAGE gel for 45 minutes at 200V. The gel was then stained with Simply blue stain for 1 hour and then destained overnight. CL=Cell Lysate, SN=Supernatant, FT=Flow Through, W1=Wash 1, W2=Wash 2, and E= Elution.

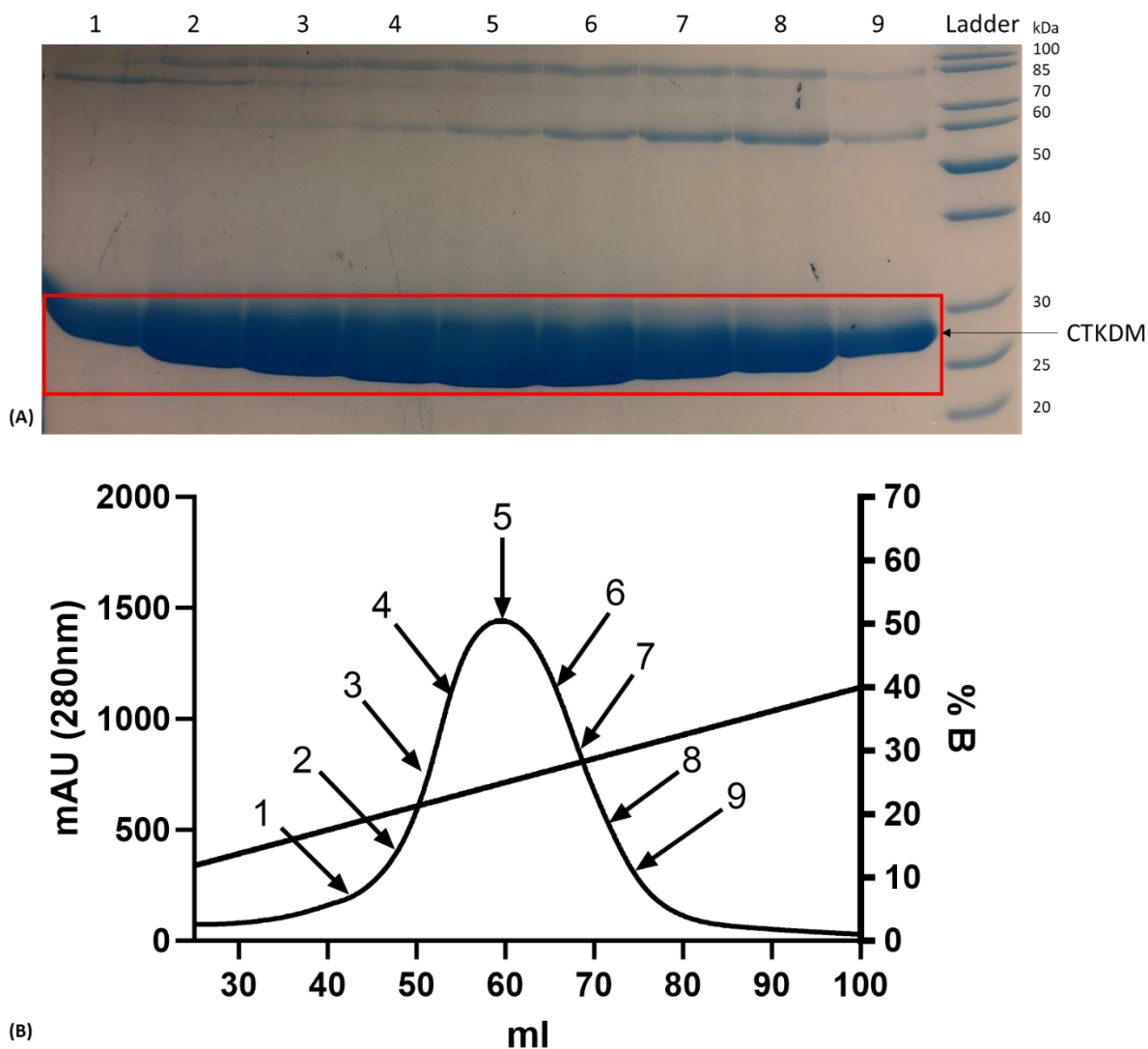


Figure 3.4.1.6 – SDS PAGE analysis and chromatogram of RSK4 CTKDM anion exchange (LB expression) – A) The purification was completed on a 5ml HiTrap Q HP where 1ml/min flow rate was used. 5 μ l of ladder and 10 μ l of samples mixed with 2X lamelli loading dye were loaded onto an SDS-PAGE gel for 45 minutes at 200V. The gel was then stained with Coomassie blue stain for 1 hour and then destained overnight. Numbers above SDS correspond to the points on B in which samples were taken. B) Chromatogram data for corresponding experiment. The x-axis represents volume of buffer (ml) which had been applied to the column, the left Y-axis shows the absorbance (mAU) at 280nm and the right Y-axis depicts the % of buffer B.

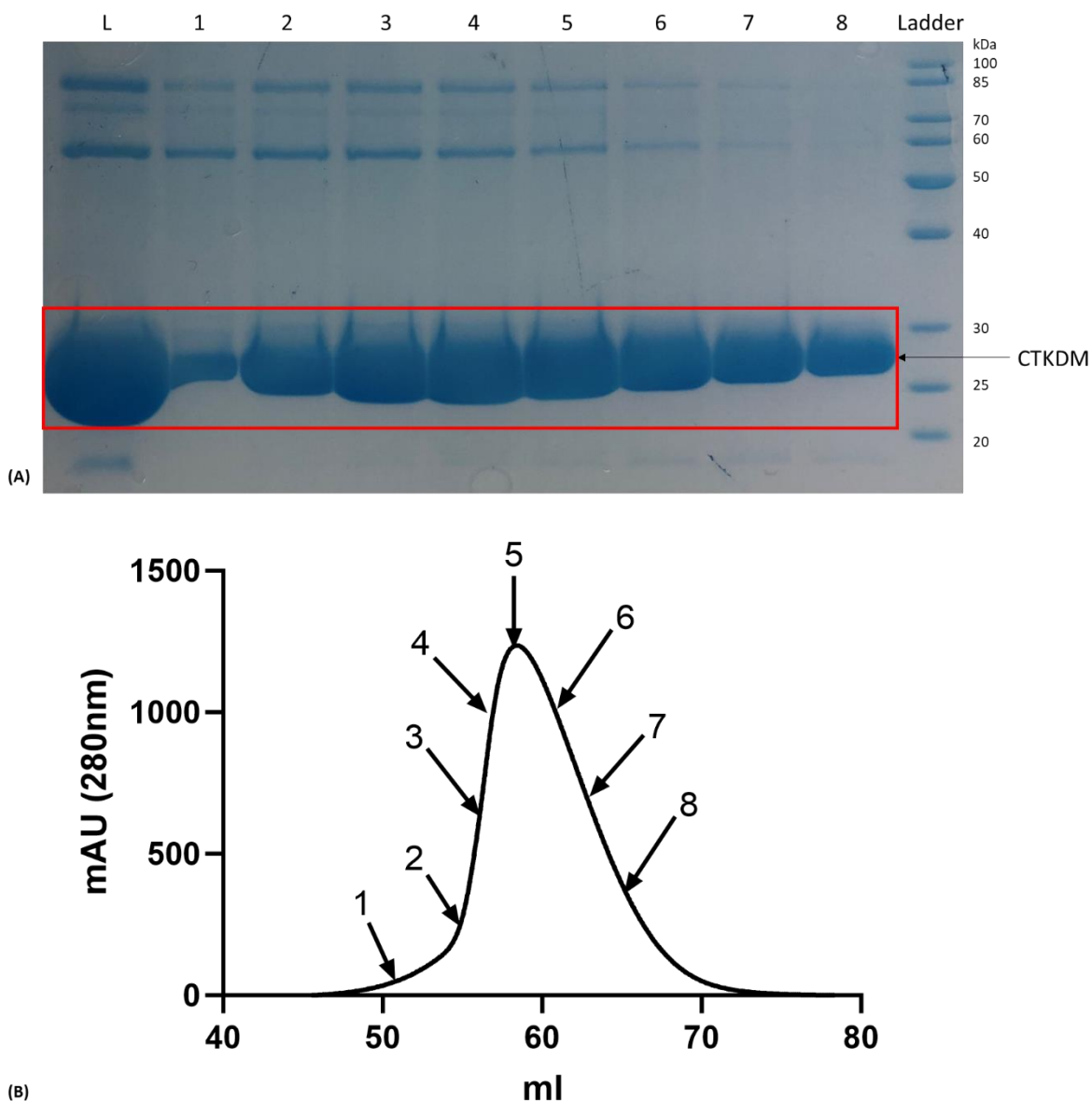


Figure 3.4.1.7 – SDS PAGE analysis and chromatogram of RSK4 CTKDM Size exclusion (LB expression) – A) A Superdex 75 G 16/60 was used for the size exclusion purification, flow rate of 1ml/min was used. 5 μ l of ladder and 10 μ l of samples mixed with 2X lamelli loading dye were loaded onto an SDS-PAGE gel for 45 minutes at 200V. The gel was then stained with Simply blue stain for 1 hour and then destained with destain buffer overnight. Numbers above SDS correspond to the points on B in which samples were taken. B) Chromatogram data for corresponding experiment. The x-axis represents volume of buffer (ml) which had been applied to the column, the Y-axis shows the absorbance (mAU) at 280nm.

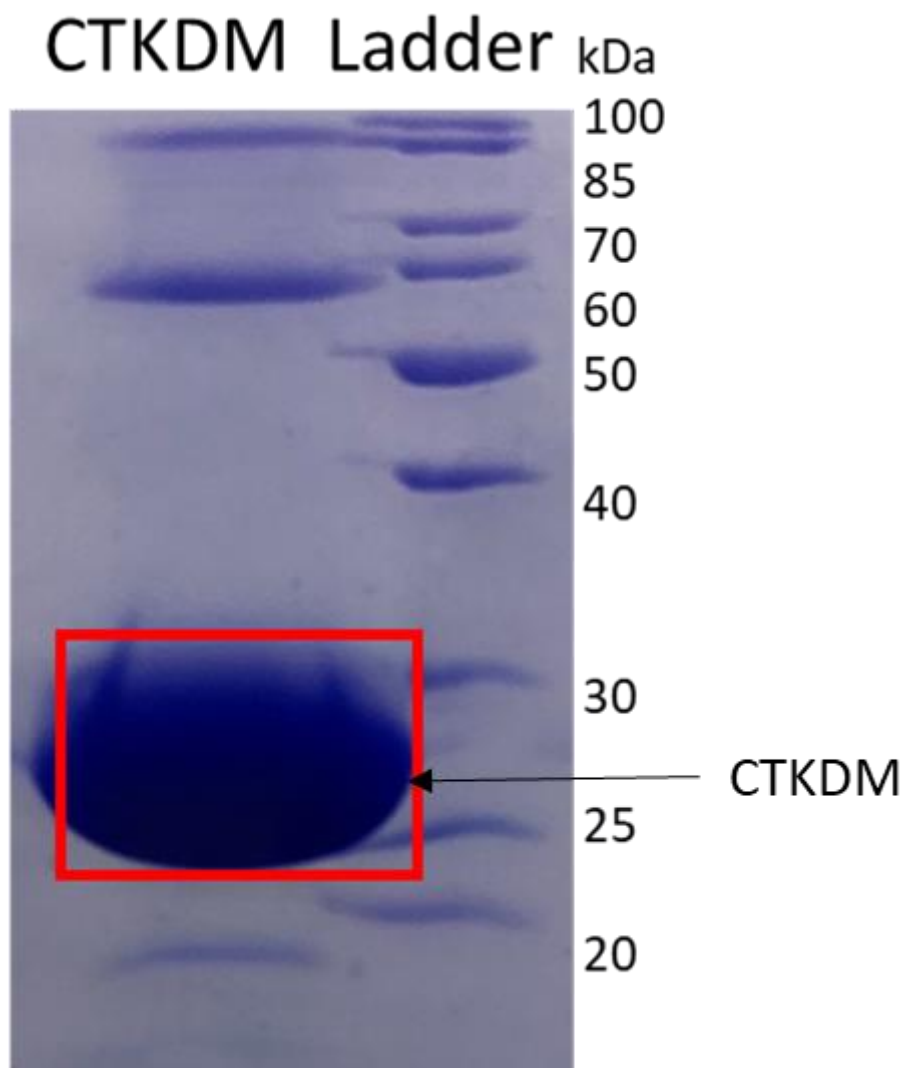


Figure 3.4.1.8 – SDS PAGE analysis of RSK4 CTKDM at 10mg/ml (LB expression) - 5 μ l of ladder and 10 μ l of sample was mixed with 2X lamelli loading dye were loaded onto an SDS-PAGE gel for 45 minutes at 200V. The gel was then stained with Coomassie blue stain for 1 hour and then destained overnight. Red box depicts which band is the protein of interest RSK4 CTKDM.



Figure 3.4.1.9 – 100x magnification of RSK4 CTKDM crystal – 7 mg/ml of RSK4 CTKDM in 0.1M HEPES buffer pH 7. 100 nl protein with 100 nl buffer. Red box highlights where the crystal is located.

3.5 – RSK4 C-Terminal Kinase Domains role in activation

3.5.1 RSK4 CTKDM is catalytically active

As previously described in chapter 1.3.3, RSKs are activated through a phosphorylation cascade. RSK4 CTKD is activated by ERK1/2 phosphorylation of T577 on the activation loop (Romeo *et al.* 2012). This results in activation of the CTKD and the sequential activation of RSK4. To determine if the phospho-mimetic mutation introduced into RSK4 CTKD created a catalytically active protein, purified RSK4 CTKD and RSK4 CTKDM constructs were used in a HTRF KinEASE assay. In this method, a proprietary substrate peptide is presented for hetero phosphorylation by the kinase domain of target protein. RSK4 CTKD and RSK4 CTKDM were incubated for 3 hours with saturating concentration of ATP and MgCl₂ (Chapter 2.6.1). Activities of RSK4 CTKD and RSK4 CTKDM were tested using a constant concentration of enzyme and substrate and monitored over time by the amount of phosphorylated substrate produced. As expected, RSK4 CTKD does not show any appreciable kinase activity (Figure 3.5.1.1). On the contrary, RSK4 CTKDM has a higher activity than RSK4 CTKD at the same time points (Figure 3.5.1.1) and follows a classic Michaelis-Menten trend. This has been seen before for related kinases with phospho-mimetic mutations (Chrysostomou *et al.* 2021). Taken together these data suggest that phosphorylation on T577 is indispensable for RSK4-CTKD activity and the protein is active only after phosphorylation on T577.

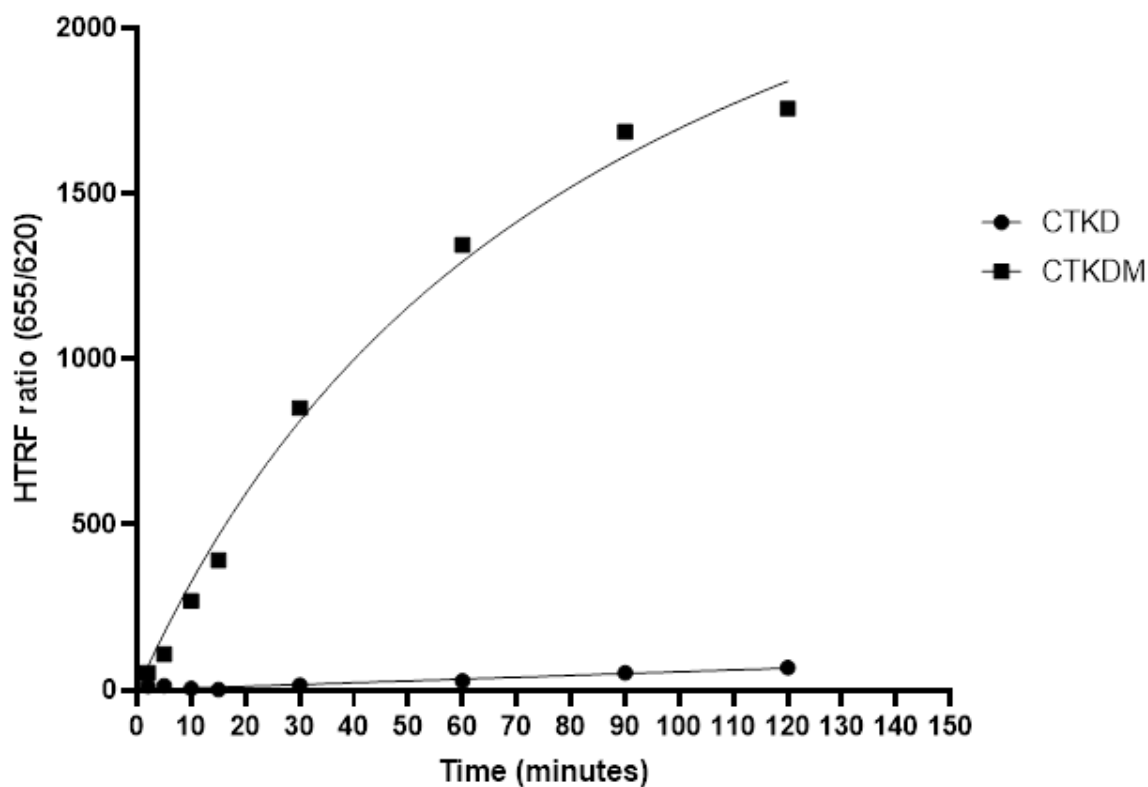


Figure 3.5.1.1 – HTRF KinEASE assay of RSK4 CTKD and CTKDM – 5 μ M of kinase, kinase buffer, 2 μ l of substrate and 2 μ l of ATP were added to wells and mixed. Over a timecourse the reaction was quenched with 2mM EDTA. 5 μ l of Streptavidin-XL665 and 5 μ l of STK antibody-cryptate were then added and incubated for 1hr at RT. The samples were then quantified on a clariostar plate reader.

3.5.2 – Cross Talk between the RSK4 NTKD and the RSK4 CTKD

RSK4 contains two distinct kinase domains in the same polypeptide chain. The CTKD is pivotal in regulation of RSK4 activity via the autoinhibitory loop (Ranganathan *et al.* 2006). Additionally, the CTKD is responsible for keeping RSK4 in inactive state via ERK1/2 binding (Ranganathan *et al.* 2006). The only known substrate of the RSK4-CTKD is RSK4 itself, via phosphorylation of the HM. This in turn leads to the sequential activating phosphorylations of RSK4 including the NTKD which allows for phosphorylation of a wide range of substrates (Pearce *et al.* 2010). Most recently it has been suggested that the phosphorylated HM is essential in NTKD activity (Chrysostomou *et al.* 2021). This highlights the high level of interaction between the two kinase domains. To further expand on the relationship between the RSK4 NTKD and CTKD interactions between the two domains were monitored using a pull-down assay. Prior to the assay the RSK4 NTKD and NL constructs needed to be purified as they were not readily available from previous experiments. Both proteins were purified in a similar manner to the C-term constructs. However, as the purpose of purification was not for crystallography, cleavage of the N-terminal GST tag was not needed. As such, both RSK4 NTKD and NL were purified using a two steps purification approach, with affinity chromatography (chapter 2.4.2) followed by size exclusion chromatography (chapter 2.4.4). This achieved suitable protein purity for pull down assays. For the pull-down, three different RSK4 N-Terminal constructs were used: RSK4 NTKD, encompassing only the inactive kinase domain (residues 48-349) (Chrysostomou *et al.* 2021), RSK4 NL, including inactive kinase domain and AGC regulatory region (residues 48-401) and RSK4 NL3M, the NL domain containing S232E S389E S372E phospho-mimetic mutations, mimicking the fully active state of RSK4 N-terminal. These three constructs had an N-Terminal GST

fusion tag and were used as baits. GST-tag proteins were immobilized on a GSTrap resin and incubated with RSK4 CTKD or RSK4 CTKDM. Both RSK4 CTKD and RSK4 CTKDM had a His-tag, which allowed cross-validation of the elution sample via western blot (Figure 3.5.2.1). Indeed, the N-terminal constructs, the C-terminal constructs, and GST contaminations in the NTKD samples have similar MW and are virtually undistinguishable on an SDS-PAGE thus the need for western blotting.

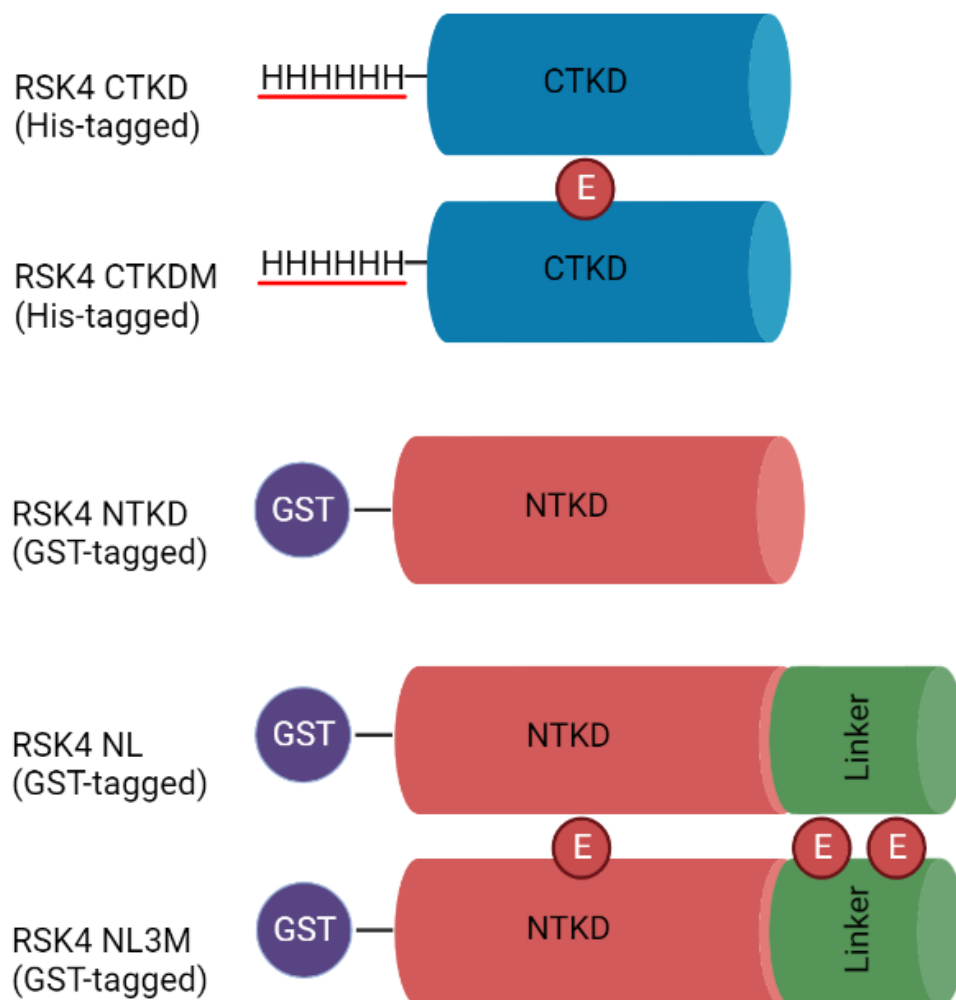


Figure 3.5.2.1 – RSK4 truncations used in western blotting – schematic representation of the RSK domains purified for western blotting. Grey represents the NTKD represented in red, Linker region represented in green, CTKD represented in blue. Red E represents phosphomimetic mutations to glutamic acid. HHHHHH- represents a hexahistidine tag whilst purple GST circles represent a GST tag.

Using an anti-GST-antibody it was possible to confirm presence of bait proteins in the pull-down elution sample, while anti-His-antibody was used to visualize presence of RSK4 CTKD and RSK4 CTKDM in the elution sample. The western blots showed that the RSK4 CTKD and RSK4 CTKDM did not aspecifically bind the GST resin (Figure 3.5.2.2), while the RSK4 NTKD, NL and NL3M all bound to the resin as expected (Figure 3.5.2.2). Importantly, it is possible to see that both the RSK4 CTKD and the RSK4 CTKDM interact with RSK4 NL, but not with RSK4 NTKD (Figure 3.5.2.3) and that all GST proteins eluted as expected (Figure 3.5.2.3). This is a strong indication that the RSK4 CTKD substrate is the HM region, which is present in RSK4 NL but not in RSK4 NTKD. This is a further confirmation that RSK4 NTKD is not phosphorylated by the CTKD, but it is able to auto-phosphorylate itself on the activation loop (Chrysostomou *et al.* 2021). Interestingly, RSK4 NL3M does not interact with either the RSK4 CTKD or CTKDM (Figure 3.5.2.3). This suggests that, upon phosphorylation of the HM and TM, the RSK4 CTKD detaches, allowing the phosphorylated HM to bind the phosphate binding pocket on the NTKD, in line with the current proposed RSK4 activation model (Chrysostomou *et al.* 2021). This would also rule out presence of a large back-to-face interaction surface between RSK4 CTKD and NTKD, visible on the AlphaFold model.

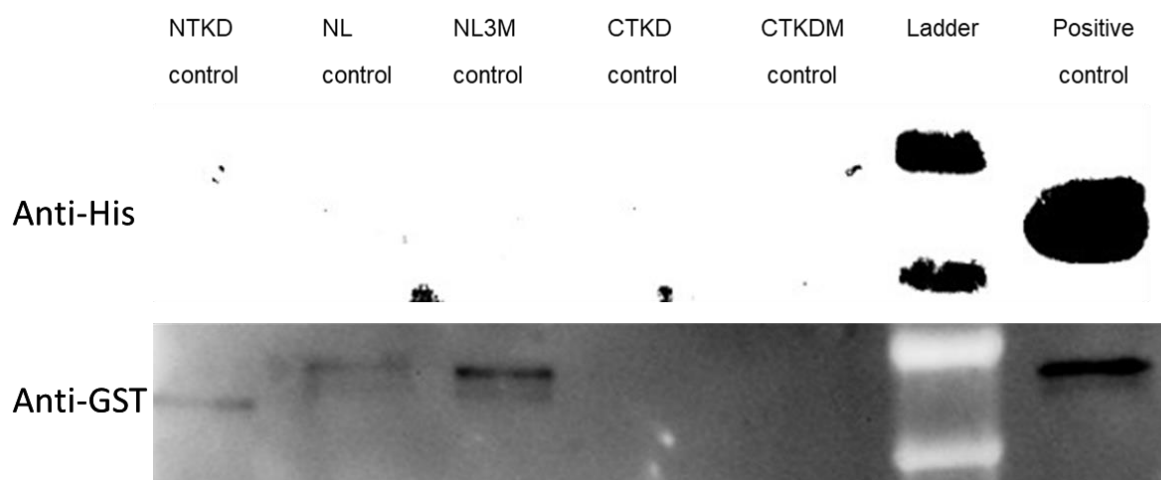


Figure 3.5.2.2 – Western blot of pull-down assay controls - The samples were run on an SDS-PAGE for 45 minutes at 200V, the gel was then transferred to a membrane. The membrane was then blocked for 1hr at RT, Primary antibody was incubated ON at 4°C then washed with PBST. The membrane was then blocked again for 1hr at RT and then incubated for 1hr with secondary antibody at RT. The membrane was then washed with PBST and then visualized with HRP substrate.

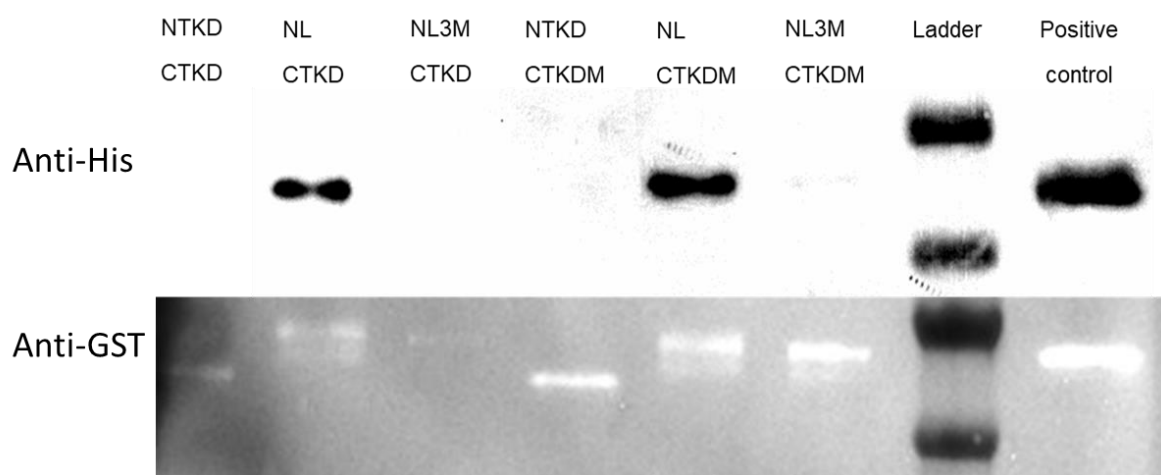


Figure 3.5.2.3 – Western blot of pull-down assay binding elutions - The samples were run on an SDS-PAGE for 45 minutes at 200V, the gel was then transferred to a membrane. The membrane was then blocked for 1hr at RT, Primary antibody was incubated ON at 4°C then washed with PBST. The membrane was then blocked again for 1hr at RT and then incubated for 1hr with secondary antibody at RT. The membrane was then washed with PBST and then visualized with HRP substrate.

3.6 – Discussion

3.6.1 – Results Overview

This chapter discusses the purification of RSK4 constructs and the attempts to elucidate the differential mechanism of activation of RSK4. A “divide and conquer” approach was adopted and RSK4 domains were split in different constructs, so to explore their structures, activation and, finally, explore their interaction. RSK4 NTKD structure and activation mechanism have been described before (Lara *et al.* 2013), however, the RSK4 NTKD lack the HM region which is key in AGC kinase activation. As such, a construct containing the NTKD and HM bearing 3 phosphomimetic mutations (S232E S389E S372E), mimicking the active state of this domain, was cloned into a pETM-14 vector. Unfortunately, attempts to crystalize this domain failed to produce crystals. The other catalytic domain of RSK4 for which we have little information is the CTKD. Two constructs were cloned, a CTKD and a CTKDM bearing a phosphomimetic mutation on the activation loop (T581E). Importantly, kinase activity assay showed that the phospho-mimetic mutation incorporated into RSK4 CTKDM causes constitutive activation of the protein while the RSK4 CTKD wt was catalytically inactive. Despite RSK4 CTKD and CTKDM produced protein in large quantities at a reasonably high purity, crystal trials were pursued but yielded no crystals. Optimization studies helped increase the purity of protein, thus increasing likelihood of obtaining protein crystals. Crystallization trials yielded one potential crystal, which lacked well defined edges. Follow-up optimization tests failed to reproduce the crystal, which would suggest the initial hit was a salt crystal. Despite the lack of structural information, the protein samples were pure enough to carry out intra-domain binding studies. Pull down assay showed that the RSK4-CTKD and RSK4-CTKDM interacted with NL but did not interact with NTKD or NL3M, which

suggests that the CTKD is bound to the HM in a resting state and detaches upon activation (Figure 3.6.1.1)

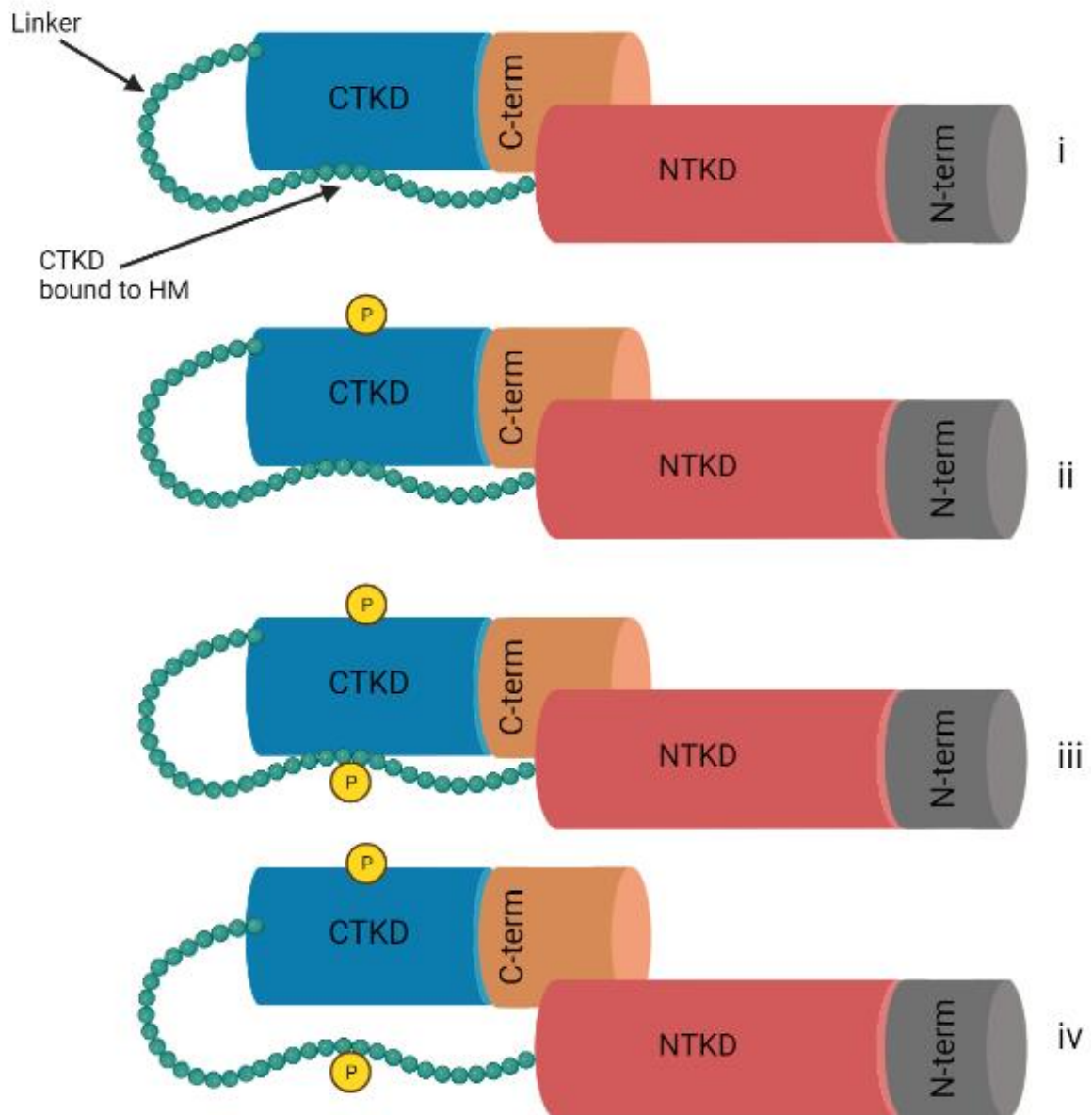


Figure 3.6.1.1 – Model of RSK4 N-C terminal interaction – the C-term is represented in orange, the CTKD is represented in blue, the linker region is represented in green amino acid chain, the NTKD is represented in red, and the N-term is represented in grey. Phosphorylation events are depicted by yellow P spheres. i) The CTKD is bound to the HM of the linker region in an inactive state. ii) The CTKD is phosphorylated. iii) the CTKD phosphorylates the linker. iv) The CTKD then detaches from the HM.

3.6.2 – RSK4 NL3M proteolysis

In RSK4 NL3M, it is possible to see additional bands at a lower molecular weight (Figures 3.2.1.1-3). While it was not validated by mass spectrometry, considering the consistent presence of discreet band(s) at a lower MW than RSK4 NL3M, the presence of a relatively high amount of protein (unlikely to be a bacterial protein), suggest the presence of proteolytic cleavage. This may be the result of a direct cleavage of the protein or a concomitant event of misfolding and cleavage. Indeed, in unstructured protein are more susceptible to proteolytic targeting (Hayat *et al.* 2018; Wingfield 2015).

Proteolysis occurs due to endogenous proteases, as *E. coli* express both endo- and exoproteases. Endoproteases cleave proteins within the polypeptide chain relevant to specific recognition sequences, whereas exoproteases cleave at the end of the polypeptide (Rozkov & Enfors 2004). As part of the purification protocol, several steps are normally, and were specifically here, introduced to reduce proteolysis. As shown by Yang *et al.* (1997), reduction of temperature during expression reduces proteases activity. Specifically, the effect of using cold incubation on enzymatic activity was demonstrated with two orthologs, chicken and rat liver 6-phosphofructo-2-kinase/fructose-2,6-bisphosphatase. Both were liable to proteolysis and formation of inclusion bodies when expressed at 37 °C, but not at 22 °C (Yang *et al.* 1997). Similarly a reduction in incubation temperature from 37 °C to 25 °C caused a reduction in interferon (IFN) α -2 proteolysis (Chesshyre & Hipkiss 1989). Additionally, low temperatures help promote correct folding of recombinant protein which can give additional protection against proteolysis by concealing target

proteolytic sequences inside secondary and tertiary structure (Ryan & Henehan 2013). Unfortunately, temperature is not sufficient to reduce proteolysis, especially during cell lysis stages. As such, protease inhibitor cocktail and EDTA were added to the lysis buffer. EDTA specifically inhibits metalloproteases, (many *E. coli* proteases are metalloproteases) by removing the metal ions in solution which are needed for metalloprotease function. Protease inhibitor cocktails contain a mixture of different protease inhibitors with the aim to inhibit multiple proteases simultaneously which removes the need to add multiple different inhibitors separately (Ryan 2011). The protein inhibitor cocktail used (Thermo Fisher scientific) should inhibit all major protease groups except metalloproteases (Table 3.6.2.1), but only achieve an inhibition of cysteine proteases at around 70% as opposed to approximately 95% and 85% for trypsin proteases and metalloproteases (with EDTA), respectively.

Table 3.6.2.1 – Components of Protease Inhibitor cocktail

Inhibitor	Target Protease
Aprotinin	Serine proteases
Bestatin	Aminopeptidases
E-64	Cysteine proteases
Leupeptin	Serine and cysteine proteases
AEBSF	Serine proteases
Pepstatin A	Aspartic acid proteases

Despite this, it seems proteolytic cleavage may be occurring at the early stage of RSK4 purification. The AGC region of RSK4 NL3M exists in an unstructured state,

making it more accessible to proteases (Suskiewicz *et al.* 2011). A potential cleavage at the N-term is unlikely, as the protein is N-term GST-tagged, while it is highly possible at the C-term of the construct since the cleaved products co-eluted with GST during affinity purification (Figure 3.2.1.1-3). Therefore, it seemed logical to suspect that cleavage would occur at the C-terminal AGC region of RSK4 NL3M. Presence of potential cleavage sites were also identified using the bioinformatic tools PeptideCutter (Gasteiger *et al.* 2005) and PROSPER (Song *et al.* 2012), which define a theoretical cleavage sites based on the recognition sequences of several proteases. Of the four families, cysteine and serine proteases had most cleavage sites in the C-terminus of RSK4 NL3M which would create suitable fragments as seen in the SDS-PAGE (Figure 3.2.1.1-3) (Gasteiger *et al.* 2005; Song *et al.* 2012). Coincidentally, the protease inhibitor cocktail used has reduced inhibition of Cysteine proteases which could explain why the construct was subject to proteolytic cleavage. Previous studies have shown that it is possible to identify a tailored mix of inhibitors by using protease inhibitor panels, where several inhibitors are tested simultaneously and then analyzed using SDS-PAGE to infer a reduction in proteolysis (Rozkov & Enfors 2004; Ryan 2011). The inhibitors which cause a reduction in proteolysis could then be incorporated in lysis buffer (Rozkov & Enfors 2004; Ryan 2011). This principle was illustrated well by Robert *et al.* (2009), showing that the cleavage of their recombinant protein created a 22 amino acid peptide. Using inhibitor panels, they showed that an aspartic protease was responsible for the cleavage, and specifically, using Edman degradation, they were able to identify the protease as cathepsin D. Importantly, similar to NL3M purification, they showed that high concentrations of EDTA alone were not sufficient to inhibit proteolysis completely (Robert *et al.* 2009).

3.6.3 – C-terminal kinase domain does not crystallize

Purification of RSK4 CTKD resulted in relatively pure but heterogenous samples not suitable for crystal trials (Figures 3.3.1.5 and 3.3.1.9). Conversely, purification of RSK4 CTKDM resulted in purer sample more suitable for crystallography (Figures 3.4.1.4 and 3.1.4.8). For both RSK4 CTKD and CTKDM expression in LB media caused an increase in the RSK:contaminants ratio without a substantial loss in protein folding. Considering an overall estimated sample purity of about 90%, RSK4 CTKD and CTKDM (AIM and LB) were subjected to crystallization trials, but none resulted in production of crystals. This would suggest that the heterogeneity observed affected crystallization more than expected. Interestingly, by carefully analyzing all 10 mg/ml samples (Figures 3.3.1.5, 3.3.1.9, 3.4.1.4 and 3.4.1.8), it is possible to notice a clear pattern with recurring contaminations across all samples: three single bands at approximately 80-85 kDa, 60-65 kDa and 15-20 kDa (here ranges were used to allow for some discrepancies between reported size and how it appears on gels – this occurred for both RSK4 CTKD and CTKDM). It is possible that the higher contaminations (60kDa and 80kDa) could be the formation of dimers and trimers respectively, this could be determined through western blotting, if they are in fact dimers or trimers, then the His-tag would confirm this. Alternatively, A common artefact of recombinant expression in *E. coli* cells is the presence of chaperons in protein samples. In fact, *E.coli* possesses several protein folding machinaries: Hsp100 (ClpA), Hsp90 (HtpG), Hsp70 (DnaK), Hsp60 (GroEL) and sHsps (small heat-shock proteins; IbpA and IbpB) (Hoffmann & Rinas 2004). By utilizing the data from SDS-analysis several of these chaperones can be identified based on their MW, as ClpA, GroEL and IbpA or IbpB correspond to the bands at

84.2 kDa, 60 kDa, 15.7 kDa and 16 kDa respectively (Consortium 2017). Chaperones operate in a synergistic manner, working co-operatively to assess the extent of misfolding, traffic the misfolded protein to the correct chaperone, assist refolding or disaggregate the protein but if this process is unsuccessful the protein is degraded (Calloni *et al.* 2012; Santra *et al.* 2017). However, when recombinant proteins are overexpressed proteostasis becomes imbalanced causing an increase in misfolding, which would recapitulate the common presence of chaperones in purified recombinant proteins (Baneyx & Mujacic 2004; Kress *et al.* 2009). When comparing the final samples of both RSK4 CTKD (Figures 3.3.1.5 and 3.3.1.9) and CTKDM (Figures 3.4.1.4 and 3.4.1.8) there is a clear reduction in the amount of chaperone contamination in RSK4 CTKDM samples suggesting an increase in proportion of protein sample folded in native state thus a more homogeneous final sample. The difference between the two constructs could be due to the 139thosphor-mimetic mutation of RSK4 CTKDM results in a difference of charge. The threonine of RSK4 CTKD, has no net charge, while the glutamic acid of RSK4 CTKDM which has one negative charge. The mechanism underlying the protein stabilization has not been elucidated, however, it is likely that inserting a 139thosphor-mimetic mutation in the kinase domains could induce conformational changes resulting in protein stabilization. This was illustrated by Haase *et al.* (2004) by mutating 14 different serine or threonine sites to aspartic or glutamic acid across different regions of tau. Mutations in different regions both suppressed and enhanced aggregation of Tau (Haase *et al.* 2004).

Protein expression and purification conditions were optimized to increase sample stability and overall purity. Following Vera *et al.* (2007) guidelines, expression

temperature was reduced to 18 °C as it has been demonstrated that lower temperatures during induction can reduce aggregation and increase the correct folding of proteins. The authors showed that by comparing expression of GFP induced at the same OD with the same IPTG concentration (1mM) at different temperatures, the proportion of GFP in the insoluble fraction reduced significantly from 58.8% at 37 °C, to 54.4% at 30 °C and 16.9% at 16 °C, strongly supporting the relevance of lower temperature in promoting native fold. This was further expanded with the use of Infrared spectroscopy, which showed a progressive band shift in the spectra of the insoluble GFP fraction as temperature was decreased which was attributed to conformational transition to a native-like α -helix structure (Vera *et al.* 2007). In a similar manner of monitoring the accumulation of aggregate in the insoluble fraction, ClpA5 protein accumulation in the insoluble fraction at 20-25 °C showed dramatically less intense bands via SDS-PAGE than when incubated 30-37 °C (Schultz *et al.* 2006). Furthermore, optimization of IPTG concentration can reduce the overall amount of protein produced which in turn relieves the refolding pathways. Across several studies it was shown that lower concentrations of IPTG produced yields of active and soluble protein (Larentis *et al.* 2014; Silaban *et al.* 2019). Indeed, conditions utilized in these experiments are in line with those of another MAPK, p38, which was optimized to the conditions of 0.25 mM IPTG and OD₆₀₀ of 0.8 at 18 °C (Sunil K. Khattar *et al.* 2007). In contrast, Einsfeldt *et al.* (2011) showed that IPTG concentration caused no change in expression of their recombinant protein ClpP (Einsfeldt *et al.* 2011). These literatures illustrate that the expression conditions to produce soluble protein in a fully folded state is protein specific, requiring protein specific optimization, which could be adopted for RSK4 CTKD.

Bacterial chaperones have been shown to often co-elute with recombinant protein during purification and routine purification approaches (i.e., affinity and size exclusion chromatography) fail to remove them. In fact, chaperones can be removed only using specific chaperone removal protocols. The first instance of experimental separation was shown by Thain *et al.* (1996) where GroEL was removed from their recombinantly GST-tagged protein human papillomavirus type 16 (HPV 16). This was done by binding the recombinant protein onto a GST column and washing the protein with a buffer supplemented with 5mM ATP and 20mM MgCl₂. Washing the column with high concentrations of ATP induces a conformational change in GroEL thus releasing it from the recombinant protein (Thain *et al.* 1996). A similar approach was applied to purify the kinase domain of Interleukin-2 tyrosine kinase (Itk) (Joseph & Andreotti 2008) expressed in ArcticExpress *E. coli*, which express higher levels of GroEL/ES to aid correct folding and expression at 12 °C (Joseph & Andreotti 2008). Although similar to the work by Thain *et al.* (1996), the subtle differences shown here are more suited toward a kinase which often have poor thermal stability (Joseph & Andreotti 2008). Another method has also been used which approaches this problem in a different manner. Rohman & Harrison-Lavoie (2000), prior to purification the bacterial proteins of the soluble fraction of untransformed cells were denatured. The recombinant protein was then incubated in a high ATP concentration buffer in a similar manner to the previous techniques. The denatured bacterial proteins were then used to compete with the recombinant protein as GroEL preferentially binds the most misfolded protein present. The recombinant protein is then recovered using GST affinity, washed and eluted (Rohman & Harrison-Lavoie 2000).

3.6.4 – RSK4 NTKD and CTKD interact via the AGC regulatory region

RSK1-3 are dependent on PDK1 for activation (Jensen *et al.* 1999). ERK binds and phosphorylates RSK in the CTKD activation loop (Roux *et al.* 2003), the CTKD then autophosphorylates the HM which creates a binding site for PDK1 (Frödin *et al.* 2000, 2002). ERK also phosphorylates two additional residues in the TM which stabilizes PDK1 interaction, which in turn phosphorylates the activation loop of the NTKD (Dalby *et al.* 1998; Lara *et al.* 2013). RSK4 differs from other isoforms as it is activated in a PDK1 independent manner and exists in a constitutively active state (Dümmeler *et al.* 2005), which lead to the hypothesis that RSK4 could be activated through a different mechanism. RSK4 NTKD structure revealed the presence of a non-canonical kinase folding, where the β B-sheet is in place of the C-helix (Chrysostomou *et al.* 2021), previously observed also in RSK2 NTKD and MSK1 (Malakhova *et al.* 2009). Chrysostomou *et al.* 2021 speculated that this may represent a unique feature of kinases with two kinase domains (i.e., RSK and MSK families). Indeed, using docking simulations the authors showed that the phosphorylated HM interacts with the NTKD in the phosphate binding pocket and may be responsible for facilitating the NTKD autophosphorylation. This is in line with the results of the RSK4 constructs pull-down, which show that the HM is bound to the CTKD while inactive and is released upon phosphorylation, supporting a dynamic role of the HM in autoinhibition-activation of the kinase (Figures 3.5.2.2 – 3.5.2.3). Importantly, in line with earlier RSK1-3 characterization data (Frödin *et al.* 2000, 2002), no binding between the NTKD and CTKD was detected. This is in clear contrast with the AlphaFold model (Figure 3.3.1.1), which fails to recapitulate this mechanism of activation and shows presence of a large interaction surface directly between the two kinase domains. This is very likely due to a lack in appropriate

training data for the AI tool, since RSKs and MSKs are the only 6 kinases among the 518 human kinases to possess 2 kinase domains in a single polypeptide (Endicott *et al.* 2012; Manning *et al.* 2002).

3.6.5 – Conclusion

When considering these data it seems that further expression and purification optimization of the RSK4 constructs are needed; RSK4 NL3M is likely being proteolytically cleaved; RSK4 CTKD samples still contain a significant proportion of chaperone contaminant that suggests the sample is heterogeneous; RSK4 CTKDM has minor chaperon contaminants which could be removed through specialist protocols. Despite this the pull down assay experimentally demonstrated that RSK4 CTKD binds the HM in an inactive state and releases upon activation. To push forward the characterization of the regulation mechanisms of the different RSKs isoforms, the full-length structure of RSKs is required. Previous attempts to crystallize the full-length RSK4 have failed, and cryo-EM is likely the most suitable technique for such a challenging task. Herzik *et al.* (2019) pushed the boundaries of cryo-EM by solving the structure of a protein amassing less than 100 kDa to near atomic resolution (Herzik *et al.* 2019). Despite the name (p90 ribosomal kinase), RSK4 has a MW 83.8kDa and no symmetrical shape, which could create challenges with data collection and image quality (Cianfrocco & Kellogg 2020). Additionally, RSK4 has shown low solubility in low salt buffers, which is not ideal in the freezing process (Bhella 2019). Nevertheless, there are examples of proteins which have been solved via cryo-EM which share some similarities. The 80 kDa protein, haemagglutinin-esterase (HE), was solved to a resolution of 3.4 Å (Hurdiss *et al.* 2020). HE, is similarly size to RSK4 but exhibits a moderate symmetry which would

in aid in processing (Hurdiss *et al.* 2020). A major advantage of working with ribosomal proteins is the possibility of solving the structure of the kinase bound to the ribosome. This kind of experiment has been demonstrated previously with Hepatitis C virus (HCV) Internal ribosome entry site (IRES) and the 40S ribosomal subunit to 3.9 Å. The cryo-EM structure showed novel molecular details between the IRES and the 40S subunit which rationalizes previous biochemical evidence regarding the HCV initiation mechanism, furthermore, the refinement was driven by a 80S ribosome-HCV IRES complex (Quade *et al.* 2015). Cryo-EM could also be useful to elucidate the activation mechanism of RSK4 by using a combination of phospho-mimetic and phospho-dead mutants to capture different stages of protein activation. Indeed, this has been done before for the Ryanodine Receptors Ca^{2+} channels. Loss of a positively charged Arginine from the R164C mutation caused distortion of a salt bridge network which induced rotation of the cytoplasmic domain and partial progression to an open state and hyperactive state (Iyer *et al.* 2020). Considering these literatures cryo-EM could be a feasible expansion of the pulldown between RSK4 NTD and CTD.

Chapter 4 – Results – The role of RSKs in AR signalling and Prostate Cancer

4.1 - Introduction

PCa is the leading cause of cancer related death in men in the UK. Patients with non-aggressive disease can often be managed or treated (Filson *et al.* 2015). However, for many, diagnosis of the disease is often too late and as such have advanced disease which is more aggressive and malignant. The most common treatment for this disease state are antiandrogens, luteinizing hormone-releasing hormone (LHRH) agonists or a combination of both. These elicit their effects by targeting AR signalling; antiandrogens bind and inhibit the AR directly whereas LHRHs reduce the amount of androgens circulating the body. Both result in the same outcome, reduced activation of the AR transcriptional program (Pine *et al.* 2016). The necessity to reduce activation of the AR transcriptional program is because the AR is the key regulator of PCa. This means many accumulated genetic alterations translate to changes in AR function. These can occur through direct changes to AR function, for example, mutations in the ligand binding domain can lead to promiscuous ligand activation of the AR. Alternatively mutations to signalling molecules or AR co-regulators can also alter regulation of AR function (Matsumoto *et al.* 2013; Taylor *et al.* 2010).

The AR is activated in a ligand-dependent manner and upon stimulation pre-bound chaperones (e.g. HSP 70/90) dissociate from the receptor. This allows homodimerization of AR monomers and facilitates translocation from the cytoplasm to the nucleus. Once inside the nucleus the AR recognizes and binds to regulatory regions of DNA, termed AREs, which regulate gene expression. The AR then recruits co-regulators and the basal transcriptional machinery before initiating gene

expression (Tan *et al.* 2015). The RSKs have been shown to influence PCa via multiple ways, modulating proliferation, cell cycle, cell motility, and therapy resistance (Cronin *et al.* 2021). However, the significance of RSK-AR signalling remains unclear. To investigate this relationship between RSKs activity and AR a series of experiments were undertaken; (i) AR activity reporter luciferase assays were used to determine if the RSKs can influence the AR transcriptional activity (ii) mammalian 2 hybrid assays were conducted to assess interaction (iii) siRNA knockdown of RSK isoforms coupled with qPCR of AR target genes was used to assess if the RSKs influence the AR transcriptional program and (iv) siRNA was used to assess the impact of RSK knockdown on the proliferation of PCa cell line LNCaP.

4.2 – RSK-AR signalling pathway

4.2.1 – RSKs increase AR transcriptional activity

Studies have shown that individual RSK isoforms can influence the AR transcriptional program, RSK2 was shown to form a complex with the AR co-regulator p300/CBP and in turn upregulate PSA expression (Clark *et al.* 2005), RSK1 phosphorylation of YB1 S102 was shown to enhance binding to its cognate Y-box and in turn regulate the AR transcriptional program (Shiota *et al.* 2011, 2014). However, there are no studies which investigate the RSKs in a comprehensive manner and most have little focus on RSK3/4. COS-1 cells were used for these experiments as they do not express steroid receptors. In preparation for the experiments, the RSKs were cloned into pCDNA 3.1 (+) (Chapter 2.2.2). To determine if the RSKs cause transcription of the luciferase reporter system COS-1 cells were transfected with AR and RSKs independently (Chapter 2.7.3) and then treated with the synthetic androgen mibolerone (MIB) (Chapter 2.7.4). As expected, AR activity was significantly increased in the presence of MIB (Figure 4.2.1.1) and the RSKs produced a significantly lower relative activity than the positive control (AR in the presence of MIB) (Figure 4.2.1.1). This indicated that the reporter system was functioning correctly as the AR becomes transcriptionally active in a ligand dependent manner (Rastinejad *et al.* 2013) and the RSKs caused no significant activation of the reporter system (Figure 4.2.1.1). To investigate the effects of all RSKs on AR activity COS-1 cells were co-transfected with plasmids encoding the RSKs and AR (Chapter 2.7.3) and treated with the synthetic androgen mibolerone (MIB) (Chapter 2.7.4). All of the RSKs were found to significantly increase AR activity (Figure 4.2.1.2). RSKs 2-4 increased AR activity approximately 3-fold, whereas RSK1 increased AR activity approximately 6-fold.

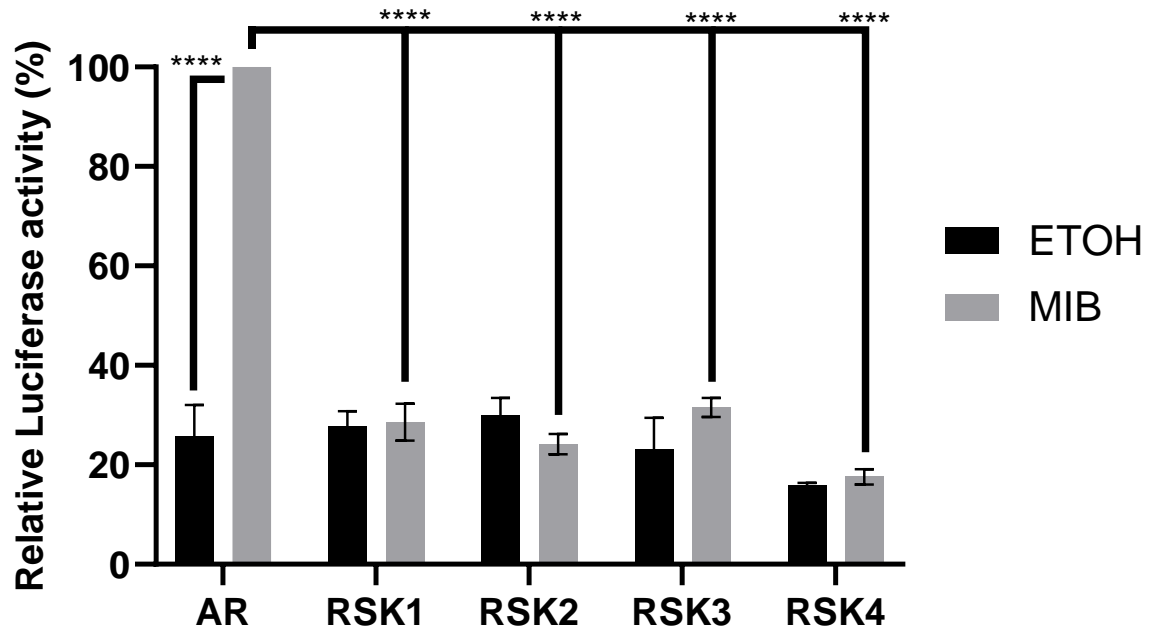


Figure 4.2.1.1 – RSK luciferase activity assay control - COS-1 cells were transfected with the reporter plasmid TAT-GRE-E1B-LUC and plasmids coding for AR or the RSKs and β -galactosidase. Cells were incubated for 20-24 hours, prior to treatment with Ethanol (EtOH) or 1 nM Mibolerone (MIB) for a further 20-24 hours. AR activity was measured using luciferase activity and normalised to β -GAL activity. Results are given as means \pm SE, three experimental repeats were performed. One-way ANOVA test was performed with Sidak's post hoc test, * $P < 0.05$, **** $P < 0.0001$.

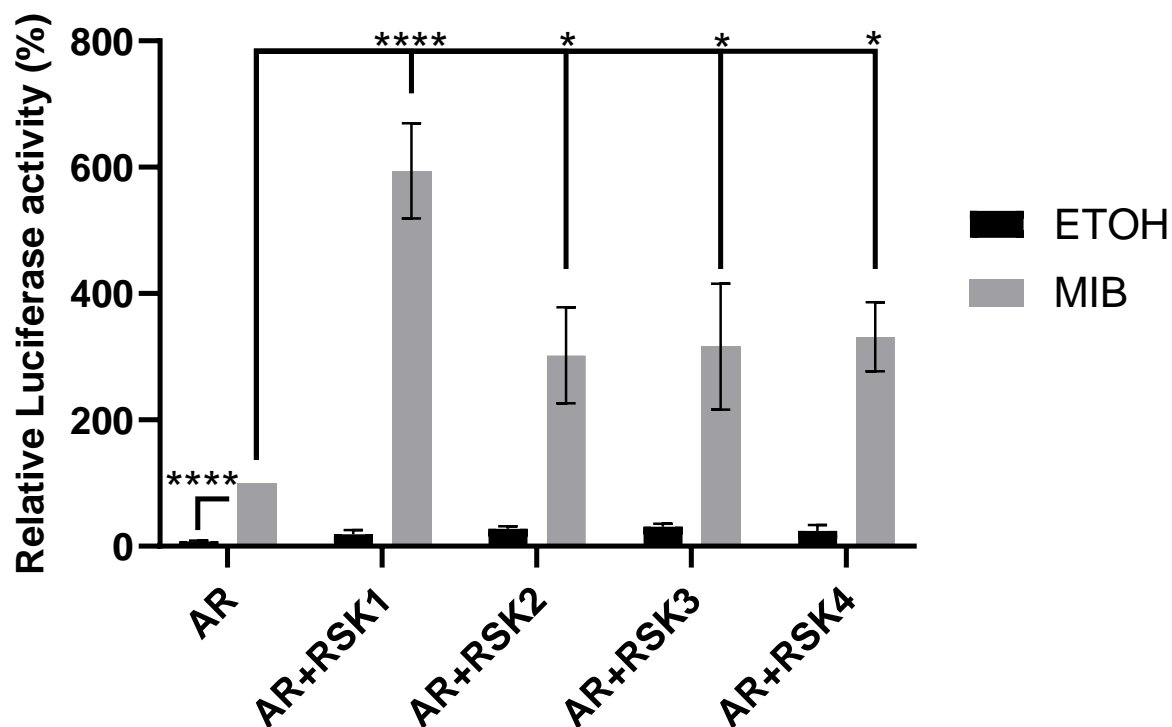


Figure 4.2.1.2 – RSKs increase AR transcriptional activity in model system – COS-1 cells were transfected with the reporter plasmid TAT-GRE-E1B-LUC and plasmids coding for AR, the RSKs and β -galactosidase. Cells were incubated for 20-24 hours, prior to treatment with Ethanol (EtOH) or 1 nM Mibolerone (MIB) for a further 20-24 hours. AR activity was measured using luciferase activity and normalised to β -GAL activity. Results are given as means \pm SE, four experimental repeats were performed. One-way ANOVA test was performed with Sidak's post hoc test, * $P < 0.05$, **** $P < 0.0001$.

4.2.2 – RSKs interact with the AR in close proximity

AR transcriptional activity can be influenced by post-translational modifications (Gioeli & Paschal 2012) or by regulation via co-regulators (Golias *et al.* 2009). The RSKs are downstream kinases of a ubiquitous proliferation pathway, the MAPK pathway, thus it would seem plausible that the AR could be a unknown RSK phosphorylation target. This is even more conceivable knowing that the AR possesses many known and established phosphorylation sites (Koryakina *et al.* 2014). There is also literature which highlighted the role of RSK2 on AR signalling through forming a complex with p300/CBP (Clark *et al.* 2005). These prior works could explain the mechanisms through which the RSKs increase AR transcriptional activity. Both of these mechanisms would require the RSK to interact with the AR in proximity and to investigate this, mammalian 2-hybrid assays were performed. Cloning was performed to produce fusion proteins (Chapter 2.2.2) - the RSKs and AR were fused with Gal4-DBD and VP16 domains, respectively.

The principle of mammalian-2-hybrid assays is based on two domains, Gal4-DBD and VP16, which when in close proximity to each other it leads to the transcription of a reporter gene, which in this case is the enzyme luciferase, conversely, when the domains are kept separate transcription of the reporter gene does not occur (Figure 4.2.2.1). By separating these domains and fusing the truncations with proteins of interest it can be used as a tool to infer proximity/interaction between the two fusion proteins. If the two proteins of interest interact then the Gal4-DBD and VP16 are brought in close enough proximity to lead to transcription of the reporter gene and thus interaction between the two proteins of interest is quantifiable, similarly if the

proteins of interest do not interact then luciferase transcription does not occur (Figure 4.2.2.1). The assignment of which protein of interest, RSK or AR, is fused to which reporter domain, Gal4-DBD or VP16, was specifically assigned with the consideration that AR is a transcription factor. If Gal4-DBD was selected as the fusion partner for the AR, it would bring the AR in close proximity with DNA which could potentially lead to unintentional transcription of the luciferase reporter gene without interaction of both the Gal4-DBD and VP16 domains. However, by choosing Gal4-DBD as the fusion protein for the RSKs, which have no known transcriptional activity it removes this possibility, which means if transcription of the reporter occurs it is due to interaction between the AR and RSKs which facilitates the proximity Gal4-DBD and VP16 for luciferase transcription (Figure 4.2.2.1).

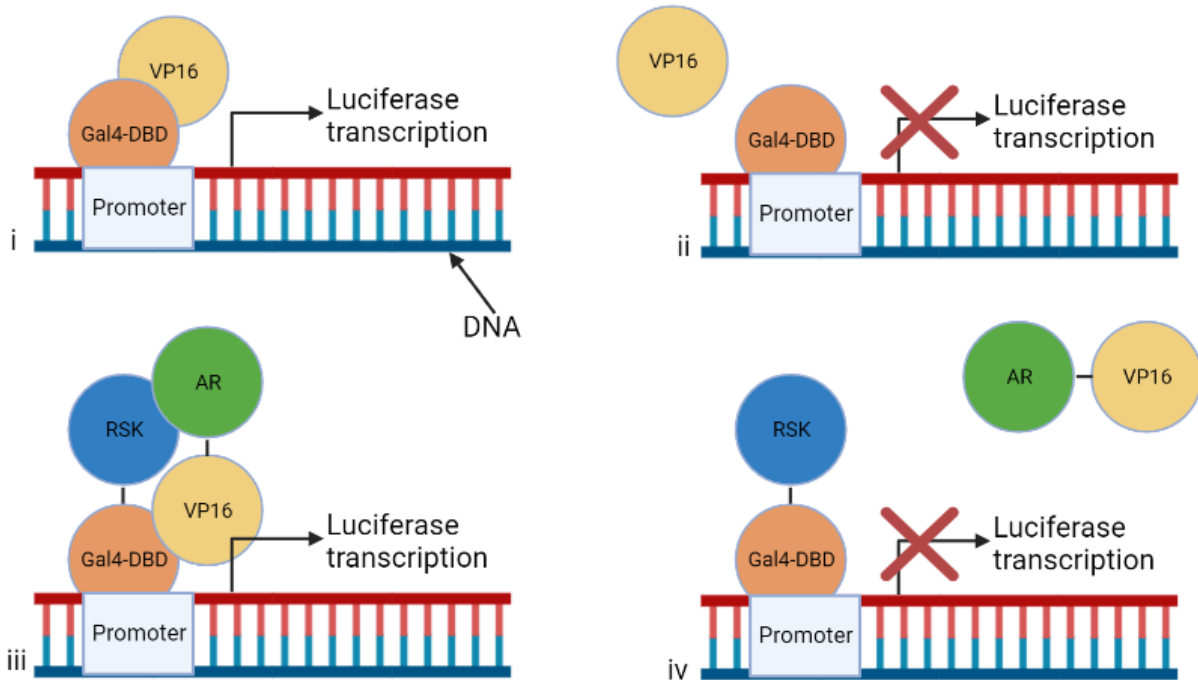


Figure 4.2.2.1 – Schematic representation of mammalian-2-hybrid mode of action – Gal4-DBD is represented by an orange circle, VP16 is represented by a yellow circle, AR is represented by a green circle, RSK is represented by a blue circle, the right angle arrow represents transcription, the light blue box represents the promoter region of DNA, the lines between circle represents fusion proteins. i) When both Gal4-DBD and VP16 are in close proximity it results in the transcription of the luciferase reporter gene. ii) When Gal4-DBD and VP16 are not in close proximity then transcription of the luciferase reporter gene does not occur. iii) If the AR and RSK interact then it brings Gal4-DBD and VP16 into proximity and transcription of the luciferase reporter gene. iv) If the AR and RSK don't interact then the fusion partners necessary for transcription are not brought into proximity and transcription of the luciferase reporter gene does not occur.

To confirm that the luciferase reporter system was functioning as intended and that the RSKs do not have intrinsic transcriptional activity, control experiments were performed: pVP16-AR and pMe-LxxLL (Figure 4.2.2.1); pMe-RSK1-4 and pVP16-empty; pM-empty and AR; pVP16-empty and pM-LxxLL were transfected into COS-1 cells. As expected, MIB promoted an interaction between the AR and the LxxLL interaction motif (Figure 4.2.2.1). This acted as a positive control experiment as LxxLL is a known interaction motif for the AR which is found in many coactivators (Jehle *et al.* 2014). The RSKs did not significantly activate the system confirming that they do not have intrinsic transcriptional activity (Figure 4.2.2.1). Combinations of empty vectors with their corresponding tested components did not significantly activate the system (Figure 4.2.2.1).

Co-expression of each RSK isoform with the AR resulted in luciferase activity similar to that of the AR+LXXLL positive control, signifying an interaction (Figure 4.2.2.2). Interestingly, there are two different modes of interaction: (i) a ligand independent interaction for RSK1, for which interaction with the AR is not significantly influenced by the binding of MIB to AR, and (ii) a ligand dependent interaction for RSK2/3/4, which are able to interact with the AR only in its ligand bound state (Figure 4.2.2.2). Indeed, these results reinforce a relationship between the RSKs and AR but does not divulge whether the RSKs are binding to the AR directly or indirectly through a complex.

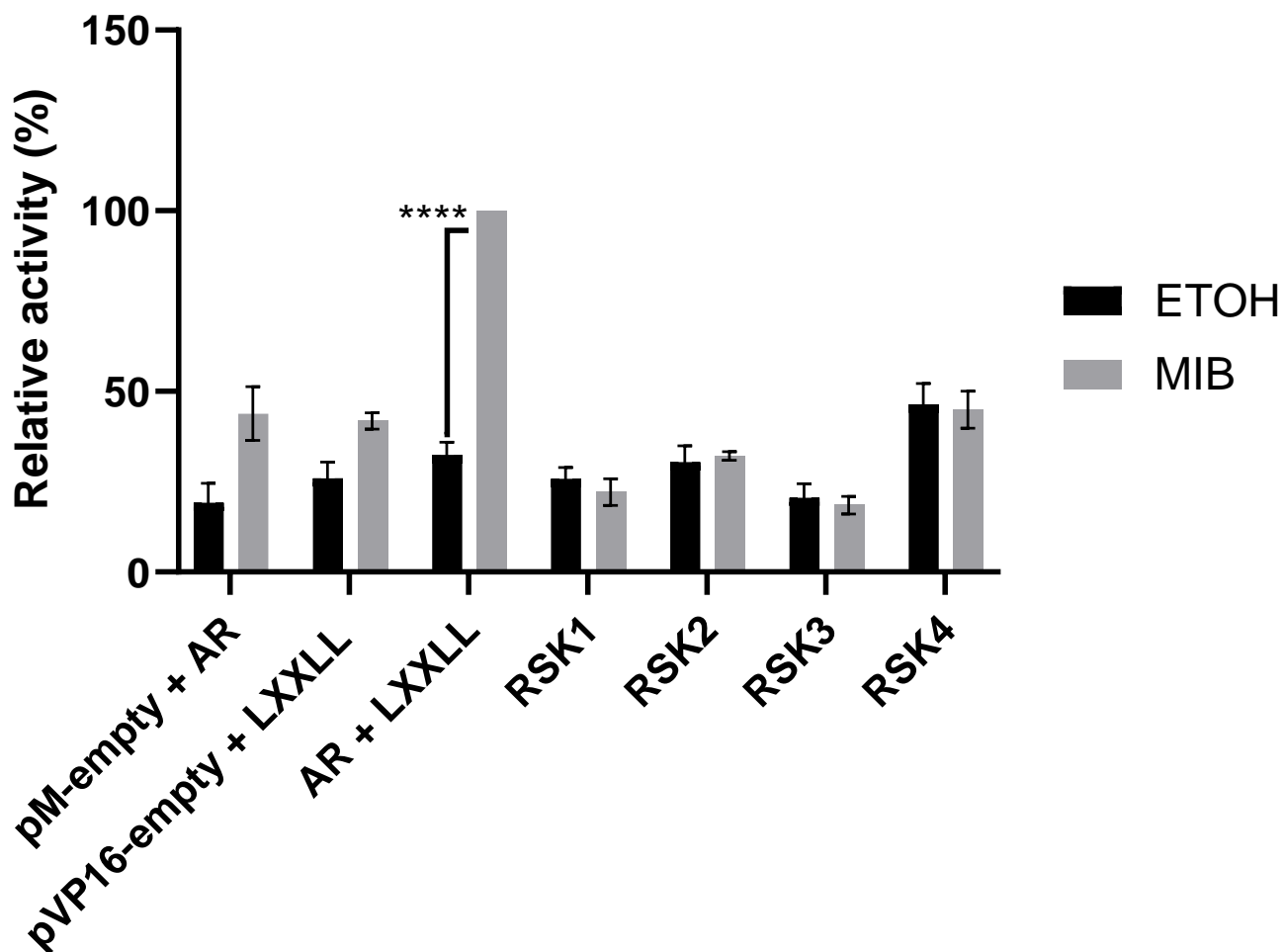


Figure 4.2.2.1 – Mammalian-2-hybrid assay of controls – COS-1 cells were transfected with the reporter plasmid 5GAL-LUC and DNA plasmids encoding for the genes, β -galactosidase, and one RSK isoform (excluding the positive control, which was transfected with AR and LXXLL) or a combination of AR, LXXLL, empty PM vector and empty pVP16 and incubated for 20-24 hours. Cells were then treated with either EtOH or 1nM of MIB 20-24 hours. AR Activity was measured using luciferase and normalised to β -GAL activity. Results are given as means \pm SE, four experimental repeats were performed. One-way ANOVA test was performed with Sidak's post hoc test, ****P<0.0001.

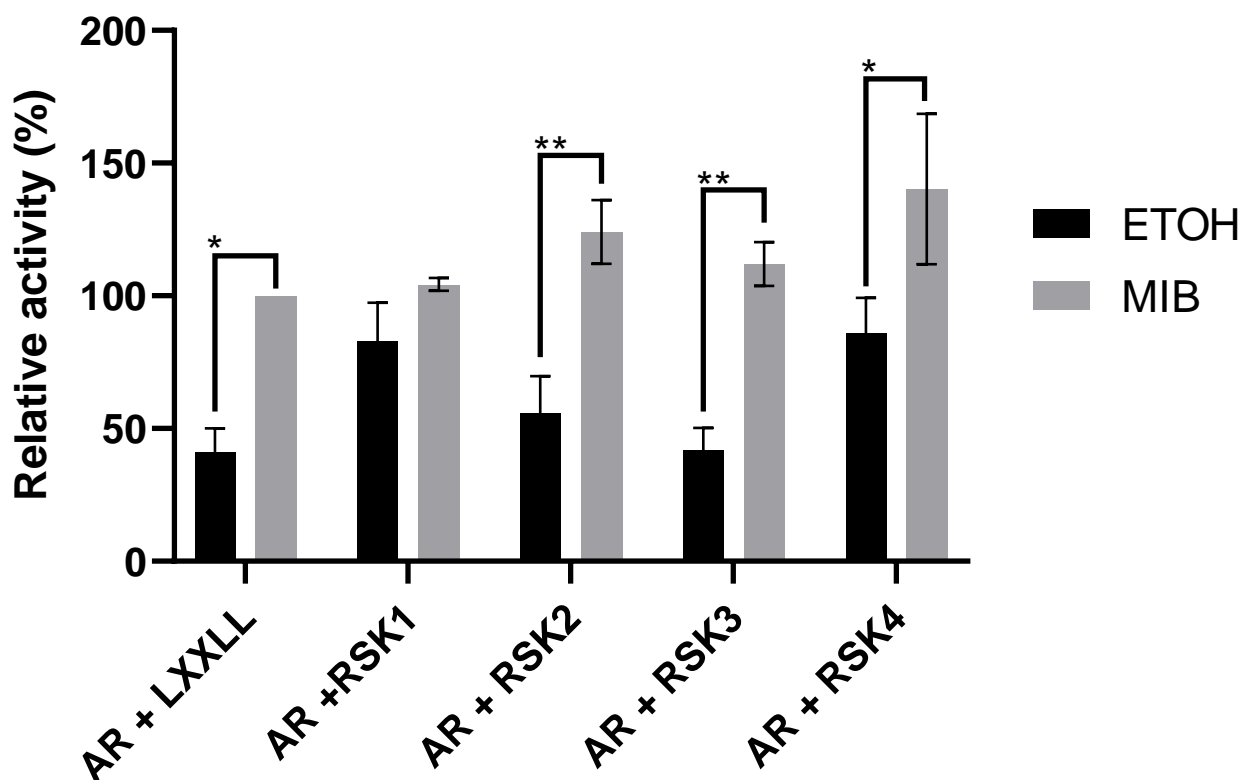


Figure 4.2.2.2 – Mammalian-2-hybrid assay of AR-RSK – COS-1 cells were transfected with the reporter plasmid 5GAL-LUC and DNA plasmids encoding for the genes, β -galactosidase, one RSK isoform and the AR (excluding the positive control AR+LXXLL) and then incubated for 20-24 hours. Cells were then treated with either EtOH or 1nM of MIB for 20-24 hours. AR Activity was measured using luciferase and normalised to β -GAL activity. Results are given as means \pm SE, four experimental repeats were used. One-way ANOVA test was performed with Sidak's post hoc test, *P<0.05, **P<0.005.

4.2.3 – RSKs influence the AR transcriptional program

As described above, the RSKs enhance AR activity. However, these experiments were performed in COS-1 cells and the proteins were expressed ectopically.

Transitioning to a more relevant disease related cell line was necessary to depict the importance of this RSK/AR signalling in a more biologically relevant context. To determine which cell line to choose, and to get a better understanding of RSK expression in PCa lines, RSK levels were investigated via qPCR (Figure 4.2.3.1). Further consideration must also be made to the AR state of these cells lines, as we intend to investigate the relationship between AR-RSK signalling it is important that the RSKs and AR are expressed endogenously and the cell line responds to treatment with synthetic androgens (Table 4.2.3.1).

Table 4.2.3.1 – Cell line, AR expression state and Ligand responsiveness – negative AR expression status depicts that no AR expression is traceable by western blotting whilst positive depicts that AR is detectable. Androgen unresponsive depicts no increase in growth occurs in response to androgen stimulation, androgen responsive depicts that increased growth rate is observed in response to androgen stimulation whilst androgen independent depicts increased growth rate despite the absence of androgens.

Cell Line	AR expression status	Response to androgen stimulation
PNT1A	Negative	Androgen unresponsive
LNCaP	Positive	Androgen responsive
C42	Positive	Androgen independent
C42B	Positive	Androgen responsive
22RV1	Positive	Androgen responsive
DU145	Negative	Androgen independent

In the healthy control cell line PNT1A, expression of RSK3/4 were significantly lower than the expression of both RSK1/2, in agreement with the literature (Houles & Roux 2018). RSK1 levels were reasonably constant across the cancer cell lines, although it was found to be significantly higher in 22RV1 cells compared to PNT1A. In contrast, RSK2 expression was significantly higher in LNCaP, C42 and C42B cell lines compared to the non-tumorigenic control. The expression of RSK3 and 4 were significantly higher than the PNT1A control across all cell lines except 22RV1 and DU145, respectively (Figure 4.2.3.1). Due to the RSK expression profile and the fact that the cell line is AR positive, it was decided that future experiments would be performed with LNCaP.

To investigate potential crosstalk between the AR and the RSKs, the initial focus was to determine if the AR regulates RSK1-4 expression at the transcriptional level. LNCaP were incubated in hormone-depleted media for 2 days and then treated with ETOH or 1 nM MIB for 24 hrs. No evidence of RSK1-4 regulation, at the RNA level, was found for the AR as addition of MIB resulted in no statistically significant changes in the expression of RSK1-4 (Figure 4.2.3.2). To determine if RSK signalling influences the AR transcriptional program, siRNA was used to deplete RSK1-4 levels. siRNA knockdowns were performed, followed by qPCR. Initial experiments were conducted to determine the efficacy of the siRNA knockdown; if siRNA was indeed causing a reduction in the desired isoform but also to determine if changes in expression of one isoform occurred when another is reduced by knockdown. In all cases the expression of the target RSK was significantly reduced when LNCaPs were transfected with the corresponding siRNA (Figures 4.2.3.3 A-D).

No significant changes were seen in the expression of the other RSKs when the individual RSKs were depleted, demonstrating that they siRNA have specificity.

The knock-down experiments were subsequently repeated to assess if depletion of the RSKs had an effect upon AR target genes PSA, Transmembrane protease serine 2 (TMPRSS2), N-Myc Downstream Regulated 1 (NDRG1), Zinc Finger And BTB Domain Containing 16 (ZBTB16), FK506 binding protein 5 (FKBP5) expression (Figure 4.2.3.4 A-E). siRNA knockdown of RSK2 resulted in a significant decrease in PSA expression (Figure 4.2.3.4.A). RSK1 and RSK2 siRNA knockdown significantly decreased TMPRSS2 expression (Figure 4.2.3.4.B) whereas siRNA knockdown of RSK1 and RSK4 caused a significant increase in MIB-induced expression of NDRG1 (Figure 4.2.3.4.C) There were no significant changes in FKBP5 (Figure 4.2.3.4.D) or ZBT116 (Figure 4.2.3.4.E) in response to RSK1-4 knock-down. Further, RSK3 knock-down had no impact on any of the AR target genes examined. The effect of the RSKs upon AR signalling is therefore isoform and target gene specific.

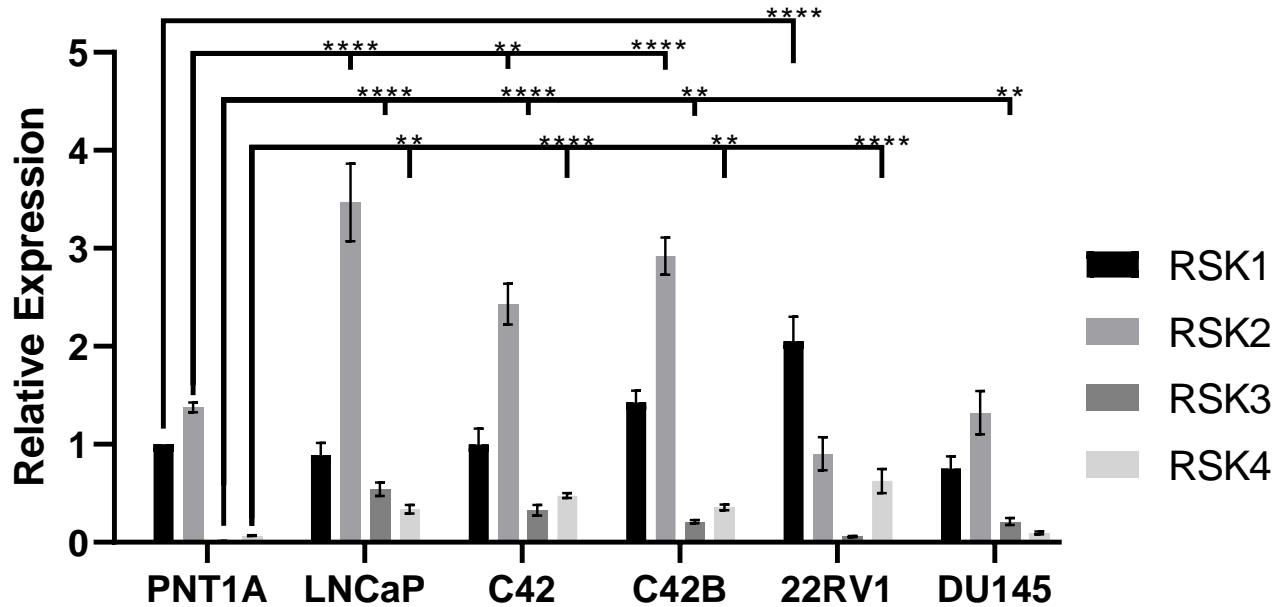


Figure 4.2.3.1– qPCR to monitor RSK expression in PCa cell lines – PCa cell lines were incubated until 80% confluency. RNA was then extracted, and reverse transcribed into cDNA before qPCR. Expression of the gene was measured by fluorescence with SYBR green dye. Results are given as means \pm SE, six experimental repeats were performed. One-way ANOVA test was performed with Sidak's post hoc test, ** $P < 0.005$, **** $P < 0.0001$.

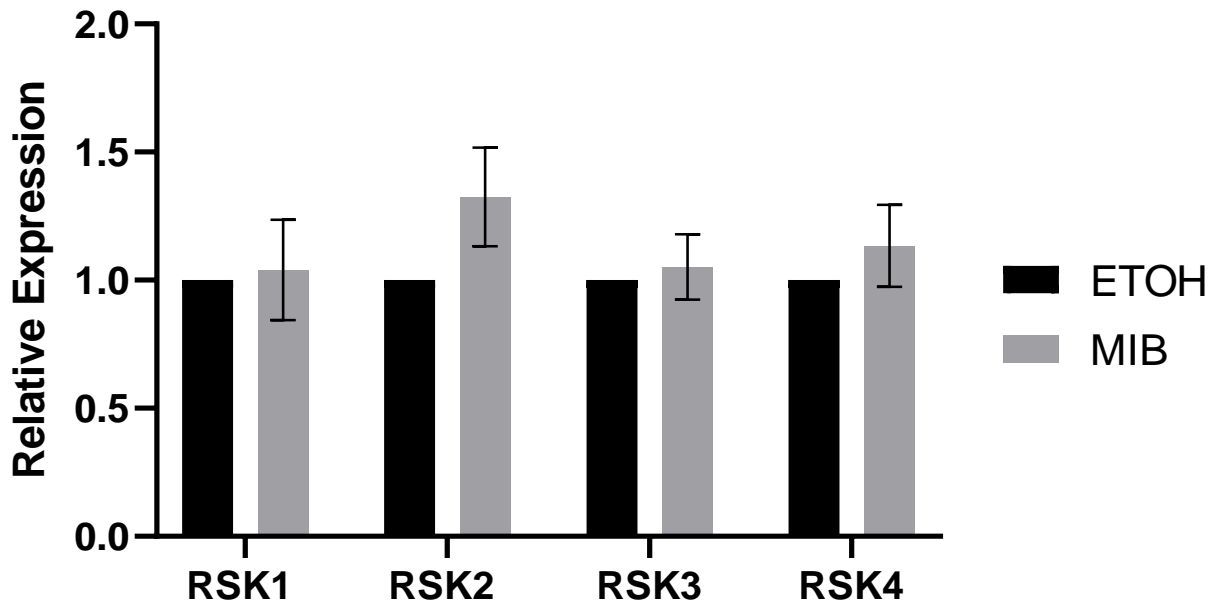


Figure 4.2.3.2– RSK expression is not altered by androgen stimulation - LNCAP cells were seeded into a 6 well plate in hormone rich media for 20-24 hours prior to a media change to hormone-depleted media for a further 20-24 hours. Cells were treated with either EtOH or 1nM MIB for 20-24 hours. RNA was then extracted, and reverse transcribed into cDNA before qPCR. Expression of the gene was measured by fluorescence with SYBR green dye. Results are given as means \pm SE, four experimental repeats were performed. One-way ANOVA test was performed with Sidak's post hoc test.

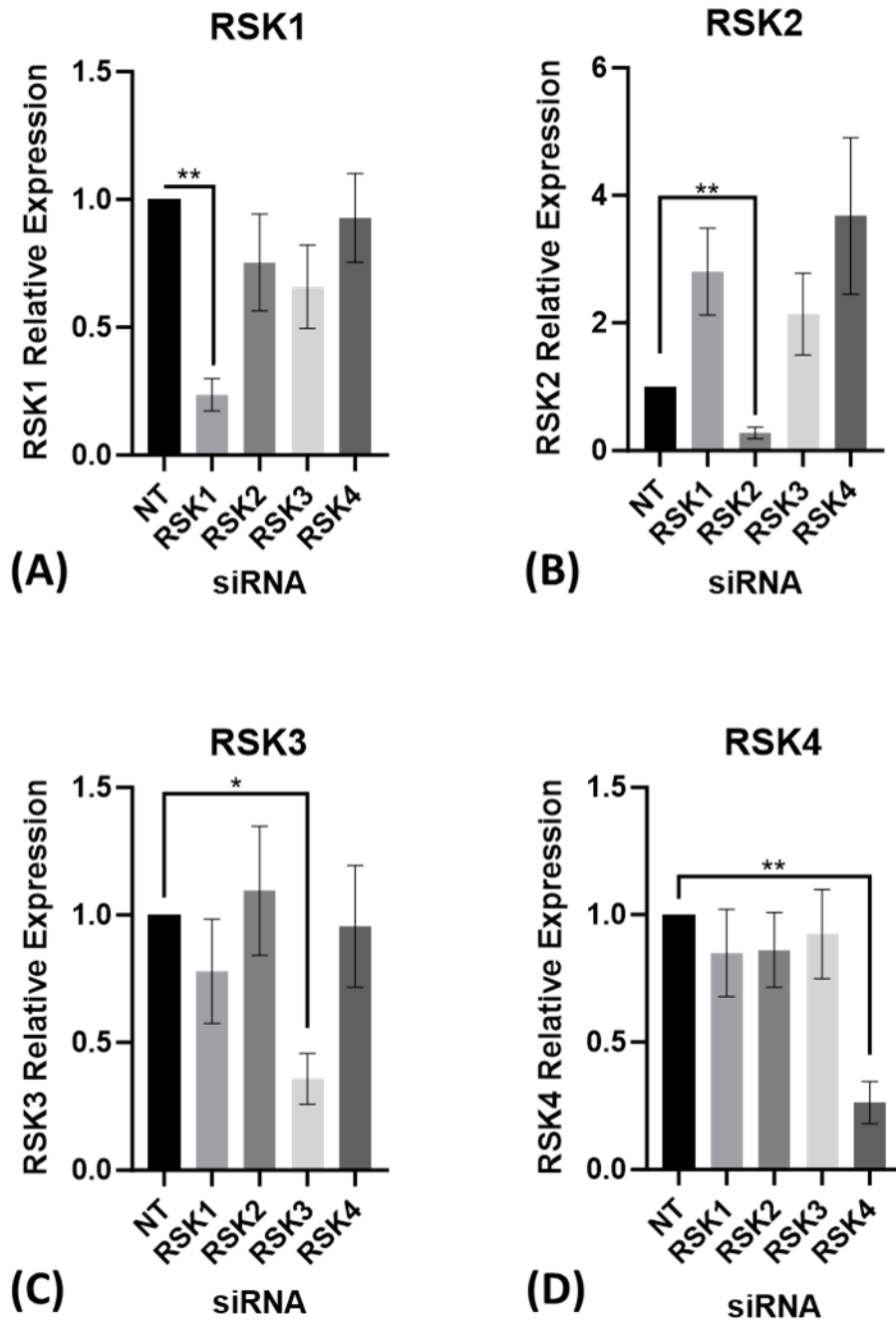


Figure 4.2.3.3 – siRNA knockdown of RSK coupled with qPCR of RSK1-4 expression in the presence of MIB - LNCAP cells were seeded into a 6 well plate in hormone rich media for 20-24 hours prior to a media change to hormone-depleted media for a further 20-24 hours. Cells were transfected with a pool of three siRNAs to knockdown one RSK isoform at a time (excluding the control (NT) which was transfected with non-targeting RNA) and then incubated for 72 hours. Cells were then treated with 1nM MIB for 20-24 hours. RNA was then extracted, and reverse transcribed into cDNA before qPCR. Expression of the gene was measured by fluorescence with SYBR green dye. Results are given as means \pm SE, five experimental repeats were performed. One-way ANOVA test was performed with Sidak's post hoc test, *P<0.05, **P<0.005.

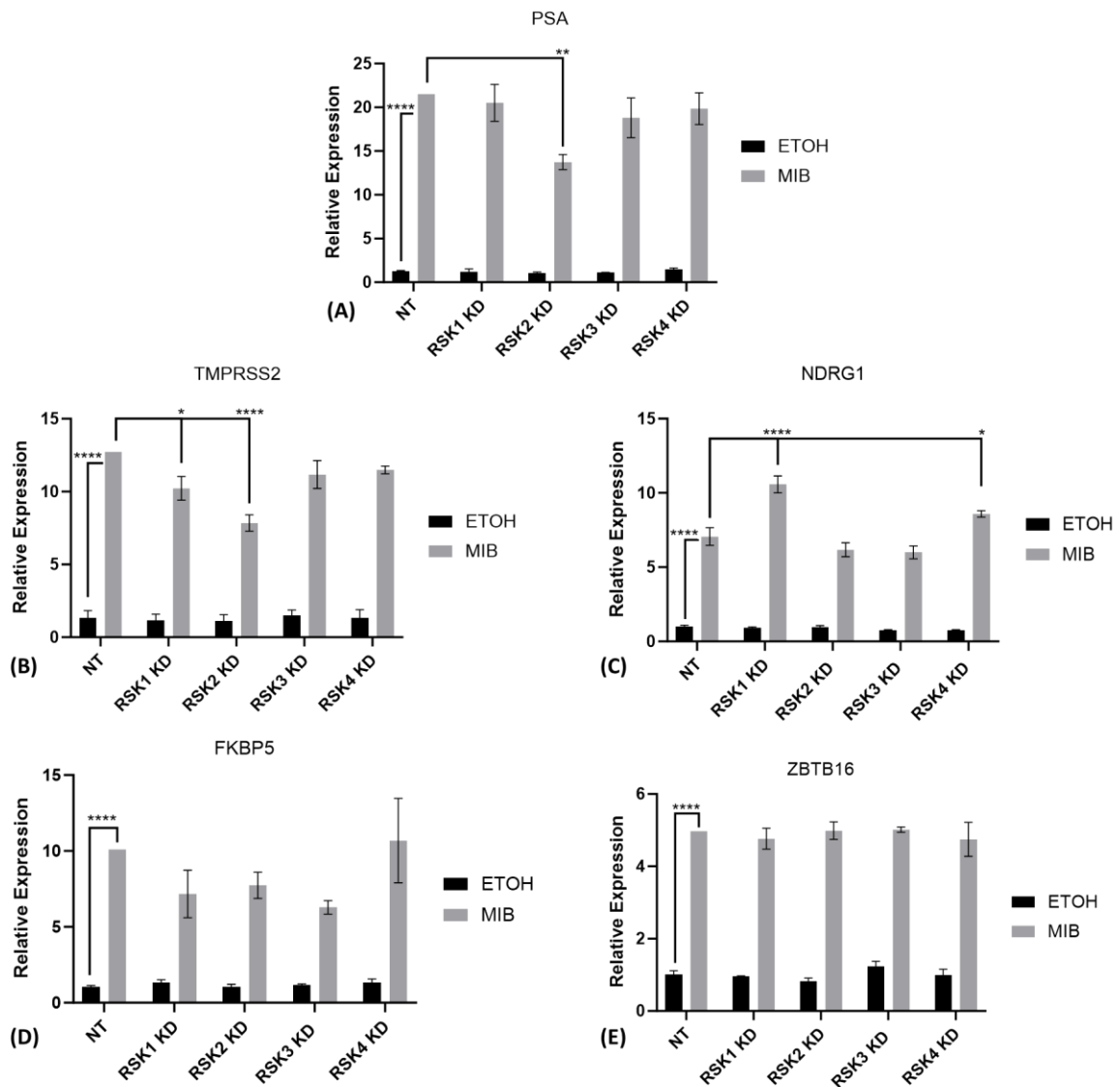


Figure 4.2.3.4 – siRNA knockdown of RSK coupled with qPCR to monitor expression of AR target genes – LNCaP cells were seeded into a 6 well plate in hormone rich media for 20-24 hours prior to a media change to hormone-depleted media for a further 20-24 hours. Cells were transfected with a pool of three siRNAs to knockdown one RSK isoform at a time (excluding the control (NT) which was transfected with non-targeting RNA) and then incubated for 72 hours. Cells were then treated with either EtOH or 1nM MIB for 20-24 hours. RNA was then extracted, and reverse transcribed into cDNA before qPCR. Expression of the gene was measured by fluorescence with SYBR green dye. Results are given as means \pm SE, three experimental repeats were performed. One-way ANOVA test was performed with Sidak's post hoc test, * $P < 0.05$, ** $P < 0.005$, **** $P < 0.0001$. A) PSA. B) TMPRSS2. C) NDRG1. D) FKBP5. E) ZBT.

4.2.4 – The RSKs reduce proliferation in LNCaPs

The MAPK pathway has been shown to contribute to PCa proliferation through several downstream components (Mukherjee *et al.* 2011), including RSKs (Clark *et al.* 2005; Yu *et al.* 2015). However, no studies have comprehensively investigated the effect of RSK isoforms on PCa proliferation. To answer this important question, WST proliferation assays were performed in LNCaP cells. Initially, the concentration of mibolerone and duration, to be used in the experiments, was optimized. These experiments clearly highlighted that a 5-day incubation was optimal compared to the 3-day and 7-day time periods. A significant increase in proliferation was evident for 1nM, 10nM and 100nM of mibolerone. To remain consistent with previous experiments 1nM was chosen with an incubation period of 5 days (Figure 4.2.4.1). Cells were subsequently transfected with siRNA and incubated for 72 hours, and then treated with 1 nM MIB for 5 days prior to the WST assay. A significant increase in proliferation was observed when cells were treated with MIB using cells transfected with non-targeting control (NT) siRNA. RSK2 and RSK4 knockdown resulted in a significant decrease in the androgen-induced proliferation of LNCaPs, whilst RSK1/3 had no significant effect upon proliferation (Figure 4.2.4.2). This therefore highlights the contribution of RSK2/4 to the proliferation of LNCaP cells.

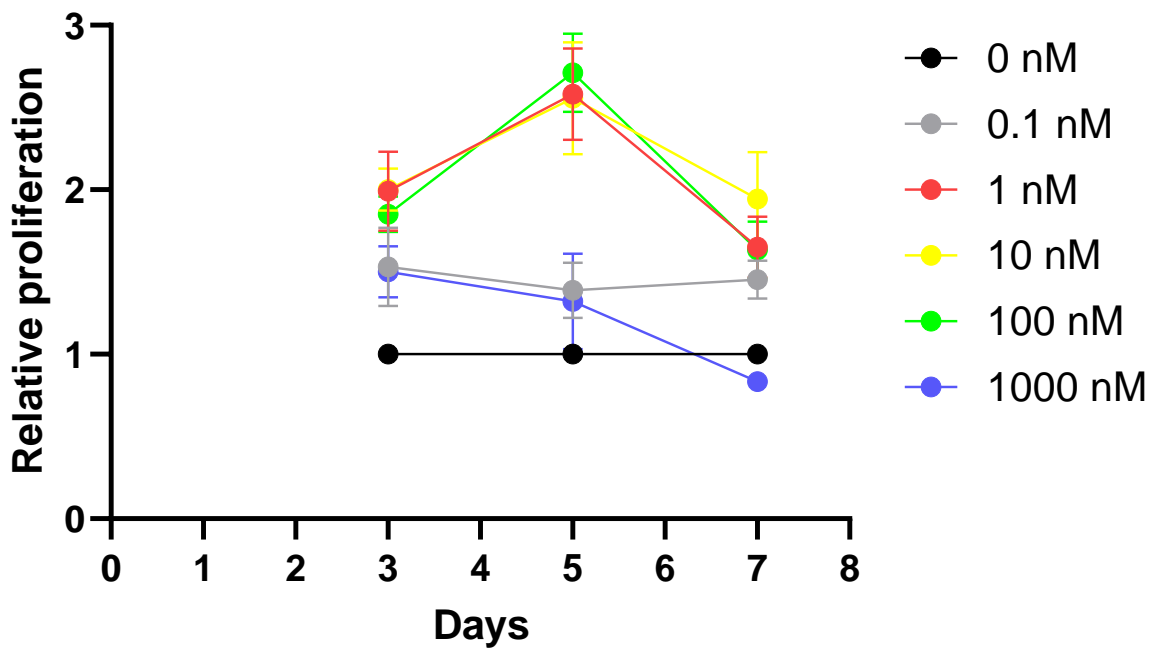


Figure 4.2.4.1 – WST hormone optimisation assay – LNCaP cells were seeded in a 96 well plate in hormone-depleted media for 20-24 hours prior to transfection with non-targeting siRNA and incubated for 72 hours. Cells were then treated with a dose range of MIB over three different time periods, 3 days, 5 days, and 7 days. The WST assay was then performed. Three experimental repeats were performed.

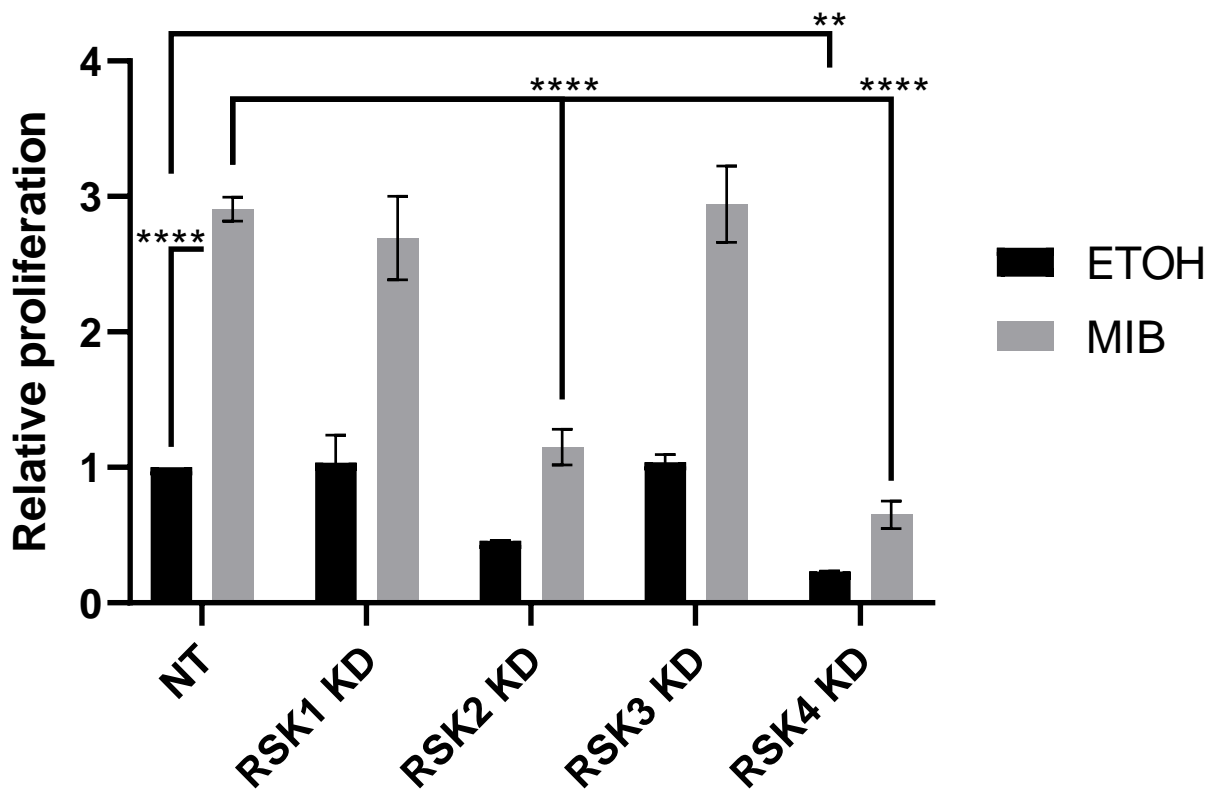


Figure 4.2.4.2 – RSK siRNA knockdown WST assay – LNCAP cells seeded in a 96 well plate in hormone-depleted media for 20-24hours. Cells were then transfected with a pool of three siRNAs to knockdown one RSK isoform at a time (excluding the control (NT) which was transfected with non-targeting RNA) and incubated for 72 hours. Cells were then treated with either EtOH or 1nM MIB for 120 hours. WST assay was then performed. Results are given as means \pm SE, three experimental repeats were performed. One-way ANOVA test was performed with Sidak's post hoc test, **P<0.005, ****P<0.0001.

4.3 – Discussion

4.3.1 – Results Overview

This chapters investigated the role of the RSKs in AR signalling and PCa proliferation. Luciferase reporter assays showed that all RSKs significantly increased AR transcriptional activity (Chapter 4.2.1). Further, the mammalian 2 hybrid assays demonstrated that the RSKs interact, or are in proximity, with the AR (Chapter 4.2.2). qPCR of PCa cell lines highlighted that RSKs showed a general increase across all PCa cell lines, most significantly RSK2, but more interestingly RSK3/4 which goes against current literature (Houles & Roux 2018) (Chapter 4.2.3). Based on this, further experiments were expanded to the LNCaP PCa cell line, so that the effects of the RSKs upon AR signalling could be investigated using endogenous proteins. siRNA knockdown coupled with qPCR was used to infer if the RSKs influence the AR transcriptional program. RSK expression was investigated which determined that all siRNA knockdowns were significantly reducing expression of the desired isoform (Chapter 4.2.3). Importantly, expression of key AR target genes was differentially regulated by the RSKs; RSK1 and RSK4 knockdown resulted in an increase in the expression of *NDRG1*; RSK1 and RSK2 knockdown induced a decrease in *TMPRSS2*; RSK2 knocked down produced a significant decrease in *PSA*, respectively. Differently from the other RSKs, RSK3 knockdown caused no significant changes in any of the investigated genes of interest (Chapter 4.2.3). To investigate if the RSKs affect cell growth, WST proliferation assays were undertaken. These experiments showed that RSK2 and RSK4 knockdown significantly reduced LNCaP proliferation (Chapter 4.2.3).

4.3.2 – RSK expression is elevated in Prostate Cancer

PCa arises through the accumulation of mutations which results in prostatic intraepithelial neoplasia, which is an abnormal state of prostate cells with different growth and morphology. Accumulation of further mutations drives development of prostate cells into an adenocarcinoma (Gandhi *et al.* 2018; Packer & Maitland 2016). Many of the mutations acquired are centered around altering the activation and regulation of the AR transcriptional program (Pine *et al.* 2016; Taylor *et al.* 2010). This is often achieved through constitutively active signalling pathways which cause altered cellular function such as increased growth rate. The MAPK pathway is one such pathway which is upregulated across many cancers (Romeo *et al.* 2012) and there are several common mutations across these cancer types which have also been shown to contribute to PCa progression, such as B-Raf or K-Ras (Aronchik *et al.* 2014; Mukherjee *et al.* 2011). Aberrant activation of the MAPK pathway often results in the activation of the RSKs which are contributing to PCa signalling.

It was demonstrated that the RSKs generally exhibited increased expression across PCa cell lines compared to the nontumorigenic control (PNT1A). RSK1/2 expression was consistently higher than that of RSK3/4 (Figure 4.2.3.1) which agrees with the literature (Houles & Roux 2018); these studies have suggested that RSK1/2 possess a more dominant role with oncogenic characteristics whilst RSK3/4 expression is suppressed due to tumour suppressor activity. Indeed, RSK2 expression was significantly higher in LNCaP and its derivatives C42 and C42B compared to PNT1A. Additionally, RSK2 expression was higher than all of the other RSKs in all cell lines, with the exception of RSK1 in 22RV1 (Figure 4.2.3.1). This

expression pattern also agrees with the previous investigation of RSKs in PCa by Clark *et al.* (2005), who highlighted that RSK1/2 protein levels were elevated 2.5-3.5 fold in PCa patient biopsies compared to normal prostate tissue (Clark *et al.* 2005). However, in this study, RSK1 expression was relatively consistent across the PCa cell lines, except for 22RV1 which showed a significant increase in expression.

As described previously, RSK1/2 are thought to have oncogenic activity whereas RSK3/4 appear to have tumour suppressor activity and so it was hypothesized that the expression of these isoforms would differ between cells. In support of this, RSK3/4 expression was barely detectable in the healthy control cell line PNT1A. However, RSK3/4 expression was significantly increased in all PCa cell lines except for 22RV1 and DU145 respectively (Figure 4.2.3.1). This is therefore contradictory to the suggestion that these are tumour suppressors, as the expression of RSK3/4 was up-regulated in these models of castrate resistant disease. This could suggest that RSK3/4 play an important role in tumour progression to castrate resistance. However, it should be noted that only one non-tumorigenic line was used here and it is unclear of how representative this line is of normal prostate tissues. Future analysis of healthy control/patient samples will therefore be important to better understand alterations in RSK expression in the development and/or progression of prostate cancer.

4.3.3 – RSKs regulate AR activity

Members of the RSK family have previously been shown to regulate the AR in PCa. Specifically, RSK2 has been linked to PCa, as overexpression or hyperactivation of RSK2 led to an increase in PSA expression. Furthermore, this regulation of the AR transcriptional program was demonstrated to be through RSK2 binding to p300/CBP (Clark *et al.* 2005). Additionally, RSK1 has been shown to indirectly regulate the transcription of AR through phosphorylation of YB1 at S102. This phosphorylation of YB1 enhances its translocation to the nucleus and binding to its cognate Y-box which in turn regulates the AR transcriptional program (Shiota *et al.* 2011, 2014).

Luciferase assays were used to investigate RSK regulation on AR activity.

Interestingly, all RSK isoforms were found to significantly increase AR transcriptional activity (Figure 4.2.1.2). This agrees with the literature that demonstrated that RSK1 and RSK2 can enhance the AR transcriptional program (Clark *et al.* 2005; Nabbi *et al.* 2017; Yu *et al.* 2015). In contrast, to date, no studies have investigated the involvement of RSK3/4 in AR signalling which makes this result more significant and novel. Additionally, these results contradict the notion that RSK3/4 have tumour suppressor qualities. If that were the case, it would be expected that RSK3/4 would reduce AR transcriptional activity. It could be argued that this result is due to the use of a model system (COS-1) and perhaps an artefact of overexpression of exogenous proteins, furthermore, there are no western blots to confirm the expression of the AR within the COS-1 cells which could question if the RSKs are affecting the cells via another mode of action. Therefore, additional experiments were conducted in the more physiologically relevant PCa cell line LNCaP. siRNA

knockdown of the RSKs coupled with qPCR of known AR target genes produced interesting results.

RSK2 knockdown caused a significant decrease in *PSA* expression (Figure 4.2.3.4.A), suggesting that this RSK enhances the expression of this gene. *PSA* is a serine protease which is secreted into the prostate lumen to cleave semenogelin I and II. In PCa, *PSA* expression is elevated and is a well-established biomarker which has been used as a diagnostic and prognostic tool to assist with clinical decision making (Balk *et al.* 2003). Previous literature showed that overexpression and hyperactivation of RSK2 caused an increase in expression of *PSA* (Clark *et al.* 2005). Considering this, it would suggest that RSK2 enhances AR regulation of *PSA* expression in an oncogenic manner.

RSK1 and RSK2 knockdown caused a significant decrease in *TMPRSS2* expression (Figure 4.2.3.4.B), suggesting that these RSKs enhance the transcription of this gene. *TMPRSS2* is type II transmembrane serine protease which is highly expressed in the prostate and is associated with PCa progression (Chen *et al.* 2010).

Immunohistochemistry has identified *TMPRSS2* expression on the apical plasma membrane of the healthy prostate luminal cells and expression was elevated and mislocalized across the whole cell membrane in PCa patient samples (Chen *et al.* 2010). In addition, it has been shown that *TMPRSS2* stimulates a proteolytic cascade which promotes tumour growth and metastasis in a DHT-dependent manner (Ko *et al.* 2015). Furthermore, *TMPRSS2* is commonly involved in a gene fusion event linked to PCa development/progression (Dudka *et al.* 2020). Taken

together this could suggest an oncogenic role of RSK1/2 because they enhance *TMPRSS2* expression in LNCaP which has a strong oncogenic association.

Knockdown of RSK1 and RSK4 led to an increase in the expression of the AR regulated gene *NDRG1* (Figure 4.2.3.4.C). This suggests that both RSKs were repressing the expression of *NDRG1*. *NDRG1* is ubiquitously expressed but has elevated expression in the prostate and has been shown to act as a tumour suppressor in many different cancer types including PCa (Bae *et al.* 2013). An example of this was demonstrated by using both inhibitors and siRNA knockdown on both PC3 cells. The inhibitor Valporic acid (VPA), which is a histone deacetylase inhibitor was shown to upregulate *NDRG1* in PC3 cells which inhibited the metastatic characteristics of PC3 cells. In a converse manner siRNA knockdown of *NDGR1* caused an increase in cell invasion, as such, it was the expression of *NDGR1* exhibiting tumour suppressor properties by inhibiting this invasion program (Lee & Kim 2015). Concurrently, knockdown of *NDRG1* in LNCaP cells promoted expression of metastatic proteins and an increase in metastasis (Quan *et al.* 2021). In further agreement, *NDRG1* overexpression in DU145 prostate cancer cells attenuated transforming growth factor beta (TGF- β) induced EMT. This was achieved by inhibiting downstream signalling of TGF- β and maintain E-cadherin and β -catenin which are significantly decreased in the absence of *NDRG1* (Chen *et al.* 2012). Taken together this data would suggest an oncogenic role of RSK1/4, through suppression of *NDRG1* expression.

Two additional AR regulated genes were investigated, *FKBP5* (Figure 4.2.3.4.D) and *ZBTB16* (Figure 4.2.3.4.E) and No RSK knockdowns caused a significant change in expression of these genes. *FKBP5* has recently been shown to also act as a tumour suppressor, utilizing a conserved mechanism of repression in multiple types of cancer including PCa (Mall *et al.* 2022). *ZBTB16* is a transcription factor and is known to regulate several essential facets of cell function. More specifically, *ZBTB16* has been shown to act as a tumour suppressor; overexpression was shown to inhibit proliferation multiple PCa cells lines whilst siRNA/shRNA knockdown of *ZBTB16* results in increased proliferation (Jin *et al.* 2017). The fact that none of the RSKs were shown to influence the expression of these two AR target genes could be seen as a negative result, however, it is understood that the AR transcriptional activity can be influenced differentially. Transcription of AR genes is not simply an 'on or off' scenario meaning all genes, or no genes are transcribed. The AR selectively regulates genes and the transcriptome appears to be regulated by post-translational modifications (Anbalagan *et al.* 2012; Gioeli & Paschal 2012; Wen *et al.* 2020) and/or co-regulators function (Golias *et al.* 2009; Heemers & Tindall 2007; Heinlein 2004).

To conclude, these results highlight that the RSKs can influence AR transcriptional activity and that they regulate the AR transcriptional program in LNCaP cells. These results also suggest that RSK2 has the most pronounced effect upon the AR transcriptional program. Further, and perhaps more interesting, RSK4 may regulate the AR transcriptional program in an oncogenic manner. Knowing this information now poses the question as to how the RSKs modulate AR activity.

4.3.4 – RSKs interact with the AR in proximity

As previously mentioned, RSK2 directly influences the AR through a complex with p300/CBP (Clark *et al.* 2005) and RSK1 indirectly modulates AR activity through phosphorylation of the co-regulator YB1 (Shiota *et al.* 2011, 2014). To investigate potential interactions further, M2H assays were performed. The assay demonstrated that all RSKs interact with/are in proximity to the AR (Figure 4.2.2.2) and two modes of action can be seen. RSK2/3/4 interact with the AR in a ligand dependent manner whereas RSK1 interacts with the AR in a ligand independent manner (Figure 4.2.2.2).

Taken alone, the M2H assays are unable to verify if the RSKs and AR interact directly as a positive result in this assay could be interpreted in different ways: i) the RSKs could be binding to the AR directly ii) the RSKs could be binding to the AR indirectly as part of a complex. Initial work with RSK2 and Estrogen receptor alpha (ER α) showed that RSK2 directly binds to the LBD and phosphorylates ER α at S167 which induces conformational changes in the AF-2 which enhanced transcriptional activity (Clark *et al.* 2001). However, more recent work reported that ER α sequesters RSK2 into the nucleus via direct interaction but not phosphorylation of S167 which activated the pro-neoplastic transcriptional program (Ludwik *et al.* 2018). This completely contradicts the work by Clark *et al.* 2001. When considering the evidence presented by both Clark *et al.* 2001 and Ludwik *et al.* 2018, the evidence presented by Ludwik *et al.* 2018 is more compelling due to the more diverse and sophisticated techniques used. This is apparent through the use of BCa cell lines and mouse models by Ludwik *et al.* 2018 as opposed to the use of one cell line, BHK cells, and

more basic techniques by Clark *et al.* 2001 (Although these differences may partly be due to the techniques available at the time of research). Similar to the work of Ludwik *et al.* 2018, RSK2 has also been shown to participate in larger complex formation in PCa (Clark *et al.* 2005) through association of with p300/CBP and the AR which was validated by using a p300 competitive inhibitor E1A. Within their research, to emulate earlier work (Clark *et al.* 2001), which highlighted RSK2 phosphorylation of S167, Clark *et al.* 2005 attempted to show that RSK2 phosphorylates the AR in the same manner. Using kinase phosphorylation assays they showed that RSK2 does not phosphorylate the known activating sites of the AR (S208 and S778) as RSK2 only caused a 2-fold increase in phosphorylation of the AR peptide compared to a 150-fold increase in phosphorylation of the ER α peptide. However, while the authors excluded the direct phosphorylation of AR, the peptides used were created based upon the RSK recognition site RXRXXS/T. This has several limitations since the RSKs have been shown to preferentially but not exclusively phosphorylate this motif. For example C-Fos (S362), YB1 (S102) and p65 (S536) are phosphorylated by the RSKs but lack the recognition sequence (Lara *et al.* 2013). Furthermore, the AR has many phosphorylation sites (at least 25) which makes it unlikely that all were discovered at the time (Wen *et al.* 2020). It is still therefore a matter of debate as to whether RSK2 may phosphorylate the AR. Independently from RSK-SR complexes/phosphorylation RSK1 has been shown to form a complex with ERK and the S100B protein which in turn contributes to malignant melanoma. Furthermore this formation of the complex was shown to sequester RSK1 in the cytoplasm, which inhibits ERK phosphorylation of RSK1 CTKD at T573 thus may contribute to anti-metastatic signalling in malignant melanoma (Hartman *et al.* 2014). Considering this literature and the vast literature of

AR being regulated by co-regulators (Golias *et al.* 2009; Heemers & Tindall 2007; Heinlein 2004) and post-translational modifications (Anbalagan *et al.* 2012; Gioeli & Paschal 2012; Wen *et al.* 2020) it seems feasible that the RSKs could regulate the AR by either mechanism and further experiments are needed to determine this.

4.3.5 – RSKs regulate LNCaP proliferation

The RSKs have been shown to regulate several aspects of PCa including cell proliferation (chapter 1.4.1), cell cycle regulation (chapter 1.4.2), cell motility (chapter 1.4.3) and therapy resistance (chapter 1.4.4). Proliferation assays were conducted to determine if the RSKs regulation of the AR could elicit a global effect on the PCa cells. This was achieved by using siRNA to knockdown the RSKs and then the effect upon proliferation was quantified by WST assay. LNCaP proliferation was significantly decreased when RSK2 or RSK4 were knocked down (Figure 4.2.4.2). This suggests that RSK2/4 may act in an oncogenic capacity within PCa signalling. This coincides with previous literature about RSK2 (Chen *et al.* 2013; Clark *et al.* 2005; Doehn *et al.* 2009; Gawecka *et al.* 2012; Wu *et al.* 2014) but provides new insight into the role of RSK4 in PCa signalling. Similar to these results, both RSK2 and RSK4 knockdown in A549 lung cancer cells inhibited metastasis suggesting oncogenic qualities in this cell type (Lara *et al.* 2011). Conversely, RSK4 has been shown to act as a tumour suppressor in BCa cell line MDA-MB-231, reducing metastasis and proliferation (Thakur *et al.* 2008). This data presents a novel insight into RSK signalling, suggesting that the different RSKs may have different activities in different tumour types, and proves why research should be comprehensive

especially when considering protein isoforms because although they have high similarity, they possess distinct and varied functions.

4.3.6 – Conclusion

When considering these data, the RSKs are likely involved in AR signalling and in turn contribute to PCa progression. Further investigations are therefore warranted. Indeed, RSK expression across PCa cell lines was intriguing, especially considering RSK3/4 expression. However, the number of cell lines utilized was limited. This could be expanded to give a broader understanding by using additional PCa cell lines and analyzing patient samples. Luciferase assays showed that all RSKs activated the AR which highlighted a potential mechanism of PCa regulation; this was validated using siRNA knockdowns coupled with qPCR for AR target genes in LNCaP cells. siRNA knockdowns highlighted the ability of RSK1, RSK2 and RSK4 to influence expression of AR target genes. These experiments give useful insight into the cross-talk between the RSKs and AR but these experiments can be expanded; i) using additional PCa cell lines as RSK levels vary between lines ii) using RNA-seq to understand global changes in the transcriptome. Nevertheless, the qPCR results can be used to support the hypothesis that the RSK family modulates AR signalling. The proliferations assays showed that RSK2/4 knockdown significantly decreased LNCaP proliferation; this coincides with the data obtained for RSK2/4 from qPCR which is important as RSK4 has been identified as a novel regulator of the AR activity. Additionally, the fact that the RSK2 data presented here agrees with previous studies further validates the approach and likelihood of these data showing true insight into this signalling cross-talk. Beyond these experiments there are several avenues to

follow. Additional assays could be performed to investigate if the RSKs regulate more processes than proliferation such as cell motility and therapy resistance.

Transitioning to mouse models and patient derived models would also be a sensible progression as it would allow for further intricacies such as the immune system to be introduced and also allow for experimentation on the method of drug delivery.

4.4 - Final conclusion

RSK1/2 have been implicated in PCa signalling but there are no studies investigating the involvement of RSK3/4 to date. The underrepresentation of RSK3/4 is undoubtedly leaving gaps of knowledge surrounding RSK signalling, a comprehensive study into the role of RSKs in PCa signalling was undertaken. Here I demonstrate that the RSKs regulate the AR transcriptional program in a differential manner and that RSK2/4 regulate the proliferation in PCa cell line LNCaP. This carries some significance due to the novelty of RSK4 in PCa signalling. However, the role of the RSKs varies in different tissues and cancers, for example, here we show RSK4 may exhibit oncogenic characteristics which coincides with the role of RSK4 in lung cancer (Chrysostomou *et al.* 2021) but differs from its reported tumour suppressor qualities in BCa (Jiang *et al.* 2017). The differential mechanisms of regulation must arise from structural differences between isoforms, despite having high sequence identity in conserved regions. To expand on this the structure and mechanism of activation of RSK4 was investigated. While protein purification yielded no protein crystals, pull down assays experimentally confirmed the proposed mechanism of the interaction between RSK4 CTKD and the HM which has not previously been confirmed. Expansion of both RSK-AR signalling and RSK4 structural studies could be used to develop future therapeutic treatments for PCa.

Bibliography

- Alexa, A., Gógl, G., Glatz, G., Garai, Á., Zeke, A., Varga, J., Dudás, E., Jeszenői, N., Bodor, A., Hetényi, C., & Reményi, A. (2015). Structural assembly of the signaling competent ERK2–RSK1 heterodimeric protein kinase complex. *Proceedings of the National Academy of Sciences*, **112**(9), 2711–2716.
- Almami, A., Hegazy, S. A., Nabbi, A., Alshalalfa, M., Salman, A., Abou-Ouf, H., Riabowol, K., & Bismar, T. A. (2016). ING3 is associated with increased cell invasion and lethal outcome in ERG-negative prostate cancer patients. *Tumor Biology*, **37**(7), 9731–9738.
- Anbalagan, M., Huderson, B., Murphy, L., & Rowan, B. G. (2012). Post-translational modifications of nuclear receptors and human disease. *Nuclear Receptor Signaling*, **10**(Figure 1), nrs.10001.
- Anjum, R., & Blenis, J. (2008). The RSK family of kinases: Emerging roles in cellular signalling. *Nature Reviews Molecular Cell Biology*, **9**(10), 747–758.
- Aronchik, I., Appleton, B. A., Basham, S. E., Crawford, K., Del Rosario, M., Doyle, L. V., Estacio, W. F., Lan, J., Lindvall, M. K., Luu, C. A., Ornelas, E., Venetsanakos, E., Shafer, C. M., & Jefferson, A. B. (2014). Novel potent and selective inhibitors of p90 ribosomal S6 kinase reveal the heterogeneity of RSK function in MAPK-driven cancers. *Molecular Cancer Research*, **12**(5), 803–812.
- Bae, D.-H., Jansson, P. J., Huang, M. L., Kovacevic, Z., Kalinowski, D., Lee, C. S., Sahni, S., & Richardson, D. R. (2013). The role of NDRG1 in the pathology and potential treatment of human cancers. *Journal of Clinical Pathology*, **66**(11), 911–917.
- Balk, S. P., Ko, Y.-J., & Bubley, G. J. (2003). Biology of Prostate-Specific Antigen. *Journal of Clinical Oncology*, **21**(2), 383–391.
- Baneyx, F., & Mujacic, M. (2004). Recombinant protein folding and misfolding in *Escherichia coli*. *Nature Biotechnology*, **22**(11), 1399–1408.
- Boutros, R., Lobjois, V., & Ducommun, B. (2007). CDC25 phosphatases in cancer cells: Key players? Good targets? *Nature Reviews Cancer*, **7**(7), 495–507.
- Boutros, R., Mondesert, O., Lorenzo, C., Astuti, P., & McArthur, G. (2013). CDC25B Overexpression Stabilises Centrin 2 and Promotes the Formation of Excess Centriolar Foci. *PLoS ONE*, **8**(7), 67822.
- Brooke, G., & Bevan, C. (2009). The Role of Androgen Receptor Mutations in Prostate Cancer Progression. *Current Genomics*, **10**(1), 18–25.
- Calloni, G., Chen, T., Schermann, S. M., Chang, H., Genevaux, P., Agostini, F., Tartaglia, G. G., Hayer-Hartl, M., & Hartl, F. U. (2012). DnaK Functions as a Central Hub in the *E. coli* Chaperone Network. *Cell Reports*, **1**(3), 251–264.
- Campi, R., Brookman-May, S. D., Subiela Henríquez, J. D., Akdoğan, B., Brausi, M., Klatte, T., Langenhuijsen, J. F., Linares-Espinos, E., Marszalek, M., Roupret, M., Stief, C. G., Volpe, A., Minervini, A., & Rodriguez-Faba, O. (2019). Impact of Metabolic Diseases, Drugs, and Dietary Factors on Prostate Cancer Risk, Recurrence, and Survival: A Systematic Review by the European Association of Urology Section of Oncological Urology. *European Urology Focus*, **5**(6), 1029–

1057.

- Cancer Research UK. Prostate cancer statistics.
<https://www.cancerresearchuk.org/health-professional/cancer-statistics/statistics-by-cancer-type/prostate-cancer#heading-Five>. Retrieved April 8, 2020, from <https://www.cancerresearchuk.org/health-professional/cancer-statistics/statistics-by-cancer-type/prostate-cancer#heading-Five>
- Cargnello, M., & Roux, P. P. (2011). Activation and Function of the MAPKs and Their Substrates, the MAPK-Activated Protein Kinases. *Microbiology and Molecular Biology Reviews*, **75**(1), 50–83.
- Chan, H. M., & La Thangue, N. B. (2001). p300/CBP proteins: HATs for transcriptional bridges and scaffolds. *Journal of Cell Science*, **114**(13), 2363–2373.
- Chao, O. S. P., & Clément, M. V. (2006). Epidermal growth factor and serum activate distinct pathways to inhibit the BH3 only protein BAD in prostate carcinoma LNCaP cells. *Oncogene*, **25**(32), 4458–4469.
- Chen, C., Zhang, L., Huang, N. J., Huang, B., & Kornbluth, S. (2013). Suppression of DNA-damage checkpoint signaling by Rsk-mediated phosphorylation of Mre11. *Proceedings of the National Academy of Sciences of the United States of America*, **110**(51), 20605–20610.
- Chen, Y.-W., Lee, M.-S., Lucht, A., Chou, F.-P., Huang, W., Havighurst, T. C., Kim, K., Wang, J.-K., Antalis, T. M., Johnson, M. D., & Lin, C.-Y. (2010). TMPRSS2, a Serine Protease Expressed in the Prostate on the Apical Surface of Luminal Epithelial Cells and Released into Semen in Prostatomes, Is Misregulated in Prostate Cancer Cells. *The American Journal of Pathology*, **176**(6), 2986–2996.
- Chen, Z., Zhang, D., Yue, F., Zheng, M., Kovacevic, Z., & Richardson, D. R. (2012). The Iron Chelators Dp44mT and DFO Inhibit TGF- β -induced Epithelial-Mesenchymal Transition via Up-Regulation of N-Myc Downstream-regulated Gene 1 (NDRG1). *Journal of Biological Chemistry*, **287**(21), 17016–17028.
- Chesshyre, J. A., & Hipkiss, A. R. (1989). Low temperatures stabilize interferon α -2 against proteolysis in *Methylophilus methylotrophus* and *Escherichia coli*. *Applied Microbiology and Biotechnology*, **31**, 158–162.
- Chrysostomou, S., Roy, R., Prischi, F., ... Pardo, O. E. (2021). Repurposed floxacins targeting RSK4 prevent chemoresistance and metastasis in lung and bladder cancer. *Science Translational Medicine*, **13**(602).
 doi:10.1126/scitranslmed.aba4627
- Clark, D. E., Errington, T. M., Smith, J. A., Frierson, H. F. J., Weber, M. J., & Lannigan, D. A. (2005). The serine/threonine protein kinase, p90 ribosomal S6 kinase, is an important regulator of prostate cancer cell proliferation. *Cancer Research*, **65**(8), 3108–3116.
- Clark, D. E., Poteet-Smith, C. E., Smith, J. A., & Lannigan, D. A. (2001). Rsk2 allosterically activates estrogen receptor α by docking to the hormone-binding domain. *EMBO Journal*, **20**(13), 3484–3494.
- Collier, A., Ghosh, S., McGlynn, B., & Hollins, G. (2012). Prostate cancer, androgen

- deprivation therapy, obesity, the metabolic syndrome, type 2 diabetes, and cardiovascular disease: A review. *American Journal of Clinical Oncology: Cancer Clinical Trials*, **35**(5), 504–509.
- Consortium, T. U. (2017). UniProt: the universal protein knowledgebase. *Nucleic Acids Research*, **45**(D1), 158–169.
- Cronin, R., Brooke, G. N., & Prischi, F. (2021). The role of the p90 ribosomal S6 kinase family in prostate cancer progression and therapy resistance. *Oncogene*, **40**(22), 3775–3785.
- Culig, Z., & Santer, F. R. (2012). Androgen receptor co-activators in the regulation of cellular events in prostate cancer. *World Journal of Urology*, **30**(3), 297–302.
- Cuzick, J., Thorat, M. A., Andriole, G., ... Wolk, A. (2014). Prevention and early detection of prostate cancer. *The Lancet Oncology*, **15**(11), 484–492.
- Dalby, K. N., Morrice, N., Caudwell, F. B., Avruch, J., & Cohen, P. (1998). Identification of Regulatory Phosphorylation Sites in Mitogen-activated Protein Kinase (MAPK)-activated Protein Kinase-1a/p90. *Journal of Biological Chemistry*, **273**(3), 1496–1505.
- Dart, D. A., Waxman, J., Aboagye, E. O., & Bevan, C. L. (2013). Visualising Androgen Receptor Activity in Male and Female Mice. *PLoS ONE*, **8**(8), 1–16.
- Doehn, U., Hauge, C., Frank, S. R., Jensen, C. J., Duda, K., Nielsen, J. V., Cohen, M. S., Johansen, J. V., Winther, B. R., Lund, L. R., Winther, O., Taunton, J., Hansen, S. H., & Frödin, M. (2009). RSK Is a Principal Effector of the RAS-ERK Pathway for Eliciting a Coordinate Promotile/Invasive Gene Program and Phenotype in Epithelial Cells. *Molecular Cell*, **35**(4), 511–522.
- Dong, J., Wu, Z., Wang, D., Pascal, L. E., Nelson, J. B., Wipf, P., & Wang, Z. (2019). Hsp70 binds to the androgen receptor N-terminal domain and modulates the receptor function in prostate cancer cells. *Molecular Cancer Therapeutics*, **18**(1), 39–50.
- Dudka, I., Thysell, E., Lundquist, K., Antti, H., Iglesias-Gato, D., Flores-Morales, A., Bergh, A., Wikström, P., & Gröbner, G. (2020). Comprehensive metabolomics analysis of prostate cancer tissue in relation to tumor aggressiveness and TMPRSS2-ERG fusion status. *BMC Cancer*, **20**(1), 437.
- Dümmler, B. A., Hauge, C., Silber, J., Yntema, H. G., Kruse, L. S., Kofoed, B., Hemmings, B. A., Alessi, D. R., & Frödin, M. (2005). Functional Characterization of Human RSK4, a New 90-kDa Ribosomal S6 Kinase, Reveals Constitutive Activation in Most Cell Types. *Journal of Biological Chemistry*, **280**(14), 13304–13314.
- Einsfeldt, K., Severo Júnior, J. B., Corrêa Argondizzo, A. P., Medeiros, M. A., Alves, T. L. M., Almeida, R. V., & Larentis, A. L. (2011). Cloning and expression of protease ClpP from *Streptococcus pneumoniae* in *Escherichia coli*: Study of the influence of kanamycin and IPTG concentration on cell growth, recombinant protein production and plasmid stability. *Vaccine*, **29**(41), 7136–7143.
- Eisenmann, K. M., VanBrocklin, M. W., Staffend, N. A., Kitchen, S. M., & Koo, H. M. (2003). Mitogen-Activated Protein Kinase Pathway-Dependent Tumor-Specific

- Survival Signaling in Melanoma Cells through Inactivation of the Proapoptotic Protein Bad. *Cancer Research*, **63**(23), 8330–8337.
- Endicott, J. A., Noble, M. E. M., & Johnson, L. N. (2012). The structural basis for control of eukaryotic protein kinases. *Annual Review of Biochemistry*, **81**, 587–613.
- Erikson, E., & Maller, J. L. (1986). Purification and characterization of a protein kinase from *Xenopus* eggs highly specific for ribosomal protein S6. *J. Biol. Chem.*, **261**, 350–355.
- Estébanez-Perpiñá, E., Arnold, L. A., Nguyen, P., Rodrigues, E. D., Mar, E., Bateman, R., Pallai, P., Shokat, K. M., Baxter, J. D., Guy, R. K., Webb, P., & Fletterick, R. J. (2007). A surface on the androgen receptor that allosterically regulates coactivator binding. *Proceedings of the National Academy of Sciences of the United States of America*, **104**(41), 16074–16079.
- Fabbro, D., Cowan-Jacob, S. W., & Moebitz, H. (2015). Ten things you should know about protein kinases: IUPHAR Review 14. *British Journal of Pharmacology*, **172**(11), 2675–2700.
- Faus, H., & Haendler, B. (2006). Post-translational modifications of steroid receptors. *Biomedicine and Pharmacotherapy*, **60**(9), 520–528.
- Ferlay, J., Shin, H. R., Bray, F., Forman, D., Mathers, C., & Parkin, D. M. (2010). Estimates of worldwide burden of cancer in 2008: GLOBOCAN 2008. *International Journal of Cancer*, **127**(12), 2893–2917.
- Filson, C. P., Marks, L. S., & Litwin, M. S. (2015). Expectant management for men with early stage prostate cancer. *CA: A Cancer Journal for Clinicians*, **65**(4), 264–282.
- Frödin, M., Antal, T. L., Dümmler, B. A., Jensen, C. J., Deak, M., Gammeltoft, S., & Biondi, R. M. (2002). A phosphoserine/threonine-binding pocket in AGC kinases and PDK1 mediates activation by hydrophobic motif phosphorylation. *EMBO Journal*, **21**(20), 5396–5407.
- Frödin, M., Jensen, C. J., Merienne, K., & Gammeltoft, S. (2000). A phosphoserine-regulated docking site in the protein kinase RSK2 that recruits and activates PDK1. *The EMBO Journal*, **19**(12), 2924–34.
- Fu, M., Rao, M., Wang, C., Sakamaki, T., Wang, J., Di Vizio, D., Zhang, X., Albanese, C., Balk, S., Chang, C., Fan, S., Rosen, E., Palvimo, J. J., Jänne, O. A., Muratoglu, S., Avantaggiati, M. L., & Pestell, R. G. (2003). Acetylation of Androgen Receptor Enhances Coactivator Binding and Promotes Prostate Cancer Cell Growth. *Molecular and Cellular Biology*, **23**(23), 8563–75.
- Gandhi, J., Afridi, A., Vatsia, S., Joshi, G., Joshi, G., Kaplan, S. A., Smith, N. L., & Khan, S. A. (2018). The molecular biology of prostate cancer: Current understanding and clinical implications. *Prostate Cancer and Prostatic Diseases*, **21**(1), 22–36.
- Gao, X., Chaturvedi, D., & Patel, T. B. (2012). Localization and retention of p90 ribosomal S6 kinase 1 in the nucleus: Implications for its function. *Molecular Biology of the Cell*, **23**(3), 503–515.

- Gasteiger, E., Hoogland, C., Gattiker, A., Duvaud, S., Wilkins, M. R., Appel, R. D., & Bairoch, A. (2005). *The Proteomics Protocols Handbook*. (J. M. Walker, Ed.) *The Proteomics Protocols Handbook*, Totowa, NJ: Humana Press.
doi:10.1385/1592598900
- Gaughan, L., Stockley, J., Wang, N., McCracken, S. R. C., Treumann, A., Armstrong, K., Shaheen, F., Watt, K., McEwan, I. J., Wang, C., Pestell, R. G., & Robson, C. N. (2011). Regulation of the androgen receptor by SET9-mediated methylation. *Nucleic Acids Research*, **39**(4), 1266–1279.
- Gawecka, J. E., Young-Robbins, S. S., Sulzmaier, F. J., Caliva, M. J., Heikkila, M. M., Matter, M. L., & Ramos, J. W. (2012). RSK2 protein suppresses integrin activation and fibronectin matrix assembly and promotes cell migration. *Journal of Biological Chemistry*, **287**(52), 43424–43437.
- Gilmore, A. P., Valentijn, A. J., Wang, P., Ranger, A. M., Bundred, N., O'Hare, M. J., Wakeling, A., Korsmeyer, S. J., & Streuli, C. H. (2002). Activation of BAD by therapeutic inhibition of epidermal growth factor receptor and transactivation by insulin-like growth factor receptor. *Journal of Biological Chemistry*, **277**(31), 27643–27650.
- Gioeli, D., & Paschal, B. M. (2012). Post-translational modification of the androgen receptor. *Molecular and Cellular Endocrinology*, **352**(1–2), 70–78.
- Gógl, G., Biri-Kovács, B., Póti, Á. L., Vadász, H., Szeder, B., Bodor, A., Schlosser, G., Ács, A., Turiák, L., Buday, L., Alexa, A., Nyitray, L., & Reményi, A. (2018). Dynamic control of RSK complexes by phosphoswitch-based regulation. *The FEBS Journal*, **285**(1), 46–71.
- Goldsmith, E. J., Akella, R., Min, X., Zhou, T., & Humphreys, J. M. (2007). Substrate and Docking Interactions in Serine/Threonine Protein Kinases. *Chemical Reviews*, **107**(11), 5065–5081.
- Golias, C., Iliadis, I., Peschos, D., & Charalabopoulos, K. (2009). Amplification and co-regulators of androgen receptor gene in prostate cancer. *Experimental Oncology*, **31**(1), 3–8.
- Gordon, V., Bhadel, S., Wunderlich, W., Zhang, J., Ficarro, S. B., Mollah, S. A., Shabanowitz, J., Hunt, D. F., Xenarios, I., Hahn, W. C., Conaway, M., Carey, M. F., & Gioeli, D. (2010). CDK9 Regulates AR Promoter Selectivity and Cell Growth through Serine 81 Phosphorylation. *Molecular Endocrinology*, **24**(12), 2267–2280.
- Greschik, H., Wurtz, J.-M., Sanglier, S., Bourguet, W., van Dorsselaer, A., Moras, D., & Renaud, J.-P. (2002). Structural and Functional Evidence for Ligand-Independent Transcriptional Activation by the Estrogen-Related Receptor 3. *Molecular Cell*, **9**(2), 303–313.
- Gronemeyer, H., Gustafsson, J. Å., & Laudet, V. (2004). Principles for modulation of the nuclear receptor superfamily. *Nature Reviews Drug Discovery*, **3**(11), 950–964.
- Haase, C., Stieler, J. T., Arendt, T., & Holzer, M. (2004). Pseudophosphorylation of tau protein alters its ability for self-aggregation. *Journal of Neurochemistry*, **88**(6), 1509–1520.

- Hanahan, D., & Weinberg, R. A. (2000). The Hallmarks of Cancer. *Cell*, **100**(1), 57–70.
- Hanahan, D., & Weinberg, R. A. (2011). Hallmarks of cancer: The next generation. *Cell*, Elsevier Inc., , pp. 646–674.
- Hartman, K. G., Vitolo, M. I., Pierce, A. D., Fox, J. M., Shapiro, P., Martin, S. S., Wilder, P. T., & Weber, D. J. (2014). Complex Formation between S100B Protein and the p90 Ribosomal S6 Kinase (RSK) in Malignant Melanoma Is Calcium-dependent and Inhibits Extracellular Signal-regulated Kinase (ERK)-mediated Phosphorylation of RSK. *Journal of Biological Chemistry*, **289**(18), 12886–12895.
- Hayat, S. M. G., Farahani, N., Golichenari, B., & Sahebkar, A. (2018). Recombinant Protein Expression in Escherichia coli (E.coli): What We Need to Know. *Current Pharmaceutical Design*, **24**(6), 718–725.
- Heemers, H. V., & Tindall, D. J. (2007). Androgen receptor (AR) coregulators: A diversity of functions converging on and regulating the AR transcriptional complex. *Endocrine Reviews*, **28**(7), 778–808.
- Heinlein, C. A. (2004). Androgen Receptor (AR) Coregulators: An Overview. *Endocrine Reviews*, **23**(2), 175–200.
- Helsen, C., & Claessens, F. (2014). Molecular and Cellular Endocrinology Looking at nuclear receptors from a new angle, **382**, 97–106.
- Herzik, M. A., Wu, M., & Lander, G. C. (2019). High-resolution structure determination of sub-100 kDa complexes using conventional cryo-EM. *Nature Communications*, **10**(1), 1032.
- Hilger, R. A., Scheulen, M. E., & Strumberg, D. (2002). Focus : Experimental Oncology · Review Article The Ras-Raf-MEK-ERK Pathway in the Treatment of Cancer. *Onkologie*, **25**, 511–518.
- Hindie, V., Stroba, A., Zhang, H., Lopez-Garcia, L. A., Idrissova, L., Zeuzem, S., Hirschberg, D., Schaeffer, F., Jørgensen, T. J. D., Engel, M., Alzari, P. M., & Biondi, R. M. (2009). Structure and allosteric effects of low-molecular-weight activators on the protein kinase PDK1. *Nature Chemical Biology*, **5**(10), 758–764.
- Hoffmann, F., & Rinas, U. (2004). Roles of Heat-Shock Chaperones in the Production of Recombinant Proteins in Escherichia coli. In *Advances in biochemical engineering/biotechnology*, Vol. 89, , pp. 143–161.
- Houles, T., & Roux, P. P. (2018). Defining the role of the RSK isoforms in cancer. *Seminars in Cancer Biology*, **48**, 53–61.
- Hurdiss, D. L., Drulyte, I., Lang, Y., Shamorkina, T. M., Pronker, M. F., van Kuppeveld, F. J. M., Snijder, J., & de Groot, R. J. (2020). Cryo-EM structure of coronavirus-HKU1 haemagglutinin esterase reveals architectural changes arising from prolonged circulation in humans. *Nature Communications*, **11**(1), 4646.
- Ikeda, Y., Aihara, K. I., Sato, T., Akaike, M., Yoshizumi, M., Suzaki, Y., Izawa, Y., Fujimura, M., Hashizume, S., Kato, M., Yagi, S., Tamaki, T., Kawano, H.,

- Matsumoto, T. T. T., Azuma, H., Kato, S., & Matsumoto, T. T. T. (2005). Androgen receptor gene knockout male mice exhibit impaired cardiac growth and exacerbation of angiotensin II-induced cardiac fibrosis. *Journal of Biological Chemistry*, **280**(33), 29661–29666.
- Iyer, K. A., Hu, Y., Nayak, A. R., Kurebayashi, N., Murayama, T., & Samsó, M. (2020). Structural mechanism of two gain-of-function cardiac and skeletal RyR mutations at an equivalent site by cryo-EM. *Science Advances*, **6**(31), 1–13.
- Jackson, S. P. (2001). Detecting, signalling and repairing DNA double-strand breaks. *Biochemical Society Transactions*, **29**(6), 655–661.
- Jakobsen, N. A., Hamdy, F. C., & Bryant, R. J. (2016). Novel biomarkers for the detection of prostate cancer. *Journal of Clinical Urology*, **9**(2_suppl), 3–10.
- Jehle, K., Cato, L., Neeb, A., Muhle-Goll, C., Jung, N., Smith, E. W., Buzon, V., Carbó, L. R., Estebanez-Perpiña, E., Schmitz, K., Fruk, L., Luy, B., Chen, Y., Cox, M. B., Braše, S., Brown, M., & Cato, A. C. B. (2014). Coregulator control of androgen receptor action by a novel nuclear receptor-binding motif. *Journal of Biological Chemistry*, **289**(13), 8839–8851.
- Jensen, C. J., Buch, M. B., Krag, T. O., Hemmings, B. A., Gammeltoft, S., & Frödin, M. (1999). 90-kDa ribosomal S6 kinase is phosphorylated and activated by 3-phosphoinositide-dependent protein kinase-1. *Journal of Biological Chemistry*, **274**(38), 27168–27176.
- Jiang, Y., Ye, X., Ji, Y., Zhou, X., Yang, H., Wei, W., & Li, Q. (2017). Aberrant expression of RSK4 in breast cancer and its role in the regulation of tumorigenicity. *International Journal of Molecular Medicine*, **40**(3), 883–890.
- Jin, L., Li, D., Lee, J. S., Elf, S., Alesi, G. N., Fan, J., Kang, H.-B., Wang, D., Fu, H., Taunton, J., Boggon, T. J., Tucker, M., Gu, T.-L., Chen, Z. G., Shin, D. M., Khuri, F. R., & Kang, S. (2013). p90 RSK2 Mediates Antiankist Signals by both Transcription-Dependent and -Independent Mechanisms. *Molecular and Cellular Biology*, **33**(13), 2574–2585.
- Jin, Y., Nenseth, H. Z., & Saatcioglu, F. (2017). Role of PLZF as a tumor suppressor in prostate cancer. *Oncotarget*, **8**(41), 71317–71324.
- Jones, S. W., Erikson, E., Blenis, J., Maller, J. L., & Erikson, R. L. (1988). A *Xenopus* ribosomal protein S6 kinase has two apparent kinase domains that are each similar to distinct protein kinases. *Proceedings of the National Academy of Sciences of the United States of America*, **85**(10), 3377–81.
- Joo, S. S., & Yoo, Y.-M. (2009). Melatonin induces apoptotic death in LNCaP cells via p38 and JNK pathways: therapeutic implications for prostate cancer. *Journal of Pineal Research*, **47**(1), 8–14.
- Joseph, R. E., & Andreotti, A. H. (2008). Bacterial expression and purification of Interleukin-2 Tyrosine kinase: Single step separation of the chaperonin impurity. *Protein Expression and Purification*, **60**(2), 194–197.
- Kaikkonen, S., Jääskeläinen, T., Karvonen, U., Rytinki, M. M., Makkonen, H., Gioeli, D., Paschal, B. M., & Palvimo, J. J. (2009). SUMO-Specific Protease 1 (SEN1) Reverses the Hormone-Augmented SUMOylation of Androgen Receptor and

- Modulates Gene Responses in Prostate Cancer Cells. *Molecular Endocrinology*, **23**(3), 292–307.
- Kastan, M. B., & Lim, D. S. (2000). The many substrates and functions of ATM. *Nature Reviews Molecular Cell Biology*, **1**(3), 179–186.
- Katzenwadel, A., & Wolf, P. (2015). Androgen deprivation of prostate cancer: Leading to a therapeutic dead end. *Cancer Letters*, **367**(1), 12–17.
- Kavya, K., Kumar, M. N., Patil, R. H., Hegde, S. M., Kiran Kumar, K. M., Nagesh, R., Babu, R. L., Ramesh, G. T., & Chidananda Sharma, S. (2017). Differential expression of AP-1 transcription factors in human prostate LNCaP and PC-3 cells: role of Fra-1 in transition to CRPC status. *Molecular and Cellular Biochemistry*, **433**(1–2), 13–26.
- Kim, S.-T., Lim, D.-S., Canman, C. E., & Kastan, M. B. (1999). Substrate Specificities and Identification of Putative Substrates of ATM Kinase Family Members. *Journal of Biological Chemistry*, **274**(53), 37538–37543.
- Kim, Y., Bigelow, L., Borovilos, M., Dementieva, I., Duggan, E., Eschenfeldt, W., Hatzos, C., Joachimiak, G., Li, H., Maltseva, N., Mulligan, R., Quartey, P., Sather, A., Stols, L., Volkart, L., Wu, R., Zhou, M., & Joachimiak, A. (2008). High-Throughput Protein Purification for X-Ray Crystallography and NMR. In *Advances in Protein Chemistry and Structural Biology*, Vol. 75, , pp. 85–105.
- Ko, C.-J., Huang, C.-C., Lin, H.-Y., Juan, C.-P., Lan, S.-W., Shyu, H.-Y., Wu, S.-R., Hsiao, P.-W., Huang, H.-P., Shun, C.-T., & Lee, M.-S. (2015). Androgen-Induced TMPRSS2 Activates Matriptase and Promotes Extracellular Matrix Degradation, Prostate Cancer Cell Invasion, Tumor Growth, and Metastasis. *Cancer Research*, **75**(14), 2949–2960.
- Ko, S., Ahn, J., Song, C. S., Kim, S., Knapczyk-Stwora, K., & Chatterjee, B. (2011). Lysine Methylation and Functional Modulation of Androgen Receptor by Set9 Methyltransferase. *Molecular Endocrinology*, **25**(3), 433–444.
- Kolch, W. (2000). Meaningful relationships: the regulation of the Ras/Raf/MEK/ERK pathway by protein interactions. *Biochemical Journal*, **351**(2), 289–305.
- Kornev, A. P., Haste, N. M., Taylor, S. S., & Ten Eyck, L. F. (2006). Surface comparison of active and inactive protein kinases identifies a conserved activation mechanism. *Proceedings of the National Academy of Sciences of the United States of America*, **103**(47), 17783–17788.
- Koryakina, Y., Ta, H. Q., & Gioeli, D. (2014). Androgen receptor phosphorylation: biological context and functional consequences. *Endocrine-Related Cancer*, **21**(4), T131–T145.
- Kress, W., Maglica, Ž., & Weber-Ban, E. (2009). Clp chaperone–proteases: structure and function. *Research in Microbiology*, **160**(9), 618–628.
- Lai, J. J., Lai, K. P., Zeng, W., Chuang, K. H., Altuwaijri, S., & Chang, C. (2012). Androgen receptor influences on body defense system via modulation of innate and adaptive immune systems: Lessons from conditional AR knockout mice. *American Journal of Pathology*, **181**(5), 1504–1512.
- Lara, R., Mauri, F. A., Taylor, H., Derua, R., Shia, A., Gray, C., Nicols, A., Shiner, R.

- J., Schofield, E., Bates, P. A., Waelkens, E., Dallman, M., Lamb, J., Zicha, D., Downward, J., Seckl, M. J., & Pardo, O. E. (2011). An siRNA screen identifies RSK1 as a key modulator of lung cancer metastasis. *Oncogene*, **30**(32), 3513–3521.
- Lara, R., Seckl, M. J., & Pardo, O. E. (2013). The p90 RSK family members: Common functions and isoform specificity. *Cancer Research*, **73**(17), 5301–5308.
- Larentis, A. L., Nicolau, J. F. M. Q., Esteves, G. D. S., Vareschini, D. T., de Almeida, F. V. R., dos Reis, M. G., Galler, R., & Medeiros, M. A. (2014). Evaluation of pre-induction temperature, cell growth at induction and IPTG concentration on the expression of a leptospiral protein in *E. coli* using shaking flasks and microbioreactor. *BMC Research Notes*, **7**(1), 671.
- Lavin, M. F. (2007). ATM and the Mre11 complex combine to recognize and signal DNA double-strand breaks. *Oncogene*, **26**(56), 7749–7758.
- Law, J. H., Li, Y., To, K., Wang, M., Astanehe, A., Lambie, K., Dhillon, J., Jones, S. J. M., Gleave, M. E., Eaves, C. J., & Dunn, S. E. (2010). Molecular decoy to the Y-box binding protein-1 suppresses the growth of breast and prostate cancer cells whilst sparing normal cell viability. *PLoS ONE*, **5**(9), 1–11.
- Lee, J. E., & Kim, J. H. (2015). Valproic acid inhibits the invasion of PC3 prostate cancer cells by upregulating the metastasis suppressor protein NDRG1. *Genetics and Molecular Biology*, **38**(4), 527–533.
- Leighton, I. A., Dalby, K. N., Barry Caudwell, F., Cohen, P. T. W., & Cohen, P. (1995). Comparison of the specificities of p70 S6 kinase and MAPKAP kinase-1 identifies a relatively specific substrate for p70 S6 kinase: the N-terminal kinase domain of MAPKAP kinase-1 is essential for peptide phosphorylation. *FEBS Letters*, **375**(3), 289–293.
- Li, D., Fu, T. M., Nan, J., Liu, C., Li, L. F., & Su, X. D. (2012). Structural basis for the autoinhibition of the C - Terminal kinase domain of human RSK1. *Acta Crystallographica Section D: Biological Crystallography*, **68**(6), 680–685.
- Liu, X., Feng, C., Liu, J., Cao, L., Xiang, G., Liu, F., Wang, S., Jiao, J., & Niu, Y. (2018). Androgen receptor and heat shock protein 27 co-regulate the malignant potential of molecular apocrine breast cancer. *Journal of Experimental and Clinical Cancer Research*, **37**(1), 1–12.
- Löbrich, M., & Jeggo, P. A. (2007). The impact of a negligent G2/M checkpoint on genomic instability and cancer induction. *Nature Reviews Cancer*, **7**(11), 861–869.
- Ludwik, K. A., McDonald, O. G., Brenin, D. R., & Lannigan, D. A. (2018). ER α -mediated nuclear sequestration of RSK2 is required for ER β breast cancer tumorigenesis. *Cancer Research*, **78**(8), 2014–2025.
- MacLean, H. E., Chiu, W. S. M., Notini, A. J., Axell, A.-M., Davey, R. A., McManus, J. F., Ma, C., Plant, D. R., Lynch, G. S., & Zajac, J. D. (2008). Impaired skeletal muscle development and function in male, but not female, genomic androgen receptor knockout mice. *The FASEB Journal*, **22**(8), 2676–2689.

- Malakhova, M., Kurinov, I., Liu, K., Zheng, D., D'Angelo, I., Shim, J.-H., Steinman, V., Bode, A. M., & Dong, Z. (2009). Structural Diversity of the Active N-Terminal Kinase Domain of p90 Ribosomal S6 Kinase 2. *PLoS ONE*, **4**(11), e8044.
- Mall, D. P., Basu, S., Ghosh, K., Kumari, N., Lahiri, A., Paul, S., & Biswas, D. (2022). Human FKBP5 Negatively Regulates Transcription through Inhibition of P-TEFb Complex Formation. *Molecular and Cellular Biology*, **42**(1). doi:10.1128/MCB.00344-21
- Manning, B. D., & Cantley, L. C. (2007). AKT/PKB Signaling: Navigating Downstream. *Cell*, **129**(7), 1261–1274.
- Manning, G., Whyte, D. B., Martinez, R., Hunter, T., & Sudarsanam, S. (2002). The protein kinase complement of the human genome. *Science (New York, N.Y.)*, **298**(5600), 1912–34.
- Marinkovich, M. P. (2007). Tumour microenvironment: Laminin 332 in squamous-cell carcinoma. *Nature Reviews Cancer*, **7**(5), 370–380.
- Matsumoto, T., Sakari, M., Okada, M., Yokoyama, A., Takahashi, S., Kouzmenko, A., & Kato, S. (2013). The Androgen Receptor in Health and Disease. *Annual Review of Physiology*, **75**(1), 201–224.
- Meharena, H. S., Chang, P., Keshwani, M. M., Oruganty, K., Nene, A. K., Kannan, N., Taylor, S. S., & Kornev, A. P. (2013). Deciphering the Structural Basis of Eukaryotic Protein Kinase Regulation. *PLoS Biology*, **11**(10), e1001680.
- Meharena, H. S., Fan, X., Ahuja, L. G., Keshwani, M. M., McClendon, C. L., Chen, A. M., Adams, J. A., & Taylor, S. S. (2016). Decoding the Interactions Regulating the Active State Mechanics of Eukaryotic Protein Kinases. *PLoS Biology*, **14**(11). doi:10.1371/journal.pbio.2000127
- Mendoza, M. C., Er, E. E., & Blenis, J. (2011). The Ras-ERK and PI3K-mTOR pathways: Cross-talk and compensation. *Trends in Biochemical Sciences*, **36**(6), 320–328.
- Miller, C. J., & Turk, B. E. (2018). Homing in: Mechanisms of Substrate Targeting by Protein Kinases. *Trends in Biochemical Sciences*, **43**(5), 380–394.
- Modi, V., & Dunbrack, R. L. (2019). Defining a new nomenclature for the structures of active and inactive kinases. *Proceedings of the National Academy of Sciences*, **116**(14), 6818–6827.
- Mukherjee, R., McGuinness, D. H., McCall, P., Underwood, M. A., Seywright, M., Orange, C., & Edwards, J. (2011). Upregulation of MAPK pathway is associated with survival in castrate-resistant prostate cancer. *British Journal of Cancer*, **104**(12), 1920–1928.
- Nabbi, A., McClurg, U. L., Thalappilly, S., Almami, A., Mobahat, M., Bismar, T. A., Binda, O., & Riabowol, K. T. (2017). ING3 promotes prostate cancer growth by activating the androgen receptor. *BMC Medicine*, **15**(1), 103.
- Nagy, L., & Schwabe, J. W. R. (2004). Mechanism of the nuclear receptor molecular switch. *Trends in Biochemical Sciences*, **29**(6), 317–324.
- Packer, J. R., & Maitland, N. J. (2016). The molecular and cellular origin of human

- prostate cancer. *Biochimica et Biophysica Acta - Molecular Cell Research*, **1863**(6), 1238–1260.
- Pearce, L. R., Komander, D., & Alessi, D. R. (2010). The nuts and bolts of AGC protein kinases. *Nature Reviews Molecular Cell Biology*, **11**(1), 9–22.
- Perez-Cornago, A., Key, T. J., Allen, N. E., Fensom, G. K., Bradbury, K. E., Martin, R. M., & Travis, R. C. (2017). Prospective investigation of risk factors for prostate cancer in the UK Biobank cohort study. *British Journal of Cancer*, **117**(10), 1562–1571.
- Pine, A. C., Fioretti, F. F., Brooke, G. N., & Bevan, C. L. (2016). Advances in genetics: widening our understanding of prostate cancer. *F1000Research*, **5**(0), 1512.
- Pinna, L. A., & Ruzzene, M. (1996). How do protein kinases recognize their substrates? *Biochimica et Biophysica Acta (BBA) - Molecular Cell Research*, **1314**(3), 191–225.
- Quan, Y., Zhang, X., Butler, W., Du, Z., Wang, M., Liu, Y., & Ping, H. (2021). The role of N-cadherin/c-Jun/NDRG1 axis in the progression of prostate cancer. *International Journal of Biological Sciences*, **17**(13), 3288–3304.
- Rana, K., Fam, B. C., Clarke, M. V., Pang, T. P. S., Zajac, J. D., & MacLean, H. E. (2011). Increased adiposity in DNA binding-dependent androgen receptor knockout male mice associated with decreased voluntary activity and not insulin resistance. *American Journal of Physiology-Endocrinology and Metabolism*, **301**(5), E767–E778.
- Ranganathan, A., Pearson, G. W., Chrestensen, C. A., Sturgill, T. W., & Cobb, M. H. (2006). The MAP kinase ERK5 binds to and phosphorylates p90 RSK. *Archives of Biochemistry and Biophysics*, **449**(1–2), 8–16.
- Rastinejad, F. (2001). Retinoid X receptor and its partners in the nuclear receptor family. *Current Opinion in Structural Biology*, **11**(1), 33–38.
- Rastinejad, F., Huang, P., Chandra, V., & Khorasanizadeh, S. (2013). Understanding nuclear receptor form and function using structural biology. *Journal of Molecular Endocrinology*, **51**(3). doi:10.1530/JME-13-0173
- Rellos, P., Pike, A. C. W., Niesen, F. H., Salah, E., Lee, W. H., von Delft, F., & Knapp, S. (2010). Structure of the CaMKII δ /Calmodulin Complex Reveals the Molecular Mechanism of CaMKII Kinase Activation. *PLoS Biology*, **8**(7), e1000426.
- Rhee, H., Gunter, J. H., Heathcote, P., Ho, K., Stricker, P., Corcoran, N. M., & Nelson, C. C. (2015). Adverse effects of androgen-deprivation therapy in prostate cancer and their management. *BJU International*, **115**(S5), 3–13.
- Robert, F., Bierau, H., Rossi, M., Agugiaro, D., Soranzo, T., Broly, H., & Mitchell-Logean, C. (2009). Degradation of an Fc-fusion recombinant protein by host cell proteases: Identification of a CHO cathepsin D protease. *Biotechnology and Bioengineering*, **104**(6), 1132–1141.
- Roemer, S. C., Donham, D. C., Sherman, L., Pon, V. H., Edwards, D. P., & Churchill, M. E. A. (2006). Structure of the Progesterone Receptor-Deoxyribonucleic Acid

Complex: Novel Interactions Required for Binding to Half-Site Response Elements. *Molecular Endocrinology*, **20**(12), 3042–3052.

- Rohman, M., & Harrison-Lavoie, K. J. (2000). Separation of copurifying GroEL from glutathione-S-transferase fusion proteins. *Protein Expression and Purification*, **20**(1), 45–47.
- Romeo, Y., Moreau, J., Zindy, P. J., Saba-El-Leil, M., Lavoie, G., Dandachi, F., Baptissart, M., Borden, K. L. B., Meloche, S., & Roux, P. P. (2013). RSK regulates activated BRAF signalling to mTORC1 and promotes melanoma growth. *Oncogene*, **32**(24), 2917–2926.
- Romeo, Y., Zhang, X., & Roux, P. P. (2012). Regulation and function of the RSK family of protein kinases. *The Biochemical Journal*, **441**, 553–569.
- Roux, P. P., Richards, S. A., & Blenis, J. (2003). Phosphorylation of p90 Ribosomal S6 Kinase (RSK) Regulates Extracellular Signal-Regulated Kinase Docking and RSK Activity Phosphorylation of p90 Ribosomal S6 Kinase (RSK) Regulates Extracellular Signal-Regulated Kinase Docking and RSK Activity. *Molecular and Cellular Biology*, **23**(14), 4796–4804.
- Roux, P. P., Shahbazian, D., Vu, H., Holz, M. K., Cohen, M. S., Taunton, J., Sonenberg, N., & Blenis, J. (2007). RAS/ERK signaling promotes site-specific ribosomal protein S6 phosphorylation via RSK and stimulates cap-dependent translation. *Journal of Biological Chemistry*, **282**(19), 14056–14064.
- Rozkov, A., & Enfors, S.-O. (2004). Analysis and Control of Proteolysis of Recombinant Proteins in Escherichia coli. In *Advances in biochemical engineering/biotechnology*, Vol. 89, pp. 163–195.
- Ryan, B. J. (2011). Avoiding Proteolysis During Protein Chromatography. In *Methods in molecular biology*, pp. 61–71.
- Sakkiah, S., Cao, G. P., Gupta, S. P., & Lee, K. W. (2017). Overview of the Structure and Function of Protein Kinases. *Current Enzyme Inhibition*, **13**(2). doi:10.2174/1573408013666161226155608
- Santra, M., Farrell, D. W., & Dill, K. A. (2017). Bacterial proteostasis balances energy and chaperone utilization efficiently. *Proceedings of the National Academy of Sciences*, **114**(13), E2654–E2661.
- Sato, T., Matsumoto, T., Kawano, H., ... Kato, S. (2004). Brain masculinization requires androgen receptor function. *Proceedings of the National Academy of Sciences*, **101**(6), 1673–1678.
- Schultz, T., Martinez, L., & de Marco, A. (2006). The evaluation of the factors that cause aggregation during recombinant expression in E. coli is simplified by the employment of an aggregation-sensitive reporter. *Microbial Cell Factories*, **5**(1), 28.
- Schwabe, J., Chapman, L., Finch, J., & Rhodes, D. (1993). The crystal structure of the estrogen receptor DNA-binding domain bound to DNA: how receptors discriminate between their response elements. *Cell*, **75**, 567–78.
- Shaffer, P. L., Jivan, A., Dollins, D. E., Claessens, F., & Gewirth, D. T. (2004). Structural basis of androgen receptor binding to selective androgen response

- elements. *Proceedings of the National Academy of Sciences of the United States of America*, **101**(14), 4758–4763.
- Shiota, M., Takeuchi, A., Song, Y. H., Yokomizo, A., Kashiwagi, E., Uchiumi, T., Kuroiwa, K., Tatsugami, K., Fujimoto, N., Oda, Y., & Naito, S. (2011). Y-box binding protein-1 promotes castration-resistant prostate cancer growth via androgen receptor expression. *Endocrine-Related Cancer*, **18**(4), 505–517.
- Shiota, M., Yokomizo, A., Takeuchi, A., Itsumi, M., Imada, K., Kashiwagi, E., Inokuchi, J., Tatsugami, K., Uchiumi, T., & Naito, S. (2014). Inhibition of RSK/YB-1 Signaling Enhances the Anti-Cancer Effect of Enzalutamide in Prostate Cancer. *The Prostate*, **74**(9), 959–969.
- Shiraishi, K., & Matsuyama, H. (2017). Gonadotropin actions on spermatogenesis and hormonal therapies for spermatogenic disorders [Review]. *Endocrine Journal*, **64**(2), 123–131.
- Silaban, S., Gaffar, S., Simorangkir, M., Maksum, I. P., & Subroto, T. (2019). Effect of IPTG Concentration on Recombinant Human Prethrombin-2 Expression in Escherichia coli BL21(DE3) ArcticExpress. *IOP Conference Series: Earth and Environmental Science*, **217**(1), 012039.
- Song, J., Tan, H., Perry, A. J., Akutsu, T., Webb, G. I., Whisstock, J. C., & Pike, R. N. (2012). PROSPER: An Integrated Feature-Based Tool for Predicting Protease Substrate Cleavage Sites. *PLoS ONE*, **7**(11), e50300.
- Stokoe, D., Caudwell, B., Cohen, P. T. W., & Cohen, P. (1993). The substrate specificity and structure of mitogen-activated protein (MAP) kinase-activated protein kinase-2. *Biochemical Journal*, **296**(3), 843–849.
- Studier, F. W. (2005). Protein production by auto-induction in high-density shaking cultures. *Protein Expression and Purification*, **41**(1), 207–234.
- Sulzmaier, F., & Ramos, J. (2013). RSK Isoforms in Cancer Cell Invasion and Metastasis. *Cancer Research*, **73**(20), 6099–6105.
- Sun, G. G., Lu, Y. F., Zhang, J., & Hu, W. N. (2014). Filamin A regulates MMP-9 expression and suppresses prostate cancer cell migration and invasion. *Tumor Biology*, **35**(4), 3819–3826.
- Sunil K. Khatrar, Pankaj Gulati, Prabuddha K. Kundu, Vibhuti Singh, Usha Bughani, Malini Bajpai, & Kulvinder. S. Saini. (2007). Enhanced Soluble Production of Biologically Active Recombinant Human p38 Mitogen-Activated-Protein Kinase (MAPK) in Escherichia coli. *Protein & Peptide Letters*, **14**(8), 756–760.
- Suskiewicz, M. J., Sussman, J. L., Silman, I., & Shaul, Y. (2011). Context-dependent resistance to proteolysis of intrinsically disordered proteins. *Protein Science*, **20**(8), 1285–1297.
- Tan, M. E., Li, J., Xu, H. E., Melcher, K., & Yong, E. L. (2015). Androgen receptor: Structure, role in prostate cancer and drug discovery. *Acta Pharmacologica Sinica*, **36**(1), 3–23.
- Taylor, B. S., Schultz, N., Hieronymus, H., ... Gerald, W. L. (2010). Integrative Genomic Profiling of Human Prostate Cancer. *Cancer Cell*, **18**(1), 11–22.

- Thain, A., Gaston, K., Jenkins, O., & Clarke, A. R. (1996). A method for the separation of GST fusion proteins from co-purifying GroEL. *Trends in Genetics*, **12**(6), 209–210.
- Thakur, A., Sun, Y., Bollig, A., Wu, J., Biliran, H., Banerjee, S., Sarkar, F. H., & Liao, D. J. (2008). Anti-invasive and antimetastatic activities of ribosomal protein S6 kinase 4 in breast cancer cells. *Clinical Cancer Research : An Official Journal of the American Association for Cancer Research*, **14**(14), 4427–36.
- Ting, H.-J., Yeh, S., Nishimura, K., & Chang, C. (2002). Supervillin associates with androgen receptor and modulates its transcriptional activity. *Proceedings of the National Academy of Sciences*, **99**(2), 661–666.
- Ushijima, M., Shiota, M., Matsumoto, T., Kashiwagi, E., Inokuchi, J., & Eto, M. (2022). An oral first-in-class small molecule RSK inhibitor suppresses AR variants and tumor growth in prostate cancer. *Cancer Science*, **113**(5), 1731–1738.
- van Royen, M. E., van Cappellen, W. A., de Vos, C., Houtsmuller, A. B., & Trapman, J. (2012). Stepwise androgen receptor dimerization. *Journal of Cell Science*, **125**(8), 1970–1979.
- Vera, A., González-Montalbán, N., Arís, A., & Villaverde, A. (2007). The conformational quality of insoluble recombinant proteins is enhanced at low growth temperatures. *Biotechnology and Bioengineering*, **96**(6), 1101–1106.
- Verze, P., Cai, T., & Lorenzetti, S. (2016). The role of the prostate in male fertility, health and disease. *Nature Reviews Urology*, **13**(7), 379–386.
- Vial, D., & McKeown-Longo, P. J. (2012). Epidermal Growth Factor (EGF) Regulates $\alpha 5 \beta 1$ Integrin Activation State in Human Cancer Cell Lines through the p90RSK-dependent Phosphorylation of Filamin A. *Journal of Biological Chemistry*, **287**(48), 40371–40380.
- Wadosky, K. M., & Koochekpour, S. (2017). Androgen receptor splice variants and prostate cancer: From bench to bedside. *Oncotarget*, **8**(11), 18550–18576.
- Walters, K. A., McTavish, K. J., Seneviratne, M. G., Jimenez, M., McMahon, A. C., Allan, C. M., Salamonsen, L. A., & Handelsman, D. J. (2009). Subfertile female androgen receptor knockout mice exhibit defects in neuroendocrine signaling, intraovarian function, and uterine development but not uterine function. *Endocrinology*, **150**(7), 3274–3282.
- Wen, S., Niu, Y., & Huang, H. (2020). Posttranslational regulation of androgen dependent and independent androgen receptor activities in prostate cancer. *Asian Journal of Urology*, **7**(3), 203–218.
- Wingfield, P. T. (2015). Overview of the Purification of Recombinant Proteins. *Current Protocols in Protein Science*, **80**(1), 1–35.
- Wu, C. F., Liu, S., Lee, Y. C., Wang, R., Sun, S., Yin, F., Bornmann, W. G., Yu-Lee, L. Y., Gallick, G. E., Zhang, W., Lin, S. H., & Kuang, J. (2014). RSK promotes G2/M transition through activating phosphorylation of Cdc25A and Cdc25B. *Oncogene*, **33**(18), 2385–2394.
- Yang, J., Cron, P., Good, V. M., Thompson, V., Hemmings, B. A., & Barford, D.

- (2002a). Crystal structure of an activated Akt/Protein Kinase B ternary complex with GSK3-peptide and AMP-PNP. *Nature Structural Biology*, **9**(12), 940–944.
- Yang, J., Cron, P., Thompson, V., Good, V. M., Hess, D., Hemmings, B. A., & Barford, D. (2002b). *Molecular Mechanism for the Regulation of Protein Kinase B/Akt by Hydrophobic Motif Phosphorylation activity, termed PDK2, phosphorylates PKB at Ser 474 of its C-terminal hydrophobic motif. Phosphorylation of Ser 474 augments the activity of PDK1-phosphorylated PKB by 7- to 10-fold (Alessi et al., 1996), such that phosphorylation of both residues results in greater than. Molecular Cell*, Vol. 9.
- Yang, Q.-H., Wu, C.-L., Lin, K., & Li, L. (1997). Low Concentration of Inducer Favors Production of Active Form of 6-Phosphofructo-2-kinase/Fructose-2,6-bisphosphatase in *Escherichia coli*. *Protein Expression and Purification*, **10**(3), 320–324.
- Yu, G., Lee, Y. C., Cheng, C. J., Wu, C. F., Song, J. H., Gallick, G. E., Yu-Lee, L. Y., Kuang, J., & Lin, S. H. (2015). RSK promotes prostate cancer progression in bone through ING3, CKAP2, and PTK6-mediated cell survival. *Molecular Cancer Research*, **13**(2), 348–357.
- Yu, X., Yi, P., Hamilton, R. A., Shen, H., Chen, M., Foulds, C. E., Mancini, M. A., Ludtke, S. J., Wang, Z., & O'Malley, B. W. (2020). Structural Insights of Transcriptionally Active, Full-Length Androgen Receptor Coactivator Complexes. *Molecular Cell*, **79**(5), 812-823.e4.
- Zarif, J. C., & Miranti, C. K. (2016). The importance of non-nuclear AR signaling in prostate cancer progression and therapeutic resistance. *Cellular Signalling*, **28**(5), 348–356.
- Zheng, Y., Asara, J. M., & Tyner, A. L. (2012). Protein-tyrosine kinase 6 promotes peripheral adhesion complex formation and cell migration by phosphorylating p130 CRK-associated substrate. *Journal of Biological Chemistry*, **287**(1), 148–158.
- Zheng, Y., Wang, Z., Bie, W., Brauer, P. M., Perez White, B. E., Li, J., Nogueira, V., Raychaudhuri, P., Hay, N., Tonetti, D. A., Macias, V., Kajdacsy-Balla, A., & Tyner, A. L. (2013). PTK6 Activation at the Membrane Regulates Epithelial-Mesenchymal Transition in Prostate Cancer. *Cancer Research*, **73**(17), 5426–5437.
- Zoubeidi, A., Zardan, A., Beraldi, E., Fazli, L., Sowery, R., Rennie, P., Nelson, C., & Gleave, M. (2007). Cooperative Interactions between Androgen Receptor (AR) and Heat-Shock Protein 27 Facilitate AR Transcriptional Activity. *Cancer Research*, **67**(21), 10455–10465.
- Zoubeidi, A., Zardan, A., Wiedmann, R. M., Locke, J., Beraldi, E., Fazli, L., & Gleave, M. E. (2010). Hsp27 promotes insulin-like growth factor-I survival signaling in prostate cancer via p90Rsk-dependent phosphorylation and inactivation of BAD. *Cancer Research*, **70**(6), 2307–2317.

Appendix

Appendix table 1 – Primers used in cloning for structural studies – F/R represent forward or reverse primer respectively. S/AS represent sense or anti-sense primer respectively. Regions in bold and highlighted yellow represent the restriction enzyme site. Regions in bold and highlighted in green represent the amino acid mutation.

Primer	Sequence
RSK4 CTKD F (NcoI)	GGAATT CCATGG CAATGTATTACCAATTG
RSK4CTKD R (XhoI)	TTC CTCGAG TCTGTGAGTTATCCATGA
RSK4 NL F (NcoI)	TTG CCATGG ATGAAGGAGTTGTAAAG
RSK4 NL R (XhoI)	GGAATTC CTCGAG TTAGATTTTATATTCTTCTG
RSK4 NL3M F (NcoI)	TTG CCATGG ATGAAGGAGTTGTAAAG
RSK4 NL3M R (XhoI)	GGAATTC CTCGAG TTAGATTTTATATTCTTCTG
RSK4 T581E (S)	TTGCAGTGTAGCATGG TTC TAAGAGAAGTCCATTTTCTCCTCGAAGTTGT
RSK4 T581E (AS)	ACAACCTCGAGGAGAAAATGGACTTCTCTTA GAA CCATGCTACACTGCAA

Appendix table 2 – Primers used in cloning for – F/R represent forward or reverse primer respectively. Regions in bold and highlighted represent the restriction enzyme site.

Primer	Sequence
RSK1 KpnI (F)	GCAATTC GGTACC ATGCCGCTCGCCCAGCT
RSK1 NotI (R)	GGAATTCGC GGCCGCT CACAGGGTGGTGGATGG
RSK2 KpnI (F)	GCAATTC GGTACC ATGCCGCTGGCGCAGCTGGC
RSK2 NotI (R)	GGAATTCGC GGCCGC TTACAGGGCTGTTGAGGTGA
RSK3 KpnI (F)	GCAATTC GGTACC ATGGACCTGAGCATGAAGAA
RSK3 NotI (R)	GGAATTCGC GGCCGC TCACAGCCGCGT
RSK4 KpnI (F)	GCAATTC GGTACC ATGCTACCATTGCTCCTCAG
RSK4 NotI (R)	GGAATTCGC GGCCGC TTACAGGCCAGTTGATGTTCCG
RSK1 EcoRI (F)	CCG GAATTC ATGCCGCTCGCCCAGCT
RSK1 Sall (R)	CGC GTCGAC TCACAGGGTGGTGGATGGCAA
RSK2 BamHI (F)	GGATCC GCATGCCGCTGGCGCAGCT
RSK2 HindIII (R)	CCC AAGCTT TCACAGGGCTGTTGAGGTGAT
RSK3 EcoRI (F)	CCG GAATTC ATGGACCTGAGCATGAAGAAGTTCGC
RSK3 Sall (R)	CGC GTCGAC CAGCCGCGTGGACGTGAGT
RSK4 EcoRI (F)	CCG GAATTC ATGCTACCATTGCT
RSK4 BamHI (F)	CGC GGATCC TTACAGGCCAGTTGAT

Appendix Table 3 – Purification buffers – RSK4 CTKD(M) dictates that both CTKD and CTKDM share these buffers.

Buffer	Buffer Composition
RSK4 NL3M W1	50 mM Tris-HCl pH 8.00, 300 mM NaCl, 5 % (v/v) glycerol, 0.01% (v/v) triton 100X, 5 mM β -mercaptoethanol, 1 mM EDTA
RSK4 NL3M W2	50 mM Tris-HCl pH 8.00, 1M NaCl, 5 % (v/v) glycerol, 0.01% (v/v) triton 100X, 1mM $MgCl_2$, 500 μ M ATP, 5 mM β -mercaptoethanol.
RSK4 NL3M E	50 mM Tris-HCl pH 8.00, 150 mM NaCl, 5 % (v/v) glycerol, 0.01% (v/v) triton 100X, 1mM $MgCl_2$, 500 μ M ATP, 5 mM β -mercaptoethanol 10 mM reduced glutathione.
RSK4 NL3M DIAL	50 mM Tris-HCl pH 7.00, 50 mM NaCl, 5 mM β -mercaptoethanol, 5 % (v/v) glycerol, 1mM $MgCl_2$, 500 μ M ATP
RSK4 NL3M Buffer A	50 mM Tris-HCl pH 7, 5 mM β -mercaptoethanol, 5 % (v/v) glycerol
RSK4 NL3M Buffer B	50 mM Tris-HCl pH 7, 1M NaCl, 5 mM β -mercaptoethanol, 5 % (v/v) glycerol
RSK4 NL3M SEC buffer	25 mM Tris-HCl pH 7, 150 mM NaCl, 5 % (v/v) glycerol)
RSK4 CTKD(M) W1	50 mM Tris-HCl pH 8.00, 300 mM NaCl, 20 mM Imidazole, 5 % (v/v) glycerol, 0.01% (v/v) triton 100X, 1mM $MgCl_2$, 500 μ M ATP
RSK4 CTKD(M) W2	50 mM Tris-HCl pH 8.00, 1 M NaCl, 20 mM Imidazole, 5 % (v/v) glycerol, 0.1% (v/v) triton 100X, 1mM $MgCl_2$, 1mM ATP
RSK4 CTKD(M) E	50 mM Tris-HCl pH 8.00, 300 mM NaCl, 300 mM Imidazole, 5 % (v/v) glycerol, 0.01% (v/v) triton 100X, 1mM $MgCl_2$, 500 μ M ATP
RSK4 CTKD(M) DIAL	50 mM Tris-HCl pH 8.00, 75 mM NaCl, 5 mM β -mercaptoethanol, 5 % (v/v) glycerol
RSK4 CTKD(M) Buffer A	50 mM Tris-HCl pH 8, 5 mM β -mercaptoethanol, 5 % (v/v) glycerol
RSK4 CTKD(M) Buffer B	50 mM Tris-HCl pH 8, 1M NaCl, 5 mM β -mercaptoethanol, 5 % (v/v) glycerol
RSK4 CTKD(M) SEC buffer	25 mM Tris-HCl pH 8, 150 mM NaCl, 5 % (v/v) glycerol)
RSK4 NTKD/NL W1	50 mM Tris-HCl pH 8.00, 300 mM NaCl, 5 % (v/v) glycerol, 0.01% (v/v) triton 100X, 5 mM β -mercaptoethanol, 1 mM EDTA
RSK4 NTKD/NL W2	50 mM Tris-HCl pH 8.00, 1M NaCl, 5 % (v/v) glycerol, 0.01% (v/v) triton 100X, 5 mM β -mercaptoethanol.
RSK4 NTKD/NL E	50 mM Tris-HCl pH 8.00, 150 mM NaCl, 5 % (v/v) glycerol, 5 mM β -mercaptoethanol 10 mM reduced glutathione
RSK4 NTKD/NL SEC BUFFER	25 mM Tris-HCl pH 8, 150 mM NaCl, 5 % (v/v) glycerol)

Appendix table 4 – Antibodies used in Western Blotting of Pull down assay – Rb denotes rabbit and Gt denotes goat.

Antibody	Primary/Secondary	Supplier, identification code	Dilution used
Anti-Hexahistidine (Rb)	Primary	Abcam, ab137839	1:5000
Anti-GST (Rb)	Primary	Abcam, ab9085	1:500
Anti-Rabbit (Gt)	Secondary	Sigma, A6154	1:2000

Appendix table 5 – QPCR primers

RSK1 F	CGGAAGGAGACCATGACACTGA
RSK1 R	GTTGGCAGGATTCCGCTTGAAC
RSK2 F	CCAGTGCTGTCCTGTTCACT
RSK2 R	GACCATTTTCCGCTCTCAGC
RSK3 F	GAAATTAAGCGCCATCCCTTCT
RSK3 R	CCACTGCTGGTTTGAACGGT
RSK4 F	ACTCACAAGAGACCAGTTG
RSK4 R	GAGTCAGGGCAGAGTATG
L19 F	GGTTAGACCCCAATGAGACC
L19 R	CATCTTTGATGAGCTTCAGG
NDRG1 F	CTCCTGCAAGAGTTTGGATGTCC
NDRG1 R	TCATGCCGATGTCATGGTAGG
TMPRSS2 F	CCTGTGTGCCAAGACGACTG
TMPRSS2 R	TTATAGCCCATGTCCCTGCAG
PSA F	TTGTCTTCCTCACCTGTCC
PSA R	AGCTGTGGCTGACCTGAAAT
ZBT F	CTGGATAGTTTGCGGCTGAG
ZBT R	ATGTCAGTGCCAGTATGGGT
FKBP5 F	ATTATCCGGAGAACCAAACG
FKBP5 R	CAAACATCCTTCCACCACAG

Appendix table 6 – RSK siRNA pool sequences

siRNA name	Sequence
Rsk-1 siRNA sc-29475A	Sense: CCAACAUCAUCACUCUGAATT Antisense: UUCAGAGUGAUGAUGUUGGTT
Rsk-1 siRNA sc-29475B	Sense: GCAUCUGUGACUUUGGUUUTT Antisense: AAACCAAAGUCACAGAUGCTT
Rsk-1 siRNA sc-29475C	Sense: GGAAAGCGAUUCACUGUAUTT Antisense: AUACAGUGAAUCGCUUUCCTT
Rsk-2 siRNA sc-36441A	Sense: GAAGGGAAGUUGUAUCUUAtt Antisense: UAAGAUACAACUCCCUUctt
Rsk-2 siRNA sc-36441B	Sense: CCAGAUGGAGUUGAAGAAAtt Antisense: UUUCUUCAACUCCAUCUGGtt
Rsk-2 siRNA sc-36441C	Sense: CAGCAUCCAAACAUAUCAAtt Antisense: UGAUAAUGUUUGGAUGCUGtt
Rsk-3 siRNA sc-36443A	Sense: CCGAGUAACAUCUGUACAtt Antisense: UGUACAGGAUGUUACUCGGtt
Rsk-3 siRNA sc-36443B	Sense: GGAUCCUGUUGUACACCAUtt Antisense: AUGGUGUACAACAGGAUCctt
Rsk-3 siRNA sc-36443C	Sense: CUGUGCUCUACUUCAUUGAtt Antisense: UCAAUGAAGUAGAGCACAGtt
Rsk-4 siRNA sc-39212A	Sense: GAGCAAUGGUUGCAACAUAAtt Antisense: UAUGUUGCAACCAUUGCUCtt
Rsk-4 siRNA sc-39212B	Sense: CAACUGGCCUGUAAGAUAUUtt Antisense: AAAUCUUAACAGGCCAGUUGtt
Rsk-4 siRNA sc-39212C	Sense: GCAGUAGUGUUCAAGUGUUtt Antisense: AACACUUGAACACUACUGctt

Appendix table 7 – PEG/ION Crystalization screen buffers – Tube no. refers to tube number. 1-48 are from PEG/ION 1 and 49-96 are from PEG/ION 2

Tube No.	Components
1	0.2 M Sodium fluoride, 20% w/v Polyethylene glycol 3,350
2	0.2 M Potassium fluoride, 20% w/v Polyethylene glycol 3,350
3	0.2 M Ammonium fluoride, 20% w/v Polyethylene glycol 3,350
4	0.2 M Lithium chloride, 20% w/v Polyethylene glycol 3,350
5	0.2 M Magnesium chloride hexahydrate, 20% w/v Polyethylene glycol 3,350
6	0.2 M Sodium chloride, 20% w/v Polyethylene glycol 3,350
7	0.2 M Calcium chloride dihydrate, 20% w/v Polyethylene glycol 3,350
8	0.2 M Potassium chloride, 20% w/v Polyethylene glycol 3,350
9	0.2 M Ammonium chloride, 20% w/v Polyethylene glycol 3,350
10	0.2 M Sodium iodide, 20% w/v Polyethylene glycol 3,350
11	0.2 M Potassium iodide, 20% w/v Polyethylene glycol 3,350
12	0.2 M Ammonium iodide, 20% w/v Polyethylene glycol 3,350
13	0.2 M Sodium thiocyanate, 20% w/v Polyethylene glycol 3,350
14	0.2 M Potassium thiocyanate, 20% w/v Polyethylene glycol 3,350
15	0.2 M Lithium nitrate, 20% w/v Polyethylene glycol 3,350
16	0.2 M Magnesium nitrate hexahydrate, 20% w/v Polyethylene glycol 3,350
17	0.2 M Sodium nitrate, 20% w/v Polyethylene glycol 3,350
18	0.2 M Potassium nitrate, 20% w/v Polyethylene glycol 3,350
19	0.2 M Ammonium nitrate, 20% w/v Polyethylene glycol 3,350
20	0.2 M Magnesium formate dihydrate, 20% w/v Polyethylene glycol 3,350
21	0.2 M Sodium formate, 20% w/v Polyethylene glycol 3,350
22	0.2 M Potassium formate, 20% w/v Polyethylene glycol 3,350
23	0.2 M Ammonium formate, 20% w/v Polyethylene glycol 3,350
24	0.2 M Lithium acetate dihydrate, 20% w/v Polyethylene glycol 3,350
25	0.2 M Magnesium acetate tetrahydrate, 20% w/v Polyethylene glycol 3,350
26	0.2 M Zinc acetate dihydrate, 20% w/v Polyethylene glycol 3,350
27	0.2 M Sodium acetate trihydrate, 20% w/v Polyethylene glycol 3,350
28	0.2 M Calcium acetate hydrate, 20% w/v Polyethylene glycol 3,350
29	0.2 M Potassium acetate, 20% w/v Polyethylene glycol 3,350
30	0.2 M Ammonium acetate, 20% w/v Polyethylene glycol 3,350
31	0.2 M Lithium sulfate monohydrate, 20% w/v Polyethylene glycol 3,350
32	0.2 M Magnesium sulfate heptahydrate, 20% w/v Polyethylene glycol 3,350
33	0.2 M Sodium sulfate decahydrate, 20% w/v Polyethylene glycol 3,350
34	0.2 M Potassium sulfate, 20% w/v Polyethylene glycol 3,350
35	0.2 M Ammonium sulfate, 20% w/v Polyethylene glycol 3,350
36	0.2 M Sodium tartrate dibasic dihydrate, 20% w/v Polyethylene glycol 3,350
37	0.2 M Potassium sodium tartrate tetrahydrate, 20% w/v Polyethylene glycol 3,350
38	0.2 M Ammonium tartrate dibasic, 20% w/v Polyethylene glycol 3,350
39	0.2 M Sodium phosphate monobasic monohydrate, 20% w/v Polyethylene glycol 3,350
40	0.2 M Sodium phosphate dibasic dihydrate, 20% w/v Polyethylene glycol 3,350
41	0.2 M Potassium phosphate monobasic, 20% w/v Polyethylene glycol 3,350
42	0.2 M Potassium phosphate dibasic, 20% w/v Polyethylene glycol 3,350
43	0.2 M Ammonium phosphate monobasic, 20% w/v Polyethylene glycol 3,350
44	0.2 M Ammonium phosphate dibasic, 20% w/v Polyethylene glycol 3,350
45	0.2 M Lithium citrate tribasic tetrahydrate, 20% w/v Polyethylene glycol 3,350
46	0.2 M Sodium citrate tribasic dihydrate, 20% w/v Polyethylene glycol 3,350
47	0.2 M Potassium citrate tribasic monohydrate, 20% w/v Polyethylene glycol 3,350
48	0.2 M Ammonium citrate dibasic, 20% w/v Polyethylene glycol 3,350

49	0.1 M Sodium malonate pH 4.0, 12% w/v Polyethylene glycol 3,350
50	0.2 M Sodium malonate pH 4.0, 20% w/v Polyethylene glycol 3,350
51	0.1 M Sodium malonate pH 5.0, 12% w/v Polyethylene glycol 3,350
52	0.2 M Sodium malonate pH 5.0, 20% w/v Polyethylene glycol 3,350
53	0.1 M Sodium malonate pH 6.0, 12% w/v Polyethylene glycol 3,350
54	0.2 M Sodium malonate pH 6.0, 20% w/v Polyethylene glycol 3,350
55	0.1 M Sodium malonate pH 7.0, 12% w/v Polyethylene glycol 3,350
56	0.2 M Sodium malonate pH 7.0, 20% w/v Polyethylene glycol 3,350
57	4% v/v TacsimateTM pH 4.0, 12% w/v Polyethylene glycol 3,350
58	8% v/v TacsimateTM pH 4.0, 20% w/v Polyethylene glycol 3,350
59	4% v/v TacsimateTM pH 5.0, 12% w/v Polyethylene glycol 3,350
60	8% v/v TacsimateTM pH 5.0, 20% w/v Polyethylene glycol 3,350
61	4% v/v TacsimateTM pH 6.0, 12% w/v Polyethylene glycol 3,350
62	8% v/v TacsimateTM pH 6.0, 20% w/v Polyethylene glycol 3,350
63	4% v/v TacsimateTM pH 7.0, 12% w/v Polyethylene glycol 3,350
64	8% v/v TacsimateTM pH 7.0, 20% w/v Polyethylene glycol 3,350
65	4% v/v TacsimateTM pH 8.0, 12% w/v Polyethylene glycol 3,350
66	8% v/v TacsimateTM pH 8.0, 20% w/v Polyethylene glycol 3,350
67	0.1 M Succinic acid pH 7.0, 12% w/v Polyethylene glycol 3,350
68	0.2 M Succinic acid pH 7.0, 20% w/v Polyethylene glycol 3,350
69	0.1 M Ammonium citrate tribasic pH 7.0, 12% w/v Polyethylene glycol 3,350
70	0.2 M Ammonium citrate tribasic pH 7.0, 20% w/v Polyethylene glycol 3,350
71	0.1 M DL-Malic acid pH 7.0, 12% w/v Polyethylene glycol 3,350
72	0.2 M DL-Malic acid pH 7.0, 20% w/v Polyethylene glycol 3,350
73	0.1 M Sodium acetate trihydrate pH 7.0, 12% w/v Polyethylene glycol 3,350
74	0.2 M Sodium acetate trihydrate pH 7.0, 20% w/v Polyethylene glycol 3,350
75	0.1 M Sodium formate pH 7.0, 12% w/v Polyethylene glycol 3,350
76	0.2 M Sodium formate pH 7.0, 20% w/v Polyethylene glycol 3,350
77	0.1 M Ammonium tartrate dibasic pH 7.0, 12% w/v Polyethylene glycol 3,350
78	0.2 M Ammonium tartrate dibasic pH 7.0, 20% w/v Polyethylene glycol 3,350
79	2% v/v TacsimateTM pH 4.0, 0.1 M Sodium acetate trihydrate pH 4.6, 16% w/v Polyethylene glycol 3,350
80	2% v/v TacsimateTM pH 5.0, 0.1 M Sodium citrate tribasic dihydrate pH 5.6, 16% w/v Polyethylene glycol 3,350
81	2% v/v TacsimateTM pH 6.0, 0.1 M BIS-TRIS pH 6.5, 20% w/v Polyethylene glycol 3,350
82	2% v/v TacsimateTM pH 7.0, 0.1 M HEPES pH 7.5, 20% w/v Polyethylene glycol 3,350
83	2% v/v TacsimateTM pH 8.0, 0.1 M Tris pH 8.5, 16% w/v Polyethylene glycol 3,350
84	(0.07 M Citric acid, 0.03 M BIS-TRIS propane / pH 3.4), 16% w/v Polyethylene glycol 3,350
85	(0.06 M Citric acid, 0.04 M BIS-TRIS propane / pH 4.1), 16% w/v Polyethylene glycol 3,350
86	(0.05 M Citric acid, 0.05 M BIS-TRIS propane / pH 5.0), 16% w/v Polyethylene glycol 3,350
87	(0.04 M Citric acid, 0.06 M BIS-TRIS propane / pH 6.4), 20% w/v Polyethylene glycol 3,350
88	(0.03 M Citric acid, 0.07 M BIS-TRIS propane / pH 7.6), 20% w/v Polyethylene glycol 3,350
89	(0.02 M Citric acid, 0.08 M BIS-TRIS propane / pH 8.8), 16% w/v Polyethylene glycol 3,350
90	0.02 M Calcium chloride dihydrate, 0.02 M Cadmium chloride hydrate,
91	0.02 M Cobalt(II) chloride hexahydrate, 20% w/v Polyethylene glycol 3,350
92	0.01 M Magnesium chloride hexahydrate, 0.005 M Nickel(II) chloride hexahydrate
93	0.1 M HEPES sodium pH 7.0, 15% w/v Polyethylene glycol 3,350
94	0.02 M Zinc chloride, 20% w/v Polyethylene glycol 3,350
95	0.15 M Cesium chloride, 15% w/v Polyethylene glycol 3,350
96	0.2 M Sodium bromide, 20% w/v Polyethylene glycol 3,350

Appendix table 8 – JCSG+ crystallization screen buffers – Tube no. refers to tube number. All numbers refer to exactly as the come in the box.

Tube No.	Buffer components
1-1	0.2 M Lithium sulfate, 0.1 M Sodium acetate pH 4.5, 50 % w/v PEG 400
1-2	0.1 M Sodium citrate pH 5.5, 20 % w/v PEG 3000
1-3	0.2 M Ammonium citrate dibasic, 20 % w/v PEG 3350
1-4	0.02 M Calcium chloride dihydrate, 0.1 M Sodium acetate pH 4.6, 30 % v/v MPD
1-5	0.2 M Magnesium formate dihydrate, 20 % w/v PEG 3350
1-6	0.2 M Lithium sulfate, 0.1 M Phosphate/citrate pH 4.2, 20 % w/v PEG 1000
1-7	0.1 M CHES pH 9.5, 20 % w/v PEG 8000
1-8	0.2 M Ammonium formate, 20 % w/v PEG 3350
1-9	0.2 M Ammonium chloride, 20 % w/v PEG 3350
1-10	0.2 M Potassium formate, 20 % w/v PEG 3350
1-11	0.2 M Ammonium phosphate monobasic, 0.1 M Tris pH 8.5, 50 % v/v MPD
1-12	0.2 M Potassium nitrate, 20 % w/v PEG 3350
1-13	0.8 M Ammonium sulfate, 0.1 M Citrate pH 4.0
1-14	0.2 M Sodium thiocyanate, 20 % w/v PEG 3350
1-15	0.1 M BICINE pH 9.0, 20 % w/v PEG 6000
1-16	0.1 M HEPES pH 7.5, 10 % w/v PEG 8000, 8 % v/v Ethylene glycol
1-17	0.1 M Sodium cacodylate pH 6.5, 40 % v/v MPD, 5 % w/v PEG 8000
1-18	0.1 M Phosphate/citrate pH 4.2, 40 % v/v Ethanol, 5 % w/v PEG 1000
1-19	0.1 M Sodium acetate pH 4.6, 8 % w/v PEG 4000
1-20	0.2 M Magnesium chloride hexahydrate, 0.1 M Tris pH 7, 10 % w/v PEG 8000
1-21	0.1 M Citrate pH 5.0, 20 % w/v PEG 6000
1-22	0.2 M Magnesium chloride hexahydrate, 0.1 M Sodium cacodylate pH 6.5, 50 % v/v PEG 200
1-23	1.6 M Sodium citrate tribasic dihydrate pH 6.5
1-24	0.2 M Potassium citrate tribasic monohydrate, 20 % w/v PEG 3350
1-25	0.2 M Sodium chloride, 0.1 M Phosphate/citrate pH 4.2, 20 % w/v PEG 8000
1-26	1.0 M Lithium chloride, 0.1 M Citrate pH 4.0, 20 % w/v PEG 6000
1-27	0.2 M Ammonium nitrate, 20 % w/v PEG 3350
1-28	0.1 M HEPES pH 7.0, 10 % w/v PEG 6000
1-29	0.8 M Sodium phosphate monobasic monohydrate, 0.80 M Potassium phosphate monobasic, 0.1 M Sodium HEPES pH 7.5
1-30	0.1 M Phosphate/citrate pH 4.2, 40 % v/v PEG 300
1-31	0.2 M Zinc acetate dihydrate, 0.1 M Sodium acetate pH 4.5, 10 % w/v PEG 3000
1-32	0.1 M Tris pH 8.5, 20 % v/v Ethanol
1-33	0.1 M Sodium/potassium phosphate pH 6.2, 25 % v/v 1,2-Propandiol, 10 %v/v Glycerol
1-34	0.1 M BICINE pH 9.0, 10 % w/v PEG 20,000, 2 % v/v 1,4-Dioxane
1-35	2.0 M Ammonium sulfate, 0.1 M Sodium acetate pH 4.6
1-36	10 % w/v PEG 1000, 10 % w/v PEG 8000
1-37	24 % w/v PEG 1500, 20 % v/v Glycerol
1-38	0.2 M Magnesium chloride hexahydrate, 0.1 M Sodium HEPES pH 7.5, 30 % v/v PEG 400
1-39	0.2 M Sodium chloride 0.1 M, Sodium/potassium phosphate pH 6.2, 50 % v/v PEG 200

1-40	0.2 M Lithium sulfate, 0.1 M Sodium acetate pH 4.5, 30 % w/v PEG 8000
1-41	0.1 M HEPES pH 7.5, 70 % v/v MPD
1-42	0.2 M Magnesium chloride hexahydrate, 0.1 M Tris pH 8.5, 20 % w/v PEG 8000
1-43	0.2 M Lithium sulfate, 0.1 M Tris pH 8.5, 40 % v/v PEG 400
1-44	0.1 M Tris 8.0, 40 % v/v MPD
1-45	0.17 M Ammonium sulfate, 25.5 % w/v PEG 4000
1-46	0.2 M Calcium acetate hydrate, 0.1 M Sodium cacodylate pH 6.5, 40 % v/v PEG 300
1-47	0.14 M Calcium chloride dihydrate, 0.07 M Sodium acetate pH 4.6, 14 % v/v 2-Propanol, 30 % v/v Glycerol
1-48	0.04 M Potassium phosphate monobasic, 16 % w/v PEG 8000 20 % v/v Glycerol
2-1	1.0 M Sodium citrate tribasic dihydrate, 0.1 M Sodium cacodylate pH 6.5
2-2	2.0 M Ammonium sulfate, 0.2 M Sodium chloride, 0.1 M Sodium cacodylate 6.5
2-3	0.2 M Sodium chloride, 0.1 M HEPES pH 7.5, 10 % v/v 2-Propanol
2-4	1.26 M Ammonium sulfate, 0.1 M Tris pH 8.5, 0.2 M Lithium sulfate
2-5	0.1 M CAPS pH 10.5, 40 % v/v MPD
2-6	0.2 M Zinc acetate dihydrate, 0.1 M Imidazole pH 8.0, 20 % w/v PEG 3000
2-7	0.2 M Zinc acetate dihydrate, 0.1 M Sodium cacodylate pH 6.5, 10 % v/v 2-Propanol
2-8	1.0 M Ammonium phosphate dibasic, 0.1 M Sodium acetate pH 4.5
2-9	1.6 M Magnesium sulfate heptahydrate, 0.1 M MES pH 6.5
2-10	0.1 M BICINE pH 9.0, 10 % w/v PEG 6000
2-11	0.16 M Calcium acetate hydrate, 0.08 M Sodium cacodylate pH 6.5, 14.4 % w/v PEG 8000, 20 % v/v Glycerol
2-12	0.1 M Imidazole pH 8.0, 10 % w/v PEG 8000
2-13	0.05 M Cesium chloride, 0.1 M MES pH 6.5, 30 % v/v Jeffamine® M-600
2-14	3.2 M Ammonium sulfate, 0.1 M Citrate pH 5.0
2-15	0.1 M Tris pH 8.0, 20 % v/v MPD
2-16	0.1 M HEPES pH 7.5, 20 % v/v Jeffamine® M-600
2-17	0.2 M Magnesium chloride hexahydrate, 0.1 M Tris pH 8.5 50 % v/v Ethylene glycol
2-18	0.1 M BICINE pH 9.0, 10 % v/v MPD
2-19	0.8 M Succinic acid pH 7.0
2-20	2.1 M DL-Malic acid pH 7.0
2-21	2.4 M Sodium malonate dibasic monohydrate pH 7.0
2-22	1.1 M Sodium malonate dibasic monohydrate, 0.1 M HEPES pH 7.0, 0.5 % v/v Jeffamine® ED-2003
2-23	1.0 M Succinic acid, 0.1 M HEPES pH 7.0, 1 % w/v PEG 2000 MME
2-24	0.1 M HEPES pH 7.0, 30 % v/v Jeffamine® M-600
2-25	0.1 M HEPES pH 7.0, 30 % v/v Jeffamine® ED-2003
2-26	0.02 M Magnesium chloride hexahydrate, 0.1 M HEPES pH 7.5, 22 % w/v Poly(acrylic acid sodium salt) 5100
2-27	0.01 M Cobalt(II) chloride hexahydrate, 0.1 M Tris pH 8.5, 20 % w/v Polyvinylpyrrolidone
2-28	0.2 M TMAO, 0.1 M Tris pH 8.5, 20 % w/v PEG 2000 MME
2-29	0.005 M Cobalt(II) chloride hexahydrate, 0.1 M HEPES pH 7.5, 12 % w/v PEG 3350, 0.005 M Cadmium chloride hemi(pentahydrate), 0.005 M Magnesium chloride hexahydrate, 0.005 M Nickel(II) chloride hexahydrate
2-30	0.2 M Sodium malonate dibasic monohydrate, 20 % w/v PEG 3350
2-31	0.1 M Succinic acid, 15 % w/v PEG 3350

2-32	0.15 M DL-Malic acid, 20 % w/v PEG 3350
2-33	0.1 M Potassium thiocyanate, 30 % w/v PEG 2000 MME
2-34	0.15 M Potassium bromide, 30 % w/v PEG 2000 MME
2-35	2.0 M Ammonium sulfate, 0.1 M BIS-Tris pH 5.5
2-36	3.0 M Sodium chloride, 0.1 M BIS-Tris pH 5.5
2-37	0.3 M Magnesium formate dihydrate, 0.1 M BIS-Tris pH 5.5
2-38	1.0 M Ammonium sulfate, 0.1 M BIS-Tris pH 5.5, 1 % w/v PEG 3350
2-39	0.1 M BIS-Tris pH 5.5, 25 % w/v PEG 3350
2-40	0.2 M Calcium chloride dihydrate, 0.1 M BIS-Tris pH 5.5, 45 % v/v MPD
2-41	0.2 M Ammonium acetate, 0.1 M BIS-Tris pH 5.5, 45 % v/v MPD
2-42	0.1 M Ammonium acetate, 0.1 M BIS-Tris pH 5.5, 17 % w/v PEG 10,000
2-43	0.2 M Ammonium sulfate, 0.1 M BIS-Tris pH 5.5, 25 % w/v PEG 3350
2-44	0.2 M Sodium chloride 0.1, M BIS-Tris pH 5.5, 25 % w/v PEG 3350
2-45	0.2 M Lithium sulfate, 0.1 M BIS-Tris pH 5.5, 25 % w/v PEG 3350
2-46	0.2 M Ammonium acetate, 0.1 M BIS-Tris pH 5.5, 25 % w/v PEG 3350
2-47	0.2 M Magnesium chloride hexahydrate, 0.1 M BIS-Tris pH 5.5, 25 % w/v PEG 3350
2-48	0.2 M Ammonium acetate, 0.1 M HEPES pH 7.5, 45 % v/v MPD

Appendix Table 9 – Structure screen crystallization screen buffers – Tube no. refers to tube number of the buffers from the screen.

Tube No.	Components
A 1	0.02 M Calcium chloride dihydrate, 0.1 M Sodium acetate pH 4.6, 30 % v/v MPD
A 2	0.2 M Ammonium acetate, 0.1 M Sodium acetate pH 4.6, 30 % w/v PEG 4000
A 3	0.2 M Ammonium sulfate, 0.1 M Sodium acetate pH 4.6, 25 % w/v PEG 4000
A 4	2.0 M Sodium formate, 0.1 M Sodium acetate pH 4.6
A 5	2.0 M Ammonium sulfate, 0.1 M Sodium acetate pH 4.6
A 6	0.1 M Sodium acetate pH 4.6, 8 % w/v PEG 4000
A 7	0.2 M Ammonium acetate, 0.1 M Sodium citrate pH 5.6, 30 % w/v PEG 4000
A 8	0.2 M Ammonium acetate, 0.1 M Sodium citrate pH 5.6, 30 % v/v MPD
A 9	0.1 M Sodium citrate pH 5.6, 20 % w/v PEG 4000, 20 % v/v 2-Propanol
A10	1.0 M Ammonium phosphate monobasic, 0.1 M Sodium citrate pH 5.6
A11	0.2 M Calcium chloride dihydrate, 0.1 M Sodium acetate pH 4.6, 20 % v/v 2-Propanol
A12	1.4 M Sodium acetate trihydrate, 0.1 M Sodium cacodylate pH 6.5
B1	0.2 M Sodium citrate tribasic dihydrate, 0.1 M Sodium cacodylate pH 6.5, 30 % v/v 2-Propanol
B2	0.2 M Ammonium sulfate, 0.1 M Sodium cacodylate pH 6.5, 30 % w/v PEG 8000
B3	0.2 M Magnesium acetate tetrahydrate, 0.1 M Sodium cacodylate pH 6.5, 20 % w/v PEG 8000
B4	0.2 M Magnesium acetate tetrahydrate, 0.1 M Sodium cacodylate pH 6.5, 30 % v/v MPD
B5	1.0 M Sodium acetate trihydrate, 0.1 M Imidazole pH 6.5
B6	0.2 M Sodium acetate trihydrate, 0.1 M Sodium cacodylate pH 6.5, 30 % w/v PEG 8000
B7	0.2 M Zinc acetate dihydrate, 0.1 M Sodium cacodylate pH 6.5, 18 % w/v PEG 8000
B8	0.2 M Calcium acetate hydrate, 0.1 M Sodium cacodylate pH 6.5, 18 % w/v PEG 8000
B9	0.2 M Sodium citrate tribasic dihydrate, 0.1 M Sodium HEPES pH 7.5, 30 % v/v MPD
B10	0.2 M Magnesium chloride hexahydrate, 0.1 M Sodium HEPES pH 7.5, 30 % v/v 2-Propanol
B11	0.2 M Calcium chloride dihydrate, 0.1 M Sodium HEPES pH 7.5, 28 % v/v PEG 400
B12	0.2 M Magnesium chloride hexahydrate, 0.1 M Sodium HEPES pH 7.5, 30 % v/v PEG 400
C1	0.2 M Sodium citrate tribasic dihydrate, 0.1 M Sodium HEPES pH 7.5, 20 % v/v 2-Propanol
C2	0.8 M Potassium sodium tartrate tetrahydrate, 0.1 M Sodium HEPES pH 7.5
C3	1.5 M Lithium sulfate, 0.1 M Sodium HEPES pH 7.5
C4	0.8 M Sodium phosphate monobasic monohydrate, 0.8 M Potassium phosphate monobasic, 0.1 M Sodium HEPES pH 7.5
C5	1.4 M Sodium citrate tribasic dihydrate, 0.1 M Sodium HEPES pH 7.5
C6	2.0 M Ammonium sulfate, 0.1 M Sodium HEPES pH 7.5, 2 % v/v PEG 400
C7	0.1 M Sodium HEPES pH 7.5, 20 % w/v PEG 4000, 10 % v/v 2-Propanol
C8	2.0 M Ammonium sulfate, 0.1 M Tris pH 8.5

C9	0.2 M Magnesium chloride hexahydrate, 0.1 M Tris pH 8.5, 30 % w/v PEG 4000
C10	0.2 M Sodium citrate tribasic dihydrate, 0.1 M Tris pH 8.5, 30 % v/v PEG 400
C11	0.2 M Lithium sulfate, 0.1 M Tris pH 8.5, 30 % w/v PEG 4000
C12	0.2 M Ammonium acetate, 0.1 M Tris pH 8.5, 30 % v/v 2-Propanol
D1	0.2 M Sodium acetate trihydrate, 0.1 M Tris pH 8.5, 30 % w/v PEG 4000
D2	0.1 M Tris pH 8.5, 8 % w/v PEG 8000
D3	2.0 M Ammonium phosphate monobasic, 0.1 M Tris pH 8.5
D4	0.4 M Potassium sodium tartrate tetrahydrate
D5	0.4 M Ammonium phosphate monobasic
D6	0.2 M Ammonium sulfate, 30 % w/v PEG 8000
D7	0.2 M Ammonium sulfate, 30 % w/v PEG 4000
D8	2.0 M Ammonium sulfate
D9	4.0 M Sodium formate
D10	0.05 M Potassium phosphate monobasic, 20 % w/v PEG 8000
D11	30 % w/v PEG 1500
D12	0.2 M Magnesium formate dihydrate
E1	0.1 M Sodium chloride, 0.1 M BICINE pH 9.0, 30 % v/v PEG 500 MME
E2	2.0 M Magnesium chloride hexahydrate, 0.1 M BICINE pH 9.0
E3	0.1 M BICINE pH 9.0, 10 % w/v PEG 20000, 2 % v/v 1,4-Dioxane
E4	0.2 M Magnesium chloride hexahydrate, 0.1 M Tris pH 8.5, 3.4 M 1,6-Hexanediol
E5	0.1 M Tris pH 8.5, 25 % v/v tert-Butanol
E6	1.0 M Lithium sulfate/0.01 M Nickel(II) chloride hexahydrate, 0.1 M Tris pH 8.5
E7	1.5 M Ammonium sulfate, 0.1 M Tris pH 8.5
E8	0.2 M Ammonium phosphate monobasic, 0.1 M Tris pH 8.5
E9	0.1 M Tris pH 8.5
E10	0.01 M Nickel (II) chloride hexahydrate, 0.1 M Tris pH 8.5
E11	0.5 M Ammonium sulfate, 0.1 M Sodium HEPES pH 7.5
E12	0.1 M Sodium HEPES pH 7.5, 5 % v/v MPD
F1	0.1 M Sodium HEPES pH 7.5
F2	1.6 M Ammonium sulfate/0.1 M Sodium chloride, 0.1 M Sodium HEPES pH 7.5
F3	2.0 M Ammonium formate, 0.1 M Sodium HEPES pH 7.5
F4	1.0 M Sodium acetate trihydrate/0.05 M Cadmium sulfate 8/3 -hydrate, 0.1 M Sodium HEPES pH 7.5
F5	0.1 M Sodium HEPES pH 7.5, 70 % v/v MPD
F6	4.3 M Sodium chloride, 0.1 M Sodium HEPES pH 7.5
F7	0.1 M Sodium HEPES pH 7.5, 8 % v/v Ethylene glycol
F8	1.6 M Magnesium sulfate heptahydrate 0.1 M MES 6.5
F9	2.0 M Sodium chloride/0.1 M Potassium phosphate monobasic/0.1 M Sodium phosphate monobasic monohydrate, 0.1 M MES pH 6.5
F10	0.1 M MES pH 6.5, 12 % w/v PEG 20000
F11	1.6 M Ammonium sulfate, 0.1 M MES pH 6.5
F12	0.05 M Cesium chloride, 0.1 M MES pH 6.5
G1	0.01 M Cobalt(II) chloride hexahydrate, 0.1 M MES pH 6.5, 1.8 M Ammonium sulfate
G2	0.2 M Ammonium sulfate, 0.1 M MES pH 6.5
G3	0.01 M Zinc sulfate heptahydrate, 0.1 M MES pH 6.5
G4	0.1 M Sodium HEPES pH 7.5
G5	2.0 M Ammonium sulfate, 0.2 M Potassium sodium tartrate tetrahydrate, 0.1 M Sodium citrate pH 5.6
G6	1.0 M Lithium sulfate, 0.5 M Ammonium sulfate, 0.1 M Sodium citrate pH 5.6

G7	0.5 M Sodium chloride, 0.1 M Sodium citrate pH 5.6
G8	0.1 M Sodium citrate pH 5.6
G9	0.01 M Iron(III) chloride hexahydrate, 0.1 M Sodium citrate pH 5.6
G10	0.01 M Manganese(II) chloride tetrahydrate, 0.1 M Sodium citrate pH 5.6
G11	2.0 M Sodium chloride, 0.1 M Sodium acetate pH 4.6
G12	0.2 M Sodium chloride, 0.1 M Sodium acetate pH 4.6
H1	0.01 M Cobalt(II) chloride hexahydrate, 0.1 M Sodium acetate pH 4.6
H2	0.1 M Cadmium chloride hemi(pentahydrate), 0.1 M Sodium acetate pH 4.6
H3	0.2 M Ammonium sulfate, 0.1 M Sodium acetate pH 4.6
H4	2.0 M Sodium chloride
H5	0.5 M Sodium chloride/0.1 M Magnesium chloride hexahydrate
H6	25 % v/v Ethylene glycol
H7	35 % v/v 1,4-Dioxane
H8	2.0 M Ammonium sulfate, 5 % v/v 2-Propanol
H9	1.0 M Imidazole pH 7.0
H10	10 % w/v PEG 1000, 10 % w/v PEG 8000
H11	1.5 M Sodium chloride, 10 % v/v Ethanol
H12	1.6 M Sodium citrate pH 6.5

Appendix Table 10 – PACT premier crystallization screen buffers – Tube no. refers to tube number of the buffers from the screen.

Tube No.	Buffer Components
1-1	0.1 M SPG pH 4.0, 25 % w/v PEG 1500
1-2	0.1 M SPG pH 5.0, 25 % w/v PEG 1500
1-3	0.1 M SPG pH 6.0, 25 % w/v PEG 1500
1-4	0.1 M SPG pH 7.0, 25 % w/v PEG 1500
1-5	0.1 M SPG pH 8.0, 25 % w/v PEG 1500
1-6	0.1 M SPG pH 9.0, 25 % w/v PEG 1500
1-7	0.2 M Sodium chloride, 0.1 M Sodium acetate pH 5.0, 20 % w/v PEG 6000
1-8	0.2 M Ammonium chloride, 0.1 M Sodium acetate pH 5.0, 20 % w/v PEG 6000
1-9	0.2 M Lithium chloride, 0.1 M Sodium acetate pH 5.0, 20 % w/v PEG 6000
1-10	0.2 M Magnesium chloride hexahydrate, 0.1 M Sodium acetate pH 5.0, 20 % w/v PEG 6000
1-11	0.2 M Calcium chloride dihydrate, 0.1 M Sodium acetate pH 5.0, 20 % w/v PEG 6000
1-12	0.01 M Zinc chloride, 0.1 M Sodium acetate pH 5.0, 20 % w/v PEG 6000
1-13	0.1 M MIB pH 4.0, 25 % w/v PEG 1500
1-14	0.1 M MIB pH 5.0, 25 % w/v PEG 1500
1-15	0.1 M MIB pH 6.0, 25 % w/v PEG 1500
1-16	0.1 M MIB pH 7.0, 25 % w/v PEG 1500
1-17	0.1 M MIB pH 8.0, 25 % w/v PEG 1500
1-18	0.1 M MIB pH 9.0, 25 % w/v PEG 1500
1-19	0.2 M Sodium chloride, 0.1 M MES pH 6.0, 20 % w/v PEG 6000
1-20	0.2 M Ammonium chloride, 0.1 M MES pH 6.0, 20 % w/v PEG 6000
1-21	0.2 M Lithium chloride, 0.1 M MES pH 6.0, 20 % w/v PEG 6000
1-22	0.2 M Magnesium chloride hexahydrate, 0.1 M MES pH 6.0 20 % w/v PEG 6000
1-23	0.2 M Calcium chloride dihydrate, 0.1 M MES pH 6.0, 20 % w/v PEG 6000
1-24	0.01 M Zinc chloride, 0.1 M MES pH 6.0, 20 % w/v PEG 6000
1-25	0.1 M PCTP pH 4.0, 25 % w/v PEG 1500
1-26	0.1 M PCTP pH 5.0, 25 % w/v PEG 1500
1-27	0.1 M PCTP pH 6.0, 25 % w/v PEG 1500
1-28	0.1 M PCTP pH 7.0, 25 % w/v PEG 1500
1-29	0.1 M PCTP pH 8.0, 25 % w/v PEG 1500
1-30	0.1 M PCTP pH 9.0, 25 % w/v PEG 1500
1-31	0.2 M Sodium chloride, 0.1 M HEPES pH 7.0, 20 % w/v PEG 6000
1-32	0.2 M Ammonium chloride, 0.1 M HEPES pH 7.0, 20 % w/v PEG 6000
1-33	0.2 M Lithium chloride, 0.1 M HEPES pH 7.0, 20 % w/v PEG 6000
1-34	0.2 M Magnesium chloride hexahydrate, 0.1 M HEPES pH 7.0, 20 % w/v PEG 6000
1-35	0.2 M Calcium chloride dihydrate, 0.1 M HEPES pH 7.0, 20 % w/v PEG 6000
1-36	0.01 M Zinc chloride, 0.1 M HEPES pH 7.0, 20 % w/v PEG 6000
1-37	0.1 M MMT pH 4.0, 25 % w/v PEG 1500
1-38	0.1 M MMT pH 5.0, 25 % w/v PEG 1500
1-39	0.1 M MMT pH 6.0, 25 % w/v PEG 1500
1-40	0.1 M MMT pH 7.0, 25 % w/v PEG 1500
1-41	0.1 M MMT pH 8.0, 25 % w/v PEG 1500

1-42	0.1 M MMT pH 9.0, 25 % w/v PEG 1500
1-43	0.2 M Sodium chloride, 0.1 M Tris pH 8.0, 20 % w/v PEG 6000
1-44	0.2 M Ammonium chloride, 0.1 M Tris pH 8.0, 20 % w/v PEG 6000
1-45	0.2 M Lithium chloride, 0.1 M Tris pH 8.0, 20 % w/v PEG 6000
1-46	0.2 M Magnesium chloride hexahydrate, 0.1 M Tris pH 8.0, 20 % w/v PEG 6000
1-47	0.2 M Calcium chloride dihydrate, 0.1 M Tris pH 8.0, 20 % w/v PEG 6000
1-48	0.002 M Zinc chloride, 0.1 M Tris 8.0, 20 % w/v PEG 6000
2-1	0.2 M Sodium fluoride, 20 % w/v PEG 3350
2-2	0.2 M Sodium bromide, 20 % w/v PEG 3350
2-3	0.2 M Sodium iodide 20, % w/v PEG 3350
2-4	0.2 M Potassium thiocyanate 20, % w/v PEG 3350
2-5	0.2 M Sodium nitrate, 20 % w/v PEG 3350
2-6	0.2 M Sodium formate, 20 % w/v PEG 3350
2-7	0.2 M Sodium acetate trihydrate, 20 % w/v PEG 3350
2-8	0.2 M Sodium sulfate 20, % w/v PEG 3350
2-9	0.2 M Potassium sodium tartrate tetrahydrate, 20 % w/v PEG 3350
2-10	0.02 M Sodium/potassium phosphate, 20 % w/v PEG 3350
2-11	0.2 M Sodium citrate tribasic dihydrate, 20 % w/v PEG 3350
2-12	0.2 M Sodium malonate dibasic monohydrate, 20 % w/v PEG 3350
2-13	0.2 M Sodium fluoride, 0.1 M Bis-Tris propane pH 6.5, 20 % w/v PEG 3350
2-14	0.2 M Sodium bromide, 0.1 M Bis-Tris propane pH 6.5, 20 % w/v PEG 3350
2-15	0.2 M Sodium iodide, 0.1 M Bis-Tris propane pH 6.5, 20 % w/v PEG 3350
2-16	0.2 M Potassium thiocyanate, 0.1 M Bis-Tris propane pH 6.5, 20 % w/v PEG 3350
2-17	0.2 M Sodium nitrate, 0.1 M Bis-Tris propane pH 6.5, 20 % w/v PEG 3350
2-18	0.2 M Sodium formate, 0.1 M Bis-Tris propane pH 6.5, 20 % w/v PEG 3350
2-19	0.2 M Sodium acetate trihydrate, 0.1 M Bis-Tris propane pH 6.5, 20 % w/v PEG 3350
2-20	0.2 M Sodium sulfate, 0.1 M Bis-Tris propane pH 6.5, 20 % w/v PEG 3350
2-21	0.2 M Potassium sodium tartrate tetrahydrate, 0.1 M Bis-Tris propane pH 6.5, 20 % w/v PEG 3350
2-22	0.02 M Sodium/potassium phosphate, 0.1 M Bis-Tris propane pH 6.5, 20 % w/v PEG 3350
2-23	0.2 M Sodium citrate tribasic dihydrate, 0.1 M Bis-Tris propane pH 6.5, 20 % w/v PEG 3350
2-24	0.2 M Sodium malonate dibasic monohydrate, 0.1 M Bis-Tris propane pH 6.5, 20 % w/v PEG 3350
2-25	0.2 M Sodium fluoride, 0.1 M Bis-Tris propane pH 7.5, 20 % w/v PEG 3350
2-26	0.2 M Sodium bromide, 0.1 M Bis-Tris propane pH 7.5, 20 % w/v PEG 3350
2-27	0.2 M Sodium iodide, 0.1 M Bis-Tris propane pH 7.5, 20 % w/v PEG 3350
2-28	0.2 M Potassium thiocyanate, 0.1 M Bis-Tris propane pH 7.5, 20 % w/v PEG 3350
2-29	0.2 M Sodium nitrate, 0.1 M Bis-Tris propane pH 7.5, 20 % w/v PEG 3350
2-30	0.2 M Sodium formate, 0.1 M Bis-Tris propane pH 7.5, 20 % w/v PEG 3350
2-31	0.2 M Sodium acetate trihydrate, 0.1 M Bis-Tris propane pH 7.5, 20 % w/v PEG 3350

2-32	0.2 M Sodium sulfate, 0.1 M Bis-Tris propane pH 7.5, 20 % w/v PEG 3350
2-33	0.2 M Potassium sodium tartrate tetrahydrate, 0.1 M Bis-Tris propane pH 7.5, 20 % w/v PEG 3350
2-34	0.02 M Sodium/potassium phosphate, 0.1 M Bis-Tris propane pH 7.5, 20 % w/v PEG 3350
2-35	0.2 M Sodium citrate tribasic dihydrate, 0.1 M Bis-Tris propane pH 7.5, 20 % w/v PEG 3350
2-36	0.2 M Sodium malonate dibasic monohydrate, 0.1 M Bis-Tris propane pH 7.5, 20 % w/v PEG 3350
2-37	0.2 M Sodium fluoride, 0.1 M Bis-Tris propane pH 8.5, 20 % w/v PEG 3350
2-38	0.2 M Sodium bromide, 0.1 M Bis-Tris propane pH 8.5, 20 % w/v PEG 3350
2-39	0.2 M Sodium iodide, 0.1 M Bis-Tris propane pH 8.5, 20 % w/v PEG 3350
2-40	0.2 M Potassium thiocyanate, 0.1 M Bis-Tris propane pH 8.5, 20 % w/v PEG 3350
2-41	0.2 M Sodium nitrate, 0.1 M Bis-Tris propane pH 8.5, 20 % w/v PEG 3350
2-42	0.2 M Sodium formate, 0.1 M Bis-Tris propane pH 8.5, 20 % w/v PEG 3350
2-43	0.2 M Sodium acetate trihydrate, 0.1 M Bis-Tris propane pH 8.5, 20 % w/v PEG 3350
2-44	0.2 M Sodium sulfate, 0.1 M Bis-Tris propane pH 8.5, 20 % w/v PEG 3350
2-45	0.2 M Potassium sodium tartrate tetrahydrate, 0.1 M Bis-Tris propane pH 8.5, 20 % w/v PEG 3350
2-46	0.02 M Sodium/potassium phosphate, 0.1 M Bis-Tris propane pH 8.5, 20 % w/v PEG 3350
2-47	0.2 M Sodium citrate tribasic dihydrate, 0.1 M Bis-Tris propane pH 8.5, 20 % w/v PEG 3350
2-48	0.2 M Sodium malonate dibasic monohydrate 0.1, M Bis-Tris propane pH 8.5, 20 % w/v PEG 3350

Appendix Table 11 – PGA crystallization screen buffers – Tube no. refers to tube number of the buffers from the screen.

Tube No.	Buffer components
1-1	0.3 M Potassium bromide, 0.1 M Sodium acetate pH 5.0, 8 % w/v γ -PGA (Na ⁺ form, LM)
1-2	0.2 M Magnesium chloride, 0.1 M Sodium acetate pH 5.0, 8 % w/v γ -PGA (Na ⁺ form, LM)
1-3	0.3 M Sodium malonate dibasic monohydrate, 0.1 M Sodium acetate pH 5.0, 8 % w/v γ -PGA (Na ⁺ form, LM)
1-4	0.6 M Sodium formate, 0.1 M Sodium acetate pH 5.0, 8 % w/v γ -PGA (Na ⁺ form, LM)
1-5	1 M Ammonium formate, 0.1 M Sodium acetate pH 5.0, 8 % w/v γ -PGA (Na ⁺ form, LM)
1-6	0.2 M Potassium thiocyanate, 0.1 M Sodium acetate pH 5.0, 8 % w/v γ -PGA (Na ⁺ form, LM)
1-7	0.2 M L-Proline, 0.1 M Sodium acetate pH 5.0, 8 % w/v γ -PGA (Na ⁺ form, LM)
1-8	0.2 M L-Arginine, 0.1 M Sodium acetate pH 5.0, 8 % w/v γ -PGA (Na ⁺ form, LM)
1-9	0.1 M Sodium acetate pH 5.0, 5 % w/v γ -PGA (Na ⁺ form, LM), 30 % v/v PEG 400
1-10	0.1 M Sodium acetate pH 5.0, 5 % w/v γ -PGA (Na ⁺ form, LM), 30 % v/v PEG 500 MME
1-11	0.1 M Sodium acetate pH 5.0, 5 % w/v γ -PGA (Na ⁺ form, LM), 30 % v/v MPD
1-12	0.1 M Sodium acetate pH 5.0, 5 % w/v γ -PGA (Na ⁺ form, LM), 20 % w/v PEG 2000 MME
1-13	0.1 M Sodium acetate pH 5.0, 5 % w/v γ -PGA (Na ⁺ form, LM), 20 % w/v PEG 3350
1-14	0.1 M Sodium acetate pH 5.0, 5 % w/v γ -PGA (Na ⁺ form, LM), 15 % w/v PEG 4000
1-15	0.1 M Sodium acetate pH 5.0, 5 % w/v γ -PGA (Na ⁺ form, LM), 12 % w/v PEG 8000
1-16	0.1 M Sodium acetate pH 5.0, 5 % w/v γ -PGA (Na ⁺ form, LM), 8 % w/v PEG 20000
1-17	0.2 M Potassium bromide, 0.2 M Potassium thiocyanate, 0.1 M Sodium acetate pH 5.0, 3 % w/v γ -PGA (Na ⁺ form, LM), 30 % v/v PEG 400
1-18	0.2 M Potassium bromide, 0.2 M Potassium thiocyanate, 0.1 M Sodium acetate pH 5.0, 3 % w/v γ -PGA (Na ⁺ form, LM), 20 % v/v PEG 500 MME
1-19	0.2 M Potassium bromide, 0.2 M Potassium thiocyanate, 0.1 M Sodium acetate pH 5.0, 3 % w/v γ -PGA (Na ⁺ form, LM), 20 % v/v MPD
1-20	0.2 M Potassium bromide, 0.2 M Potassium thiocyanate, 0.1 M Sodium acetate pH 5.0, 3 % w/v γ -PGA (Na ⁺ form, LM), 10 % w/v PEG 2000 MME
1-21	0.2 M Potassium bromide, 0.2 M Potassium thiocyanate, 0.1 M Sodium acetate pH 5.0, 3 % w/v γ -PGA (Na ⁺ form, LM), 5 % w/v PEG 3350
1-22	0.2 M Potassium bromide, 0.2 M Potassium thiocyanate, 0.1 M Sodium acetate pH 5.0, 3 % w/v γ -PGA (Na ⁺ form, LM), 5 % w/v PEG 4000
1-23	0.2 M Potassium bromide, 0.2 M Potassium thiocyanate, 0.1 M Sodium acetate pH 5.0, 3 % w/v γ -PGA (Na ⁺ form, LM), 5 % w/v PEG 8000
1-24	0.2 M Potassium bromide, 0.2 M Potassium thiocyanate, 0.1 M Sodium acetate pH 5.0, 3 % w/v γ -PGA (Na ⁺ form, LM), 3 % w/v PEG 20000
1-25	0.1 M Ammonium sulfate, 0.3 M Sodium formate, 0.1 M Sodium acetate pH 5.0, 3 % w/v γ -PGA (Na ⁺ form, LM), 30 % v/v PEG 400

1-26	0.1 M Ammonium sulfate, 0.3 M Sodium formate, 0.1 M Sodium acetate pH 5.0, 3 % w/v γ -PGA (Na ⁺ form, LM), 20 % v/v PEG 500 MME
1-27	0.1 M Ammonium sulfate, 0.3 M Sodium formate, 0.1 M Sodium acetate pH 5.0, 3 % w/v γ -PGA (Na ⁺ form, LM), 20 % v/v MPD
1-28	0.1 M Ammonium sulfate, 0.3 M Sodium formate, 0.1 M Sodium acetate pH 5.0, 3 % w/v γ -PGA (Na ⁺ form, LM), 10 % w/v PEG 2000 MME
1-29	0.1 M Ammonium sulfate, 0.3 M Sodium formate, 0.1 M Sodium acetate pH 5.0, 3 % w/v γ -PGA (Na ⁺ form, LM), 5 % w/v PEG 3350
1-30	0.1 M Ammonium sulfate, 0.3 M Sodium formate, 0.1 M Sodium acetate pH 5.0, 3 % w/v γ -PGA (Na ⁺ form, LM), 5 % w/v PEG 4000
1-31	0.1 M Ammonium sulfate, 0.3 M Sodium formate, 0.1 M Sodium acetate pH 5.0, 3 % w/v γ -PGA (Na ⁺ form, LM), 5 % w/v PEG 8000
1-32	0.1 M Ammonium sulfate, 0.3 M Sodium formate, 0.1 M Sodium acetate pH 5.0, 3 % w/v γ -PGA (Na ⁺ form, LM), 3 % w/v PEG 20000
1-33	0.3 M Potassium Bromide, 0.1 M Sodium cacodylate pH 6.5, 8 % w/v γ -PGA (Na ⁺ form, LM)
1-34	0.2 M Magnesium chloride, 0.1 M Sodium cacodylate pH 6.5, 8 % w/v γ -PGA (Na ⁺ form, LM)
1-35	0.3 M Sodium malonate dibasic monohydrate, 0.1 M Sodium cacodylate pH 6.5, 8 % w/v γ -PGA (Na ⁺ form, LM)
1-36	0.6 M Sodium formate, 0.1 M Sodium cacodylate pH 6.5, 8 % w/v γ -PGA (Na ⁺ form, LM)
1-37	1 M Ammonium formate, 0.1 M Sodium cacodylate pH 6.5, 8 % w/v γ -PGA (Na ⁺ form, LM)
1-38	0.2 M Potassium thiocyanate, 0.1 M Sodium cacodylate pH 6.5, 8 % w/v γ -PGA (Na ⁺ form, LM)
1-39	0.2 M L-Proline, 0.1 M Sodium cacodylate pH 6.5, 8 % w/v γ -PGA (Na ⁺ form, LM)
1-40	0.2 M L-Arginine, 0.1 M Sodium cacodylate pH 6.5, 8 % w/v γ -PGA (Na ⁺ form, LM)
1-41	0.1 M Sodium cacodylate pH 6.5, 5 % w/v γ -PGA (Na ⁺ form, LM), 30 % v/v PEG 400
1-42	0.1 M Sodium cacodylate pH 6.5, 5 % w/v γ -PGA (Na ⁺ form, LM), 30 % v/v PEG 500 MME
1-43	0.1 M Sodium cacodylate pH 6.5, 5 % w/v γ -PGA (Na ⁺ form, LM), 30 % v/v MPD
1-44	0.1 M Sodium cacodylate pH 6.5, 5 % w/v γ -PGA (Na ⁺ form, LM), 20 % w/v PEG 2000 MME
1-45	0.1 M Sodium cacodylate pH 6.5, 5 % w/v γ -PGA (Na ⁺ form, LM), 20 % w/v PEG 3350
1-46	0.1 M Sodium cacodylate pH 6.5, 5 % w/v γ -PGA (Na ⁺ form, LM), 15 % w/v PEG 4000
1-47	0.1 M Sodium cacodylate pH 6.5, 5 % w/v γ -PGA (Na ⁺ form, LM), 12 % w/v PEG 8000
1-48	0.1 M Sodium cacodylate pH 6.5, 5 % w/v γ -PGA (Na ⁺ form, LM), 8 % w/v PEG 20000
2-1	0.2 M Potassium bromide, 0.2 M Potassium thiocyanate, 0.1 M Sodium cacodylate pH 6.5, 3 % w/v γ -PGA (Na ⁺ form, LM), 30 % v/v PEG 400
2-2	0.2 M Potassium bromide, 0.2 M Potassium thiocyanate, 0.1 M Sodium cacodylate pH 6.5, 3 % w/v γ -PGA (Na ⁺ form, LM), 20 % v/v PEG 500 MME
2-3	0.2 M Potassium bromide, 0.2 M Potassium thiocyanate, 0.1 M Sodium cacodylate pH 6.5, 3 % w/v γ -PGA (Na ⁺ form, LM), 20 % v/v MPD
2-4	0.2 M Potassium bromide, 0.2 M Potassium thiocyanate, 0.1 M Sodium cacodylate pH 6.5, 3 % w/v γ -PGA (Na ⁺ form, LM), 10 % w/v PEG 2000 MME

2-5	0.2 M Potassium bromide, 0.2 M Potassium thiocyanate, 0.1 M Sodium cacodylate pH 6.5, 3 % w/v γ -PGA (Na ⁺ form, LM), 5 % w/v PEG 3350
2-6	0.2 M Potassium bromide, 0.2 M Potassium thiocyanate, 0.1 M Sodium cacodylate pH 6.5, 3 % w/v γ -PGA (Na ⁺ form, LM), 5 % w/v PEG 4000
2-7	0.2 M Potassium bromide, 0.2 M Potassium thiocyanate, 0.1 M Sodium cacodylate pH 6.5, 3 % w/v γ -PGA (Na ⁺ form, LM), 5 % w/v PEG 8000
2-8	0.2 M Potassium bromide, 0.2 M Potassium thiocyanate, 0.1 M Sodium cacodylate pH 6.5, 3 % w/v γ -PGA (Na ⁺ form, LM), 3 % w/v PEG 20000
2-9	0.1 M Ammonium sulfate, 0.3 M Sodium formate, 0.1 M Sodium cacodylate pH 6.5, 3 % w/v γ -PGA (Na ⁺ form, LM), 30 % v/v PEG 400
2-10	0.1 M Ammonium sulfate, 0.3 M Sodium formate, 0.1 M Sodium cacodylate pH 6.5, 3 % w/v γ -PGA (Na ⁺ form, LM), 20 % v/v PEG 500 MME
2-11	0.1 M Ammonium sulfate, 0.3 M Sodium formate, 0.1 M Sodium cacodylate pH 6.5, 3 % w/v γ -PGA (Na ⁺ form, LM), 20 % v/v MPD
2-12	0.1 M Ammonium sulfate, 0.3 M Sodium formate, 0.1 M Sodium cacodylate pH 6.5, 3 % w/v γ -PGA (Na ⁺ form, LM), 10 % w/v PEG 2000 MME
2-13	0.1 M Ammonium sulfate, 0.3 M Sodium formate, 0.1 M Sodium cacodylate pH 6.5, 3 % w/v γ -PGA (Na ⁺ form, LM), 5 % w/v PEG 3350
2-14	0.1 M Ammonium sulfate, 0.3 M Sodium formate, 0.1 M Sodium cacodylate pH 6.5, 3 % w/v γ -PGA (Na ⁺ form, LM), 5 % w/v PEG 4000
2-15	0.1 M Ammonium sulfate, 0.3 M Sodium formate, 0.1 M Sodium cacodylate pH 6.5, 3 % w/v γ -PGA (Na ⁺ form, LM), 5 % w/v PEG 8000
2-16	0.1 M Ammonium sulfate, 0.3 M Sodium formate, 0.1 M Sodium cacodylate pH 6.5, 3 % w/v γ -PGA (Na ⁺ form, LM), 3 % w/v PEG 20000
2-17	0.3 M Potassium bromide, 0.1 M Tris pH 7.8, 8 % w/v γ -PGA (Na ⁺ form, LM)
2-18	0.2 M Magnesium chloride, 0.1 M Tris pH 7.8, 8 % w/v γ -PGA (Na ⁺ form, LM)
2-19	0.3 M Sodium malonate dibasic monohydrate, 0.1 M Tris pH 7.8, 8 % w/v γ -PGA (Na ⁺ form, LM)
2-20	0.6 M Sodium formate, 0.1 M Tris pH 7.8, 8 % w/v γ -PGA (Na ⁺ form, LM)
2-21	1 M Ammonium formate, 0.1 M Tris pH 7.8, 8 % w/v γ -PGA (Na ⁺ form, LM)
2-22	0.2 M Potassium thiocyanate, 0.1 M Tris pH 7.8, 8 % w/v γ -PGA (Na ⁺ form, LM)
2-23	0.2 M L-Proline, 0.1 M Tris pH 7.8, 8 % w/v γ -PGA (Na ⁺ form, LM)
2-24	0.2 M L-Arginine, 0.1 M Tris pH 7.8, 8 % w/v γ -PGA (Na ⁺ form, LM)
2-25	0.1 M Tris pH 7.8, 5 % w/v γ -PGA (Na ⁺ form, LM), 30 % v/v PEG 400
2-26	0.1 M Tris pH 7.8, 5 % w/v γ -PGA (Na ⁺ form, LM), 30 % v/v PEG 500 MME
2-27	0.1 M Tris pH 7.8, 5 % w/v γ -PGA (Na ⁺ form, LM), 30 % v/v MPD
2-28	0.1 M Tris pH 7.8, 5 % w/v γ -PGA (Na ⁺ form, LM), 20 % w/v PEG 2000 MME
2-29	0.1 M Tris pH 7.8, 5 % w/v γ -PGA (Na ⁺ form, LM), 20 % w/v PEG 3350
2-30	0.1 M Tris pH 7.8, 5 % w/v γ -PGA (Na ⁺ form, LM), 15 % w/v PEG 4000
2-31	0.1 M Tris pH 7.8, 5 % w/v γ -PGA (Na ⁺ form, LM), 12 % w/v PEG 8000
2-32	0.1 M Tris pH 7.8, 5 % w/v γ -PGA (Na ⁺ form, LM), 8 % w/v PEG 20000
2-33	0.2 M Potassium bromide, 0.2 M Potassium thiocyanate, 0.1 M Tris pH 7.8 3 % w/v γ -PGA (Na ⁺ form, LM), 30 % v/v PEG 400
2-34	0.2 M Potassium bromide, 0.2 M Potassium thiocyanate, 0.1 M Tris pH 7.8 3 % w/v γ -PGA (Na ⁺ form, LM), 20 % v/v PEG 500 MME
2-35	0.2 M Potassium bromide, 0.2 M Potassium thiocyanate, 0.1 M Tris pH 7.8 3 % w/v γ -PGA (Na ⁺ form, LM), 20 % v/v MPD
2-36	0.2 M Potassium bromide, 0.2 M Potassium thiocyanate, 0.1 M Tris pH 7.8 3 % w/v γ -PGA (Na ⁺ form, LM), 10 % w/v PEG 2000 MME
2-37	0.2 M Potassium bromide, 0.2 M Potassium thiocyanate, 0.1 M Tris pH 7.8 3 % w/v γ -PGA (Na ⁺ form, LM), 5 % w/v PEG 3350

2-38	0.2 M Potassium bromide, 0.2 M Potassium thiocyanate, 0.1 M Tris pH 7.8 3 % w/v γ -PGA (Na ⁺ form, LM), 5 % w/v PEG 4000
2-39	0.2 M Potassium bromide, 0.2 M Potassium thiocyanate, 0.1 M Tris pH 7.8 3 % w/v γ -PGA (Na ⁺ form, LM), 5 % w/v PEG 8000
2-40	0.2 M Potassium bromide, 0.2 M Potassium thiocyanate, 0.1 M Tris pH 7.8 3 % w/v γ -PGA (Na ⁺ form, LM), 3 % w/v PEG 20000
2-41	0.1 M Ammonium sulfate, 0.3 M Sodium formate, 0.1 M Tris pH 7.8 3 % w/v γ -PGA (Na ⁺ form, LM), 30 % v/v PEG 400
2-42	0.1 M Ammonium sulfate, 0.3 M Sodium formate, 0.1 M Tris pH 7.8 3 % w/v γ -PGA (Na ⁺ form, LM), 20 % v/v PEG 500 MME
2-43	0.1 M Ammonium sulfate, 0.3 M Sodium formate, 0.1 M Tris pH 7.8 3 % w/v γ -PGA (Na ⁺ form, LM), 20 % v/v MPD
2-44	0.1 M Ammonium sulfate, 0.3 M Sodium formate, 0.1 M Tris pH 7.8 3 % w/v γ -PGA (Na ⁺ form, LM), 10 % w/v PEG 2000 MME
2-45	0.1 M Ammonium sulfate, 0.3 M Sodium formate, 0.1 M Tris pH 7.8 3 % w/v γ -PGA (Na ⁺ form, LM), 5 % w/v PEG 3350
2-46	0.1 M Ammonium sulfate, 0.3 M Sodium formate, 0.1 M Tris pH 7.8 3 % w/v γ -PGA (Na ⁺ form, LM), 5 % w/v PEG 4000
2-47	0.1 M Ammonium sulfate, 0.3 M Sodium formate, 0.1 M Tris pH 7.8 3 % w/v γ -PGA (Na ⁺ form, LM), 5 % w/v PEG 8000
2-48	0.1 M Ammonium sulfate, 0.3 M Sodium formate, 0.1 M Tris pH 7.8 3 % w/v γ -PGA (Na ⁺ form, LM), 3 % w/v PEG 20000